

Departamento de Electrónica Física  
Escuela Técnica Superior de Ingenieros de Telecomunicación



**A swarm intelligence approach based  
on coupled oscillators: an application  
in demand side management with  
photovoltaic distributed generation**

**Autor**

**Manuel Castillo Cagigal**  
Ingeniero de Telecomunicación

**Directores**

**Estefanía Caamaño Martín**      **Álvaro Gutiérrez Martín**  
Doctora Ingeniera de Telecomunicación      Doctor Ingeniero de Telecomunicación

**2014**



Tribunal nombrado por el Mgfc. y Excmo. Sr. Rector de la Universidad Politécnica de Madrid.

Presidente: Dr. Félix Monasterio-Huelin Maciá.

Secretario: Dr. Miguel A. Egido Aguilera.

Vocal: Dr. Mariano Sidrach de Cardona Ortín.

Vocal: Dr. Mauro Birattari.

Vocal: Dr. Iñaki Navarro Oiza.

Suplente: Dra. Llanos Mora López.

Suplente: Dr. Manuel Ocaña Miguel.

Realizando el acto de defensa y lectura de la Tesis el día \_\_\_\_\_ de \_\_\_\_\_ de 2014.

En la E.T.S. de Ingenieros de Telecomunicación.

CALIFICACIÓN:

EL PRESIDENTE

LOS VOCALES

EL SECRETARIO



## Resumen

Esta Tesis aborda los problemas de eficiencia de las redes eléctrica desde el punto de vista del consumo. En particular, dicha eficiencia es mejorada mediante el suavizado de la curva de consumo agregado. Este objetivo de suavizado de consumo implica dos grandes mejoras en el uso de las redes eléctricas: *i)* a corto plazo, un mejor uso de la infraestructura existente y *ii)* a largo plazo, la reducción de la infraestructura necesaria para suplir las mismas necesidades energéticas. Además, esta Tesis se enfrenta a un nuevo paradigma energético, donde la presencia de generación distribuida está muy extendida en las redes eléctricas, en particular, la generación fotovoltaica (FV). Este tipo de fuente energética afecta al funcionamiento de la red, incrementando su variabilidad. Esto implica que altas tasas de penetración de electricidad de origen fotovoltaico es perjudicial para la estabilidad de la red eléctrica. Esta Tesis trata de suavizar la curva de consumo agregado considerando esta fuente energética. Por lo tanto, no sólo se mejora la eficiencia de la red eléctrica, sino que también puede ser aumentada la penetración de electricidad de origen fotovoltaico en la red. Esta propuesta conlleva grandes beneficios en los campos económicos, social y ambiental.

Las acciones que influyen en el modo en que los consumidores hacen uso de la electricidad con el objetivo producir un ahorro energético o un aumento de eficiencia son llamadas *Gestión de la Demanda Eléctrica* (GDE). Esta Tesis propone dos algoritmos de GDE diferentes para cumplir con el objetivo de suavizado de la curva de consumo agregado. La diferencia entre ambos algoritmos de GDE reside en el marco en el cual estos tienen lugar: el marco local y el marco de red. Dependiendo de este marco de GDE, el objetivo energético y la forma en la que se alcanza este objetivo son diferentes. En el marco local, el algoritmo de GDE sólo usa información local. Este no tiene en cuenta a otros consumidores o a la curva de consumo agregado de la red eléctrica. Aunque esta afirmación pueda diferir de la definición general de GDE, esta vuelve a tomar sentido en instalaciones locales equipadas con *Recursos Energéticos Distribuidos* (REDs). En este caso, la GDE está enfocada en la maximización del uso de la energía local, reduciéndose la dependencia con la red.

El algoritmo de GDE propuesto mejora significativamente el auto-consumo del generador FV local. Experimentos simulados y reales muestran que el auto-consumo es una importante estrategia de gestión energética, reduciendo el transporte de electricidad y alentando al usuario a controlar su comportamiento energético. Sin embargo, a pesar de todas las ventajas del aumento de auto-consumo, éstas no contribuyen al suavizado del consumo agregado. Se han estudiado los efectos de

---

las instalaciones locales en la red eléctrica cuando el algoritmo de GDE está enfocado en el aumento del auto-consumo. Este enfoque puede tener efectos no deseados, incrementando la variabilidad en el consumo agregado en vez de reducirlo. Este efecto se produce porque el algoritmo de GDE sólo considera variables locales en el marco local. Los resultados sugieren que se requiere una coordinación entre las instalaciones. A través de esta coordinación, el consumo debe ser modificado teniendo en cuenta otros elementos de la red y buscando el suavizado del consumo agregado.

En el marco de la red, el algoritmo de GDE tiene en cuenta tanto información local como de la red eléctrica. En esta Tesis se ha desarrollado un algoritmo auto-organizado para controlar el consumo de la red eléctrica de manera distribuida. El objetivo de este algoritmo es el suavizado del consumo agregado, como en las implementaciones clásicas de GDE. El enfoque distribuido significa que la GDE se realiza desde el lado de los consumidores sin seguir órdenes directas emitidas por una entidad central. Por lo tanto, esta Tesis propone una estructura de gestión paralela en lugar de una jerárquica como en las redes eléctricas clásicas. Esto implica que se requiere un mecanismo de coordinación entre instalaciones. Esta Tesis pretende minimizar la cantidad de información necesaria para esta coordinación. Para lograr este objetivo, se han utilizado dos técnicas de coordinación colectiva: *osciladores acoplados* e *inteligencia de enjambre*. La combinación de estas técnicas para llevar a cabo la coordinación de un sistema con las características de la red eléctrica es en sí mismo un enfoque novedoso. Por lo tanto, este objetivo de coordinación no es sólo una contribución en el campo de la gestión energética, sino también en el campo de los sistemas colectivos. Los resultados muestran que el algoritmo de GDE propuesto reduce la diferencia entre máximos y mínimos de la red eléctrica en proporción a la cantidad de energía controlada por el algoritmo. Por lo tanto, conforme mayor es la cantidad de energía controlada por el algoritmo, mayor es la mejora de eficiencia en la red eléctrica.

Además de las ventajas resultantes del suavizado del consumo agregado, otras ventajas surgen de la solución distribuida seguida en esta Tesis. Estas ventajas se resumen en las siguientes características del algoritmo de GDE propuesto:

- *Robustez*: en un sistema centralizado, un fallo o rotura del nodo central provoca un mal funcionamiento de todo el sistema. La gestión de una red desde un punto de vista distribuido implica que no existe un nodo de control central. Un fallo en cualquier instalación no afecta el funcionamiento global de la red.

- 
- *Privacidad de datos:* el uso de una topología distribuida causa de que no hay un nodo central con información sensible de todos los consumidores. Esta Tesis va más allá y el algoritmo propuesto de GDE no utiliza información específica acerca de los comportamientos de los consumidores, siendo la coordinación entre las instalaciones completamente anónimos.
  - *Escalabilidad:* el algoritmo propuesto de GDE opera con cualquier número de instalaciones. Esto implica que se permite la incorporación de nuevas instalaciones sin afectar a su funcionamiento.
  - *Bajo coste:* el algoritmo de GDE propuesto se adapta a las redes actuales sin requisitos topológicos. Además, todas las instalaciones calculan su propia gestión con un bajo requerimiento computacional. Por lo tanto, no se requiere un nodo central con un alto poder de cómputo.
  - *Rápido despliegue:* las características de escalabilidad y bajo coste de los algoritmos de GDE propuestos permiten una implementación rápida. No se requiere una planificación compleja para el despliegue de este sistema.



## Abstract

This Thesis addresses the efficiency problems of the electrical grids from the consumption point of view. In particular, such efficiency is improved by means of the aggregated consumption smoothing. This objective of consumption smoothing entails two major improvements in the use of electrical grids: *i*) in the short term, a better use of the existing infrastructure and *ii*) in long term, the reduction of the required infrastructure to supply the same energy needs. In addition, this Thesis faces a new energy paradigm, where the presence of distributed generation is widespread over the electrical grids, in particular, the **Photovoltaic (PV)** generation. This kind of energy source affects to the operation of the grid by increasing its variability. This implies that a high penetration rate of photovoltaic electricity is pernicious for the electrical grid stability. This Thesis seeks to smooth the aggregated consumption considering this energy source. Therefore, not only the efficiency of the electrical grid is improved, but also the penetration of photovoltaic electricity into the grid can be increased. This proposal brings great benefits in the economic, social and environmental fields.

The actions that influence the way that consumers use electricity in order to achieve energy savings or higher efficiency in energy use are called **Demand-Side Management (DSM)**. This Thesis proposes two different **DSM** algorithms to meet the aggregated consumption smoothing objective. The difference between both **DSM** algorithms lie in the framework in which they take place: the local framework and the grid framework. Depending on the **DSM** framework, the energy goal and the procedure to reach this goal are different. In the local framework, the **DSM** algorithm only uses local information. It does not take into account other consumers or the aggregated consumption of the electrical grid. Although this statement may differ from the general definition of **DSM**, it makes sense in local facilities equipped with **Distributed Energy Resources (DERs)**. In this case, the **DSM** is focused on the maximization of the local energy use, reducing the grid dependence.

The proposed **DSM** algorithm significantly improves the self-consumption of the local **PV** generator. Simulated and real experiments show that self-consumption serves as an important energy management strategy, reducing the electricity transport and encouraging the user to control his energy behavior. However, despite all the advantages of the self-consumption increase, they do not contribute to the smooth of the aggregated consumption. The effects of the local facilities on the electrical grid are studied when the **DSM** algorithm is focused on self-consumption maximization. This approach may have undesirable effects, increasing the variability in the aggregated

---

consumption instead of reducing it. This effect occurs because the algorithm only considers local variables in the local framework. The results suggest that coordination between these facilities is required. Through this coordination, the consumption should be modified by taking into account other elements of the grid and seeking for an aggregated consumption smoothing.

In the grid framework, the **DSM** algorithm takes into account both local and grid information. This Thesis develops a self-organized algorithm to manage the consumption of an electrical grid in a distributed way. The goal of this algorithm is the aggregated consumption smoothing, as the classical **DSM** implementations. The distributed approach means that the **DSM** is performed from the consumers side without following direct commands issued by a central entity. Therefore, this Thesis proposes a parallel management structure rather than a hierarchical one as in the classical electrical grids. This implies that a coordination mechanism between facilities is required. This Thesis seeks for minimizing the amount of information necessary for this coordination. To achieve this objective, two collective coordination techniques have been used: *coupled oscillators* and *swarm intelligence*. The combination of these techniques to perform the coordination of a system with the characteristics of the electric grid is itself a novel approach. Therefore, this coordination objective is not only a contribution in the energy management field, but in the collective systems too. Results show that the proposed **DSM** algorithm reduces the difference between the maximums and minimums of the electrical grid proportionally to the amount of energy controlled by the system. Thus, the greater the amount of energy controlled by the algorithm, the greater the improvement of the efficiency of the electrical grid.

In addition to the advantages resulting from the smoothing of the aggregated consumption, other advantages arise from the distributed approach followed in this Thesis. These advantages are summarized in the following features of the proposed **DSM** algorithm:

- *Robustness*: in a centralized system, a failure or breakage of the central node causes a malfunction of the whole system. The management of a grid from a distributed point of view implies that there is not a central control node. A failure in any facility does not affect the overall operation of the grid.
- *Data privacy*: the use of a distributed topology causes that there is not a central node with sensitive information of all consumers. This Thesis goes a step further and the proposed **DSM** algorithm does not use specific information about

---

the consumer behaviors, being the coordination between facilities completely anonymous.

- *Scalability*: the proposed **DSM** algorithm operates with any number of facilities. This implies that it allows the incorporation of new facilities without affecting its operation.
- *Low cost*: the proposed **DSM** algorithm adapts to the current grids without any topological requirements. In addition, every facility calculates its own management with low computational requirements. Thus, a central computational node with a high computational power is not required.
- *Quick deployment*: the scalability and low cost features of the proposed **DSM** algorithms allow a quick deployment. A complex schedule of the deployment of this system is not required.



**To my Family**



## Acknowledgements

I would like to express my deep gratitude to Prof. Alvaro Gutiérrez Martín for its constant support to the development of this Thesis. The Alvaro's supervision of my work has not only been a valuable contribution and a source of motivation to the development of my Thesis, but he has also taught me the intricacies of scientific publishing and management of a laboratory. Thus, Alvaro's advice and review have helped me to train as researcher and to shape me as a person.

I would also like to thank Prof. Estefanía Caamaño Martín its valuable supervision of this Thesis. Their interest and dedication to the fields discussed in this work helped to shape it from the beginning. Moreover, its thorough review of the work done has been a source of valuable improvements.

I wish to thank the international reviewer Dr. Alexander Mellor and Dr. Alexandre Campo for their congratulations on this thesis. Their criticism and contributions have been a source of improvement for the development of this manuscript.

I am grateful to have been part of ROBOLABO during the realization of my Thesis. Thanks to this work environment, I have been able to develop my skills in different techniques, from programming to scientific publishing, while passing the best moments of my thesis. I would like to thanks to Eduardo Matallanas for having accompanied me since the beginning of this Thesis and his support in the development of the software, in particular, the simulator *GridSim*. I would like to thanks to Dr. Iñaki Navarro for the interesting discussions we had and for the pleasant company during the development of the SDE12 project. I also wish to thank Prof. Félix Monasterio-Huelin the interesting and pleasant discussions we had and his help and advice in the mathematical development of this Thesis.

I am also grateful to have been part of GEDIRCI during the realization of my Thesis. I want to thank Dr. Daniel Masa, Dr. Jorge Solórzano and Prof. Miguel Angel Egido their support and advice in the energy field. I would also like to mention my thanks to my colleagues of the Solar Energy Institute who have been with me during the development of this Thesis: Iñigo Ramiro, Dr. Alexander Mellor, Rodrigo Moretón and Alvaro Ramiro between others.

I would also like to thank IRIDIA for its hospitality during my stay in this center in the Université Libre de Bruxelles. I thank Prof. Marco Dorigo for giving me the opportunity to work at IRIDIA during some months. I would also like to thank Dr. Mauro Birattari for its valuable supervision during my stay in this center. His dedication to my work and advice have helped me to improve as researcher. I wish to

---

thank the people who also helped me in the development of my work in IRIDIA: Arne Brutschy, Gianpiero Francesca, Lorenzo Garattoni and Dr. Carlo Pincioli between others.

I thank the sponsorship of the Spanish Ministry of Education with a Ph.D. Grant (FPU-2010) for the entire period of realization of this Thesis. I am grateful to GeDELOS-FV and SIGMAPLANTAS projects by the possibility of using the necessary equipment for the development of this Thesis. I also wish to thank the Escuela Técnica Superior de Ingenieros de Telecomunicación of the Technical University of Madrid for their support in the maintenance and use of “MagicBox” prototype.

My last thanks to my family for their valuable support. In particular, to Carolina Pozuelo for her understanding and patience during the hard times that arise in the development of a Ph.D. Thesis.

# Contents

<b>Resumen</b>	<b>v</b>
<b>Abstract</b>	<b>ix</b>
<b>Acknowledgements</b>	<b>xv</b>
<b>Contents</b>	<b>xvii</b>
<b>List of Figures</b>	<b>xx</b>
<b>List of Tables</b>	<b>xxvi</b>
<b>List of Algorithms</b>	<b>xxviii</b>
<b>1 Introduction</b>	<b>1</b>
1.1 Electricity management background . . . . .	1
1.1.1 Demand-Side Management . . . . .	5
1.1.2 Smart Grids . . . . .	11
1.2 The aim of this Thesis . . . . .	14
1.3 Thesis structure . . . . .	15
<b>I Local framework</b>	<b>17</b>
<b>2 Local framework background</b>	<b>19</b>
2.1 Local electric power system: facility . . . . .	19
2.1.1 Distributed generation: photovoltaic technology . . . . .	20
2.1.1.1 Photovoltaic technology . . . . .	22
2.1.2 Storage . . . . .	23

2.1.3	Consumption . . . . .	25
2.2	Assessment of local electrical behavior . . . . .	27
2.3	Experimental facility: “MagicBox” . . . . .	29
2.3.1	PV generation system . . . . .	31
2.3.2	Storage system . . . . .	33
2.3.3	Loads . . . . .	33
2.3.4	Monitoring and embedded system . . . . .	34
<b>3</b>	<b>Local Demand-Side Management</b>	<b>37</b>
3.1	Local controllers . . . . .	38
3.1.1	ADSM algorithm . . . . .	40
3.1.2	Battery controller . . . . .	43
3.2	Experiments . . . . .	45
3.2.1	Simulation campaign . . . . .	48
3.2.2	Measurement campaign . . . . .	51
3.3	Effects on the grid . . . . .	57
3.3.1	Virtual users . . . . .	59
3.3.2	PV effect on the grid . . . . .	62
3.3.3	ADSM effect on the grid . . . . .	67
3.3.4	DER effect on the grid . . . . .	70
3.3.5	ADSM and DER on the grid . . . . .	74
3.4	Discussion of results and conclusions . . . . .	78
<b>II</b>	<b>Grid framework</b>	<b>81</b>
<b>4</b>	<b>Grid framework background</b>	<b>83</b>
4.1	Coupled Oscillators . . . . .	88
4.1.1	Oscillators as signals . . . . .	94
4.2	Swarm intelligence . . . . .	99
4.2.1	Stigmergy . . . . .	101
4.2.2	Division of labor and task allocation . . . . .	106
4.3	Discussion . . . . .	112
<b>5</b>	<b>Multi-Frequency Coupled Oscillators</b>	<b>115</b>
5.1	The environment as signals . . . . .	116
5.2	Single frequency coupling . . . . .	119

## CONTENTS

---

5.2.1	Coupling equations . . . . .	119
5.2.2	Coupling strength K analysis . . . . .	124
5.3	Multi-frequency coupling . . . . .	127
5.3.1	Frequency switching . . . . .	129
5.4	Operation example . . . . .	133
5.5	Discussion . . . . .	142
<b>6</b>	<b>Swarm Grid</b>	<b>145</b>
6.1	The Swarm Grid algorithm . . . . .	145
6.1.1	Scheduling with MuFCO . . . . .	148
6.1.2	Scheduling with PV forecast . . . . .	150
6.1.3	Real-time execution . . . . .	151
6.2	Operating examples . . . . .	152
6.2.1	Virtual users . . . . .	153
6.2.2	The grid without DER . . . . .	154
6.2.3	The grid with DG . . . . .	158
6.2.4	The grid with DER . . . . .	166
6.3	Discussion . . . . .	170
<b>III</b>	<b>Conclusions and Future Works</b>	<b>175</b>
<b>7</b>	<b>Conclusions and Future Works</b>	<b>177</b>
7.1	Local Framework . . . . .	177
7.2	Grid Framework . . . . .	180
7.3	Future Work . . . . .	183
7.3.1	Energy Management Framework . . . . .	183
7.3.2	Collective System Framework . . . . .	186
7.4	Review of Contributions . . . . .	187
<b>A</b>	<b>GridSim simulation framework</b>	<b>193</b>
	<b>Bibliography</b>	<b>194</b>



# List of Figures

1.1	Schematic representation of the grid. . . . .	2
1.2	Example of the aggregated consumption of the peninsular Spanish electrical grid. . . . .	3
1.3	Three-dimensional representation of the regional disparities in the Spanish electrical grid. . . . .	4
1.4	Effects of the DSM techniques in the aggregated consumption. . . . .	7
2.1	Schematic representation of a facility connected to the electrical grid. .	20
2.2	Schematic representation of PV power generation. . . . .	22
2.3	Schematic representation of the local facility. . . . .	27
2.4	“MagicBox” pictures. . . . .	29
2.5	Electrical and communication scheme of “MagicBox”. . . . .	31
2.6	Picture of the inverter’s room and battery bank of “MagicBox”. . . . .	32
2.7	Depiction of gateway communication and Power Line Communication network of the home automation system. . . . .	33
3.1	Conceptual example of the operation of the local controllers. . . . .	39
3.2	Conceptual example of load scheduling. . . . .	40
3.3	Conceptual example of the operation of the ADSM algorithm. . . . .	41
3.4	Switching between states of the battery controller. . . . .	43
3.5	Power functions of deferrable loads used in experiments. . . . .	45
3.6	Fixed consumption function for a day of experiment. . . . .	46
3.7	Energy variables for the simulated annual experiments. . . . .	49
3.8	Self-Consumption factor relationship with the storage capacity. . . . .	50
3.9	Development of the main power flows during the experiments without storage. . . . .	51
3.10	Development of the main power flows during two days of experiments without storage. . . . .	52

## LIST OF FIGURES

---

3.11 Development of the main power flows during two days of experiments with storage. . . . .	54
3.12 Development of the main power flows during the experiments without ADSM and with storage in different seasons. . . . .	55
3.13 Development of the main power flows during the experiments with ADSM and with storage in different seasons. . . . .	56
3.14 Example of the crest factor for two different periods of the aggregated consumption. . . . .	58
3.15 Conceptual example of a virtual user operation. . . . .	59
3.16 Example of the aggregated consumption of the simulated electrical grid.	61
3.17 Climate zones of Spain. . . . .	63
3.18 Development of the crest factors for different percentages of PV penetration. . . . .	64
3.19 Example of the aggregated consumption for different PV penetrations.	65
3.20 Development of the self-consumption for different percentages of PV penetration. . . . .	66
3.21 Example of the aggregated consumption of the simulated electrical grid with $\rho^{PV} = 50\%$ . . . . .	67
3.22 Development of the crest factors for different combinations of $\rho^{PV}$ and $\rho^{ctr}$ . . . . .	69
3.23 Development of the self-consumption for different combinations of $\rho^{PV}$ and $\rho^{ctr}$ . . . . .	70
3.24 Example of the aggregated consumption of the simulated electrical grid with $\rho^{PV} = 50\%$ and $\rho^{ctr} = 50\%$ . . . . .	71
3.25 Development of the crest factors for different combinations of $\rho^{PV}$ and $Cap^*$ . . . . .	72
3.26 Development of the self-consumption for different combinations of $\rho^{PV}$ and $Cap^*$ . . . . .	73
3.27 Example of the aggregated consumption of the simulated electrical grid with $\rho^{PV} = 50\%$ , storage systems of 1 day of autonomy and without ADSM. . . . .	74
3.28 Development of the crest factors for different combinations of $\rho^{PV}$ , $\rho^{ctr}$ and storage systems with 1 day of autonomy. . . . .	75
3.29 Development of the self-consumption for different combinations of $\rho^{PV}$ and $\rho^{ctr}$ and storage systems with 1 day of autonomy. . . . .	76

## LIST OF FIGURES

---

3.30	Example of the aggregated consumption of the simulated electrical grid with $\rho^{PV} = 50\%$ , $\rho^{ctr} = 50\%$ and storage systems of 1 day of autonomy	77
4.1	Graphical representation of $P(t)$ signal as a sum of $P^{nc}(t)$ and $P^c(t)$ signals.	84
4.2	Spectrum example of the non-controllable consumption.	85
4.3	Relationship between sinusoidal functions.	86
4.4	Conceptual scheme of an electrical grid divided in local facilities.	88
4.5	Sketch of the two coupled pendulums.	90
4.6	Oscillators and order parameter representation on the unit circle in two different situations.	92
4.7	Sketch of the wave interference as sum of signals.	95
4.8	Example of oscillator coupling from their output signals.	96
4.9	Example of oscillator coupling from their output signals with negative coupling.	98
4.10	Self-organization examples in biological systems.	99
4.11	Results of the foraging experiment of J.L. Deneubourg <i>et al.</i>	102
4.12	Experiment of ant foraging.	103
4.13	Qualitative stigmergy represented by the successive stages leading to the construction of a comb.	104
4.14	The response threshold model presented in the work of E. Bonabeau <i>et al.</i>	110
4.15	Conceptual scheme of an electrical grid divided in local facilities.	113
5.1	Example of coupling between oscillators and $z(t)$ using Equation 5.10.	121
5.2	Example of coupling between oscillators and $z(t)$ using Equation 5.11.	123
5.3	Example of coupling between oscillators and $z(t)$ using Equation 5.12.	125
5.4	Result of the $K$ analysis.	126
5.5	Result of the effects of the different $W$ values in $K$ analysis with the coupling equation 5.12.	127
5.6	Conceptual scheme of the MuFCO algorithm operation.	128
5.7	MuFCO algorithm operation example in frequency.	131
5.8	MuFCO algorithm operation example in time.	132
5.9	Aggregated consumption signal of peninsular Spain during 2013.	134
5.10	Aggregated consumption signal of Spain during 2013 using MuFCO algorithm with daily optimization.	138

## LIST OF FIGURES

---

5.11	Aggregated consumption signal of Spain during 2013 using MuFCO algorithm with weekly optimization. . . . .	139
5.12	Aggregated consumption signal of Spain during 2013 using MuFCO algorithm with mixed optimization . . . . .	140
5.13	Boxplot representation of the statistical analysis of the MuFCO optimization. . . . .	141
6.1	Conceptual example of the SG algorithm's load scheduling. . . . .	146
6.2	Conceptual example of the $t_{i,j}^{act}$ calculation by SG algorithm. . . . .	147
6.3	Conceptual example of the $t_{i,j}^{act}$ calculation by SG algorithm with MuFCO sinusoidal patterns. . . . .	149
6.4	Conceptual example of the $t_{i,j}^{act}$ calculation by SG algorithm with the PV forecast. . . . .	150
6.5	Conceptual example of the deferrable consumption created by the virtual users. . . . .	154
6.6	Example of the aggregated consumption of the simulated electrical grid without DER and $\rho^{ctr} = 0\%$ . . . . .	155
6.7	Development of the crest factors for different percentages of consumption controlled by the SG algorithm. . . . .	157
6.8	Example of the aggregated consumption of the simulated electrical grid without DER and $\rho^{ctr} = 100\%$ . . . . .	159
6.9	Example of the aggregated consumption of the simulated electrical grid with $\rho^{PV} = 50\%$ and $\rho^{ctr} = 0\%$ . . . . .	160
6.10	Development of the crest factors for different combinations of $\rho^{PV}$ and $\beta$ with $\rho^{ctr} = 100\%$ . . . . .	162
6.11	Development of the self-consumption for different combinations of $\rho^{PV}$ and $\beta$ with $\rho^{ctr} = 100\%$ . . . . .	163
6.12	Example of the aggregated consumption of the simulated electrical grid with $\rho^{PV} = 50\%$ , $\rho^{ctr} = 100\%$ and $\beta = 0$ . . . . .	164
6.13	Development of the crest factors for different combinations of $\rho^{PV}$ and $\rho^{ctr}$ with $\beta = 0$ . . . . .	165
6.14	Development of the self-consumption for different combinations of $\rho^{PV}$ and $\rho^{ctr}$ with $\beta = 0$ . . . . .	166
6.15	Example of the aggregated consumption of the simulated electrical grid with $\rho^{PV} = 50\%$ , $\rho^{ctr} = 50\%$ and $\beta = 0$ . . . . .	167
6.16	Development of the crest factors for different combinations of $\rho^{PV}$ and $Cap^*$ with $\rho^{ctr} = 100\%$ and $\beta = 0$ . . . . .	169

## LIST OF FIGURES

---

6.17	Development of the self-consumption for different combinations of $\rho^{PV}$ and $Cap^*$ with $\rho^{ctr} = 100\%$ and $\beta = 0$ . . . . .	170
6.18	Example of the aggregated consumption of the simulated electrical grid with $\rho^{PV} = 50\%$ , $\rho^{ctr} = 50\%$ , $\beta = 0$ and storage systems of 1 day of autonomy. . . . .	171
A.1	Scheme of the modular architecture of <i>GridSim</i> simulator. . . . .	194



# List of Tables

3.1	Typical daily consumption in “MagicBox”. . . . .	47
3.2	Energy variables and the self-consumption for experiments without storage. . . . .	53
3.3	Energy variables and the self-consumption for experiments with storage. . . . .	57
5.1	Crest factors of the aggregated consumption example. . . . .	135
5.2	<i>irace</i> optimization results. . . . .	136



# List of Algorithms

1	ADSM algorithm . . . . .	42
2	Battery controller . . . . .	44
3	MuFCO algorithm. . . . .	129
4	Swarm Grid algorithm. . . . .	151
5	Main loop of <i>GridSim</i> simulator. . . . .	195



# Acronyms

<b>ADSM</b>	Active Demand-Side Management.
<b>DER</b>	Distributed Energy Resource.
<b>DFT</b>	Discrete Fourier Transform.
<b>DG</b>	Distributed Generation.
<b>DSM</b>	Demand-Side Management.
<b>EV</b>	Electric Vehicle.
<b>FFT</b>	Fast Fourier Transform.
<b>ICT</b>	Information and Communications Technology.
<b>MuFCO</b>	Multi-Frequency Coupled Oscillators.
<b>PV</b>	Photovoltaic.
<b>SG</b>	Swarm Grid.



# Chapter 1

## Introduction

This Thesis develops a self-organized algorithm to manage the consumption of an electrical grid in a distributed way. The objective of this algorithm is to increase the efficiency of the electrical grids from the consumption point of view. In addition, this Thesis faces a new energy paradigm, where the presence of distributed generation is widespread over the electrical grids, in particular, the **Photovoltaic (PV)** generation. The algorithm is able to schedule an unlimited number of devices in order to improve their behaviors from an energy point of view. This schedule is done with a minimum information exchange by means of coordination of the elements of the grid. This coordination is performed by using two techniques with a high potential in artificial intelligence: *coupled oscillators* and *swarm intelligence*. The combination of both techniques and the presented approach make this Thesis not only interesting in the energy management field, but also in the field of collective systems.

This Chapter introduces the energy management in electric power systems from the demand point of view. Section 1.1 begins with an electricity energy management background including demand side management and *Smart Grids*, which are seen as the future technological frameworks of the electric power system management. The aim of this Thesis is described in Section 1.2. Finally, Section 1.3 presents the structure of this manuscript.

### 1.1 Electricity management background

An electric power system is a network of electrical components used to supply, transmit and use electric power. When this system supplies electricity to consumers of a region, it is usually known as *electrical grid*. Figure 1.1 shows an schematic

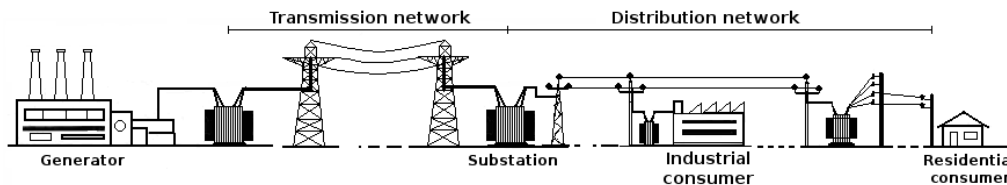


Figure 1.1: Schematic representation of the grid.

representation of a classical electrical grid which is broadly divided into four parts (Kirtley, 2010):

- *Generation*: generators supply the electric power to the grid. There are many types of generators that produce electric power from other sources of primary energy, e.g.: coal-fired power plants, combined cycle plants, photovoltaic solar plants, wind turbines, etc. These generators can also be of different sizes, from a small diesel generator to a nuclear power plant.
- *Transmission network*: the transmission network transfers large amounts of electricity from the power plants (generators) to the substations<sup>1</sup> located close to the consumers. Almost every transmission line is high-voltage, three phases and alternating current (AC). Electricity is transmitted at high voltages to reduce the energy losses in long-distance transmission. The voltage, frequency and phases depend on the regulation of each entity in charge of managing a specific grid.
- *Distribution network*: the distribution network delivers the electricity from the substations to the final consumer. The distribution lines are medium or low voltage and they broadly have one or three phases. For instance, the electricity lines that reach homes give a single phase of 230 V in Europe.
- *Consumption*: the consumption of an electrical grid is its most heterogeneous part. Any device that transforms electric power into work is considered as consumption of the system. When a set of these devices is assigned to a behavioral concept, it is called “consumer”, for example, industrial consumers, residential consumers, etc.

<sup>1</sup> A substation is a part of the electric power system that transforms voltage from high to low, or the reverse. It separates the transmission network from the distribution network.

## 1.1. Electricity management background

---

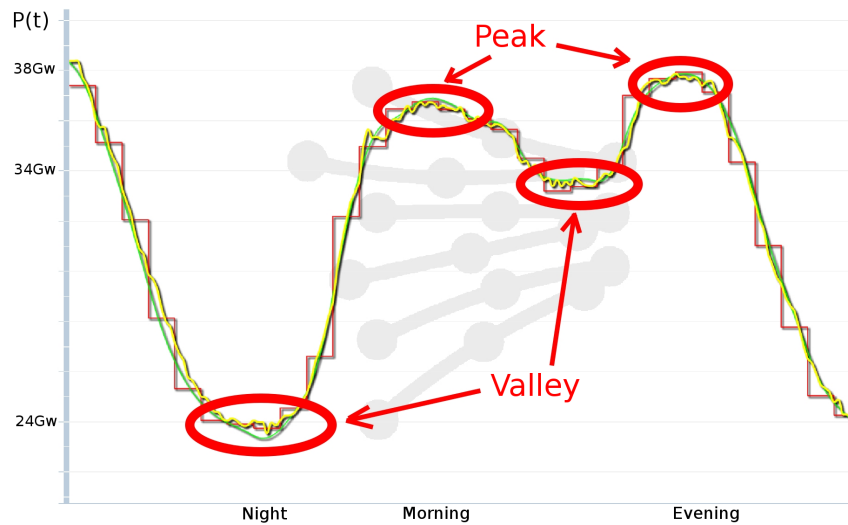


Figure 1.2: Example of the aggregated consumption of the peninsular Spanish electrical grid during a day, where peaks and valleys are marked up. Source: *Red Eléctrica Española* (R.E.E).

The electrical grid has to satisfy a single rule: the amount of active power consumed plus losses should always equal the active power produced. This rule, despite being simple, is where the main difficulties of the grid lie. If the generated power exceeds the consumed power and losses, the voltage and frequency of the system increase and vice versa. Variations in voltage and frequency are regulated by electrical regulations which depend on the country where the electrical grid is deployed. In any case, these variations may cause several damages to the grid from the generation to the consumption side. Therefore, the grid generation and consumption must be always balanced in real-time. This constraint requires a high synchronization between thousand or even millions of devices.

The balance between generation and consumption has been typically done from the generation side. The consumers demand electricity regardless of the grid status and the grid only responds to consumer requirements. These variations in the consumed power cause frequency and voltage variations that are counteracted by the generators. When the consumed power increases, the generators produce more electricity and vice versa. This mechanism is the ground of the electrical grid operation, but second order problems arise when the grid grows. The aggregated

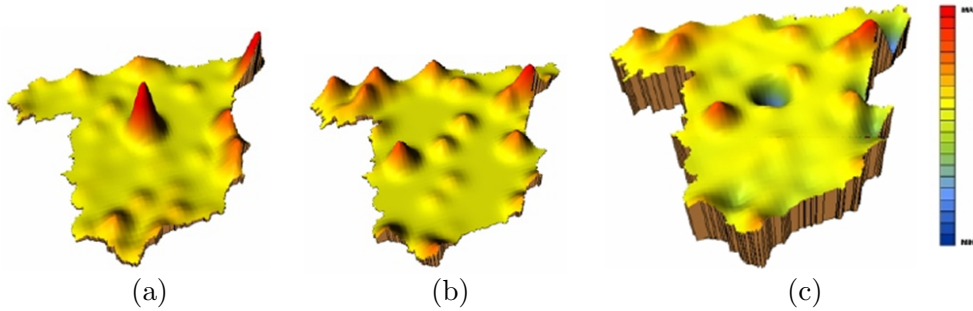


Figure 1.3: Three-dimensional representation of the regional disparities in the Spanish electrical grid during the main consumption peak in 2007, where: a) consumption map, b) generation map and c) balance between generation and consumption map. Source: *Red Eléctrica Española* (R.E.E).

consumption is defined as the sum of all consumers, thus, it represents the whole consumption of the grid. Figure 1.2 shows the aggregated consumption during a weekly day in Spain<sup>2</sup>. The low consumption periods are called *valleys* and the high consumption ones are called *peaks*. This consumption is clearly not constant along the day, triggering great variations on the generation side: in the example of the Figure 1.2, the consumption varies from 24 GW to 38 GW which implies a variation of 14 GW along a day. The installed generation capacity must be able to meet the peaks. In addition, the capacity margin over the maximum historical peak can reach values close to 20% in some countries (R.A. of Engineering, 2013). This fact causes that, during the low consumption periods, a large percentage of the grid generation is not used (the average utilization of the generation capacity is below 55%). The transmission and distribution lines must also have enough capacity to supply the historical maximum peak. Therefore, the underused problem also occurs in the transmission and distribution lines. These lines are constructed with a high degree of redundancy to provide robustness to the grid. In general, the electrical grid is able to continue to function after loss of a single line so the lines are duplicated. Under normal operation, the lines are sized to support twice the historical maximum peak. This oversizing of the grid in the generation, transmission and distribution involves an inefficient structure and high costs.

<sup>2</sup> This example shows the aggregated consumption of the peninsular Spanish electrical grid but such variations are similar in all electrical grids around the world.

## 1.1. Electricity management background

---

In addition to the problems associated with consumption peaks, the electrical grids face significant regional disparities. This problem arises because of the high centralized generation model, which implies that the electricity is generated by large generators at long distances from consumers. In areas where there is high consumption and low generation, there are problems of grid congestion because of the saturation of transmission and distribution lines. This fact creates security and quality of supply risks and increases the oversizing of the electrical infrastructure. Figure 1.3 shows an example of the regional disparities in Spain. The higher consumption areas are located in large cities—see Figure 1.3a. On the other hand, the main generation is relatively far from these cities, usually because this generation corresponds to nuclear power plants or large coal plants—see Figure 1.3b. Figure 1.3c shows the balance between generation and consumption where the regional disparities can be observed. These disparities are similar in all grids around the world.

With the growing electricity demand, the increasing cost of raw materials and the appearance of new generation technologies, to find a solution to the oversizing problem is becoming a priority in energy policies worldwide. Although generation and transmission technologies are improving and becoming more efficient, the root of the problem is the consumption variability. Significant efforts are currently being made in this direction which falls in the field of the *Demand-Side Management*.

### 1.1.1 Demand-Side Management

**Demand-Side Management (DSM)** is defined as actions that influence the way that consumers use electricity in order to achieve savings or higher efficiency in energy use. The following benefits can be achieved through DSM (Strbac, 2008; Papagiannis et al., 2008):

- *Reduce infrastructure oversizing*: as discussed above, the grid infrastructure size depends directly on the consumption peaks. By reducing the consumption during these peaks, the generation, transmission and distribution lines may reduce their oversized capacity. This, in turn, reduces the installation and maintenance costs of the grid.
- *Improve grid investment profitability*: increased consumption in low consumption periods causes a greater use of the electricity infrastructure. This entails a faster return of investment.
- *Security and ancillary services enhancement*: the implementation of DSM techniques usually leads to increased monitoring and control capability of

the electrical grid. The control capacity increment allows carrying out new emergency actions and services in the grid.

- *Integration of new generation technologies:* new generation technologies, mainly based on renewable energies, bring new management challenges. The intermittent nature of some generation technologies (e.g.: solar, wind) reduces the generation system capacity to adapt to consumption variations (Richards et al., 2012). DSM techniques may be used to link the consumption with the renewable energy generation, reducing the effects of its intermittent nature (Caamaño-Martín et al., 2007).
- *Integration of new local infrastructure:* classical electrical grids have a hierarchical structure where energy is produced in power plants that supply electricity to the consumers. This structure is changing with the appearance of **Distributed Energy Resources (DERs)**. DERs consist of a wide range of local generators and storage systems which are geographically dispersed, generally close to consumption centers, and locally managed. They bring a new conception of the electric power systems with the local user becoming not only a consumer but also a generator. DSM may be combined with DERs leading to a new grid structure called *Smart Grids*, as explained in Section 1.1.2.

DSM techniques are focused on the modification of the aggregated consumption shape. In general, these techniques seek smoothing this shape with the final goal of its flattening. This goal can be divided into the following ones:

- *Consumption reduction:* it implies the reduction of consumption without modifying the shape of the aggregated consumption—see Figure 1.4a. This effect can be produced through the efficiency improvement of the consumption appliances or increasing the society energy awareness. The consumption reduction leads to a reduction of the grid size but does not enhance its efficiency.
- *Increase valley consumption:* it implies the increase of consumption in the valleys of the aggregated consumption—see Figure 1.4b. This can be accomplished with the connection of pumping stations, storage systems or electric vehicles during the low consumption periods, among other measures. The increase of consumption along valleys improves the profitability of the grid because of a greater use of its infrastructure.
- *Decrease peak consumption:* the major cause of the oversizing problem in electrical grids are the consumption peaks. It can be reduced through the

## 1.1. Electricity management background

---

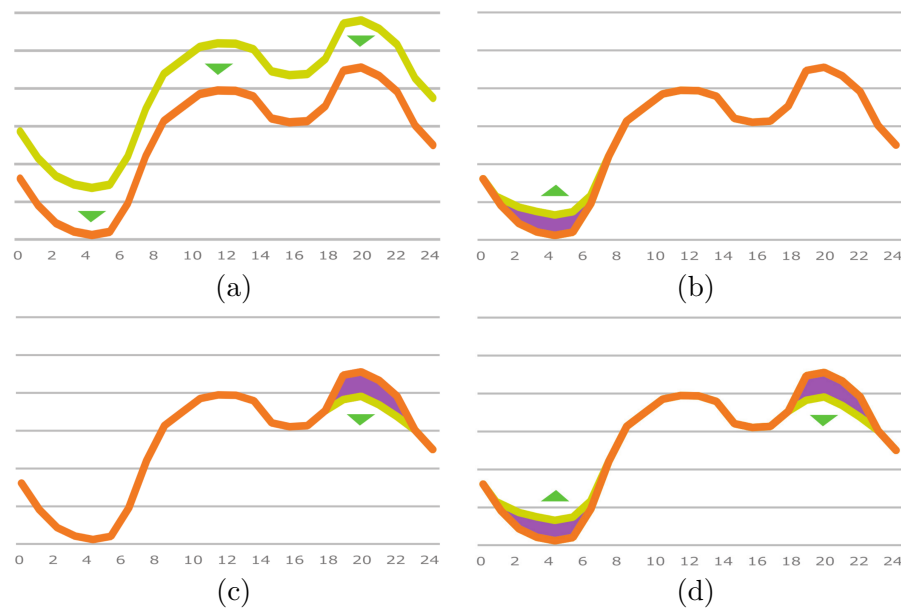


Figure 1.4: Effects of the **DSM** techniques in the aggregated consumption: a) consumption reduction, b) increase valley consumption, c) decrease peak consumption and d) load shifting. Source: *Red Eléctrica Española* (R.E.E).

**DSM**—see Figure 1.4c. The supply interruption of some consumers by the grid operators and the load automation are the main techniques to implement this effect in the aggregated consumption.

- *Load shifting*: this effect consists of displacing part of the electric loads from the peak to the valley periods—see Figure 1.4d. It may be done through a variable pricing depending on the aggregated consumption shape or the electric load automation. The load shifting combines the benefits of the increase of the valley consumption and the decrease of the peak consumption.

The **DSM** mechanisms may be varied in nature, for instance, changing the regulatory framework, encouraging consumer awareness, pursuing a reduction in the electrical appliances consumption, making possible the active participation of consumers in electricity markets, etc. **DSM** can be classified in the following classes depending on the degree of interaction between the consumer and the electric power system:

- *Saving and efficiency programs*: these are initiatives that seek to increase energy efficiency of consumption. These initiatives provoke an indirect reduction on the long-term demand in terms of power consumption, regardless of the time of consumption. Some examples are: incentive campaigns for the use of energy-saving lamps, variable speed drives in electric machines (Mecrow and Jack, 2008), energy policies (Abdelaziz et al., 2011), etc.
- *Indirect control of electric loads through pricing*: these DSM programs are based on time variation of prices, in general, depending on the costs involved for the electrical grid to meet the demand. These programs seek to discourage consumption in peak hours (Newsham and Bowker, 2010). The main instances of DSM through pricing are:
  - *Time of Use tariff* (TOU): the day is divided in time blocks with different prices. Each block reflects the historical average costs of producing and transporting the electric energy during the period covered by the block.
  - *Critical Peak Pricing* (CPP): prices in critical moments are assigned to hours in which production costs (and thus market prices) are very high, due to the difficulties of matching supply and demand (Herter, 2007). CPP aims to reduce consumption at such times.
  - *Real Time Pricing* (RTP): the retail price reflects the price established in the market, usually on an hourly basis. This type of pricing is also used with reactive power<sup>3</sup> pricing in order to control the reactive power exported to the grid (Baughman and Siddiqi, 1991). The fact that the pricing information is in real-time allows to adapt the demand to the grid status improving the use of the energy sources (Sioshansi and Short, 2009).
  - *Peak Time Rebates* (PTR): there are electricity bill rebates for not using power during the peak hours. Such programs produce a great discount on the electricity bill to committed consumers.

---

<sup>3</sup> In general, the power equation satisfies that  $P(t) = I(t) \cdot V(t)$ , where  $I(t)$  is the current and  $V(t)$  is the voltage. In AC systems, the relationship between current and voltage can be shifted because of the impedance of loads, leading to a new power equation  $P(t) = I(t) \cdot V(t + \phi)$ . This shift reduces the ability of the system to deliver power to perform useful work. Therefore, the power can be divided in *active power* and *reactive power*. The active power can perform useful work and the reactive power remains in the electric system and cannot be used to perform work until it is transformed in active power.

## 1.1. Electricity management background

---

- *Direct control of electrical loads:* in these initiatives, the system operator can directly disconnect some electrical appliances of the consumers. Although a few experiences have been reported with residential consumers, the direct control of loads is usually applied in the industry, controlling large consumers such as foundries (Torriti et al., 2010).
- *Smart metering and appliances control:* these techniques comprise market programs or structures that allow consumers to participate offering electrical load reductions by adapting the demand to the grid status. Large sophisticated customers can already tie the electricity pricing into their energy management system. Greater price differentials between high-cost and low-cost periods could result in greater shifts of energy usage. These techniques require to be accompanied by the application of intelligent appliances that facilitate the implementation of DSM (Strbac, 2008).

Although there are several practical experiences of DSM and part of its technology requirements have already been developed, its implementation is slow. The barriers faced by DSM are different in nature. In the following, a classification of these barriers is presented:

- *DSM knowledge and potential:* in classical electricity systems, consumers and generators are in two completely opposite sides. Generators supply the electricity demand in real-time and consumers usually have a complete ignorance of the system operation. This lack of knowledge leads to a lack of incentives and policies about DSM.

Additionally, there is a lack of knowledge about the costs and benefits of DSM because of a lack of methodologies to evaluate it. In Torriti et al. (2010) the authors analyze the DSM experiences in Europe and conclude that, while it is clear what DSM initiatives can achieve in terms of demand shifting from peak periods, limited knowledge has been developed about its overall energy saving capacities.

Another impediment regarding the potential of DSM is the potential impact of savings on overall financial expenditures of the consumers. Although the electricity price is increasing in most countries over time, it is still low in relation to other expenses. For instance, consumers in the U.S. spend around 2.7% of their household income on home energy bills<sup>4</sup> and the consumers in the

---

<sup>4</sup>Source: U.S. Energy Information Administration.

E.U. around 5.8%<sup>5</sup>. This implies that **DSM** programs should cause a very high reduction in the energy bill to be attractive to the consumers. However, this situation is changing because of the rising cost of electricity.

- *Lack of infrastructure*: electrical grids have always been understood as an exclusively “energy broadcast” system without information exchange. The only information that a consumer receives is a bill with the total amount of energy consumed at the end of the month. In order to perform **DSM**, the consumers may require having available energy cost information in real-time or other information related to the grid status. This information availability implies the deployment of advanced metering, control methods and **Information and Communications Technologies (ICTs)** together with the electrical grid. The slow penetration of these technologies in the electricity system and the lack of international and widespread communication standards have slowed the diffusion of **DSM**. In fact, this has been one of the central barriers to **DSM**, particularly in the residential sector, where costs tend to be high relative to savings, as compared to commercial customers (Kim and Shcherbakova, 2011).
- *Investment recovery*: the main barrier to spread **DSM** techniques are generally financial. On the consumer side, the users should make technology investments in order to exploit all benefits of **DSM**: power consumption displays, communication with the grid or even appliance automation. The recovery of this investment is slow because of the relative low electricity prices. Moreover, the troubles caused by the installation are sometimes greater than the benefits because of the difficult access to this kind of systems.

On the electricity companies side, the lack of knowledge about the costs and benefits as well as the lack of consumer interest has the consequence that the companies do not risk investing in **DSM**. This barrier is increased in liberalized energy markets because if a firm is not certain that it will recover its initial costs, it will not invest in a program that could bring future benefits to the entire industry (Kim and Shcherbakova, 2011). Therefore, **DSM** programs must take into account the whole energy industry increasing their complexity of their development.

- *Program structure and policy*: the development of a **DSM** program involves many participants, from big energy producers to small consumers. This implies

---

<sup>5</sup>Source: International Energy Agency.

## 1.1. Electricity management background

---

that the development of programs and policies that encompass the entire grid is a difficult task. The electric power sector is characterized by a very conservative stance toward innovations. This causes a slowdown in the DSM implementation. This situation is changing and the commitment of governments is growing. New energy policies are emerging motivated by improving the efficiency of the grid and fighting climate change (Edenhofer et al., 2011).

### 1.1.2 Smart Grids

Smart Grids emerge as a convergence of ICTs with power system engineering (Farhangi, 2010). It began in the late 90's as an attempt to use electronic control, metering, and monitoring in the increasingly complex electricity power systems. In Vu et al. (1997) the authors proposed that the Smart Grids should be an automated system of monitoring, control, and protection devices that improves the reliability of the transmission grid by preventing wide-spread break-ups. Indeed, they did an early definition of this technology as "Self-Managing And Reliable Transmission Grid (SMART Grid)". Smart Grid has included since then other concepts besides system reliability, for example, advanced monitoring structure, improved demand-side management, transport efficiency, self-repairing, etc. Currently, Smart Grids are a compendium of techniques to respond to the challenges of the electricity power systems. There is not a universal definition of its features, but a summary of the main ones is presented below:

- *Reliability*: in an electric power system, reliability is a key factor. The strong dependence of our societies on electricity implies that a supply problem has serious economic and social effects. The increasing complexity of grids increases the challenge of maintaining the systems reliability at the same time that the number of consumers grows. Smart Grids are envisioned to facilitate (Moslehi and Kumar, 2010): better situational awareness and operator assistance, increase resiliency against component failures and natural disasters, higher electricity quality, etc.
- *Efficiency*: the Smart Grid concept encompasses DSM and therefore all its benefits mentioned above. DSM can be integrated into a broader concept that takes into account all the elements of the Smart Grid, which in the future will consist of an interactive electric network, for generators and consumers (Rahimi and Ipakchi, 2010).

- *Flexible topology*: the appearance of **DERs** is modifying the grid topologies. They are transforming to a distributed collection of generators, consumers and storage systems spread over a region. Therefore, Smart Grids are not only focused in the local framework, but also in transmission and distribution networks (Li et al., 2010; Järventausta et al., 2010). This new structure allows improving the use of local energy resources like the renewable energies (wind, solar, etc.).
- *Additional services*: the introduction of **ICTs** in the grid leads to an improvement of the electrical power system monitoring. For instance, Smart Grids allow real-time electricity pricing. In addition, services related to the monitoring and emergency services can be implemented to prevent damages caused by grid failures.

Smart Grids should be bidirectional, in which information and energy must flow from generators to consumers and vice versa. On the other hand, it is necessary to incorporate a communication structure that allows users to adopt strategies of demand management based on information supplied by the operators of the grid (Mohsenian-Rad and Leon-Garcia, 2010). In this scenario, *smart meters* come into play. A smart meter is an advanced electricity meter that provides additional information to both consumers and electrical grid operators (Depuru et al., 2011). This information can be from different nature, from local electricity system status as voltage, frequency, active and reactive power, etc., to general grid status as instantaneous aggregated consumption, pricing, emergency signals, etc. Some smart meter proposals include also remote control capabilities so that the system operators can switch the consumer load depending on the system status (McKinstry et al., 2010; Marvin et al., 1999). Although there is not a universal definition of the characteristics and benefits of smart metering, one possible list of features is given here:

- *Consumption information*: one of the most simple and, at the same time, most powerful feature of the smart meters is digital power measurement. It has advantages on the consumer and grid operator sides. From the consumer point of view, the digitizing of these data allows to know its local consumption in real-time. Previous studies conclude that by offering consumption information to the users, the amount of energy demand at home can be reduced (Brandon and Lewis, 1999; Wood and Newborough, 2003; Leygue et al., 2014). From the grid operator point of view, the knowledge of local consumption allows to foresee more accurately the aggregated consumption. In addition, the operators

## 1.1. Electricity management background

---

can tariff the consumer bills telematically, being one of the most interesting economic benefits for them.

- *Pricing information:* consumers may adapt their consumption to pricing variations if they have that information. This is one of the greatest economic advantages that can cause the use of smart meters from the consumer point of view.
- *Emergency signals:* grid operators can send emergency signals to the consumers. They may be used to warn of a possible grid failure, enabling the consumers to disconnect their electrical appliances without risk of damage.
- *Remote load switching:* smart meters may receive control signals from the grid operators. These signals may be used to control remotely appliances, such as high power furnaces or lighting networks.
- *Grid information network:* smart meters may be use to create a parallel information network to the electrical grid. Thanks to this network, grid operators and consumers can exchange information between them. It opens up new ways of managing the grid and the implementation of advanced control algorithms. It could potentially incorporate Artificial Intelligence techniques to energy management.

It is expected that the penetration of smart meters would grow during the next years in Europe and U.S.A. (Depuru et al., 2011; Beyea, 2010; Vojdani, 2008). For example, it is expected that in 2018 one hundred percent of the electricity meters in Spain become smart meters. Most of these meters will be equipped with PRIME<sup>6</sup>, which is a narrowband Power Line Communication (PLC) technology (Sendin et al., 2012). However, the communication network is not the only challenge of the smart grids. The information transmitted through this network should be managed, where typical problems of large communications networks such as congestion, robustness, computational power, etc appear. These problems may be reduced by using a distributed management topology, where this Thesis is framed. Thus, the grid can be divided in multiple subgrids which self-organize to achieve a common energy goal. Such division into subgrids can even reach the level of consumers, being each consumer a self-organized energy entity.

From the DSM point of view, this distributed topology means that electricity consumption is managed locally without a central organizer. The previously

---

<sup>6</sup> PowerR line Intelligent Metering Evolution.

mentioned self-organized energy entities may refer to single facilities equipped with **DER** and a set of local electric loads. If every facility has the same energy goal, namely, to smooth the aggregated consumption of the electrical grid, the distributed nature of a management topology implies that the facilities must coordinate to achieve the energy goal. This coordination may be implemented by means of Artificial Intelligence techniques as discussed throughout this Thesis.

### 1.2 The aim of this Thesis

The aim of this Thesis is the development of a self-organized algorithm to manage the consumption of an electrical grid with the presence of high levels of PV penetration. The objective of this algorithm is to increase the efficiency of the electrical grids by the aggregated consumption smoothing. In this way, the oversizing of the electrical grids is reduced and the use of the existing resources is improved. In addition, this Thesis faces a new energy paradigm, where the presence of distributed generation in electrical grids is common, in particular, the photovoltaic generation. This kind of energy source affects to the operation of the grid by increasing its variability. This implies that high penetration rate of photovoltaic electricity is pernicious for the electrical grid stability. This Thesis seeks to smooth the aggregated consumption considering this energy source. Therefore, not only the efficiency of the electrical grid is improved, but also the penetration of photovoltaic electricity into the grid can be increased. This proposal brings great benefits in the economic, social and environmental fields.

In this Thesis, two distributed **DSM** algorithms have been proposed for both a local and a grid framework. The distributed approach means that the **DSM** is performed from the consumers side, without following direct commands issued by a central entity. Therefore, the grid is studied as a collective, where the basic management unit is a single facility. This means that every facility, that composes the grid, does its own energy management and seeks for the aggregated consumption smoothing. This Thesis strongly emphasizes the distributed **DSM** approach. The proposed **DSM** algorithms must satisfy the following features:

- *Robustness*: the **DSM** algorithms must be able to operate independently of the number of failures. This means that the system must continue working even if only one facility is working.

### 1.3. Thesis structure

---

- *Data privacy:* the **DSM** algorithms must avoid the information exchange between facilities, so that a facility does not have specific information about what another facility is doing. In addition, the algorithms cannot send information from the facilities to a central agent. The facilities could receive information from a central agent but this communication must be completely anonymous.
- *Scalability:* the **DSM** algorithms must be able to operate with any number of facilities. This implies that it allows the incorporation of new facilities without interfering with its operation.
- *Low cost:* the **DSM** algorithms must adapt to the current grids without any extra topological requirements. In addition, a low computing load is desired.
- *Quick deployment:* the **DSM** algorithms should be easy to install, allowing a quick deployment.

Depending on the **DSM** framework, the aim of the Thesis is reached by following a different energy goal. In the local framework, the energy goal is to maximize the self-consumption of the local generated energy of each facility. Thanks to this energy goal, the energy exchange with the electrical grid is reduced. Thus, the proposed **DSM** algorithm seeks the aggregated consumption smoothing through an “egoistic” point of view. In the grid framework, the energy goal is to smooth the aggregated consumption. This approach implies that a coordination mechanism between facilities is required. Thus, the proposed **DSM** algorithm seeks the aggregated consumption smoothing through a “cooperative” point of view.

### 1.3 Thesis structure

This Thesis is divided in two parts: local framework and grid framework. This division refers to the two situations to which the desired **DSM** algorithm has to face, as explained in Section 1.2. The local framework is composed by chapters 2 and 3. Chapter 2 reviews the different technologies used in the local context. In addition, it describes the facility used during the real experiments of this Thesis and the evaluation criteria. In Chapter 3, the local **DSM** algorithm is explained in detail. This chapter concludes with a set of simulations and real experiments that show the advantages of **DSM** for the local energy management.

The grid framework is composed by chapters 4, 5 and 6. Chapter 4 presents the distributed approach of the DSM algorithm and how it takes into account the aggregated consumption. It also describes the theoretical backgrounds of the developed mechanism: *coupled oscillators* and *swarm intelligence*. In Chapter 5, the **Multi-Frequency Coupled Oscillators (MuFCO)** is presented and described in detail; the mathematical ground of the combination of *coupled oscillators* and *swarm intelligence* is explained together with its usage on the grid framework. Chapter 6 describes the proposed DSM algorithm for the smart grid, called **Swarm Grid (SG)**. This chapter shows some experimental operation examples in which SG algorithm manages different local facilities.

The conclusions of this Thesis are in Chapter 7. The future works, Section 7.3, lists some proposals, different uses and improvements of the proposed algorithms. Finally, Section 7.4 summarizes the main contributions of the author over the course of his doctorate.

Part I

**Local framework**



## Chapter 2

# Local framework background

In this part of the Thesis, **Demand-Side Management (DSM)** is tackled from a local point view. This means that the modification of the local consumption only responds to local conditions without considering the proper operation of the electric grid. Although this statement may differ from the general definition of **DSM**, it makes sense in local facilities equipped with **Distributed Energy Resource (DER)**. These resources include small power sources and local storage that can be aggregated together with the electrical grid to provide power locally—see Figure 2.1. The use of **DERs** restructures the electric distribution networks, improving the exploitation of local resources but making new challenges appear from the management point of view (Driesen and Katiraei, 2008). **DSM** must be able to meet these challenges by taking into account the local energy situation. This Chapter gives an overview of the **DERs** used in this Thesis and their assessment. Section 2.1 contains the background of the **DERs** and the types of local consumption. The assessment methods of the energy balances of a local facility are explained in Section 2.2. Finally, Section 2.3 describes the experimental facility used in this Thesis. This facility is a real example of **DERs** connected to the grid.

### 2.1 Local electric power system: facility

A local electric power system is considered as an electric power system which belongs to a particular consumer so that the management of this system depends exclusively on its owner instead of the electric utility. Its size can be diverse, for example, from a small apartment to a large factory or even a subgrid that can contain a neighborhood of a city. For sake of simplicity, the local electric power systems are called *facilities*

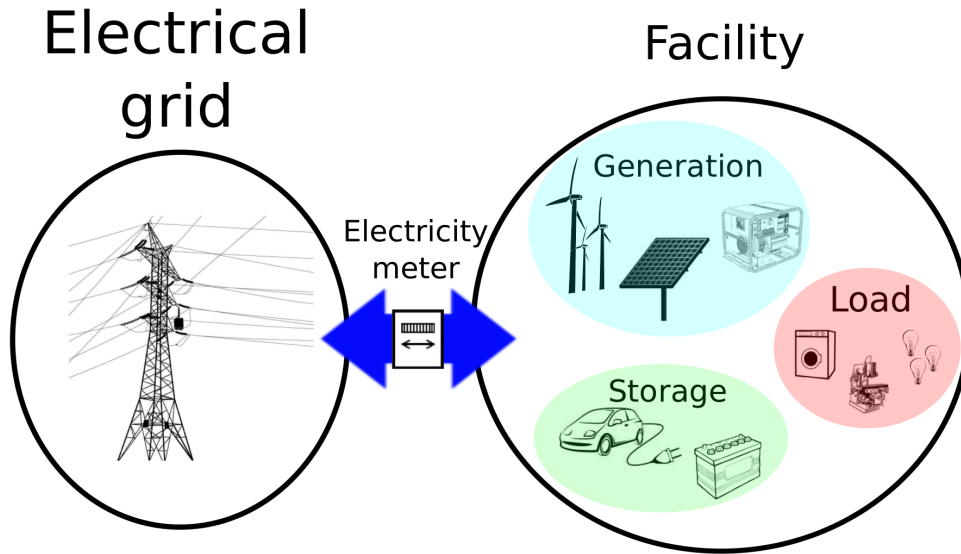


Figure 2.1: Schematic representation of a facility connected to the electrical grid.

along this Thesis. A facility usually begins, and the utility's portion of the grid ends, at the output socket of the electricity meter. This point coincides with the end of the distribution network. Figure 2.1 shows a schematic representation of a facility connected to the electrical grid.

Facilities have historically been considered as mere consumers. Electricity is generated in power plants and it is consumed by a set of different power loads. This situation is changing with the increasing deployment of **DERs** which can be found throughout the world geography. A facility may be composed by three types of elements: generation, storage and consumption. In the following sections, these elements are introduced.

### 2.1.1 Distributed generation: photovoltaic technology

Historically, electricity power systems have been designed following a vertical integration scheme. Large power generators supply energy to multiple consumers through a hierarchical transport and distribution network. On the other hand, **Distributed Generation (DG)** is a different generation structure where small generators are spread over the grid, usually on the consumer side. **DG** has been growing over the last two decades, arousing a major interest among electric power system planners

## 2.1. Local electric power system: facility

---

and operators, energy policy makers and regulators as well as developers and consumers (Lopes et al., 2007). Some examples of the benefits of DG are:

- *From an economic point of view:* DG allows local resources to be used, reducing the purchase of external resources. For example, the deployment of photovoltaic solar panels in urban areas allows to use the solar resource that comes to cities (Loulas et al., 2012). Another example are the DG units that burn landfill gasses in the proximity of landfills (Pepermans et al., 2005). In an electricity market, the local energy resources can be used depending on the electricity pricing. A proper management of these resources can offer significant economic benefits. Moreover, the installation of DG allows to increase the local consumption without increasing the transmission and distribution lines (Caamaño-Martín et al., 2008; Barker and Mello, 2000). This is of particular interest in areas of difficult access such as mountain regions.
- *From an operational point of view:* DG reduces transport and distribution power losses (Barker and Mello, 2000). The power flow in transmission and distribution networks is reduced because the electricity is generated close to the consumers. In addition, the reliability of the grid may be increased, as there are many generation spots and not only one centralized large generation (El-Khattam and Salama, 2004). The DG may also increase the electricity quality<sup>1</sup> extending the lifetime of the grid equipment (Eto et al., 2001; Dondi et al., 2002).
- *From an environmental point of view:* DG technologies contain multiple renewable and low emissions power supplies, consequently, they are much less harmful for the environment than non-renewable generation technologies (Edenhofer et al., 2011). These power supplies acquire great benefits when they are used in a distributed manner. For example, cogeneration allows generating simultaneously electricity and useful heat in the same engine. This technology is extending in the residential and commercial sectors because of its high efficiency (Onovwiona and Ugursal, 2006).

Although the widespread growth of DG is relatively recent, its existence dates back to the origins of electric power systems. Traditional combustion generators were used for isolated electric power systems, emergency systems or to ensure the electricity quality. This technology has evolved to the current micro-turbines (El-Khattam and

---

<sup>1</sup> Power quality refers to the degree to which power characteristics align with the ideal sinusoidal voltage and current waveform, with current and voltage in balance.

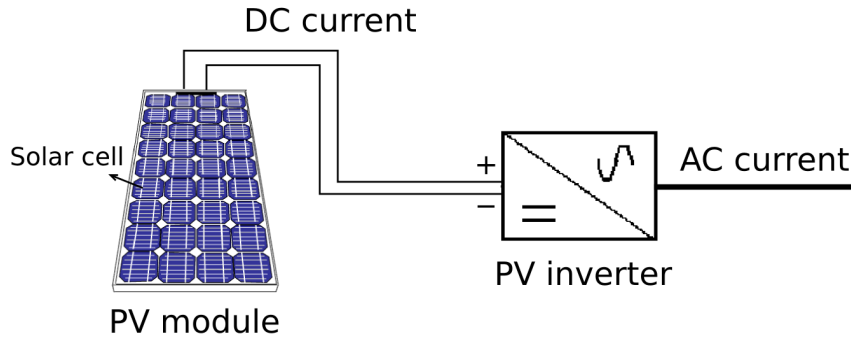


Figure 2.2: Schematic representation of PV power generation.

Salama, 2004). These systems are mainly used nowadays as auxiliary power sources. DG did not start to be used as a main generator in local facilities until the emergence of new generation technologies and its subsequent technological maturity. In this new generation framework, renewable energies have been the most innovative.

There are multiple types of renewable energies. They differ in the exploited resource and how it is exploited. For example, solar energy can be directly transformed in electricity through the Photovoltaic (PV) solar cells or it can be harnessed in a concentrated way by means of optical devices to heat molten salts to move a turbine to generate electricity. The difference may be more subtle, for example, wind power differs whether it is deployed in the sea or not. The DG technology used along this Thesis is PV technology because of its ability to integrate into local facilities and urban areas.

### 2.1.1.1 Photovoltaic technology

Figure 2.2 shows a schematic representation of PV power generation. PV technology converts the solar radiation directly into electric power (Luque and Hegedus, 2011). Its basic unit is an electrical device called *solar cell* whose operation is based on the photoelectric effect. A solar cell converts solar energy into a usable amount of direct current (DC) electricity. These cells are clustered into PV modules. A set of PV modules compound a PV generator. Since PV generator produces electricity in DC, a PV inverter to transform the DC into alternating current (AC) is required. There are multiple PV inverter technologies with different features that address the DC/AC conversion (Kjaer et al., 2005; Solórzano, 2014). These technologies are commonly

## 2.1. Local electric power system: facility

---

transparent from the **DSM** point of view because the **DSM** usually operates from the AC side. Therefore, the **PV** generator is considered in this Thesis as a “black-box” that produces electric power.

**PV** technology may achieve a better performance if it is used where the energy is consumed, for example in urban areas, where the ability of architectural integration of the **PV** modules can be exploited (Groppi, 2002). From a technical point of view, the experience with **DG** technologies shows that, as their penetration levels increase, it is necessary to have control mechanisms to contribute to the grid stability, specially in the case of failures or blackouts. This issue is being addressed by the **PV** inverter technologies which currently provide technical benefits to the local electric system and the grid such as (Caamaño-Martín et al., 2008):

- *Regulation of power factor, reactive power and voltage levels:* **PV** inverters equipped with small energy storage and an appropriate control system are able to produce or absorb reactive power. Thus, they compensate the excess or lack of reactive power in the grid, contributing to stabilize the voltage level.
- *Grid stabilization and intentional islanding:* **PV** inverters with a storage system and an adequate control system are able to actively manage their operation in order to contribute to: stabilize the voltage and frequency of the grid, maintaining a controlled island operation (isolating the grid installation) and/or support the operation of specific applications.
- *Electricity quality improvement:* **PV** inverters may operate as active filters, reducing the harmonic voltage distortion of the grid.
- *Phase symmetry control:* three phase inverters can improve the electricity quality by injecting currents to asymmetric phases and equalizing the phases of the grid.

### 2.1.2 Storage

Electrical energy storage systems have a great potential for energy management both in storage and in supply. In general, they can store energy in a wide power range as long as the maximum capacity is not reached. On the other hand, the storage systems can supply energy in a wide power range as long as there is enough energy. Despite this, the use of storage in grid-connected applications is not very common. The hydroelectric pumping stations are almost the sole storage systems that can be found in an electrical grid. They are used to store energy during

## 2. Local framework background

---

the overproduction hours (Hadjipaschalis et al., 2009). There are other situations where storage applications are beneficial, for instance, the use of storage systems for load-leveling applications for economical or technical objectives (Kiessling, 1987). *Load leveling* means that a storage system is charged with excess power during low-demand periods and it is discharged when the power demand is on peak levels. This operation may lead to financial benefits or allow higher power consumption than the power provided by the grid. Another instance is the use of storage system for frequency regulation and/or spinning reserve. *Frequency regulation* operates over a time frame of only a few minutes. The response of the power-supply system to demand fluctuations is found primarily in the frequency. Storage systems can be used to absorb the fluctuations by undergoing short-term cycles and the power generating facilities follow the trend. On the other hand, *spinning reserve* is typically used when a power station fails and others cannot take over the load immediately, a few minutes can elapse before the control can follow the consumption. The spinning reserve is a power station that runs idle and consumes but does not deliver energy until a failure in the grid occurs. Storage systems can fulfil this role without wasting energy. One remarkable example for regulation and/or spinning reserve with storage systems is the lead/acid battery storage system installed in Berlin in 1986 with 14 MWh of nominal capacity and 17 MW of nominal power (Wagner, 1997). Designed to strengthen the “island” electric grid of Berlin, it was used from the beginning of 1987 for frequency regulation and spinning reserve. In 1993, when Berlin was connected to the electricity grid of Germany, frequency regulation was no longer required but the battery was still employed for spinning reserve. Storage systems have also been widespread used in isolated systems with renewable energy sources; typically lead/acid batteries with PV solar energy where the batteries are charged during the day and the stored energy is used during the night (Bopp et al., 1998).

The main reasons of storage absence in the grid are typically its expensive cost and the generation control possibilities of the classical power stations. It makes unprofitable the deployment of new storage systems on a large scale. However, the currently technological and energy situation encourages the investment in storage systems, mainly because of the increase of the renewable energies presence in the generation side (Foidart et al., 2010; Lopes-Ferreira et al., 2013) and the hourly mismatch between the demand and the renewable energy generation (Lior, 2008; Wagner, 1997). In Koepfel and Korpas (2008), the authors analyzed the use of storage systems to fix the amount of exported energy from a renewable generator to the grid, storing energy if the generation exceeds the forecast and vice versa.

## 2.1. Local electric power system: facility

---

In [Denholm and Margolis \(2007\)](#), the authors conclude that the use of load shifting and electrical energy storage is needed to achieve **PV** high penetration levels.

Storage systems acquire a greater interest when they are used from a local point of view. In [Nair and Garimella \(2010\)](#), the authors assess the benefits of renewable energy integration with different energy storage technologies. They conclude that battery energy storage systems are likely to have a significant impact in the small-scale integration of renewable energy sources into commercial buildings and residential dwellings, providing technical and monetary benefits. Several storage technologies are in use today in multiple local applications, while others are still under research and development ([Hadjipaschalis et al., 2009](#)). This expansion and development of local storage technologies entail a lowering of costs that, together with the increasing electricity prices, make to expect an increasing number of local storage systems. In addition, the **Electric Vehicle (EV)** expansion makes possible the presence of storage systems in every building. The management of this growing storage capacity is a challenge for the local and global energy management systems, including **DSM** ([Peterson et al., 2010](#)).

### 2.1.3 Consumption

Consumption is the most heterogeneous part of an electrical power system. There are huge variety of devices that consume electricity with different characteristics: nominal power (from a LED lamp to industrial ovens), intermittent consumption (i.e. a fridge pump that activates periodically), peak power (i.e. the use of a drill), etc. For the implementation of **DSM** techniques, it is particularly interesting to classify the consumption by means of its controllability. In this Thesis, the consumption is divided in the following three types:

- *Fixed*: this consumption is uncontrollable. In general, it represents appliances whose use responds to instantaneous requirements of their users. For example, the light of a room, which must be used immediately if there is someone in the room that requires it. Other examples in buildings are elevators, computers or televisions. In previous works on **DSM**, it is also called non-deferrable consumption ([Castillo-Cagigal et al., 2011b](#)). During this Thesis, the fixed consumption is represented as a function of power demand in time  $p^{fixed}(t)$ . This consumption can be only modified by saving and efficiency programs or changing the user habits.

## 2. Local framework background

---

- *Deferrable*: this consumption represents loads that can be displaced in time. For example, the use of some home appliances as dishwashers, washing machines or dryers has certain time flexibility. The user of these appliances does not require that they run at a concrete time and their operation time could be the result of some energy or economic criteria. Out of the residential sector, part of industrial processes or even labor timetables could be modified under some energy criteria. This time displacement is usually associated to some constraints, for example: an industrial oven may run at different times of the day but in any case must run before the end of the day, its operation cannot be delayed to the next day. This consumption is represented as “energy packages”. It means that a deferrable consumption consumes an amount of energy  $E^{def}$  during a certain period of time  $\tau$ . This energy is consumed following a power demand function  $p^{def}(t)$ . The time instant at which the deferrable consumption is activated is called *activation time*  $t^{act}$ . For example, a washing machine can be activated at  $t^{act} = 17 : 00 h$ , it works during  $\tau = 1$  hour and it consumes power following the function  $p^{def}(t)$ .
- *Elastic*: this consumption represents loads whose instantaneous power can be controlled directly. For example, electric pumps whose pumping power can be controlled to regulate the water flow. Another example of elastic consumption are heating, ventilating, and air conditioning (HVAC<sup>2</sup>) equipments whose heating or cooling power can be regulated. This equipments are one of the main consumption in electrical grids and their control is the aim of several current researches (Pagliarini and Rainieri, 2012). In general, the elastic consumption is represented as a function in time  $p^{elastic}(t, x(t))$ , where  $x(t)$  is a control function.

The previous classification is not exclusionary; some devices may belong to different groups. For instance, the air conditioning may be regulated following some energy criteria but operation itself has a minimum consumption that cannot be controlled. In these cases, the device can be divided in two virtual devices, one whose consumption is fixed and other whose consumption is elastic. The controllability of a device does not only depend on its operation nature, but on its automation capabilities or the user energy awareness too. For example, a washing machine is in principle deferrable but if it is not programmable it will be only executed when the

---

<sup>2</sup> HVAC (Heating, Ventilation, and Air Conditioning) is the technology of indoor and vehicular environmental comfort. Its goal is to provide thermal comfort and acceptable indoor air quality.

## 2.2. Assessment of local electrical behavior

---

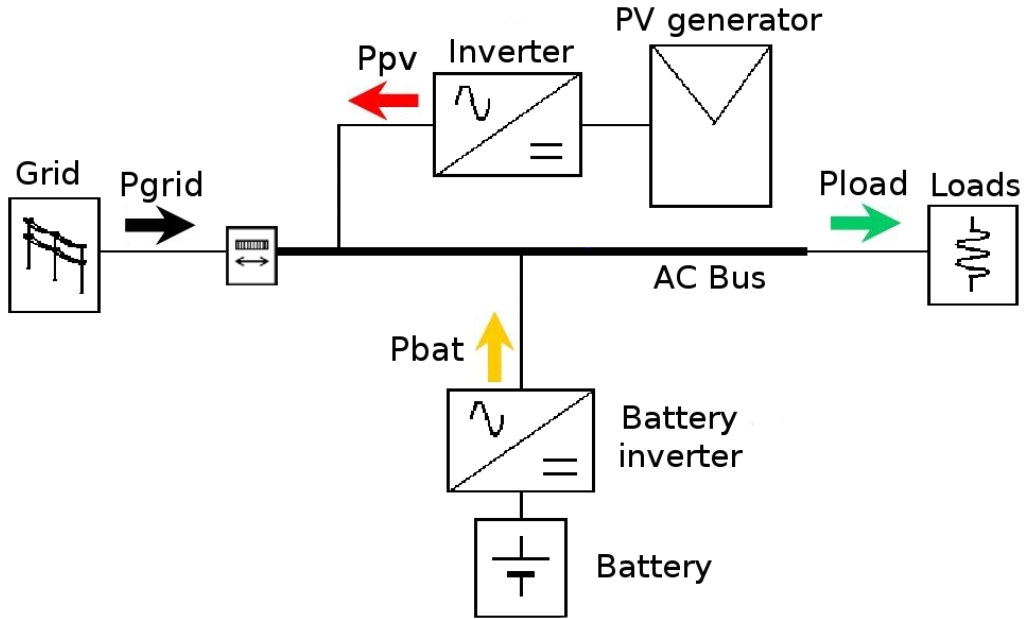


Figure 2.3: Schematic representation of the local facility, where the arrows represent the direction of positive magnitudes of the power flows considered.

user sets it up. Additionally, if the user does not have any energy awareness, even a programmable washing machine is not a deferrable consumption in practice.

## 2.2 Assessment of local electrical behavior

The Facilities considered in this Thesis are implemented based on an AC bus topology. In this topology, all elements of the system exchange energy in AC. Even the storage system stores and supplies electricity in AC through a battery inverter. Figure 2.3 shows a schematic representation of the local electrical power system with the main power flows that are considered throughout this work. There are a large number of possible energy exchanges because the presence of local generation, storage and grid connection. The sign nomenclature and criteria of the main power flows are defined as follows:

- $p_L(t)$ : power consumed by the loads. It is always positive.
- $p_{PV}(t)$ : power generated by the PV generator. It is always positive.

## 2. Local framework background

---

- $p_B(t)$ : power exchanged with the local storage system. It is positive when the storage system supplies power to the local facility and negative when the storage system stores energy.
- $p_G(t)$ : power exchanged with the grid. It is positive when the grid supplies power to the local facility and negative when the local facility exports power to the grid.

Given the spatial proximity between the generation, storage and consumption, the losses in the AC bus are considered negligible, thus, the power balance of the local facility at the AC bus is defined as follows:

$$p_{PV} + p_B + p_G = p_L \quad (2.1)$$

Time has been removed from power variables in sake of simplicity. The assessment of the local electrical behavior is based on the study of some energy variables. These variables are calculated through the integral of the power flows previously defined. The most relevant energy variables used in this Thesis are the following:

- $E_L$ : energy consumed by the loads.
- $E_{PV}$ : energy generated by the PV generator.
- $E_{G,I}$ : energy input from the grid. It is imported from the grid and may supply the local consumption or the storage system.
- $E_{G,O}$ : energy output to the grid. It is exported to the grid and may originate from both the PV generator and the storage system.
- $E_{B,I}$ : energy input from the storage system. It is discharged from the battery and may supply the local consumption or may be exported to the grid.
- $E_{B,O}$ : energy output to the storage system. It is charged in the battery and may originate from both the local generator and the grid.

The assessment factor used in the local framework is the *self-consumption factor*, denoted by the Greek letter  $\xi$  (Castillo-Cagigal et al., 2011b,a). It represents the fraction of the electrical energy consumed by the loads which is only supplied by the local generation sources. The following equation defines mathematically the self-consumption factor:

$$\xi = \frac{E_{PV,L} + E_{B,L}^{PV}}{E_L} \quad (2.2)$$

### 2.3. Experimental facility: “MagicBox”

---



Figure 2.4: “MagicBox” pictures: a) Bird eye view and b) south frontage of the solar house.

where  $E_{PV,L}$  is the energy directly supplied by the **PV** generator to the loads and  $E_{B,L}^{PV}$  is the energy from **PV** origin supplied by the storage system to the loads. The last term  $E_{B,L}^{PV}$  represents the indirect use of the locally generated energy. Notice that the storage system can contain energy from both the local generator and the grid. It implies that the origin of this energy must be considered in the calculus of the self-consumption.

Also, as expected by its own definition, the range of  $\xi$  is  $[0, 1]$ , because this factor is normalized by the total consumption of the local facility. This normalization also allows to compare the operation of different facilities regardless of their sizes.  $\xi = 0$  would be the case of a facility with no local generation available, whereas,  $\xi = 1$  means that all energy is locally supplied, for instance, a facility isolated from the electrical grid.

### 2.3 Experimental facility: “MagicBox”

During the development of the local framework part of this Thesis, a real facility has been used. It is called “MagicBox” and it is an example of **DER** in the residential sector. Simulations and real experiments are based on the devices installed in this facility. “MagicBox” is an energy self-sufficient solar house located at the Escuela Técnica Superior de Ingenieros de Telecomunicación (ETSIT) of the Universidad Politécnica de Madrid (UPM)—see Figure 2.4. It combines bioclimatic design

## 2. Local framework background

---

principles, PV solar energy integration, local energy storage technology and the use of Information and Communication Technologies (ICTs) to monitor and control the house power balance. “MagicBox” was originally designed to participate in the “Solar Decathlon<sup>3</sup> 2005”, being the first house from an European university to take part in this event (Caamaño-Martín et al., 2005; Calvo-Fernández et al., 2005). After finishing the competition, “MagicBox” was installed at the ETSIT under the Heliodomo<sup>4</sup> project framework. It hosted the R&D project GeDELOS-FV<sup>5</sup> that early studied the integration of PV hybrid and load control technologies in order to explore the possibilities of self-consumption using PV technology, local storage and controllable consumption in the residential sector (Caamaño-Martín et al., 2009a; Castillo-Cagigal et al., 2010; Matallanas et al., 2011). MagicBox also hosted the project VE2<sup>6</sup> whose main objective is the development of a software platform to manage the interaction of electric vehicles parked and connected to the electric grid of a building and the electric consumption of the whole building.

“MagicBox” is currently used as a research laboratory to assess the effect of the combination of PV generation, load management and local storage on the electric grids. From the electrical point of view, its structure is based on an AC bus topology. It works on 230 V and 50 Hz because of Spanish grid connection. From an ICT point of view, an embedded system receives information from the elements of the house (generation, storage and loads) and operates as a user interface. This embedded system can also actuate over some elements of the house to control its power balances. An schematic of the electricity and communication network of the house is shown in Figure 2.5. In the following subsections, the elements that compose this facility are explained in detail.

---

<sup>3</sup> Solar Decathlon is an award-winning program that challenges collegiate teams to design, build, and operate solar-powered houses that are cost-effective, energy-efficient, and attractive ([www.solardecathlon.gov](http://www.solardecathlon.gov)).

<sup>4</sup> *Heliodomo: nuevos conceptos de vivienda autosuficiente*, supported by the Plan Nacional de Investigación Científica, Desarrollo e Innovación Tecnológica, 2004-2007, (BIA-2004-05234).

<sup>5</sup> GeDELOS-FV: *Gestión de la demanda eléctrica doméstica con tecnología solar fotovoltaica*, supported by the Plan Nacional de Investigación Científica, Desarrollo e Innovación Tecnológica, 2007-2010, (ENE-2007-66135/ALT).

<sup>6</sup> *VE2: Sistema Inteligente de Gestión Energética del Edificio utilizando Vehículos Eléctricos*, supported by Ministerio de Economía y Competitividad, programa INNPACTO (CIN/952/2011) IPT-2012-1072-120000.

### 2.3. Experimental facility: “MagicBox”

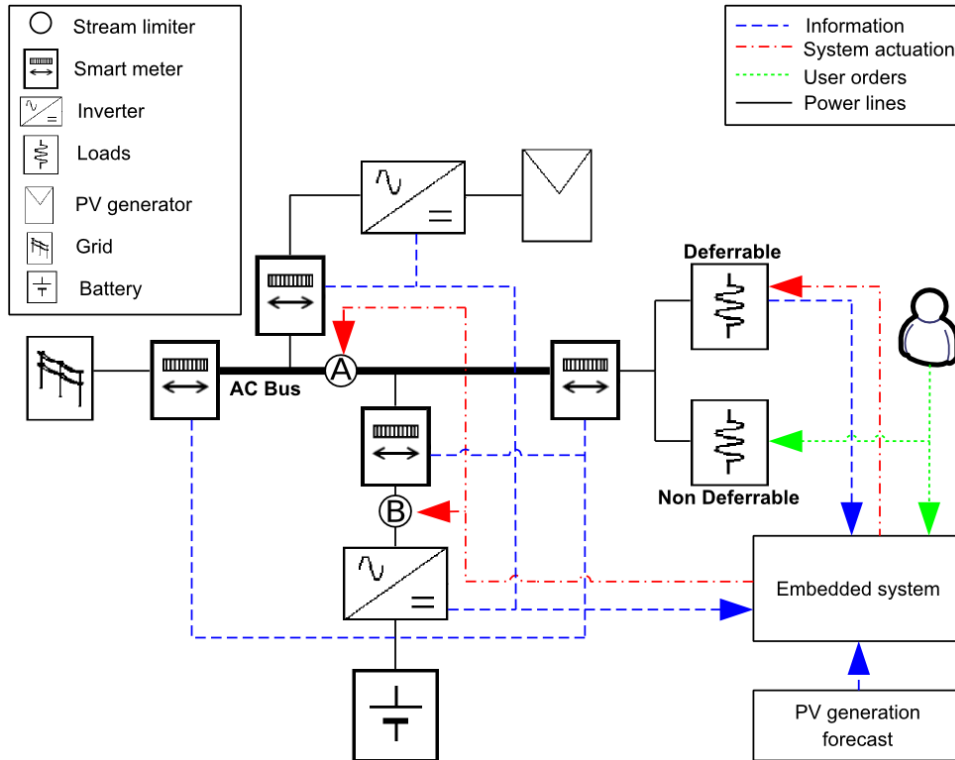


Figure 2.5: Electrical and communication scheme of “MagicBox”.

#### 2.3.1 PV generation system

The **PV** generation system of “MagicBox” consists of five independent monocrystalline silicon **PV** fields with 5.55 kW<sub>p</sub> of total generation. This system is set in order to exploit the different tilts of the sun along the year within the operational strategies of the house. To achieve this goal, the fields are distributed in different south-oriented surfaces: 1.45 kW<sub>p</sub> at 12°, 2.7 kW<sub>p</sub> at 25°, 0.8 kW<sub>p</sub> at 39° and 0.6 kW<sub>p</sub> at 90°. Each **PV** field has an associated string-type inverter—see Figure 2.6. Although there are five inverters, they are considered as a single one for simplicity. Therefore, the **PV** AC power is supplied to the AC bus, as the scheme shown in Figure 2.5. More technical parameters of the installation are not address because they are out of the scope of this Thesis. For further information see [Caamaño-Martín et al. \(2008\)](#).

## 2. Local framework background



Figure 2.6: Picture of the inverter’s room and battery bank of “MagicBox”, where: red boxes are the five **PV** inverters in use plus one of backup and the upper orange box is the battery inverter.

The photovoltaic system is equipped with a forecast **PV** generation module that communicates with the embedded system (Masa-Bote and Caamaño-Martín, 2010; Masa-Bote et al., 2014; Masa, 2014). At the beginning of the day, the system receives hourly forecasts of irradiation and ambient temperature for the next day. These meteorological forecasts are based on a numerical weather prediction model, specifically, HIRLAM<sup>7</sup> model provided by the Spanish Meteorological Agency (AEMET<sup>8</sup>) (Masa-Bote et al., 2014). They are estimated for Madrid (40.5°N, 3.7°W), where “MagicBox” is located. From these meteorological forecasts, the usable electricity from the **PV** generators is estimated taking into account site-dependent (i.e. shadowing) and technological (**PV** modules, inverters, battery, etc.) characteristics of “MagicBox”. Therefore, the **PV** generation profile for the current day is available at the beginning of each day. This information is uploaded to an exchange information area where it is collected by the control system.

<sup>7</sup> HIRLAM stands for High Resolution Limited Area Model and is a numerical short-range weather forecasting model ([www.hirlam.org](http://www.hirlam.org)).

<sup>8</sup> [www.aemet.es](http://www.aemet.es)

### 2.3. Experimental facility: “MagicBox”

---

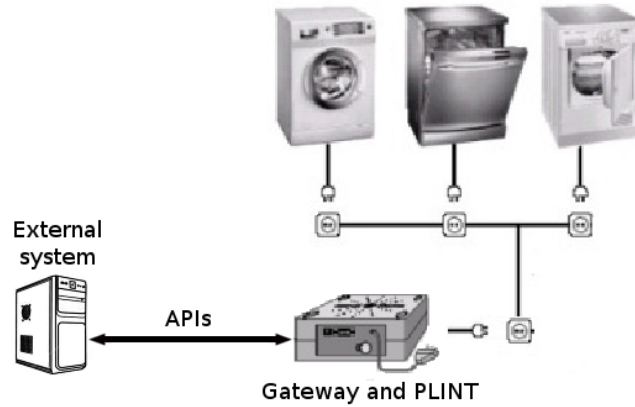


Figure 2.7: Depiction of gateway communication and Power Line Communication network of the home automation system which governs the deferrable loads.

#### 2.3.2 Storage system

The house is equipped with a lead-acid battery stationary bank. The battery bank is divided in 24 cells, each cell has a capacity of 750 Ah ( $C_{10}$ <sup>9</sup>) and a voltage of 2 V. Therefore, the total battery bank voltage is 48 V with a capacity around 36 kWh. The storage system has a bidirectional battery inverter because the battery operates at DC and all energy exchanges are produced through the AC bus—see Figure 2.6.

The battery inverter does not only implement the current conversion, but allows controlling the power flows in the house. This control is implemented through two stream limiters shown in Figure 2.5. Thanks to these limiters, high-level software battery controllers can be developed to fulfill different strategies. The limiter *A* regulates the power flow between the possible generation sources and the consumption and storage. Through this limiter, the local consumption can be isolated from the grid. The limiter *B* regulates the battery charge power.

#### 2.3.3 Loads

The house includes typical electrical appliances of a highly electrified house. The fixed appliances are monitored but not controlled: cooking appliances, fridge, freezer, lighting, computers and entertainment appliances. There are also three deferrable appliances: washing machine, dishwasher and dryer. The deferrable loads are

<sup>9</sup> Capacity for 10 hours discharge cycles.

## 2. Local framework background

---

integrated in a home automation system which allows the appliances to be monitored and controlled by a remote system. The communication of the home automation system is based on a Power Line Communication (PLC) network. Figure 2.7 shows a schematic of the home automation system communication network.

The deferrable loads incorporate PLC modems that communicate with a Power Line Interface (PLINT) using the electrical network of the house. An external system can communicate with the deferrable loads through a gateway that directly accesses the PLINT. The gateway works as a webserver that accepts requests to monitor or control the home automation system. The communication is implemented through a webserver Application Programming Interface (API) required for the access to the PLINT. The different APIs allow an external system to get data from the appliances (e.g. actual status, program duration, time to end) and to send a series of basic commands (e.g. start the appliance, choose a program, pause or stop the program). It also has different callbacks that inform about the events that occur during the operation of appliances (e.g. no water input, water tank full). The information exchange to implement the APIs between an external system and the webserver is based on WSDL<sup>10</sup> and SOAP<sup>11</sup>. The communication is implemented through Ethernet Local Area Network with TCP/IP.

### 2.3.4 Monitoring and embedded system

The house is equipped with four smart meters connected to the embedded system through an RS-485 bus—see [Castillo-Cagigal et al. \(2011c\)](#) for a detailed description of the communication protocol. Each smart meter is an energy monitoring device located at different points within the AC bus of the house. The system monitors the: *i*) PV generation, *ii*) grid exchange, *iii*) house loads and *iv*) storage system. The meters provide power and energy measurements with a sampling period of one minute. In a common situation, only one meter would be required because the PV and battery inverters are able to measure their own power and, by placing the meter

---

<sup>10</sup> The Web Services Description Language (WSDL) is an XML-based interface description language that is used for describing the functionality offered by a web service. The acronym is also used for any specific WSDL description of a web service (also referred to as a WSDL file), which provides a machine-readable description of how the service can be called, what parameters it expects, and what data structures it returns.

<sup>11</sup> SOAP, originally defined as Simple Object Access Protocol, is a protocol specification for exchanging structured information in the implementation of web services in computer networks. It relies on XML Information Set for its message format, and usually relies on other application layer protocols for message negotiation and transmission.

### 2.3. Experimental facility: “MagicBox”

---

on the load or grid line, the remainder power flow can be calculated with the power balance equation— see Equation 2.1. However, the measurements provide by the PV and battery inverters contain too many errors for a detailed study of the power balance in the house. On the other hand, a very robust monitoring system is required in “MagicBox” because it is used on multiple experimental campaigns. For these reasons, four smart meters were installed in every main power line of “MagicBox”.

The embedded system receives information of all elements previously explained. This system allows the monitoring and analysis of the overall system performance. The embedded system is equipped with a Debian operating system. Thanks to the operating system, multiple high-level controllers can be easily developed. These controllers can manage the stream limiters and deferrable loads of “MagicBox” performing a local DSM. This issue is the main purpose of the next chapter.

## 2. Local framework background

---

## Chapter 3

# Local Demand-Side Management

The combination of **Demand-Side Management (DSM)** with an automatic control of demand and local generation leads to a new concept called **Active Demand-Side Management (ADSM)** (Castillo-Cagigal et al., 2011a; Matallanas et al., 2012; Masa-Bote et al., 2014). Moreover, in this Thesis, **ADSM** is implemented together with storage technologies adding more possibilities to the energy management problem. Consumers could be the first to benefit from **ADSM** strategies, provided that there are technologies that facilitate (automate) the operation of devices without compromising the users' comfort needs and preferences. The residential sector may be a potential customer for **ADSM** systems, because it can be combined with additional comfort and security functions, improving the demand response, reducing the environmental impacts (Papagiannis et al., 2008) and offering the user information about its electrical consumption. Although **ADSM** does not directly reduce the amount of demanded energy, the work presented by Wood and Newborough (2003) concludes that by applying consumption information feedback to the users, the rates of energy consumption may be reduced. Currently, **ADSM** is increasing its viability by means of highly efficient electrical appliances that can be remotely controlled. However, to perform a true **ADSM**, several challenges must be faced up (Castillo-Cagigal et al., 2011a):

- *From a control engineering perspective:* load management should be able to deal with many parameters and variables influencing the consumption pattern (related to the user preferences and electrical appliances). In addition, it should also consider information coming from the local resources (**Photovoltaic (PV)** and storage) and the grid (price signals, remote commands, etc.).

- *From a PV engineering perspective:* supervision and management are necessary to know in real-time the status of the PV system components, as well as to forecast the expected generation in a short time scale (for example, on a 24-hour basis).

In this Chapter, a control architecture for a local facility is proposed and analyzed. This architecture implements two controllers: the *ADSM algorithm* and the *battery controller*—see Section 3.1. The *ADSM* algorithm implements a local *DSM* mechanism taking into account the local generation. The battery controller manages the charge and discharge of the local storage system. Both controllers are focused on the self-consumption maximization of the locally generated electricity. These controllers have been analyzed by means of simulations and real experiments in *MagicBox*—see Section 3.2 and 3.2.2. Although the *ADSM* algorithm and the battery controller improve the self-consumption, they have undesirable effects in the grid. Section 3.3 shows the effects of the *Distributed Generation (DG)* and the presented controllers. Finally, Section 3.4 concludes the Chapter with a discussion about the advantages and disadvantages of the use of local energy management.

## 3.1 Local controllers

The local controllers monitor the energy availability of the local facility and the consumption requirements of the user in order to maximize the self-consumption of the PV generator. Figure 3.1a shows an example of a day in which the consumption is mismatched with the PV generation. In this case, there is practically not self-consumption. This consumption should be displaced to the maximum generation hours to increase the self-consumption. Figure 3.1b shows an example of the previous consumption matched with the PV generation. The *ADSM* controller is responsible for making this adjustment. Regardless of the time when consumption occurs, the PV generation excess can be stored and used when there is not local generation. This procedure increases the self-consumption of the PV generation. Figure 3.1c shows an example of the use of an storage system to store PV energy to supply the local consumption. The battery controller is responsible for controlling the charge and discharge of the storage system to increase the use of the PV resource.

### 3.1. Local controllers

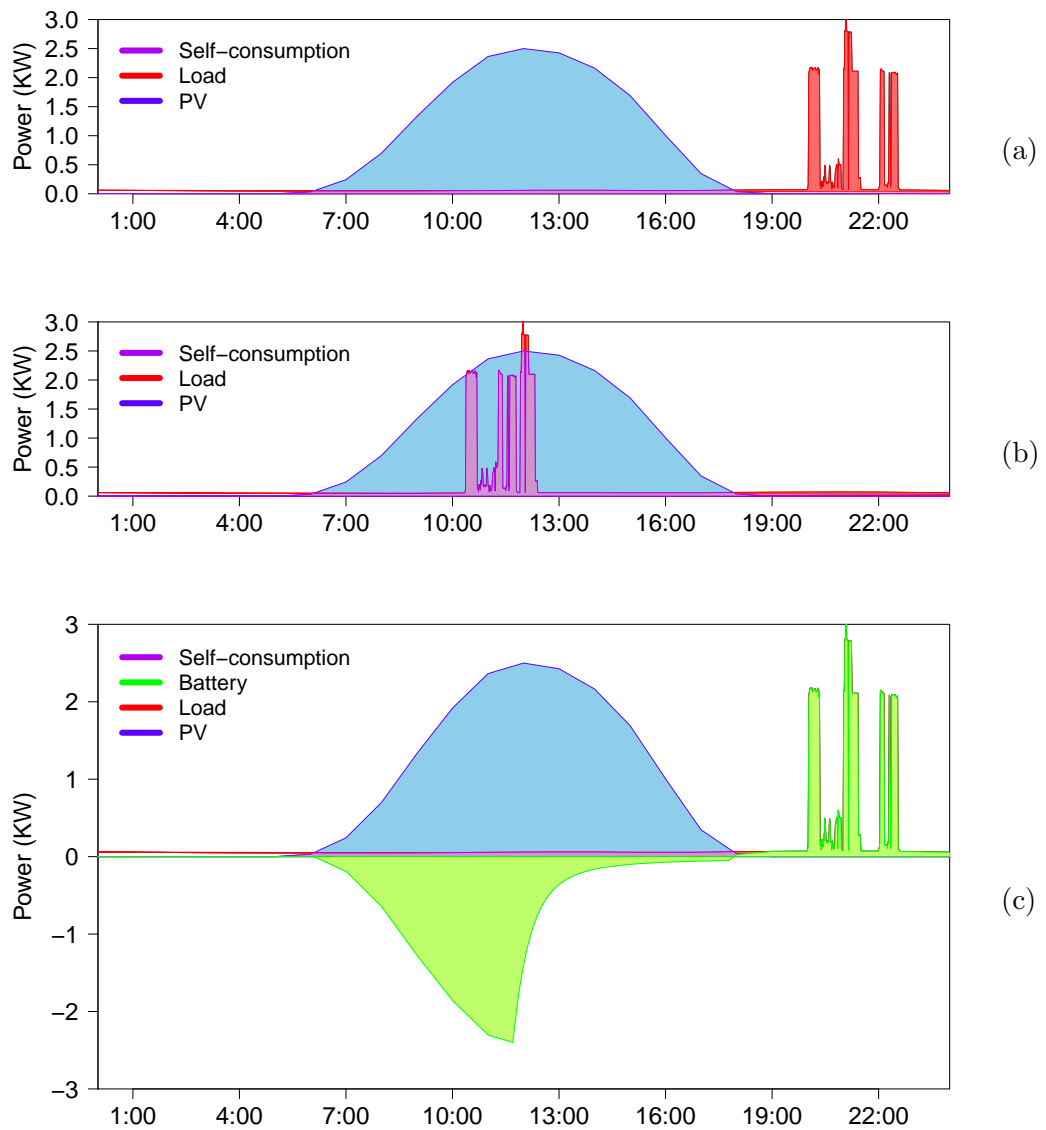


Figure 3.1: Conceptual example of the operation of the local controllers: a) consumption mismatched with the PV generation, b) consumption matched with the PV generation and c) battery storing PV energy to supply the consumption.

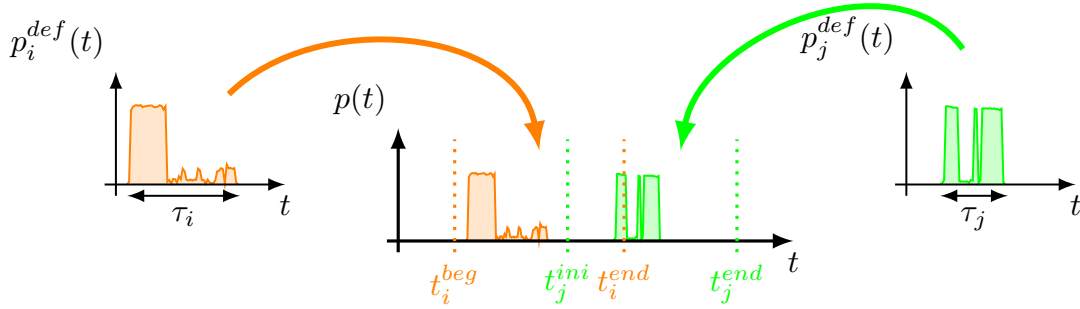


Figure 3.2: Conceptual example of load scheduling where a hypothetical user requires to run two deferrable loads  $i$  and  $j$  with different running ranges.

#### 3.1.1 ADSM algorithm

The **ADSM** algorithm is responsible for matching deferrable loads of a local facility with its **PV** generation. The instantaneous power of these loads cannot be controlled but the time instant when they are executed—see Section 2.1.3. Thus, the action of the **ADSM** algorithm is the scheduling and running of the deferrable loads of a local facility. The user indicates which particular loads should be scheduled and the time intervals in which it should be executed. Figure 3.2 shows a example of this scheduling problem where a hypothetical user requires running two deferrable loads. The user indicates the **ADSM** algorithm which load must be run and a time constraint. This time constraint is the time interval in which the deferrable load must be performed. It is called the *running range* and is defined by an initial time  $t_i^{beg}$  and a final time  $t_i^{end}$ . In Figure 3.2, each deferrable load has its own running range. The **ADSM** algorithm includes a data base containing information of every deferrable load in the system. This information of the deferrable load  $i$  is the power consumption function  $p_i^{def}(t)$  and the runtime  $\tau_i$ . In the example of the Figure 3.2, there are two different deferrable loads with different power consumption functions and runtimes. The **ADSM** algorithm schedules these loads in the running range  $[t_i^{beg}, t_i^{end}]$ . This scheduling is the allocation of an activation time  $t_i^{act}$  for each deferrable load demanded by the user.

The scheduling performed by **ADSM** algorithm is focused to meet two main objectives: *i*) efficacy in service, in the sense of satisfying the user requirements, and *ii*) optimize self-consumption of local generated electricity. The sole possibility of meeting the aforementioned objectives is through the collaboration of users, under the assumption that they do not only want to satisfy their consumption requirements, but

### 3.1. Local controllers

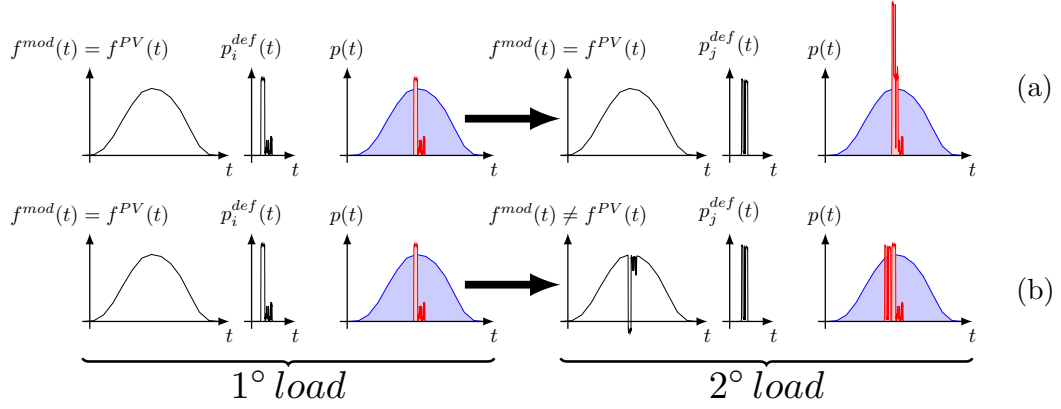


Figure 3.3: Conceptual example of the operation of the **ADSM** algorithm: a) consumption mismatched with the **PV** generation and b) consumption matched with the **PV** generation.

will accept the rationalization of them as a function of the actual energy conditions in the local system. The **ADSM** algorithm should reduce the effort of the user's decision-making, so it should have some autonomy conditioned to the user request and the actual energy status. The autonomy of the algorithm depends directly on the running ranges indicated by the user: the longer the ranges the greater the control possibilities of the **ADSM** algorithm.

The **ADSM** algorithm uses a **PV** generation forecast function  $f^{PV}(t)$  to know the local energy availability and perform scheduling. When the user requires running a deferrable load, the algorithm calculates  $t_i^{act}$  with the objective of maximizing the self-consumption of **PV** generation. To achieve this objective, the self-consumption for each possible value of  $t_i^{act}$  is calculated in the range  $[t_i^{beg}, t_i^{end}]$  using  $p_i^{def}(t)$  and the **PV** forecast information:

$$\xi_i(\hat{t}) = \int_0^{\tau_i} \min[f^{mod}(t + \hat{t}), p_i^{def}(t)] dt \quad (3.1)$$

$$t_i^{act} = \max[\hat{t} = t_i^{beg}, \hat{t} = t_i^{beg} + 1, \dots, \hat{t} = t_i^{end}]$$

where  $f^{mod}(t)$  is a function that defines the energy availability forecast, in this case  $f^{mod}(t) = f^{PV}(t)$ . Notice that the  $t_i^{act}$  calculus depends on the **PV** generation forecast and is consequently affected by forecast errors (Masa-Bote et al., 2014). Figure 3.3a shows an example of the  $t_i^{act}$  calculus where a load has been scheduled coinciding

### 3. Local Demand-Side Management

---

**Algorithm 1** High-level description of the **ADSM** algorithm.

---

```

1:  $N \leftarrow$  Number of new deferrable loads
2: if no_scheduled_load then
3:    $f^{mod}(t) = f^{PV}(t)$ 
4: end if
5: /* Main loop */
6: for  $\forall i \in N$  do
7:    $t_i^{act} \leftarrow$  Calculate activation time with Equation 3.1
8:    $f^{mod}(t) = f^{mod}(t) - p_i^{def}(t + t_i^{act})$ 
9: end for

```

---

with the maximum generation hour—see 1<sup>o</sup> *load*. The **ADSM** algorithm can schedule every load that the user requires. When a load is scheduled,  $t_i^{act}$  cannot be modified, even if the user requires new loads. The first load that is required by the user is the first to be scheduled, as a FIFO queue. Thereby the user knows at what time is going to be executed the load at the same time the load is request, ensuring the user when the consumption is doing to be done.

However, following the procedure described in Equation 3.1, a load overlapping problem arises. This problem occurs because the self-consumption maximization takes place at the maximum generation hours which are the same for every load. Figure 3.3a shows an example of this load overlapping, where the second load is scheduled at the same time as the first one. To prevent load overlapping, the **ADSM** algorithm should take into account the already scheduled load every time a new load is required by the user. This procedure is performed by modifying the **PV** generation forecast with the consumption profile of the scheduled loads:

$$f^{mod}(t) = f^{mod}(t) - p_i^{def}(t + t_i^{act}) \quad (3.2)$$

In this case,  $f^{mod}(t)$  is the **PV** generation forecast modified by the previously scheduled loads. If there is not previously scheduled loads,  $f^{mod}(t)$  is the same as  $f^{PV}(t)$ . Figure 3.3b shows an example of this process, where the second load is scheduled using  $f^{mod}(t)$ . The **ADSM** algorithm is summarized in Algorithm 1. Line 1 is the number of loads to be scheduled in an execution of the algorithm. The algorithm is executed whenever the user requires to schedule new loads. The user can request several loads at the same time. From line 2 to 4, the algorithm takes **PV** forecast or use the previous  $f^{mod}(t)$  if there is previous scheduled loads. In line 6, the main loop which scheduled the loads begins. This loop is repeated for every load

### 3.1. Local controllers

---

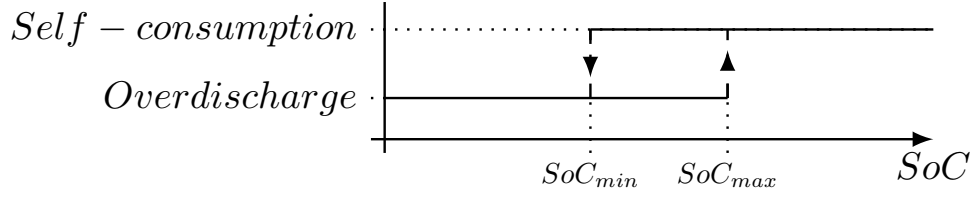


Figure 3.4: Switching between states of the battery controller.

to be scheduled. In line 7, the activation time is calculated using Equation 3.1 with the current  $f^{mod}(t)$ . In line 8,  $f^{mod}(t)$  is updated subtracting the power consumption function of the deferrable load  $i$  from the current  $f^{mod}(t)$ .

#### 3.1.2 Battery controller

The battery controller monitors the power flows and some storage system variables, and actuates over the battery power flow. The objective of this controller is to maximize the self-consumption without compromising the battery lifetime. Its main characteristics are: *i*) management of the battery inverter currents, *ii*) avoidance of electricity exchange with the grid (they only charge the battery with PV generation excess and discharge the battery to supply the loads) and *iii*) preservation of the battery life-time. The operation of the battery controller is divided in two different operation states: *self-consumption* and *overdischarge*. The switching between states depends on the *State of Charge (SoC)* of the storage system as is shown in Figure 3.4, where the x-axis is the *SoC* and the y-axis the battery controller state. Notice that there is a hysteresis area between  $SoC^{min}$  and  $SoC^{max}$ . The switching between states depends on whether the *SoC* is increasing or decreasing because this area. Each state has a different objective:

- *Self-consumption*: in this state, the local facility is virtually isolated from the grid. It means that the excess of PV generation is stored in the battery and the consumption that cannot be supplied by the PV generator is supplied by the battery. This behavior has the same effect as a physical disconnection from the electrical grid by the facility. When the system is operating in this state, all consumed energy is supplied by local sources, maximizing the self-consumption.
- *Overdischarge*: this state preserves the battery against overdischarge. The consumption that cannot be supplied by the PV generator is supplied by the

### 3. Local Demand-Side Management

---

**Algorithm 2** High-level description of the battery controller.

---

```
1: /* State switching */
2: if  $State == Overdischarge$  then
3:   if  $SoC > SoC^{max}$  then
4:      $State = Self - consumption$ 
5:   end if
6: else
7:   if  $SoC < SoC^{min}$  then
8:      $State = Overdischarge$ 
9:   end if
10: end if
11: /* Battery power flow */
12: if  $State == Overdischarge$  then
13:   if  $P_{PV} > P_{Load}$  then
14:      $p_B = p_L - p_{PV}$ 
15:   else
16:      $p_B = 0$ 
17:   end if
18: else
19:    $p_B = p_L - p_{PV}$ 
20: end if
```

---

grid. Thus, the energy stored in the battery is not used and it maintains its SoC. On the other hand, the excess of PV generation is stored in the battery, charging it until it achieves the required SoC to switch to the self-consumption state.

Algorithm 2 summarizes the operation of the battery controller. From lines 1 to 10, the algorithm updates its state switching between *Self – consumption* or *Overdischarge* depending on the value of *SoC* and the previous state value. From lines 11 to 20, the algorithm calculate the power flow of the battery inverter. If the state is *Overdischarge*, the battery is charged from the PV energy excess but it does not supply the local consumption. On the other hand, if the state is *Self – consumption*, the battery is charged with the PV energy excess (negative power) and supply the loads when there is not enough local generation (positive power). The real implementation of this battery controller depends on the local facility. The

### 3.2. Experiments

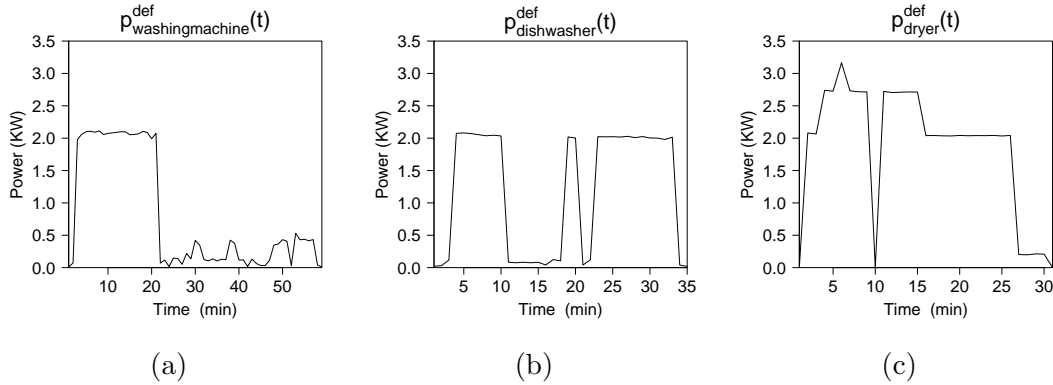


Figure 3.5: Power functions of deferrable loads used in experiments. These power consumption have been obtained through real measurements with a wattmeter with a sample period of 1 min. In addition,  $\tau_i$  has been calculated for each load: a) washing machine  $\tau_i = 60$  min, b) dishwasher  $\tau_i = 35$  min and c) dryer  $\tau_i = 30$  min.

battery inverters differ considerably depending on the manufacturer. In Section 3.2, a concrete implementation of this battery controller is presented.

### 3.2 Experiments

In this Section, the effects of the local controllers on the local energy balances are studied. The local facility chosen to perform this study is “MagicBox”—see Section 2.3. This solar house has been modeled to simulate its energy behavior in different situations. The study presented in this Section consists of a simulation campaign using the “MagicBox” model and a real experiment campaign using the real “MagicBox”.

The electrical consumption used during the experiments are based on measurements carried out in “MagicBox”. As aforementioned, the ADSM algorithm requires a data base with the deferrable load functions and their duration. The deferrable loads used in “MagicBox” are the washing machine, dryer and dishwasher. The consumption of these loads has been measured with a wattmeter with a sample period of 1 min.  $p_i^{\text{def}}(t)$  and  $\tau_i$  have been calculated from these measurements. Figure 3.5 shows the power consumption of the three deferrable loads. In the experiments presented in this section, the user requires to run these loads every day at the beginning of the day. In addition, the running range for all deferrable loads is 24 hours.

### 3. Local Demand-Side Management

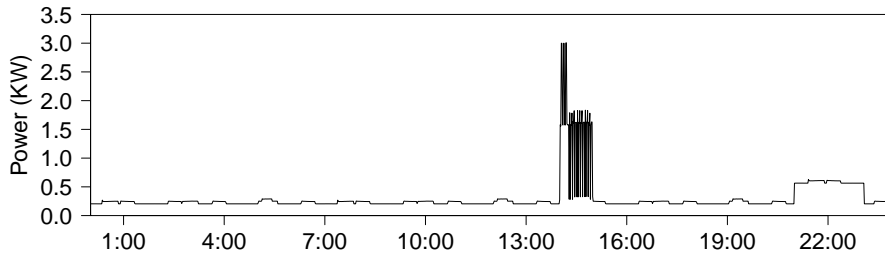


Figure 3.6: Fixed consumption function  $p^{fixed}(t)$  for a day of experiment, where the fridge, the cooking appliances, the lighting and the computers and entertainment appliances are connected. These power consumption have been obtained through real measurements with a wattmeter with a sample period of 1 min.

It means that the algorithm has three loads at the beginning of the day and it should schedule them throughout the day.

The fixed consumption is also based on measurements carried out by a wattmeter with a sample period of 1 min. Figure 3.6 shows the fixed consumption function  $p^{fixed}(t)$  for a day of experiment. There is a base consumption because of the computers and entertainment appliances. The fridge is also connected, its consumption are small peaks appearing throughout the day. The cooking appliances (oven) have been connected at midday. There is a lighting consumption in the evening. Table 3.1 shows the house's typical daily consumption divided into both types of demand. Notice that the deferrable appliances represent 21.6% of the total energy consumption. On the other hand, the main consumption comes from the computers and entertainment appliances typical of dwellings with high technology penetration. This demand pattern depends on different parameters, such as attitudinal factors, family and socio-economic groups, household type, etc. In this Thesis, a daily consumption pattern has been defined, typical of a weekly day, with the main demand at the evening, where there are more time to set up the washing appliances, and at midday because of the cooking needs (INDEL, 1998; Santiago et al., 2014; Jenkins et al., 2014). Seasonal or weekend differences have not been considered.

To analyze the effect of the ADSM algorithm in the local energy balance, there are experiments both with ADSM and without ADSM. Without ADSM implies that the deferrable loads are allocated following a typical demand pattern, in which the deferrable consumption is allocated at the evening hours regardless of the solar

### 3.2. Experiments

Appliance	Consumption (Wh/day)	Share of total (%)
<i>Deferrable</i>		
Washing machine	785.92	6.95
Dryer	962.6	8.5
Dishwasher	693.6	6.13
Total (deferrable)	2442.12	21.6
<i>Non-deferrable</i>		
Lights	1302	11.5
Oven	1255.15	11.1
Fridge	616.73	5.4
Computers and entertainment appliances (TV,DVD,etc.)	5694	50.03
Total (Non-deferrable)	8867.88	78.4
Total	11310	100

Table 3.1: Typical daily consumption in “MagicBox”.

resource. An example of this instance is show in Figure 3.1a. With **ADSM**, the algorithm allocates the deferrable consumption along the day using the running ranges defined by the user and taking into account the solar resource. An example of this instance is show in Figure 3.1b. Fixed consumption is common for both situations. In addition, the **PV** generation forecast used by the **ADSM** algorithm is the HIRLAM model, which is implemented in “MagicBox”—see Section 2.3. This model generates a forecast function every day for the next 24 hours. For this reason, the **ADSM** algorithm can only schedule the deferrable loads on the same day that they are request by the user.

The battery controller has also been implemented in “MagicBox”. This control is done through the two stream limiters shown in Figure 2.5. The equations that control the limiters depend on the operation state of the battery controller:

- *Self-consumption*: in this state, the consumption and battery charge are supplied only by the **PV** generation, thus the equation of the power limit of limiter  $A$  ( $p_A^{lim}$ ) is:

$$p_A^{lim} = p_{PV} \tag{3.3}$$

### 3. Local Demand-Side Management

This equation isolates the facility from the grid and the stream limiter  $B$  is not required. Thus, the power limit of limiter  $B$  ( $p_B^{lim}$ ) is set to the nominal power of the battery inverter  $p_{B,max}$ , accepting any energy exchange:

$$p_B^{lim} = p_{B,max} \quad (3.4)$$

- *Overdischarge*: in this state, the consumed power that exceed the PV generation is supplied by the grid, thus the equation of the limiter  $A$  is:

$$p_A^{lim} = \begin{cases} p_{PV} & p_{PV} \geq p_L \\ p_L & p_{PV} < p_L \end{cases} \quad (3.5)$$

The battery can be only charged with PV energy, thus the equation of the limiter  $B$  is:

$$p_B^{lim} = \begin{cases} p_{PV} - p_L & p_{PV} \geq p_L \\ 0 & p_{PV} < p_L \end{cases} \quad (3.6)$$

The real lead-acid battery storage system has a fixed physical capacity, which is not possible to modify dynamically. Thanks to the battery controller, the useful energy storage capacity and the discharge limit can be modified in real time. This feature has been simulated to perform the experiments and the effect of different battery capacities has been studied. The battery capacity has been normalized to the average daily energy consumption in order to express the capacity in the commonly used unit of days of autonomy. This capacity representation is typically used in stand-alone systems and allows comparing the results with different consumption levels.

$$Cap^* = \frac{Cap (kWh)}{\bar{E}_L^{day} (kWh)} \quad (3.7)$$

where  $Cap^*$  is the normalized capacity which is unitless,  $Cap$  is the nominal battery capacity measured in  $kWh$  and  $\bar{E}_L^{day}$  is the average daily consumption in  $kWh$ .

#### 3.2.1 Simulation campaign

In this Section, the effect of **ADSM** and storage systems on a local facility is analyzed. This analysis has been done throughout a simulation campaign of the power flows of “MagicBox”. This simulations are conducted by *GridSim* simulator—see Appendix A. The simulation campaign consists on a set of simulations for different capacity values

### 3.2. Experiments

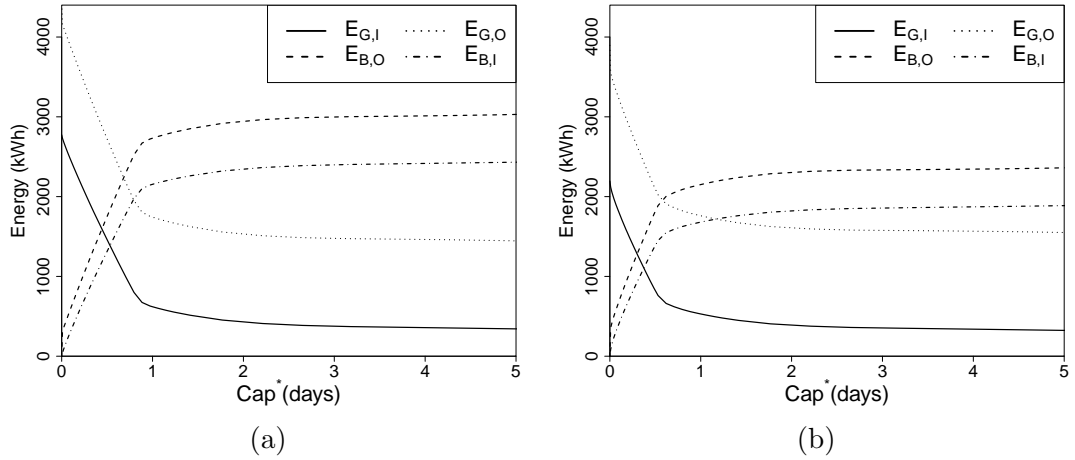


Figure 3.7: Energy variables for the simulated annual experiments: a) energy variables without ADSM and b) energy variables with ADSM.

$Cap^*$  and with and without ADSM. In each simulation, the power flows of “MagicBox” have been calculated during one year with a time step of 1 min. This means that the power flows have been calculated for each minute of the simulated year. The PV power generation use for simulations has been obtained from real measurements in “MagicBox” during the year 2010. The energy variables analyzed are  $E_{G,I}$ ,  $E_{G,O}$ ,  $E_{B,I}$ ,  $E_{B,O}$  and the self-consumption of “MagicBox”, which are defined in Section 2.2.

Figures 3.7a and 3.7b show the development of the energy variables with regard to the normalized capacity with and without ADSM respectively. Each point is the result of a yearly simulation for the capacity value represented in the abscissa axis. In general, as the storage system capacity grows the system independence from the grid increases. Figures 3.7a and 3.7b show that the influence of a storage system in the house energy behavior is not linear with its capacity. For low capacity levels, the energy variables vary severely. Close to one day of autonomy ( $Cap^* \approx 1$ ) this tendency changes and begins to soften. For high capacity levels, the variables saturate and achieve a plateau value marked by the yearly generation and demand. Notice that at  $Cap^* = 0$  there is an abrupt variation for the  $E_{G,O}$  and  $E_{B,O}$  variables because the battery float charge consumption. The float charge is activated when the battery is full-charged ( $SoC \approx 100\%$ ) and it is used to preserve the battery stored energy. This consumed energy is not useful and increases as the battery is more time in the full-charge state, a common situation for low capacity levels. Therefore, this abrupt

### 3. Local Demand-Side Management

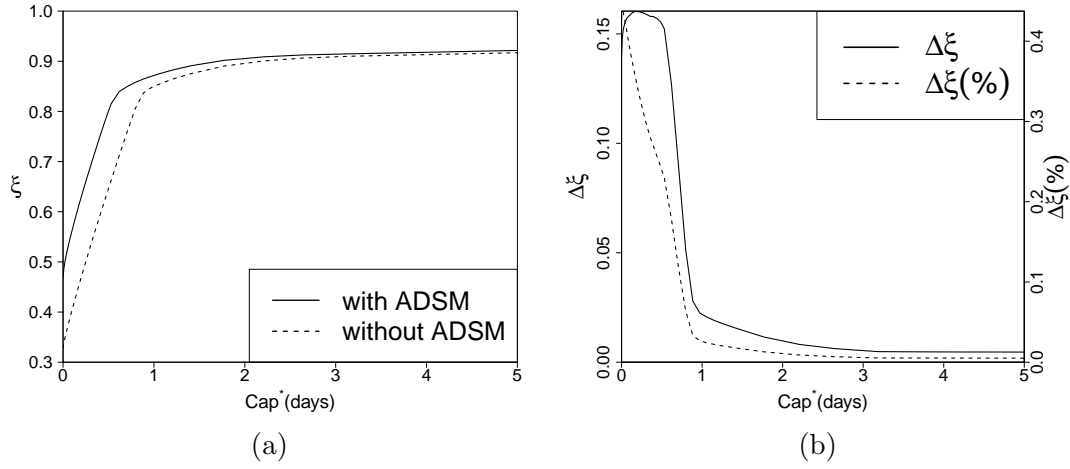


Figure 3.8: Self-Consumption factor relationship with the storage capacity: a) absolute value and b) increase because of the use of **ADSM** system.

variation on  $Cap^* = 0$  represents the energy cost which belongs to the float charge power of the battery storage system.

The self-consumption factor completes the system energy behavior analysis by applying Equation 2.2. Figure 3.8a shows the development of self-consumption  $\xi$  with regard to the normalized capacity, with and without **ADSM**. In accordance with the evaluation equations (see Section 2.2), the development of the self-consumption is inversely proportional to the imported energy from the grid. This fact can be observed by comparing Figure 3.8a with  $E_{G,I}$  in figures 3.7a and 3.7b.

The use of **ADSM** modifies considerably the house energy behavior. Generally, the **ADSM** increases  $E_{PV,L}$  and therefore the self-consumption factor. But this increase is not constant for all battery capacities. In Figure 3.8b, the increase of  $\xi$  produced by the use of **ADSM** in relation with the capacity can be observed. This improvement is represented in absolute value and relative to the results without **ADSM**. Notice that for low capacity levels, below one day of autonomy, the increase of  $\xi$  achieves its maximum. When the system capacity is higher, the effects of **ADSM** are not significant. Therefore, when the storage system has enough capacity to manage more than one day of autonomy, the demand time location is not the main parameter of the house energy behavior. In this case, the main parameter which affects to the energy balance is the **PV** daily generation.

## 3.2. Experiments

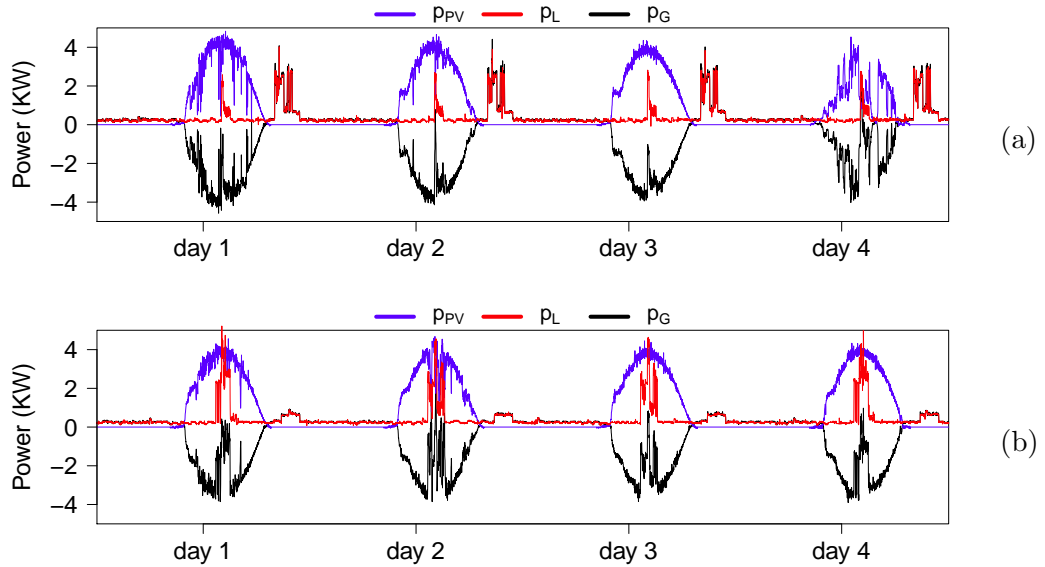


Figure 3.9: Development of the main power flows during the experiments without storage: a) without **ADSM** algorithm and b) with **ADSM** algorithm.

An important point in the  $\xi$  function is at  $Cap^* = 0$ , it means no storage system. In this situation, the self-consumption without **ADSM** represents the 32.7% of the total demand and 46.8% with **ADSM**. In order to achieve 46.8% of self-consumed energy, a 0.2 days of autonomy battery storage system is needed without **ADSM** system. This means that in this point the use of **ADSM** is equivalent to a small size storage system.

### 3.2.2 Measurement campaign

Analyzing the simulated results, the effects of **ADSM** and capacity variations have been observed. With this information, real experiments have been carried out in the solar house “MagicBox”. There are secondary effects which have not been taken into account in the simulations such as communication delays, smart meter consumption, etc., that do not affect the tendency previously observed. The power flows have been measured in the house during a week for each operation conditions, modifying the battery capacity and activating or not the **ADSM**.

### 3. Local Demand-Side Management

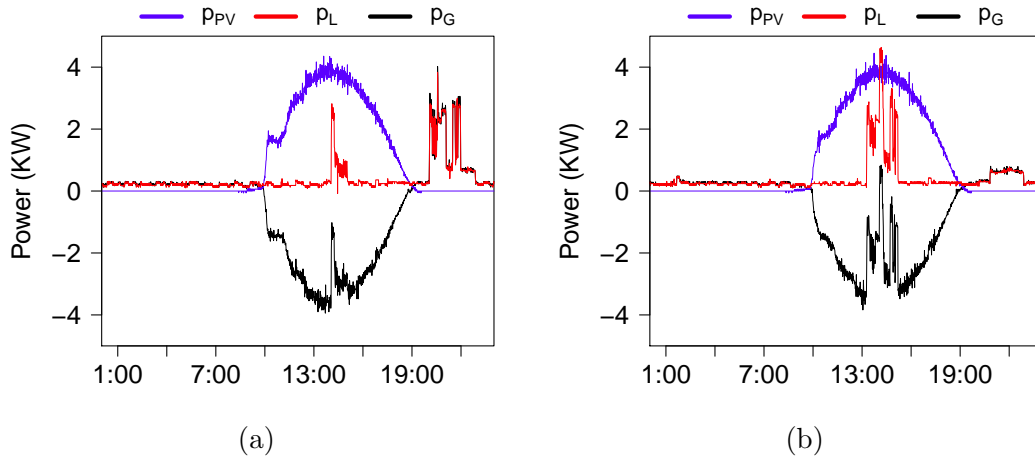


Figure 3.10: Development of the main power flows during two days of experiments without storage: a) without ADSM and b) with ADSM.

The energy behavior without storage have been studied, fixing the nominal battery capacity to  $Cap = 0$  kWh. In this situation, the effects of the ADSM can be easily observed. Two different experiments have been performed, with and without ADSM. Each experiment consists of running the house during four days with the previously explained conditions. The main power flows, the energy variables and the self-consumption has been measured along this period. Figure 3.9 shows the development of the power flows in the experiments. In the instance without ADSM, the main consumption is done during the evening without any scheduling—see Figure 3.9a. On the other hand, the main consumption is done during the maximum generation hours when the ADSM algorithm is used—see Figure 3.9b.

Figure 3.10 shows the main power flows for a day without and with ADSM. As aforementioned, the deferrable loads are set at the evening in the case without ADSM—see Figure 3.10a. This implies that the local facility imports power from the grid overnight and exports PV generation excess during the day. In the case with ADSM, the algorithm displaces the deferrable loads from the evening hours to the maximum generation hours—see Figure 3.10b. There is an important reduction of demanded power from the grid to the detriment of the exported PV electricity. This behavior is repeated throughout the week, increasing the self-consumption factor average.

### 3.2. Experiments

Parameter	Day without ADSM	Day with ADSM	Experiment without ADSM	Experiment with ADSM
$E_{PV}$ (KWh)	23.5	23.76	22.76	23.6
$E_L$ (KWh)	9.8	10.19	10.67	10.99
$E_{PV,L}$ (KWh)	3.17	6.33	3.3	6.25
$E_{G,O}$ (KWh)	20.07	17.43	19.45	17.34
$E_{G,I}$ (KWh)	7.22	4.64	7.37	4.73
$\xi$	31.5%	58%	31%	57%

Table 3.2: Energy variables and the self-consumption for two representative days and their averages for both experiments without storage.

Table 3.2 shows the average of energy variables and self-consumption measured for both experiments without storage and for the two representative days of Figure 3.10. The energy exchanged with the grid is decreased because of the use of the ADSM algorithm. In the experiment without ADSM, 85% of the locally generated energy is exported to the grid. In the experiment with ADSM, this amount of energy is reduced to 73%. On the other hand, the energy imported from the grid is also reduced, being 69% of the total energy consumed in the experiment without ADSM and 43% with ADSM. This reduction of energy exchanged with the grid is also reflected in the self-consumption of the PV generation. In these experiments, the use of ADSM has increased the self-consumption in 26%.

The next experiments have been carried out with a battery capacity of 5.4kWh which is equivalent to half day of autonomy. The presence of storage makes possible the local generated energy management, thus allowing to increase its self-consumption. Figure 3.11 shows the main power flows with the storage system for a day without and with ADSM. As in the previous experiments, the deferrable loads are set at the evening in the case without ADSM—see Figure 3.11a. In this case, the energy excess of PV generation is stored during the day to be used during the night, reducing the amount of energy imported from the grid. Although the storage system takes this energy excess, the battery capacity is not enough to absorb all this energy and part is exported to the grid. The ADSM algorithm is able to increase the amount of energy directly consumed by the loads—see Figure 3.11b. This results in a reduction of the energy exported to the grid.

Different experiments have been performed to analyze the effect of ADSM with the storage system. There are two experiments for each season of the year, with

### 3. Local Demand-Side Management

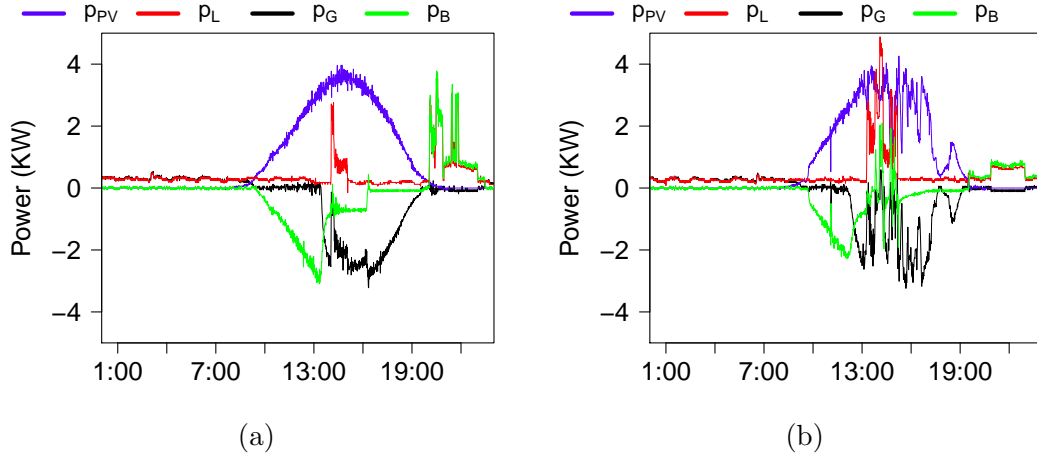


Figure 3.11: Development of the main power flows during two days of experiments with 5.4 kWh of battery capacity: a) without ADSM and b) with ADSM.

and without ADSM. Each experiment consists of running the house during four days, as those previously shown. The main power flows, the energy variables and the self-consumption has been measured along this period. Figure 3.12 shows the development of main power flows in the experiments without ADSM. The availability of the solar resource is lower during the winter period increasing in the other seasons. For this reason, the energy consumption from the grid is higher during autumn and winter and it is lower during spring and summer. The PV energy exported to the grid has the opposite behavior.

Figure 3.13 shows the development of main power flows in the experiments with ADSM. The deferrable loads are displaced to the maximum generation hours. In this case, the energy exchange with the grid is reduced. The consumption peaks during the evening are considerable reduced in comparison with the experiments without ADSM. In addition, the PV energy excess exported to the grid is also reduced.

Table 3.3 shows the average of energy variables and self-consumption measured for both experiments with 5.4 kWh of battery capacity and for the two representative days of Figure 3.11. The amount of PV generation directly used to supply the local consumption is increased by the ADSM algorithm.  $E_{PV,L}$  is the 12% of the generated energy without ADSM whereas that it is the 21% with ADSM. This increment in the direct use of the PV generation reduces the use of the storage system and energy exchange with the grid. In addition, the use of ADSM increase the self-consumption

### 3.2. Experiments

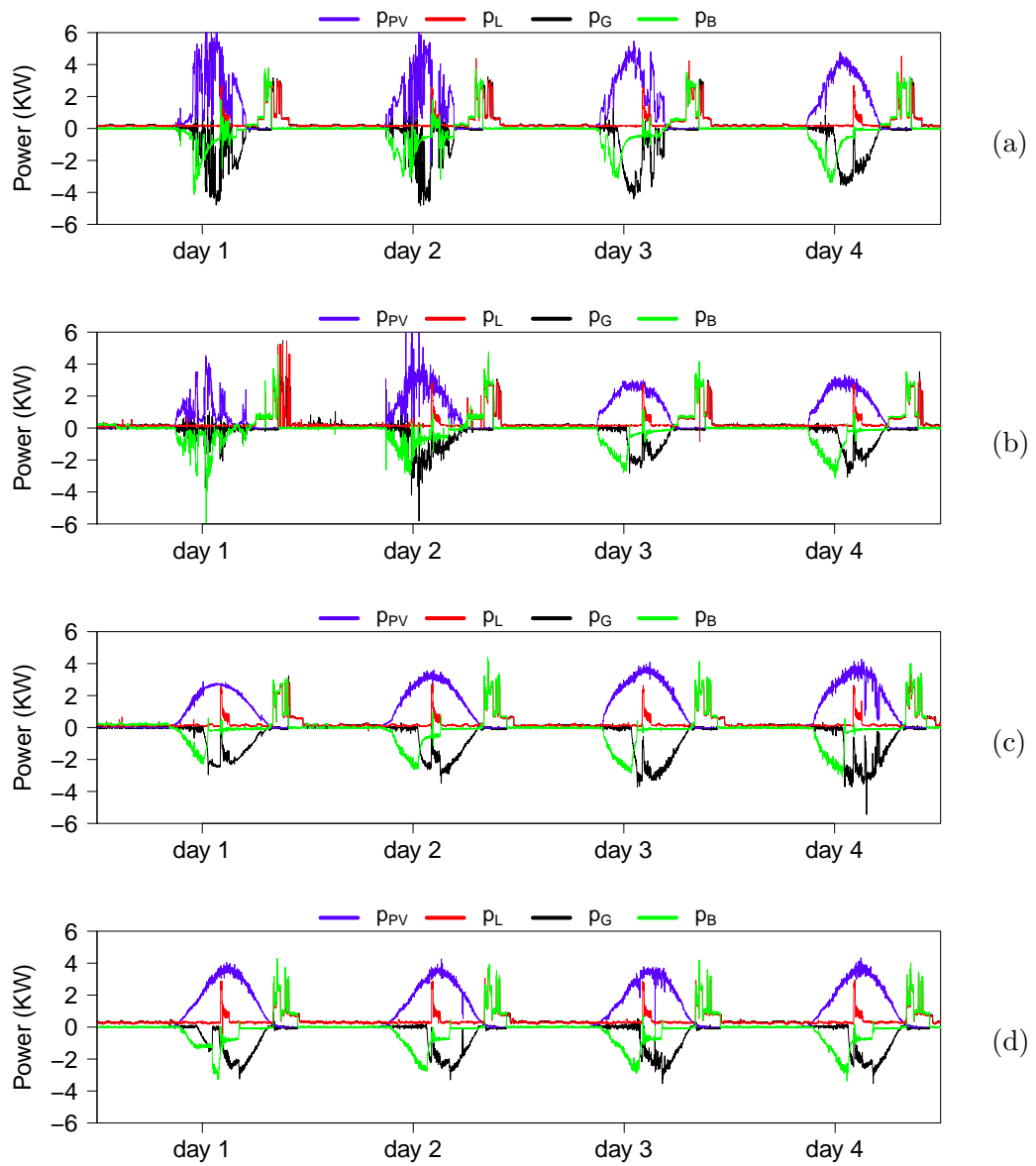


Figure 3.12: Development of the main power flows during the experiments without ADSM and with 5.4kWh of battery capacity in different seasons: a) autumn, b) winter, c) spring and d) summer.

### 3. Local Demand-Side Management

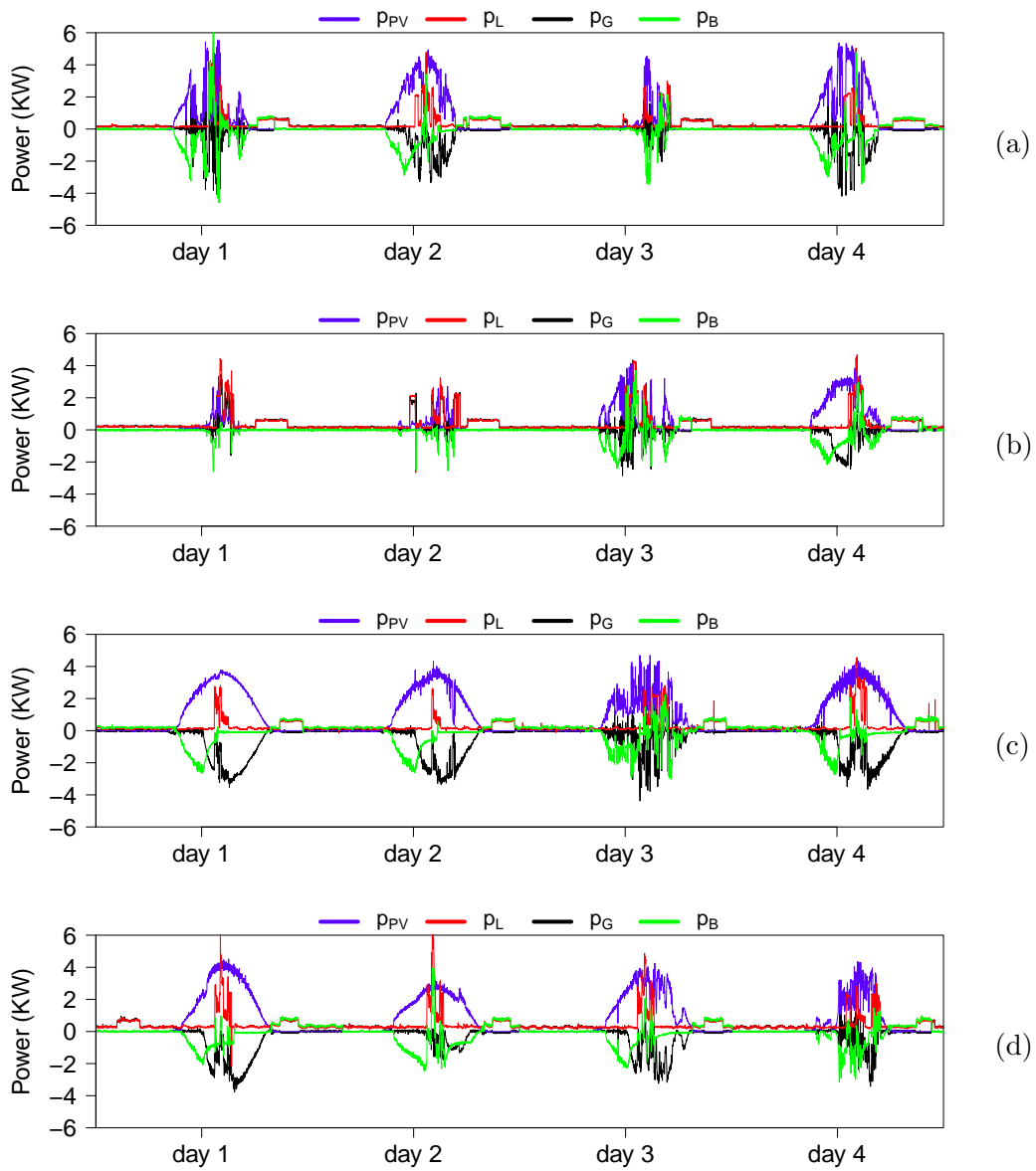


Figure 3.13: Development of the main power flows during the experiments with **ADSM** and with 5.4 kWh of battery capacity in different seasons: a) autumn, b) winter, c) spring and d) summer.

### 3.3. Effects on the grid

Parameter	Day without ADSM	Day with ADSM	Experiment without ADSM	Experiment with ADSM
$E_{PV} (KWh)$	22.9	20.8	19.16	16.86
$E_L (KWh)$	10.62	11.63	9.17	9.0
$E_{PV,L} (KWh)$	3.33	5.77	2.29	3.63
$E_{B,O} (KWh)$	8.36	5.88	4.27	3.27
$E_{B,I} (KWh)$	4.16	3.16	7.23	6.03
$E_{G,O} (KWh)$	11.2	9.13	9.35	7.02
$E_{G,I} (KWh)$	3.13	2.7	3.23	2.82
$\xi$	70.5%	77%	73%	79%

Table 3.3: Energy variables and the self-consumption for two representative days and their averages for both experiments with 5.4kWh of battery capacity.

in 6%. This increment of the self-consumption is lower than the increment in the experiments without battery—see Table 3.2. This is consistent with the results of the simulations because the use of an storage system reduces the effects of ADSM in the local energy behavior.

This measurement campaign has shown that ADSM increases the self-consumption of the local generation in real applications. In the experiments without storage, ADSM has increases in 26% the self-consumption reducing the energy dependence with the electrical grid. In the experiments with storage, this increment is lower but it reduces the energy exchange with storage system. It implies that storage system with lower capacity can be used to achieve a similar self-consumption value. On the other hand, despite the local controllers are focused on self-consumption optimization, the local facilities exchange energy with the grid. Therefore, the aggregated consumption smoothing is not guaranteed because this energy exchange is not controlled by the ADSM algorithm.

### 3.3 Effects on the grid

In this Section, the effects of ADSM and storage systems on the electrical grid are analyzed. This analysis has been done throughout simulations of an electrical grid by using *GridSim* simulator—see Appendix A. A certain number of facilities like “MagicBox” are connected in this electrical grid. The aggregated consumption is

### 3. Local Demand-Side Management

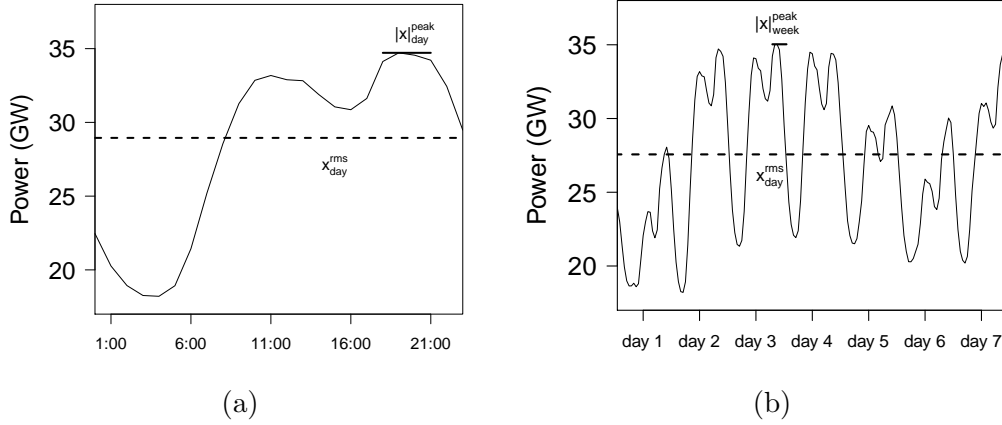


Figure 3.14: Example of the crest factor for two different periods of the aggregated consumption: a) crest factor of a day  $C_{day} = 1.19$  and b) crest factor of a week  $C_{week} = 1.27$ .

affected by the energy behavior of the local facilities. The objective of this analysis is to study how the shape of the aggregated consumption is modified because of the presence of **DG**, **Distributed Energy Resource (DER)** and **ADSM**.

In order to analyze the variability of the aggregated consumption, the *Crest Factor*  $C$  has been used. It is a measure of a waveform, showing the ratio of peak values to the average value, such that:

$$C = \frac{|x|^{peak}}{x^{rms}} \quad (3.8)$$

$$x^{rms} = \sqrt{\frac{x_1^2 + x_2^2 + \dots + x_N^2}{N}}$$

where  $N$  is the number of samples taken from the aggregated consumption,  $|x|^{peak}$  is the absolute value of the maximum peak and  $x^{rms}$  is the root mean square. The crest factor makes reference to a concrete time interval in which the signals are evaluated together with a concrete sample period. In this Thesis, the sample period to calculate the crest factor is 1 min. The time interval is denoted with a subscript, for example, the crest factor of a day is denoted by  $C_{day}$ . Figure 3.14 shows an example of the crest factor for a day and a week of the aggregated consumption. In this analysis,  $C_{year}$ ,  $C_{month}$ ,  $C_{week}$  and  $C_{day}$  have been calculated.

### 3.3. Effects on the grid

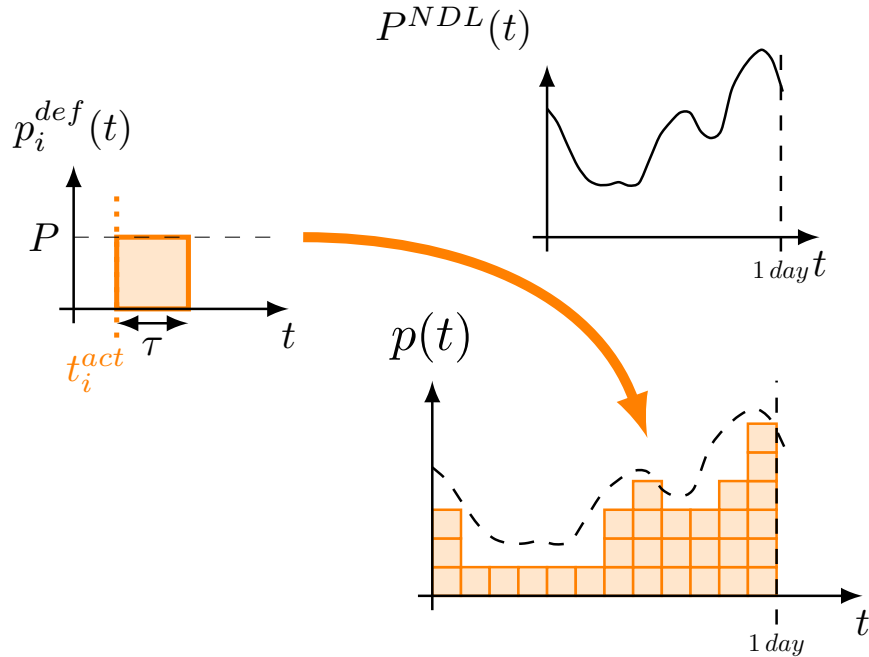


Figure 3.15: Conceptual example of a virtual user operation. The virtual user creates a number of loads for each day of simulation. The  $t_i^{act}$  of these loads is created by using the probability density function  $P^{NDL}(t)$ .

The simulated electrical grid is divided in 600 nodes which are divided in 6 different lines in groups of 100 nodes. Each line or group of nodes has different meteorological conditions as shown later. Each node is a facility with similar features to “MagicBox” as in Section 3.2. They are equipped with a PV generator, storage system and local consumption. The time step of simulation is 1 min. In this analysis, a virtual user is used in order to compose the consumption profile. This user belongs to a concrete facility, it means that if there are 600 nodes, there are 600 virtual users.

#### 3.3.1 Virtual users

A virtual user is a program inside *GridSim* simulator which emulates the behavior of a real user. It is responsible for creating the consumption function of a concrete node. In this analysis, the virtual users only create deferrable loads. It means that the whole consumption of the simulated grid is deferrable. A virtual user creates a

### 3. Local Demand-Side Management

---

certain number of deferrable loads for each day of simulation. These loads are created at the beginning of each day of a simulation. This behavior is similar to that followed in the Section 3.2, but in this case, the number of deferred loads and their position along the day is random. There is a probability density function which defines the probability that a new deferrable load is created at a given time instant. This function is denoted by  $P^{NDL}(t)$  which is discretized in minutes. Thus, the creation of a new deferrable load is a binary random variable  $NDL$  for every minute of simulation.

Figure 3.15 shows an example of a virtual user operation. A deferrable load is created with a certain probability in each minute of simulation. Thereby, whenever the virtual user creates a load, it associates a concrete  $t_i^{act}$ . If there is not a scheduling of these loads, the loads are executed following  $P^{NDL}(t)$ . It means that the consumption of the simulated facility takes the shape of  $P^{NDL}(t)$ . In this Section, the probability density function originates from the peninsular Spanish aggregated consumption in 2013. This consumption was measured by the Spanish grid operator R.E.E. with a sampling period of 1 hour. These real measurements have been interpolated in order to use an aggregated consumption with a sampling period of 1 min. In addition, this consumption has been normalized to be transformed into a probability density function. Thus, the simulated electrical grid emulates the consumption of the peninsular Spanish grid during this year. For this analysis, the deferrable loads have been simplified. They are modeled as *energy packets*. These packets consume a constant nominal power  $P$  during a certain time interval  $\tau$ —see Figure 3.15. The nominal power is  $P = 50$  MW and runtime is  $\tau = 60$  min. Although this power may seem excessive, this consumption is scaled such that the total consumed energy of the simulated grid coincides with the total consumed energy of the peninsular Spanish grid. This energy consumption reaches 246 TWh for a year of simulation. In addition, it is considered that the deferrable loads have a running range of one day (1440 min). It means that the deferrable loads which are created the day  $x$  of simulation have a running range of  $t_i^{beg} = day\ x$  and  $t_i^{end} = day\ x + 1$ .

Figure 3.16a shows an example of the aggregated consumption of the simulated electrical grid during one year. Figure 3.16b shows the aggregated consumption during a week of this simulation, where the solid line is the aggregated consumption created by the virtual users and the dashed line is the measured peninsular Spanish consumption during the year 2013. Both functions are very similar because of the large number of deferrable loads executed in the simulations. This simulation has been performed without DER and ADSM, thus, it represents the common behavior of the peninsular Spanish electrical grid. The simulated grid reaches a maximum

### 3.3. Effects on the grid

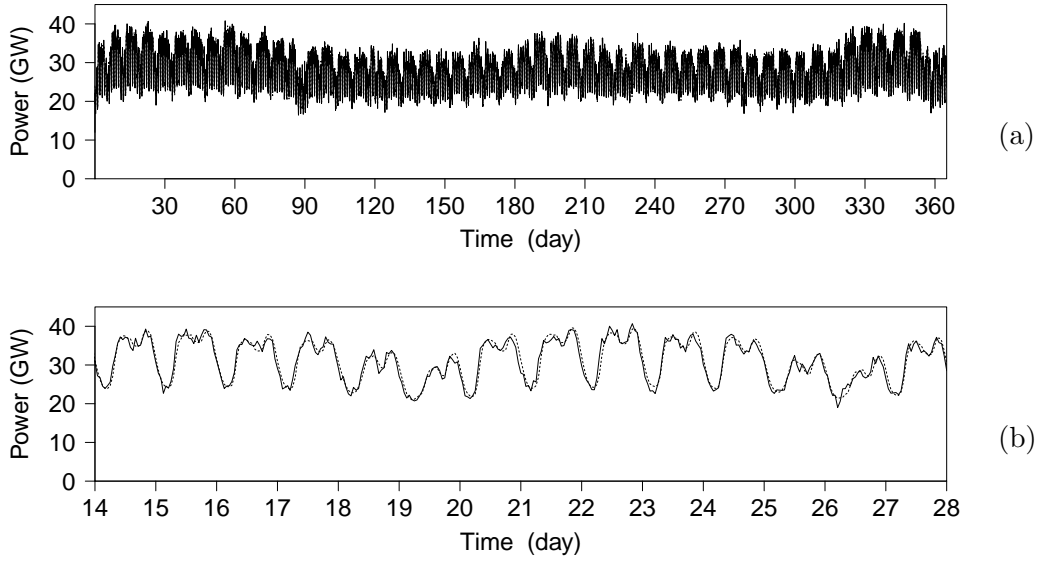


Figure 3.16: Example of the aggregated consumption of the simulated electrical grid, where the solid line is the aggregated consumption created by the virtual users and the dashed line is the measured peninsular Spanish consumption during the year 2013: a) one year of simulation and b) one week of this simulation. The crest factors for these example:  $C_{year} = 1.52$ ,  $\bar{C}_{month} = 1.38$ ,  $\bar{C}_{week} = 1.33$  and  $\bar{C}_{day} = 1.23$ .

yearly peak of 40.7 GW, a minimum valley of 16.4 GW and an average consumption of 28.1 GW. The measured consumption of the Spanish grid has a maximum yearly peak of 39.5 GW, a minimum valley of 17.2 GW and an average consumption of 28.1 GW. The daily difference between peak and valley has also been calculated so that, for the simulated grid, the maximum difference throughout the year is 19.4 GW, the minimum is 7 GW and the average is 12.3 GW. For the measured consumption, the maximum difference between peak and valley is 15.5 GW, the minimum is 7.6 GW and the average is 11.7 GW. Although the simulated grid differs from the real grid, the differences in peak and valley values do not imply a considerable difference in the dynamics of the grid. The average consumption is almost the same for both cases and the average of the daily difference between peak and valley differs by less than 5%. For this reason, the simulated grid has been taken as reference to analyze the effects of the **DER** and **ADSM** on the grid. The daily, weekly and monthly crest factors of

### 3. Local Demand-Side Management

---

the simulated grid have been averaged, so that:

$$\begin{aligned}
 C_{year} \quad \bar{C}_{month} &= \frac{1}{12} \sum_{i=1}^{12} C_{month}^i \\
 \bar{C}_{week} &= \frac{1}{52} \sum_{i=1}^{52} C_{week}^i \quad \bar{C}_{day} = \frac{1}{365} \sum_{i=1}^{365} C_{day}^i
 \end{aligned} \tag{3.9}$$

where the index  $i$  denotes the month, the week or the day of the assessed year depending on the case.  $\bar{C}_{day}$  represents the average of the crest factors of the 365 days of the simulated year,  $\bar{C}_{week}$  is the average of the 52 weeks and  $\bar{C}_{month}$  is the average of the 12 months.

#### 3.3.2 PV effect on the grid

The simulation of Figure 3.16 lacks of PV generation. It should be included in the facilities in order to use the local controllers. In addition, the effect of the PV generation on the variability of the aggregated consumption is paramount for the integration possibilities of this technology. The PV generation is considered as a negative consumption consistently with Equation 2.1: if a facility has a generation excess of 1 kW, it is consuming -1 kW. This consideration allows to introduce the PV generation in aggregated consumption and observe its effects. As a final appreciation, the aggregated consumption is always positive, it means that if the PV generation is greater than the whole consumption of the grid, the aggregated consumption will be zero instead of taking negative values. The generation profiles from six different cities of Spain have been used: Cáceres, Ciudad Real, Logroño, Madrid, Santiago and Soria. The calculus of the PV generation profiles has been done by using the real irradiance data from these cities during 2013. This irradiance has been translated to AC power by using the model of the PV generators of “MagicBox”. In addition, the PV generation forecasts have been calculated by the ARIMA model developed in Masa (2014). There are 100 virtual facilities (nodes) deployed in each city. The combination of these cities allows to consider different climate regions. This heterogeneous generation is representative of a national generation. Figure 3.17 shows a map with the studied cities and the different climate regions.

The maximum nominal PV power generation in each facility is 240 MW , such that the total power generation of all facilities is 144 GW. This generation power corresponds to a yearly energy generation around 246 TWh which is the same energy

### 3.3. Effects on the grid

---

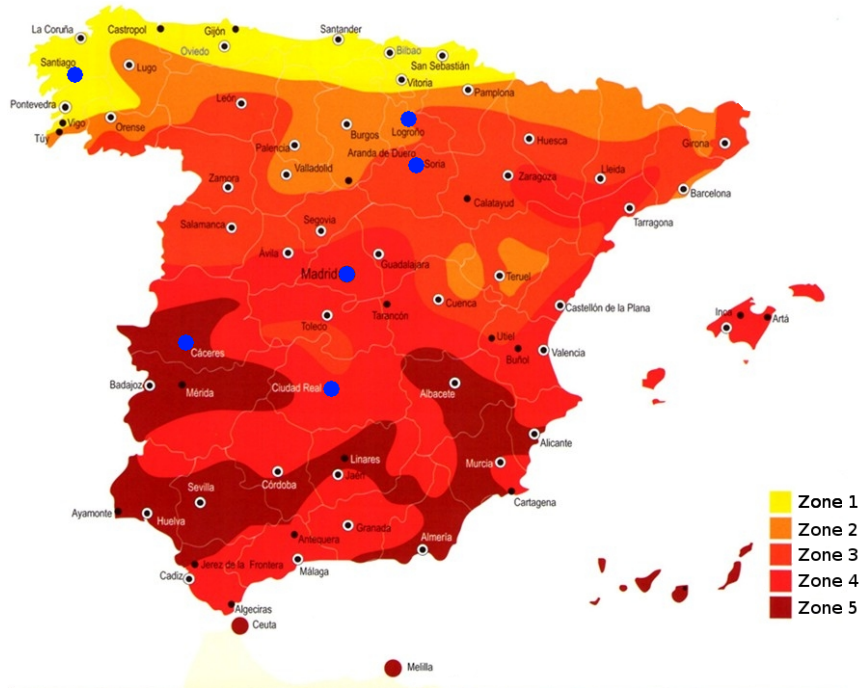


Figure 3.17: Climate zones of Spain, where the chosen cities for this analysis have been marked with blue dots.

amount than the yearly peninsular energy consumption of Spain. This amount is chosen to analyze the effects on the grid of high levels of **PV** penetration.  $\rho^{PV}$  is the *PV penetration factor* which indicates the percentage of energy generated by the **PV** generation sources. For example,  $\rho^{PV} = 50\%$  implies that the annual **PV** generated energy is the half of the whole consumption 123 TWh and an installed **PV** power of 72 GW.

A campaign of experiments has been performed to study how the **PV** penetration affects the crest factors of the aggregated consumption and the self-consumption of the local facilities. For each  $\rho^{PV}$  value, 10 experiments have been performed with different seeds of the random number generator. An experiment consists on the simulation of the electrical grid during one year (525600 min) with a concrete  $\rho^{PV}$  value and a concrete seed. The crest factors and the self-consumption of the local facilities are calculated for each experiment.

### 3. Local Demand-Side Management

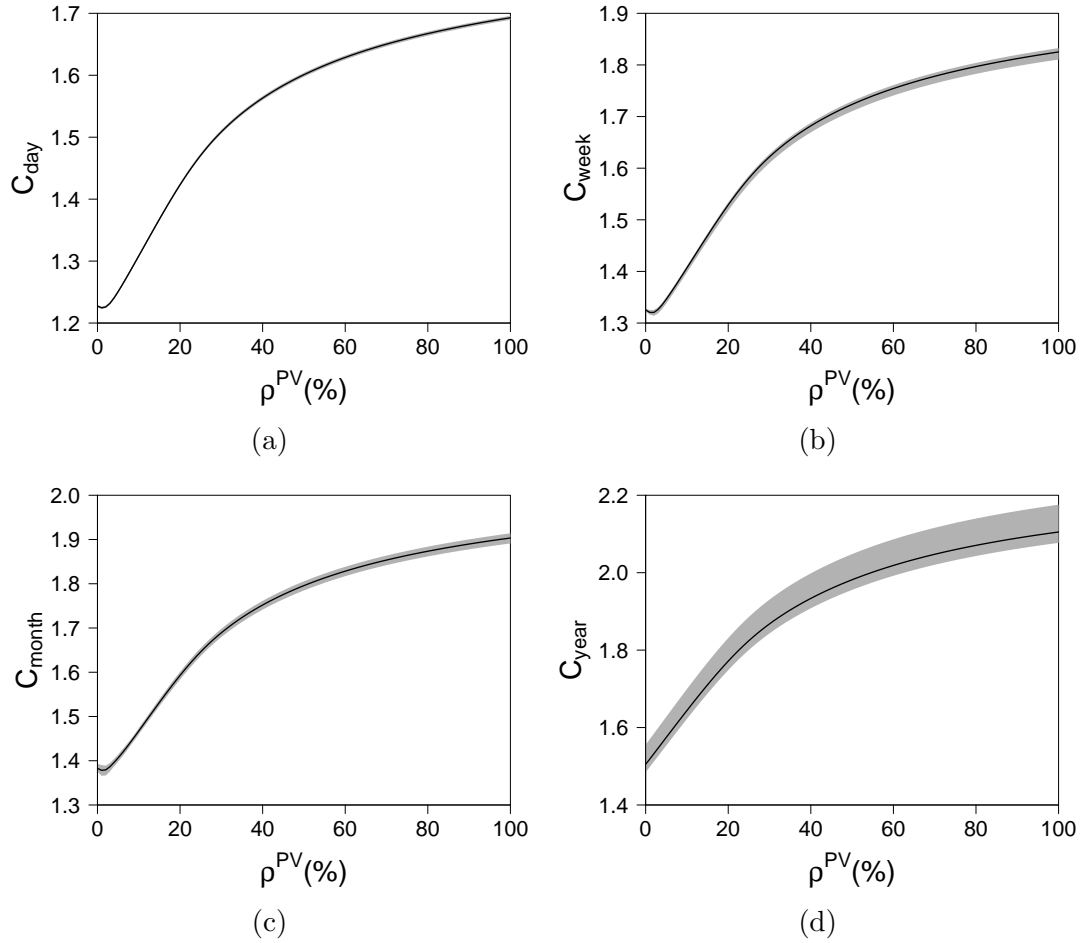


Figure 3.18: Development of the crest factors for different percentages of **PV** penetration  $\rho^{PV}$ . The solid line represents the mean of the crest factors from the 10 simulated seeds. The shaded area is between the maximum and the minimum value obtained from the 10 simulated seeds: a)  $\bar{C}_{day}$ , b)  $\bar{C}_{week}$ , c)  $\bar{C}_{month}$  and d)  $\bar{C}_{year}$ .

Figure 3.18 shows the development of the crest factors for different percentages of **PV** penetration. For each  $\rho^{PV}$  value, the mean and the maximum and minimum values have been calculated from the 10 different seeds. In general, the crest factors increase with  $\rho^{PV}$ , but this relationship is not linear. For  $\rho^{PV} < 3\%$ , that implies an

### 3.3. Effects on the grid

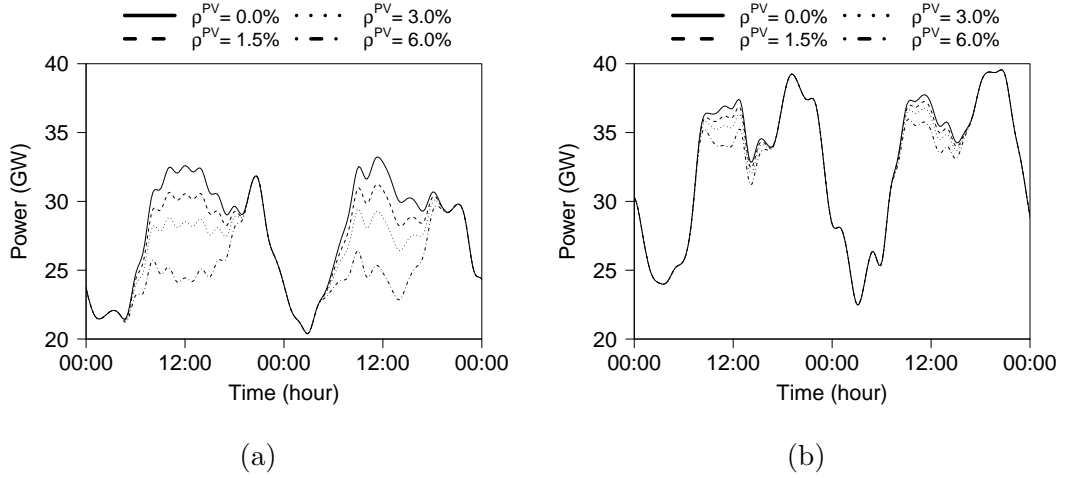


Figure 3.19: Example of the aggregated consumption for different **PV** penetrations: a) during two summer days and b) during two winter days.

installed **PV** power lower than 7.2 GW, the daily, weekly and monthly average crest factors even decrease. This happens because the **PV** generation reduces the crest factors for summer days and compensates the increase of the crest factors for winter days. Figure 3.19 shows an example of this effect. The maximum **PV** generation is at midday together with the maximum consumption peaks during summer days—see Figure 3.19a. On the other hand, the maximum consumption peaks during winter days take place at evening which cannot be reduced by the **PV** generation—see Figure 3.19b. For  $\rho^{PV} > 3\%$ , the reduction of the crest factors during summer days ceases to compensate the increase for winter days or even the crest factors during summer days increase. For  $\rho^{PV} < 35\%$ , the increment of the crest factors is linearly proportional to the **PV** penetration. After this  $\rho^{PV}$  value, the crest factor continues growing but with a lower slope. These results allow to conclude that the deployment of large amounts of **PV** generation in an electrical grid increases its variability and, thus, decreases its stability. The oversizing of the grid will increase as the **PV** generation increases. This implies that the deployment of **PV** generation must be accompanied by energy management techniques as **DSM** or storage systems.

Figure 3.20 shows the development of the self-consumption factor for different percentages of nominal **PV** generation. The higher  $\rho^{PV}$ , the higher the self-consumption in the local facilities. This relationship is almost linear, but with a

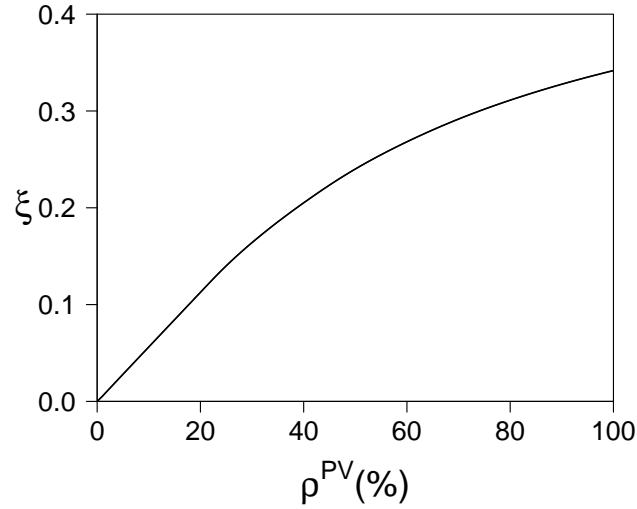


Figure 3.20: Development of the self-consumption for different percentages of **PV** penetration  $\rho^{PV}$ . The solid line represents the mean of the crest factors from the 10 simulated seeds. The shaded area is between the maximum and the minimum value obtained from the 10 simulated seeds.

slope lower than one. It implies that the increment of **PV** generated energy does not satisfy the same amount of local energy consumption. To increase this slope, the use of other techniques as **ADSM** or storage systems are required.

Figure 3.21 shows an example of the aggregated consumption of the simulated electrical grid with  $\rho^{PV} = 50\%$ . This penetration of **PV** generation in the electrical grid increases considerably its variability. The maximum yearly peak reaches 40.7 GW as the example without **PV** generation. There are times during the year where the aggregated consumption is reduced to zero. The average of the aggregated consumption is 18.3 GW. Regarding the daily difference between peak and valley, the maximum difference is 39.9 GW, the minimum is 11 GW and the average is 28.4 GW. These results imply that, regardless the **PV** generation, the electrical grid still has the same maximum yearly peak value as the situation without **PV** generation—see example of Figure 3.16. Hence, the electrical grid should have the same installed power in other generation technologies and transmission lines. The average consumption with **PV** generation is lower than the average consumption without **PV** generation. This implies that the infrastructure of the electrical grid is less exploited. Therefore,

### 3.3. Effects on the grid

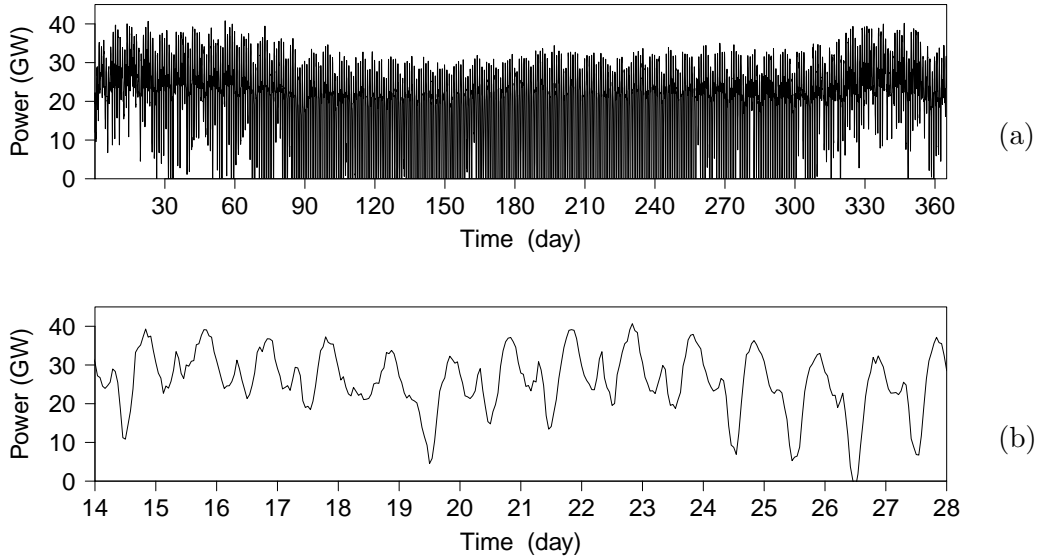


Figure 3.21: Example of the aggregated consumption of the simulated electrical grid with  $\rho^{PV} = 50\%$ : a) one year of simulation and b) one week of this simulation. The crest factors for these example:  $C_{year} = 1.98$ ,  $\bar{C}_{month} = 1.79$ ,  $\bar{C}_{week} = 1.72$  and  $\bar{C}_{day} = 1.6$ . The self-consumption for this example:  $\xi = 0.24$ .

the oversizing of the grid increases reducing the efficiency of investment. On the other hand, the self-consumption for this example is  $\xi = 0.24$ . This value is reached without **ADSM** and any storage system, thus, it is the natural self-consumption because of the natural correlation between the **PV** generation and consumption.

#### 3.3.3 ADSM effect on the grid

In this Section, the effect of the **ADSM** with **PV** generation on the electrical grid is analyzed. The simulated facilities have the same characteristics as the previous ones. Recall that these facilities are not equipped with storage system yet. A campaign of experiments has been carried out to do this analysis. In this case, there is new parameter to consider: the percentage of consumption controlled by the **ADSM** algorithm which is denoted by  $\rho^{ctr}$ . For example, if  $\rho^{ctr} = 50\%$  the **ADSM** algorithm controls the 50% deferrable loads along the year, thus, in this case where all consumption is deferrable, the algorithm controls half of the annual energy

### 3. Local Demand-Side Management

---

consumption: 123 TWh. The crest factors of the aggregated consumption and the self-consumption of the local facilities have been calculated for different combinations of  $\rho^{PV}$  and  $\rho^{ctr}$ . For each combination of these parameters, 3 experiments have been performed with different seeds of the random number generator. An experiment consists on the simulation of the electrical grid during one year (525600 min) with a concrete combination of  $\rho^{PV}$  and  $\rho^{ctr}$  and a concrete seed.

Figure 3.22 shows the development of the crest factors for different percentages of PV penetration and controlled consumption. For each combination of  $\rho^{PV}$  and  $\rho^{ctr}$ , the average has been calculated from the three different seeds. In general, the crest factors increase with  $\rho^{PV}$  as in the analysis of Figure 3.18. On the other hand, the variability of the aggregated consumption also increases with  $\rho^{ctr}$ . This effect occurs because the ADSM maximizes the self-consumption for the individual facility by executing the loads at the maximum generation hours. Those hours coincide for all facilities of a region, being all loads executed at roughly the same time. This implies that days with low PV generation or any forecast error cause a high consumption without local generation, increasing the peaks along the year. This effect is accentuated as there is more PV penetration because, in days with high PV generation, the aggregated consumption is reduced to zero but the maximum peaks remain the same value.

Figure 3.23 shows the development of the self-consumption for different percentages of PV penetration and controlled consumption. The self-consumption increases with  $\rho^{PV}$  as in the analysis of Figure 3.20. In this case, the ADSM algorithm schedules the deferrable loads to maximize the use of the PV resource. From the result, it concludes that the algorithm reaches its objective. The higher the  $\rho^{ctr}$ , the higher the self-consumption. The maximum value of self-consumption is  $\xi = 0.42$  for  $\rho^{ctr} = 100\%$  and  $\rho^{PV} = 100\%$ . This value may seem low for these parameters of the experiment, but this is because of two main reasons: the forecast errors and the natural mismatch between the generation and consumption, there are days with high generation and low consumption and vice versa.

Figure 3.24 shows an example of the aggregated consumption of the simulated electrical grid with  $\rho^{PV} = 50\%$  and  $\rho^{ctr} = 50\%$ . The maximum yearly peak reaches 51.7 GW, the minimum valley is zero and the average is 15.9 GW. The maximum yearly peak is higher than in the previous examples, it has increased from 40.7 GW to 51.7 GW. On the other hand, the average is lower in this example. This implies that the use of ADSM focus on the self-consumption maximization may even increase the variability of the aggregated consumption. The maximum daily difference between

### 3.3. Effects on the grid

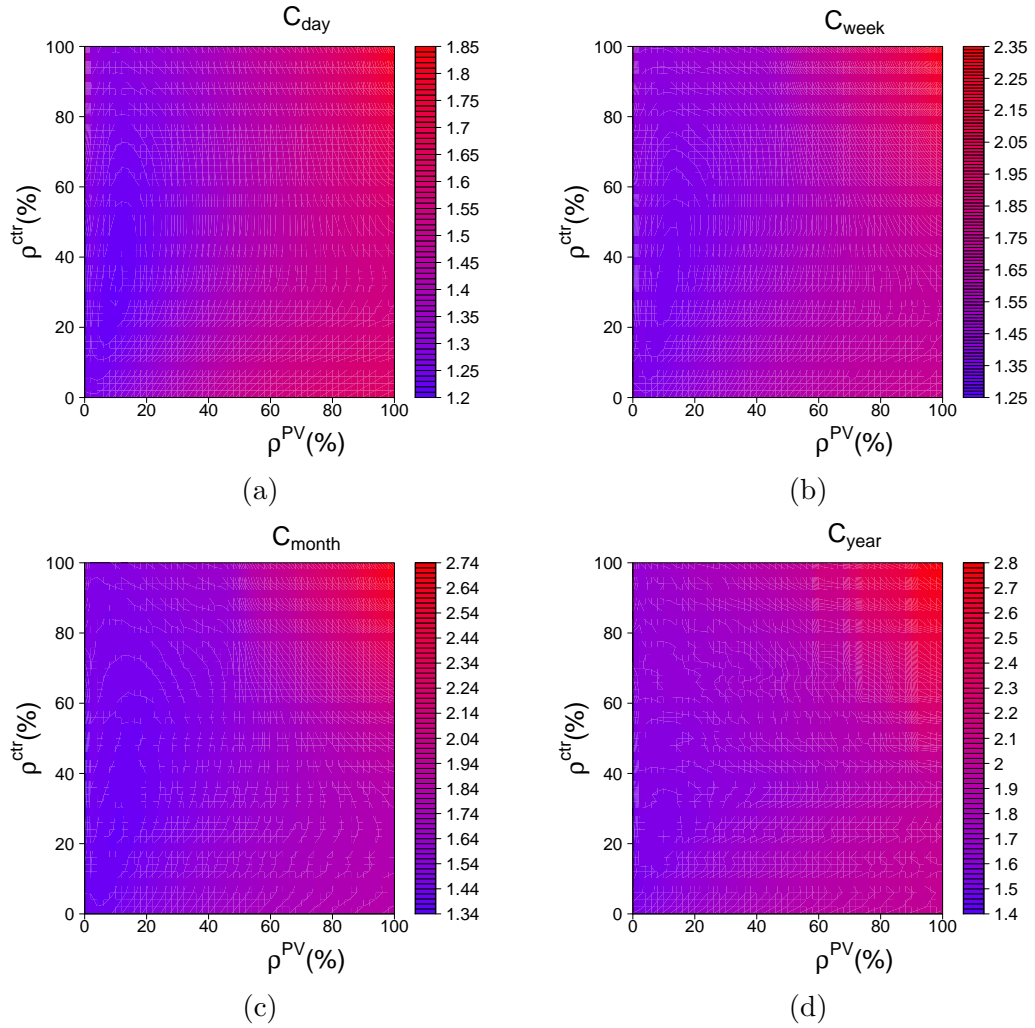


Figure 3.22: Heat map representing the development of the crest factors for different combinations of  $\rho^{PV}$  and  $\rho^{ctr}$ : a)  $\bar{C}_{day}$ , b)  $\bar{C}_{week}$ , c)  $\bar{C}_{month}$  and d)  $C_{year}$ .

peak and valley is 37.2GW, the minimum is 4.9GW and the average is 14.2GW. **ADSM** has reduced the daily difference between peak and valley from the example with **PV** generation but without **ADSM**. In addition, the self-consumption has also been increased by the **ADSM**.

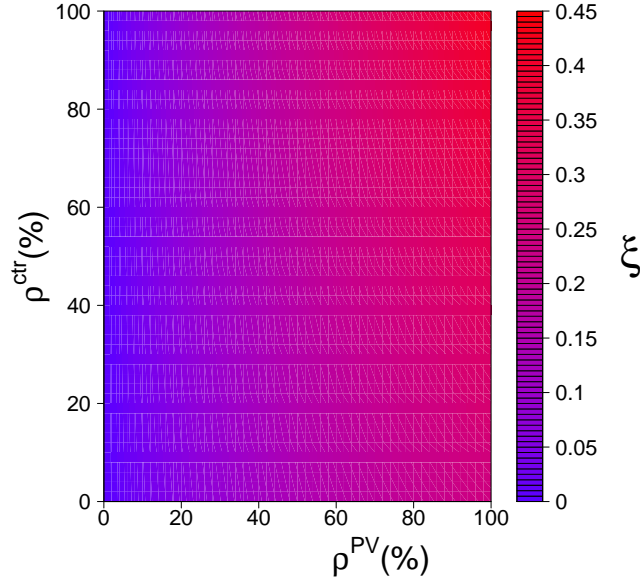


Figure 3.23: Heat map representing the development of the self-consumption for different combinations of  $\rho^{PV}$  and  $\rho^{ctr}$ .

#### 3.3.4 DER effect on the grid

The storage systems are included in the analysis of this Section. These systems together with the **DG** make up a **DER** system. They are managed by the battery controller explained in Section 3.1.2. Their capacity is a key parameter that deeply influences the effects of the storage system on the power flows. When these systems are installed in local facilities with a certain consumption, the capacity is defined in *days of autonomy*. A day of autonomy is the average consumed energy of this facility. In this scenario, each facility consumes 410 GWh per year, thus, the average daily consumption is around 1.12 GWh. The electrical grid is simulated for different capacity values  $Cap^*$ . These values are equally spaced distributed over the range  $[0, 2.4]GWh$ , representing from zero capacity (no storage system) to two days of autonomy. In addition, the battery controller is designed to optimize the self-consumption of the local facility with  $SoC^{min} = 40\%$  and  $SoC^{max} = 60\%$ .

A campaign of experiments has been performed to study how the **PV** penetration and storage system capacity affect the crest factors of the aggregated consumption and the self-consumption of the local facilities. Different combinations of  $\rho^{PV}$  and  $Cap^*$

### 3.3. Effects on the grid

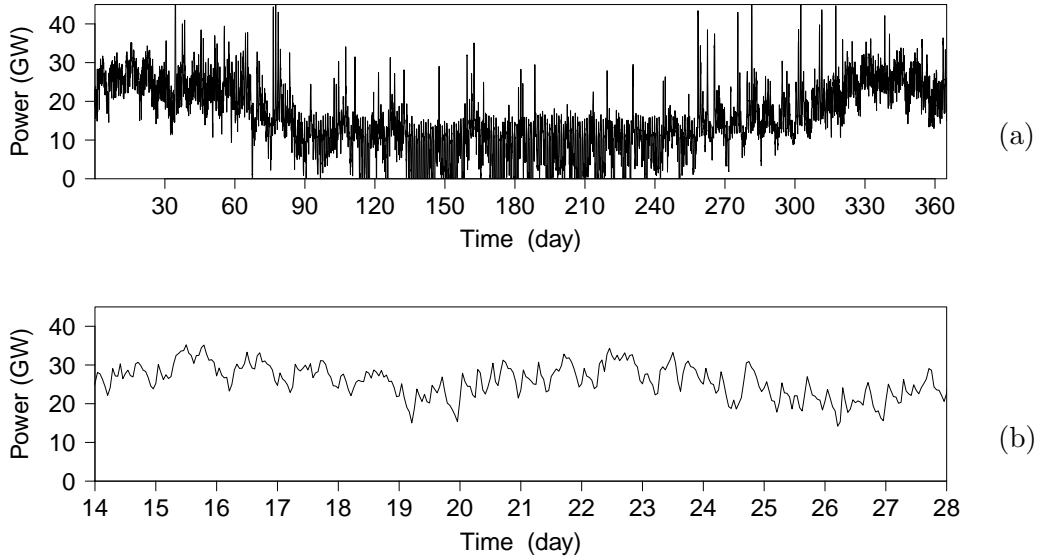


Figure 3.24: Example of the aggregated consumption of the simulated electrical grid with  $\rho^{PV} = 50\%$  and  $\rho^{ctr} = 50\%$ : a) one year of simulation and b) one week of this simulation. The crest factors for these example:  $C_{year} = 2.89$ ,  $\bar{C}_{month} = 2.57$ ,  $\bar{C}_{week} = 2.12$  and  $\bar{C}_{day} = 1.57$ . The self-consumption for this example:  $\xi = 0.33$ .

have been studied. For each combination of these parameters, 10 experiments have been performed with different seeds of the random number generator. An experiment consists on the simulation of the electrical grid during one year (525600 min) with a concrete combination of  $\rho^{PV}$  and  $Cap^*$  and a concrete seed. The crest factors and the self-consumption of the local facilities are calculated for each experiment.

Figure 3.25 shows the development of the crest factors for different percentages of PV penetration and storage system capacity. For each combination of  $\rho^{PV}$  and  $Cap^*$ , the average has been calculated from the 10 different seeds. As in the previous analysis, the crest factors increase with  $\rho^{PV}$  because the PV generation introduces deep valleys in the aggregated consumption. For low PV penetration values, the crest factors are reduced by the storage systems. These systems smooth the local power balances storing PV energy during the day and using it during evening peaks. For high PV penetration situations, the development of the crest factors changes. This is because the storage systems are able to store enough energy from the PV

### 3. Local Demand-Side Management

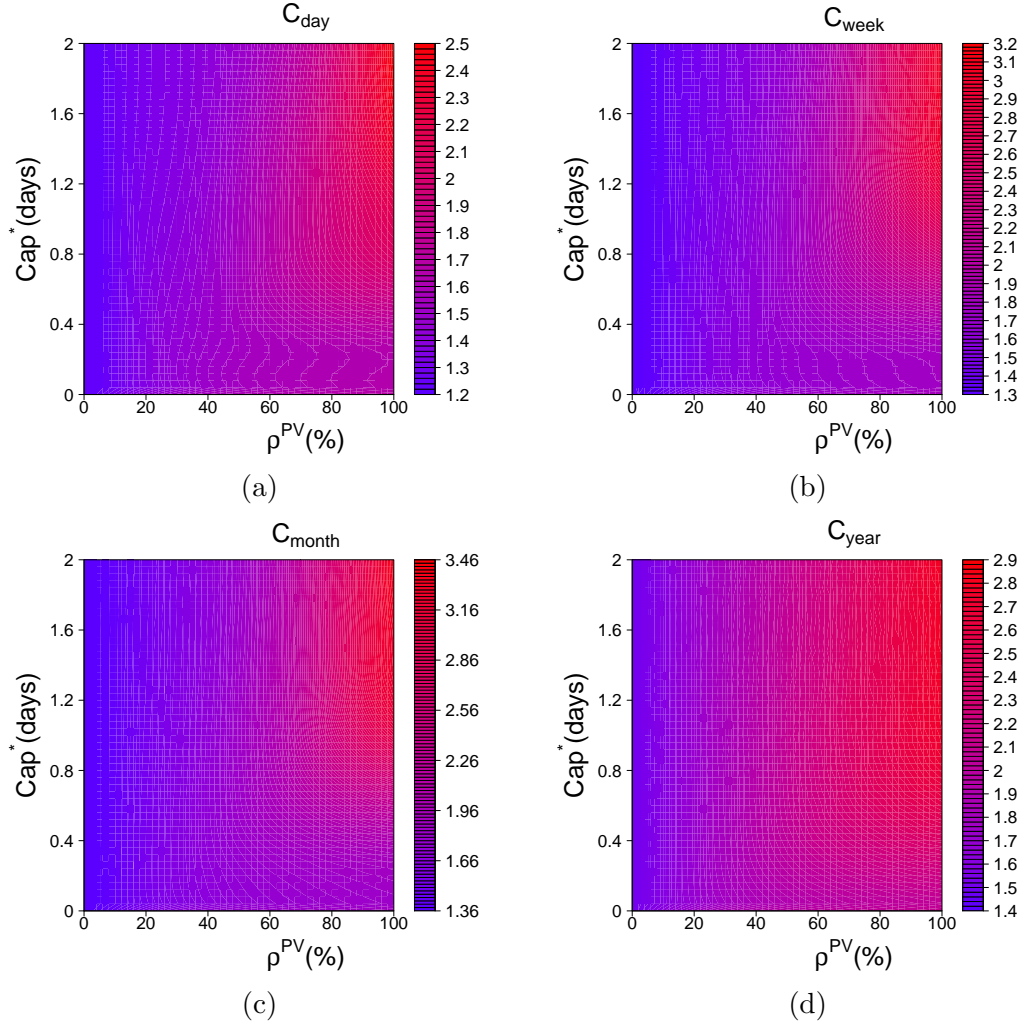


Figure 3.25: Heat map representing the development of the crest factors for different combinations of  $\rho^{PV}$  and  $Cap^*$ : a)  $\bar{C}_{day}$ , b)  $\bar{C}_{week}$ , c)  $\bar{C}_{month}$  and d)  $C_{year}$ .

generation to supply the local consumption during days, reducing the aggregated consumption to zero and being the average consumption close to zero. When there is not PV generation during few days in a row, there is not available energy and the storage systems cannot supply this consumption. Then, the aggregated consumption increases from zero to a high value. This causes a very high increment in the crest factor because these factors are a relationship between the average consumption and

### 3.3. Effects on the grid

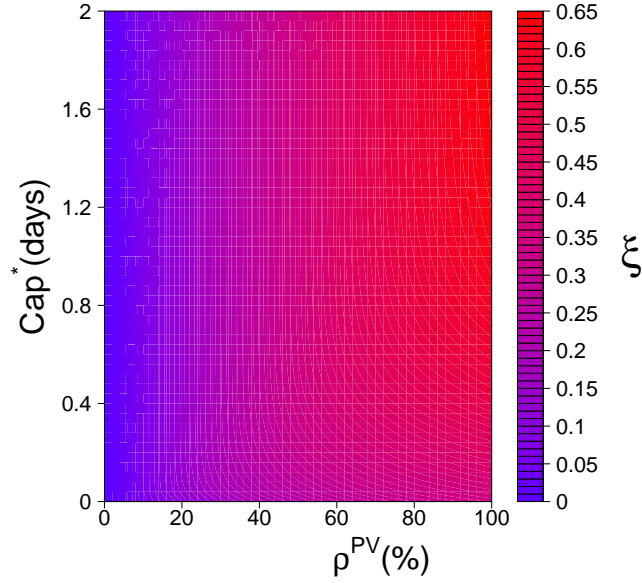


Figure 3.26: Heat map representing the development of the self-consumption for different combinations of  $\rho^{PV}$  and  $Cap^*$ .

the peaks. This effect suggests that the energy strategy of the battery controllers should take into account the grid variability for high presence of **PV** generation and storage in electrical grids.

Figure 3.26 shows the development of the self-consumption for different percentages of **PV** penetration and storage system capacity. The principal factor affecting the self-consumption is the local energy availability. If there is not local generation, the self-consumption is zero regardless of the storage capacity. For higher values of  $\rho^{PV}$ , the self-consumption is increased substantially in relation with the storage capacity. The maximum value of self-consumption in this analysis is  $\xi = 0.65$  for  $\rho^{ctr} = 100\%$  and  $Cap^* = 2$  days. Notice that this self-consumption value is greater than the value obtained in the analysis with **ADSM**—see Figure 3.23. This is because the storage systems are less dependent on the natural matching between **PV** generation and consumption than the **ADSM**.

Figure 3.27 shows an example of the aggregated consumption of the simulated electrical grid with  $\rho^{PV} = 50\%$ ,  $Cap^* = 1$  day and  $\rho^{ctr} = 0\%$ . The maximum yearly peak reaches 40.5 GW, the minimum valley is zero and the average is 18 GW. These values are similar as the example with only **PV** generation and a better than the

### 3. Local Demand-Side Management

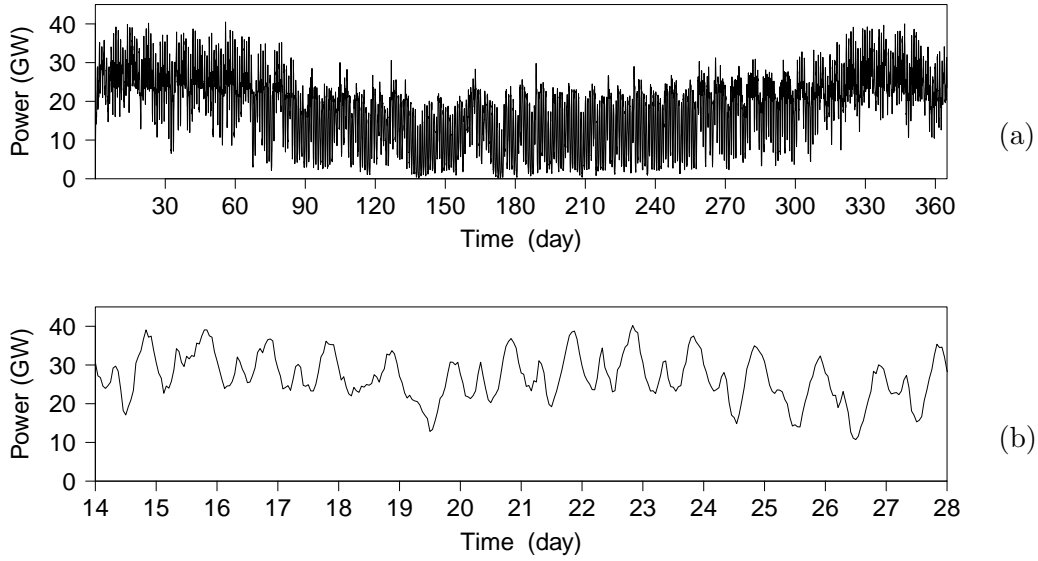


Figure 3.27: Example of the aggregated consumption of the simulated electrical grid with  $\rho^{PV} = 50\%$ , each facility with a storage systems of 1 day of autonomy and without **ADSM**: a) one year of simulation and b) one week of this simulation. The crest factors for these example:  $C_{year} = 2.09$ ,  $\bar{C}_{month} = 1.88$ ,  $\bar{C}_{week} = 1.72$  and  $\bar{C}_{day} = 1.54$ . The self-consumption for this example:  $\xi = 0.35$ .

example with **ADSM**. The maximum daily difference between peak and valley is 29.4 GW, the minimum is 10.4 GW and the average is 18.2 GW. From the daily point of view, the use of storage system reduces the difference between peak and valley from the example with only **PV** generation. This is because the aggregated consumption does not take so lower values with storage systems—compare figures 3.21 and 3.27. On the other hand, this difference increases from the example with **ADSM** because of the displacing of deferrable loads from peaks to maximum generation hours. The self-consumption takes a similar value in examples with **ADSM** and storage, being somewhat higher in the latter.

#### 3.3.5 **ADSM** and **DER** on the grid

The effect of the **ADSM** with **DER** on the electrical grid is analyzed in this Section. The simulated facilities have the same characteristics as the previous ones. A

### 3.3. Effects on the grid

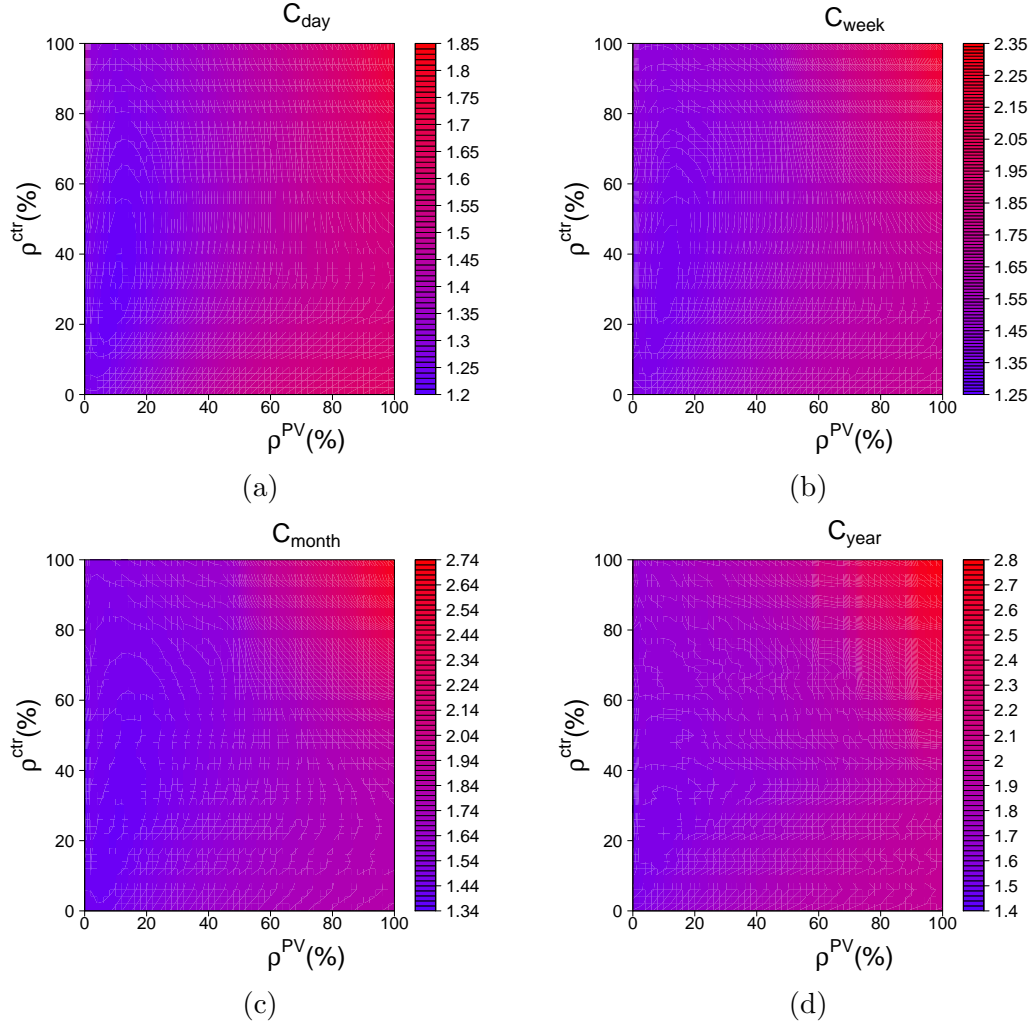


Figure 3.28: Heat map representing the development of the crest factors for different combinations of  $\rho^{PV}$  and  $\rho^{ctr}$  where the local facilities have a storage system with 1 day of autonomy: a)  $\bar{C}_{day}$ , b)  $\bar{C}_{week}$ , c)  $\bar{C}_{month}$  and d)  $C_{year}$ .

campaign of experiments has been carried out to do this analysis by following the same procedure as in Section 3.3.3. The crest factors of the aggregated consumption and the self-consumption of the local facilities have been calculated for different combinations of  $\rho^{PV}$  and  $\rho^{ctr}$ . In this case, facilities with ADSM are also equipped with a storage system with one day of autonomy. For each combination of  $\rho^{PV}$

### 3. Local Demand-Side Management

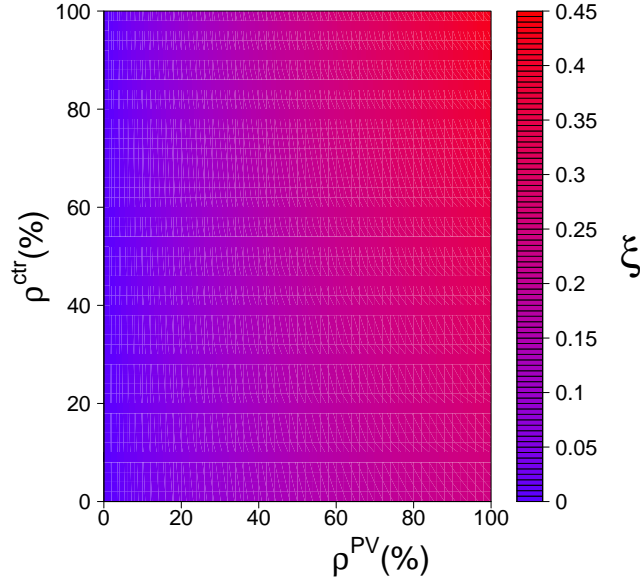


Figure 3.29: Heat map representing the development of the self-consumption for different combinations of  $\rho^{PV}$  and  $\rho^{ctr}$  where the local facilities have a storage system with 1 day of autonomy.

and  $\rho^{ctr}$ , three experiments have been performed with different seeds of the random number generator. An experiment consists on the simulation of the electrical grid during one year (525600 min) with a concrete combination of  $\rho^{PV}$  and  $\rho^{ctr}$  and a concrete seed.

Figure 3.28 shows the development of the crest factors for different percentages of PV penetration and controlled consumption. For each combination of  $\rho^{PV}$  and  $\rho^{ctr}$ , the average has been calculated from the three different seeds. The relationship between the crest factors and the values of  $\rho^{PV}$  and  $\rho^{ctr}$  is similar as the analysis with ADSM and without storage—see Figure 3.22. This is because the use of a storage system is not able to solve the problems associated with the ADSM use: the natural mismatch between the generation and consumption and the forecast errors cause high consumption without generation. These results suggest that information from the grid is required to schedule the loads in order to smooth the aggregated consumption.

Figure 3.23 shows the development of the self-consumption for different percentages of PV penetration and controlled consumption. The relationship between the self-consumption and the values of  $\rho^{PV}$  and  $\rho^{ctr}$  is also similar as the analysis

### 3.3. Effects on the grid

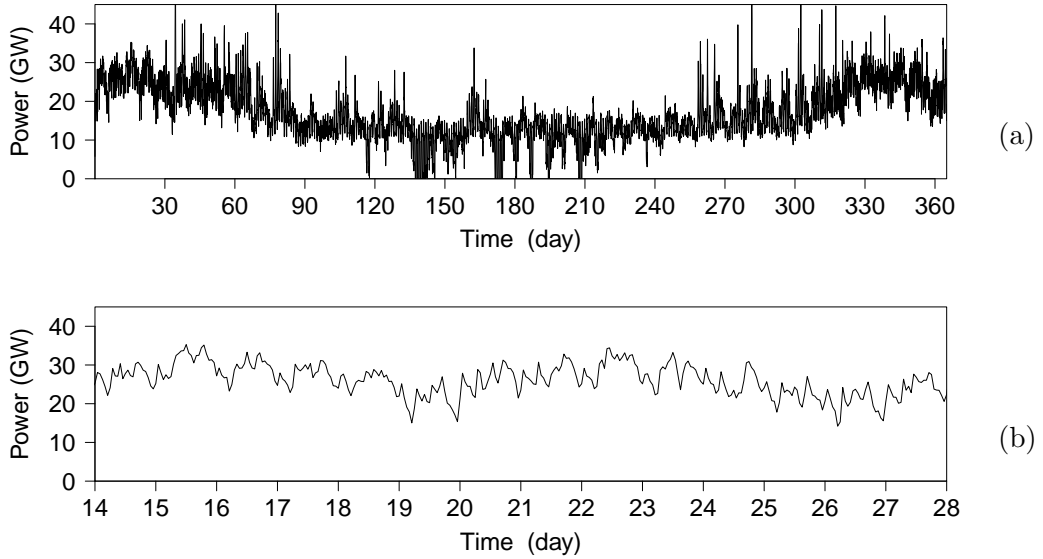


Figure 3.30: Example of the aggregated consumption of the simulated electrical grid with  $\rho^{PV} = 50\%$  and  $\rho^{ctr} = 50\%$  with storage systems of 1 day of autonomy: a) one year of simulation and b) one week of this simulation. The crest factors for these example:  $C_{year} = 2.79$ ,  $\bar{C}_{month} = 2.20$ ,  $\bar{C}_{week} = 1.79$  and  $\bar{C}_{day} = 1.42$ . The self-consumption for this example:  $\xi = 0.35$ .

with [ADSM](#) and without storage—see Figure 3.23. The maximum value of self-consumption is  $\xi = 0.43$  for  $\rho^{ctr} = 100\%$  and  $\rho^{PV} = 100\%$ . It is only  $\Delta\xi = 0.01$  higher than the case without storage. This implies that the use of the storage system does not solve the aforementioned problems.

Figure 3.30 shows an example of the aggregated consumption of the simulated electrical grid with  $\rho^{PV} = 50\%$ ,  $\rho^{ctr} = 50\%$  and  $Cap^* = 1 \text{ day}$ . The maximum yearly peak reaches 51.7 GW, the minimum valley is zero and the average is 17.3 GW. The maximum daily difference between peak and valley is 37.2 GW, the minimum is 4 GW and the average is 11.1 GW. The use of the storage system has improved the power behavior of the local facilities. The average yearly consumption is 17.3 GW in this example instead of 15.9 GW in the example without storage. This implies that the use of the electrical grid has been improved. In addition, the daily difference

between peak and valley has also been reduced. The use of the storage has affected the self-consumption, increasing from  $\xi = 0.33$  to  $\xi = 0.35$ .

## 3.4 Discussion of results and conclusions

This chapter has presented, through simulated and real experiments, the effects of storage and **ADSM** in a house equipped with **PV** generation and grid connection. Results have shown the house electrical energy balances in daily and yearly studies, activating and deactivating the **ADSM** system and modifying the battery capacity. The use of **ADSM** algorithm and battery controller increases the self-consumed energy considerably, reducing the use of the grid and supplying the highest amount of demanded electrical energy from the local sources (**PV** generation in this case).

The relationship between electrical energy variables and the storage capacity is not linear. There is a different variation of these variables for low capacity levels, achieving a plateau for capacities higher than two days of autonomy. The change of this trend takes place with storage capacities close to one day of autonomy. As expected, the relationship between the self-consumption factor and the capacity of the storage system follows a similar development as the energy variables. This relationship is an important design criterion, which involves that oversized storage systems do not produce relevant energy benefits with regard to the local energy optimization. Designers must also take into account the battery float charge consumption trends, which are not commonly considered, but are very important for small battery capacities, which will be expected to be present in the near future in these kinds of facilities.

**ADSM** presents important improvements in the local electricity power flows, integrating the generation and the user demand patterns. The effects of **ADSM** are not constant with the storage capacity, increasing considerably the self-consumption factor for low storage capacities and disappearing for high capacity levels. In conclusion, the **ADSM** brings many advantages, which the main ones are:

- *To decrease energy losses:* the use of **ADSM** increases a direct use of the local sources to the detriment of the storage use, reducing the losses with regard to the efficiency. Moreover, the **ADSM** systems have no physical contact with the energy system and therefore their use does not affect the global system efficiency.

### 3.4. Discussion of results and conclusions

---

- *To reduce the storage capacity:* the same effects produced by a system without **ADSM** can be obtained with **ADSM** by reducing at the same time the battery capacity. It involves that the storage system capacity can be reduced and therefore it decreases the related costs. Moreover, less waste will be generated when recycling the lead-acid batteries at the end of their useful life and therefore it reduces the environmental impact associated to the storage systems.
- *To increase the electricity management possibilities:* by actuating on the demand, the number of variables involved in the energy management of local electric power systems increases. In this Chapter, this management has been focused in the self-consumption maximization. By modifying this target, different energy strategies can be carried out depending on the user needs, e.g. the load displacement to low-cost electricity hours or to avoid power consumption over a defined threshold.
- *Easy scalability:* because **ADSM** can be implemented by simple electronics and software controllers, the system size is not an important constraint to this technique. On the other hand, the principal limit of **ADSM** is the percentage of deferrable loads, which in most cases is difficult to increase.
- *User awareness:* **ADSM** usually involves the user in the house energy management, by informing him about his consumption and the house energy situation. It makes the user aware of the energy demand and it usually involves the consumption reduction.

In this part of the Thesis, some of the main challenges of the **ADSM** presented in the introduction have been responded from a local point of view. An **Information and Communications Technology (ICT)** infrastructure has been developed by using the **PV** generation forecast and the house communication network supported by the electrical appliances and smart meters. The local control system takes the local conditions information and decides when loads should be placed in order to optimize the self-consumption. The complexity of the system increases, but this may be acceptable if taking into account the improvements arising from a technically and economically point of view. Also the growth in penetration of smart-metering and domotic equipments for other uses has to be taken into account.

The combination of small-scale storage with **ADSM** significantly improves the local use of the **PV** resource by means of self-consumption. However, despite all advantages of self-consumption from a local point of view, these do not contribute to

### 3. Local Demand-Side Management

---

the smoothness of the aggregated consumption of the electrical grid. In Section 3.3, the effects of the local facilities on the grid have been studied. This study began with the analysis of the PV penetration in the electrical grids. From the results, it can be concluded that the higher the PV generation power, the higher the variability of the aggregated consumption. For example, the average of the daily difference between peak and valley reaches 28.5 GW when the 50% of whole consumption of the grid is supplied by this energy source. This value is 12 GW when there is not PV generation. Therefore, this analysis shows that the massive use of PV generation in the classical electrical grid is detrimental to its stability. Despite the installed PV power, the same amount of power generation from other technologies and transmission lines are required. This implies that the problem about the electrical infrastructure oversizing is even increased by the use of PV technology.

The detrimental effects of the PV technology may be mitigate by using DSM or storage systems. The effects on the electrical grid of both technologies have been analyzed. The presented ADSM algorithm and the battery controller are focus on the self-consumption maximization. The results of the analysis have shown that the use of these techniques may even increase the variability of the aggregated consumption. This effect occurs because the criterion followed to schedule the loads is implemented by considering only local variables which are roughly common to all facilities. For example, the maximum yearly peak reaches 51 GW when the 50% of whole consumption of the grid is supplied by PV generation and 50% of whole consumption is controlled by the ADSM algorithm, regardless there is storage system or not. However, this value is 40 GW when there is not ADSM. These results suggest that coordination between these facilities is required. Through this coordination, the consumption should be modified taking into account other elements of the grid and seeking for aggregated consumption smoothing. This issue is addressed in the next part of this Thesis.

## Part II

# Grid framework



## Chapter 4

# Grid framework background

In this part of the Thesis, **Demand-Side Management (DSM)** is tackled from the electrical grid point of view. It means that the local demand should be managed to smooth the aggregated consumption of the grid. As mentioned in Chapter 1, there are different **DSM** mechanisms to address this issue, from energy savings incentives to the direct control of loads. The **DSM** mechanism proposed in this Thesis is based on the local electric load automation. The proposed mechanism is posed from a distributed point of view, thus, the **DSM** is not performed by a central agent but each consumer is actively involved in its implementation. This mechanism is defined by an algorithm whose development and operation is the main topic of this Part of the Thesis. The algorithm controls local electric loads taking into account the aggregated consumption of the electrical grid, local energy resources and the user requirements.

The main difference between this Part of the Thesis and the previous one is the addition of the aggregated consumption smoothing as a **DSM** criterion. If  $P(t)$  is the aggregated consumption signal, this criterion implies that  $P(t) \rightarrow C$ , being  $C$  a constant. In addition, the aggregated consumption of the grid may be represented as a sum of two signals, such that:

$$P(t) = P^{nc}(t) + P^c(t) \tag{4.1}$$

where  $P^{nc}(t)$  is the non-controllable consumption, either because it is not deferrable or simply because it is not equipped with any **DSM** system and  $P^c(t)$  is the consumption controlled by the algorithm.

Figure 4.1 shows a graphical representation of the signal sum. If the algorithm is not working,  $P^c(t)$  is not adapted to  $P^{nc}(t)$  and it can have any shape—see Figure 4.1a. The goal of the algorithm is to shape  $P^c(t)$  in a way that  $P(t)$  is

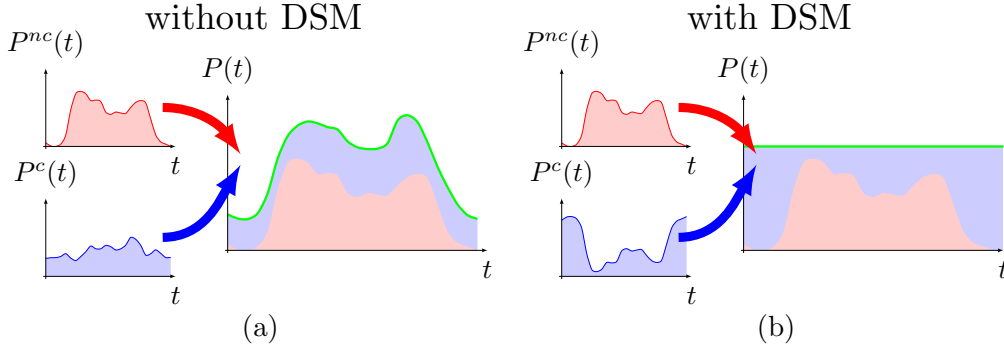


Figure 4.1: Graphical representation of  $P(t)$  signal as a sum of  $P^{nc}(t)$  and  $P^c(t)$  signals, where: a) represents the current electric grid where  $P^c(t)$  is not adapted to  $P^{nc}(t)$  and b) represents the proposed algorithm goal where  $P^c(t)$  is adapted to  $P^{nc}(t)$  in order to smooth  $P(t)$ .

smoothed. To achieve this goal,  $P^c(t)$  should be adapted to  $P^{nc}(t)$ —see Figure 4.1b. This adaptive process is the main challenge addressed by the proposed algorithm in this part of the Thesis. In particular, this process has been approached from the signal processing point of view. In general, the consumption of an electrical grid behaves periodically and, thus, there is a number of very prominent frequency components. Figure 4.2 shows the typical spectrum of the non-controllable consumption in an electrical grid. This spectrum has been obtained from the aggregated consumption of Spain during 2013<sup>1</sup>. It is similar for different countries and different years. The main frequency component of the aggregated consumption has a period of 24 hour (one day). Another prominent components are found for 12 hour period (half day) or 168 hour period (one week). Hence, this periodicity may be used to adapt  $P^c(t)$  to  $P^{nc}(t)$ .

Through the *Fourier* series, the consumption signals may be represented as a sum of sinusoidal functions plus an error term:

$$P(t) = \sum_{n=1}^N A_n \sin(n\omega_0 t + \phi_n) + e(t) \quad (4.2)$$

$$P^{nc}(t) = \sum_{n=1}^N A_n^{nc} \sin(n\omega_0 t + \phi_n^{nc}) + e^{nc}(t) \quad (4.3)$$

<sup>1</sup> The source of this data is *Red Eléctrica Española* (R.E.E)([www.ree.es](http://www.ree.es)).

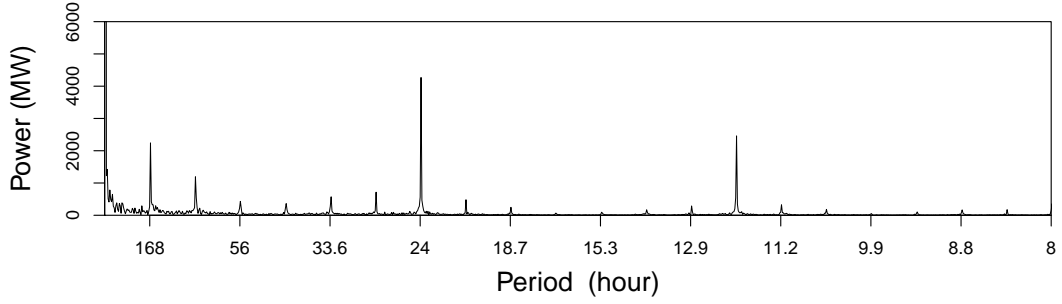


Figure 4.2: Spectrum example of the non-controllable consumption. This spectrum has been calculated by the aggregated consumption of Spain during 2013.

$$P^c(t) = \sum_{n=1}^N A_n^c \sin(n\omega_0 t + \phi_n^c) + e^c(t) \quad (4.4)$$

where  $N$  is the number of frequency components in which the signals are decomposed and  $\omega_0$  is the fundamental frequency of the *Fourier* series.  $A_n$ ,  $A_n^{nc}$  and  $A_n^c$  are the amplitudes of the frequency component  $n$  for all three signals.  $\phi_n$ ,  $\phi_n^{nc}$  and  $\phi_n^c$  are the phases of the frequency component  $n$  for all three signals.  $e(t)$ ,  $e^{nc}(t)$  and  $e^c(t)$  are the error terms of the aggregated consumption, the non-controllable consumption and the controllable consumption respectively.

Once  $P(t)$ ,  $P^{nc}(t)$  and  $P^c(t)$  are divided in sinusoidal functions, the problem can be taken apart. The relationship between the sinusoidal functions of the aggregated consumption, the non-controllable consumption and the controllable one can be established by combining equations 4.1, 4.2, 4.3 and 4.4 as:

$$A_n \sin(n\omega t + \phi_n) = A_n^{nc} \sin(n\omega t + \phi_n^{nc}) + A_n^c \sin(n\omega t + \phi_n^c) \quad (4.5)$$

Notice that all three sinusoidal functions of Equation 4.5 have the same frequency. This is applied separately to each sinusoidal function that composes the Fourier series. It implies that the amplitudes and phases of  $P(t)$  can be expressed as a combination of the amplitudes and phases of  $P^{nc}(t)$  and  $P^c(t)$ , so that:

$$A_n = \sqrt{[A_n^{nc} \cos(\phi_n^{nc}) + A_n^c \cos(\phi_n^c)]^2 + [A_n^{nc} \sin(\phi_n^{nc}) + A_n^c \sin(\phi_n^c)]^2} \quad (4.6)$$

$$\phi_n = \tan^{-1} \left[ \frac{A_n^{nc} \sin(\phi_n^{nc}) + A_n^c \sin(\phi_n^c)}{A_n^{nc} \cos(\phi_n^{nc}) + A_n^c \cos(\phi_n^c)} \right]$$

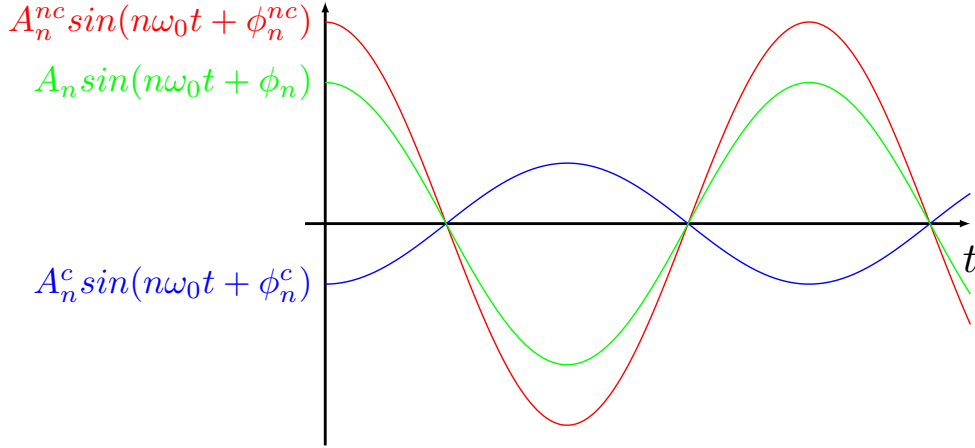


Figure 4.3: Relationship between sinusoidal functions of  $P(t)$  (green),  $P^{nc}(t)$  (red) and  $P^c(t)$  (blue).

Figure 4.3 shows an example of how the relationship of amplitudes and phases of  $P^{nc}(t)$  and  $P^c(t)$  affects the amplitudes and phases of  $P(t)$ . In this example, the phases of the controllable and non-controllable consumption signals are in counterphase, so  $\phi_n^{nc} = -\phi_n^c = \pi/2$  and the amplitudes are  $A_n^{nc} = 15$  and  $A_n^c = 5$ . Satisfying Equation 4.6, the resulting phase and amplitude of  $P(t)$  are  $\phi_n = \phi_n^{nc}$  and  $A_n = 10$ . Notice that the amplitude of the aggregated consumption is lower than the amplitude of the non-controllable consumption because the controllable consumption sinusoidal function is in counterphase. This procedure may be applied to every sinusoidal function of the Fourier series. The proposed algorithm should be able to modify  $A_n^c$  and  $\phi_n^c$  of the sinusoidal functions of  $P^c(t)$  in order to reduce the amplitudes of the sinusoidal functions of  $P(t)$ . The reduction of all  $A_n$  implies the aggregated consumption smoothing.

Dividing the grid in two parts, as in the Equation 4.1, is only a conceptual division. An electrical grid is a system with many interconnected consumers. These consumers are called facilities in this Thesis because of the technical nature of this study. Thus, the aggregated consumption signal can be represented as the sum of all facilities in the grid, such that:

$$P(t) = \sum_{i=1}^M p_i(t) \quad (4.7)$$

---

where  $M$  is the number of facilities in the electrical grid and  $p_i(t)$  is the consumption signal of the facility  $i$ . In turn, the consumption of a local facility can also be divided in controllable and non-controllable, so that:

$$p_i(t) = p_i^c(t) + p_i^{nc}(t) \quad (4.8)$$

where  $p_i^c(t)$  and  $p_i^{nc}(t)$  are the controllable and non-controllable consumption of the local facility  $i$  respectively. Figure 4.4 shows an example of two local facilities which are divided in two signals. The sum of all facilities composes the aggregated consumption. In addition, the controllable and non-controllable consumption of the electrical grid can be represented as the sum of these parts in the local facilities, such that:

$$P^c(t) = \sum_{i=1}^M p_i^c(t) \quad P^{nc}(t) = \sum_{i=1}^M p_i^{nc}(t) \quad (4.9)$$

This Equation implies that by modifying the shape of  $p_i^c(t)$ , the Fourier series of  $P^c(t)$  may also be modified. The algorithm proposed in this Thesis is based on making the local controllable consumptions behave as sinusoidal functions. Thanks to this behavior, different facilities may consume shaping different sinusoidal functions with different frequencies and phases. Thus, the summation of  $p_i^c(t)$  may be approximately equivalent to the Fourier series.

It is important to emphasize that the modification of  $p_i^c(t)$  by the proposed algorithm must be performed locally, because of the distributed nature of the proposed mechanism. It implies that in each facility there is an instance of the algorithm. It receives certain information from the grid or other facilities. This information should be enough to coordinate all consumption managed by the algorithm which is spread over the whole grid. In this Thesis, this information exchange is minimized, satisfying two constraints at the same time: i) there is no explicit information exchange between facilities and ii) the information from the grid is reduced to a single signal. To satisfy these constraints, techniques of collective systems have been used, which has not previously been used in this field. In particular, the development of the algorithm has been based on two theoretical pillars: i) the *Coupled Oscillators* that are the ground of the collective synchronization and ii) the *Swarm Intelligence* that is the ground of the cooperative behavior between distributed individuals.

The remainder of this Chapter is organized as follows. In Section 4.1, an historic overview of coupled oscillator background is presented. The Kuramoto model and further studies, which are required to understand the theoretical base of the proposed algorithm, are explained. In Section 4.2, the background of swarm intelligence

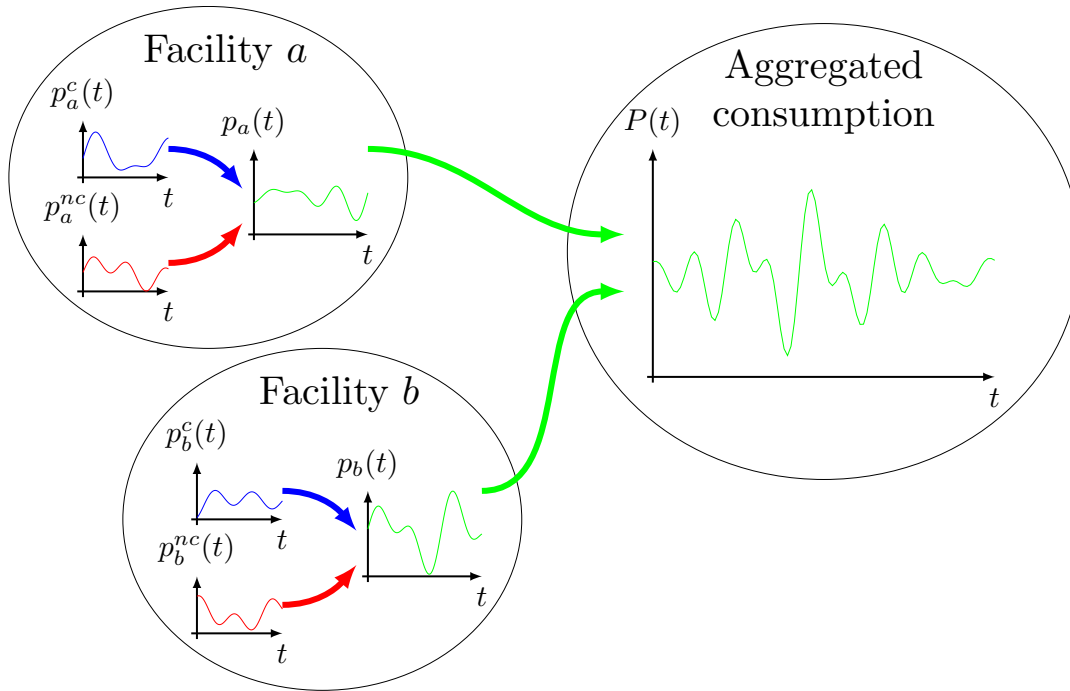


Figure 4.4: Conceptual scheme of an electrical grid divided in local facilities. There are two facilities  $a$  and  $b$  which are added to compose the aggregated consumption. Both facilities are divided in two parts: the non-controllable consumption in red lines and the controllable consumption in blue lines.

is presented. Two main theoretical concepts are explained: *self-organization* and *stigmergy*. In addition, the division of labor and task allocation of eusocial societies are explained in detailed in Section 4.2.2. This collective behavior, studied in the swarm intelligence framework, is paramount in the cooperative behavior of the proposed algorithm. Finally, in Section 4.3, a discussion about the use of these techniques is presented.

## 4.1 Coupled Oscillators

There is a wide variety of collective synchronization phenomena in which a system composed by tens, hundreds or even thousands of elements suddenly locks to a common phase causing that the collective oscillates in unison. These phenomena have

## 4.1. Coupled Oscillators

---

been observed since antiquity in the biological world through the behavior of plants and animals, for example, the migration of birds which are synchronized with the climatic cycles or the leaves of some plants species that open during the day and close at night. These observations continue nowadays, such as: networks of pacemaker cells in the heart (Michaels et al., 1987), circadian pacemaker cells in the suprachiasmatic nucleus of the brain (Liu et al., 1997), flashing fireflies (Buck, 1938, 1988), crickets that chirp in unison (Walker, 1969), etc. The synchronization phenomena may not only be found in biology, but in physics and engineering. There are also several examples of this “inanimate” synchronization, e.g.: arrays of lasers (Jiang and McCall, 1993; Glova, 2003), microwave oscillators (York and Compton, 1991), superconducting Josephson junctions (Wiesenfeld et al., 1996), etc.

The discovery of the “inanimate” synchronization happened by serendipity. It dates back to 1665 thanks to the physicist Christian Huygens as explained in detail in Strogatz (2003). Huygens had invented the pendulum clock in 1656 (Bennett et al., 2002), inspired by investigations of pendulums by Galileo Galilei beginning around 1602. With the pendulum clock help, he hoped to solve the problem of determining longitude at sea, a crucial aspect both for cartography and for ocean navigation since the *XVI* century. He had the two most accurate pendulum clocks at that time. One day, while performing some tests, he noticed that the two pendulums were oscillating in perfect synchrony.

Over the next weeks Huygens conducted a series of experiments to explore what might be causing this synchrony. His first guess was that the clocks were communicating through the air; he was wrong. Huygens then suspected that the clocks might be interacting through vibrations of their common support. To investigate this possibility, he hanged both clocks on separate planks. At the same time, he placed both planks on top of two chairs positioned back to back. Again the clocks synchronized. He disrupted their synchrony and the chairs began to shake. They continued to shake until the synchrony restored itself and the chairs stopped vibrating. Figure 4.5 shows a sketch of this experiment setup which has been further replicated (Bennett et al., 2002). In this case, the chairs, the planks and the clock structure are considered as a common support which allows the vibration propagation. The states of the pendulums are characterized by their phases,  $\theta_A$  and  $\theta_B$  in the instance of Figure 4.5. Both pendulums are synchronized if  $\theta_A = \theta_B$ .

Huygens concluded that the oscillations of the pendulum of the clocks imparted a slight movement to the planks, which shook the chairs. But when the clocks were

#### 4. Grid framework background

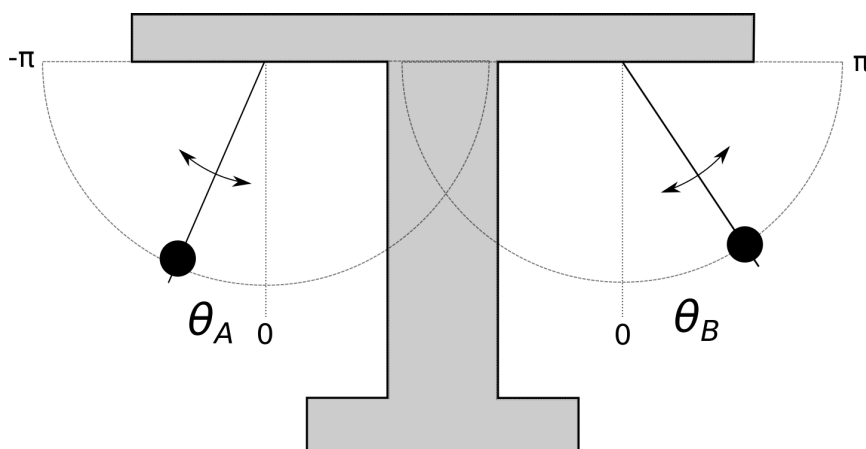


Figure 4.5: Sketch of the two coupled pendulums. They are hung on a common support that propagate the movement vibrations. The phases of both pendulums are  $\theta_A$  and  $\theta_B$  when the pendulums are synchronized it is satisfied that  $\theta_A = \theta_B$ .

in synchrony, the equal and opposite forces they exerted on the planks canceled each other out, which allowed the chairs to keep still. As Huygens wrote:

“Once the consonance is achieved the chairs will not move any more, only preventing the clocks from leaving [the state of synchrony], since as soon as they try to do that, the small movement of the chairs restores them to the previous position.”

*Christian Huygens, 1665*

Huygens had just defined the concept of stabilization by negative feedback and, at the same time, he had discovered the inanimate synchronization.

The study of the inanimate synchronization brings us to an important conclusion: the synchronization does not only originate from intelligence or life systems, but it also originates from the laws of mathematics and physics. Despite the discovery of Huygens, the collective synchronization is not rigorously studied until the mid 20th century. Wiener was the first to mathematically study the collective synchronization (Wiener, 1958). But his mathematical approach based on Fourier integrals was not successful. Some years later, in 1967, Winfree formulated the collective synchronization problem in terms of a population of limit cycles oscillators. It was a novel proposal focused on biological oscillators (Winfree, 1967):

## 4.1. Coupled Oscillators

---

“The impressive variety of biological rhythms leaves no doubt that autonomously periodic processes contribute to the coordination of life-processes. The question here raised is, What modes of temporal organization – if any – could result from weak interactions in a population of innately oscillatory devices (e.g. electronic oscillators, secretory cells, spontaneously active neurons, or individual animals)?”

*Arthur T. Winfree, 1967*

He took some assumptions and developed the following model for the biological oscillators:

$$\dot{\theta}_i = \omega_i + \left( \sum_{j=1}^N X(\theta_j) \right) \cdot Z(\theta_i) \quad (4.10)$$

where  $\theta_i$  is the phase of the oscillator  $i$ ,  $\dot{\theta}_i$  is the derivate of the phase,  $\omega_i$  is its natural frequency and  $N$  is the population of oscillators. This equation represents the phase variation of the oscillator  $i$ . It depends on the oscillator natural frequency, as in any non coupled system. Additionally, it depends on the phase of all other oscillators through the  $X(\theta_j)$  function. The effect produced by these external phases  $\theta_j$  depends in turn on the sensitive function  $Z(\theta_i)$ . Using numerical simulations and analytical approximations, Winfree discovered that such oscillator populations could exhibit the temporal analog of a phase transition.

In 1975, Kuramoto published his first paper about coupled oscillators and synchronization (Kuramoto, 1975)<sup>2</sup>. This was the first of a series of publications from which the *Kuramoto model* arises. This model is based on the study of chemical oscillators. Kuramoto established a phase description of systems of many limit cycle oscillators, as Winfree did. He showed that for any system with nearly identical weakly coupled oscillators, the long-term dynamics are given by phase equations of the following universal form:

$$\dot{\theta}_i = \omega_i + \sum_{j=1}^N \Gamma_{ij}(\theta_j - \theta_i) \quad i = 1, \dots, N \quad (4.11)$$

where  $\Gamma_{ij}$  is the coupling function that defines the effect of the group of oscillators on a single one. This equation is generally impossible to treat analytically. Therefore, Kuramoto considered a soluble model where the coupling  $\Gamma_{ij}$  and the distribution

---

<sup>2</sup> Kuramoto often uses the term *entrainment* to refer to synchronization.

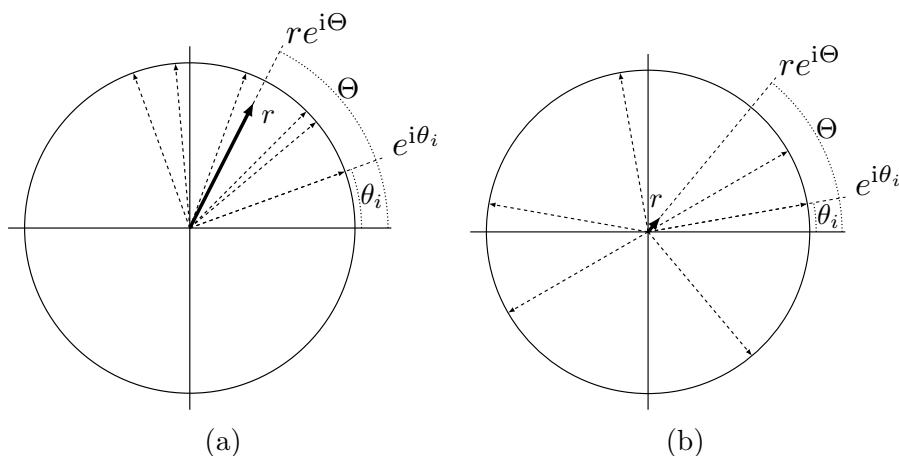


Figure 4.6: Oscillators and order parameter representation on the unit circle in two different situations: a) oscillator phases are close performing a coherent state where  $r \approx 1$  and b) oscillator phases are scattered around the circle performing an incoherent state where  $r \approx 0$ .

of the natural frequencies  $\omega_i$  are given by some simple functions. Taking this into account, he established that  $\Gamma_{ij}$  is identical for all pairs  $(i, j)$  and have a magnitude of order  $N^{-1}$ . This property ensures that the coupling strength experienced by each oscillator is independent of the total number  $N$ . The coupling function of Equation 4.11 was simplified by:

$$\Gamma_{ij}(\theta_i - \theta_j) = \frac{1}{N} \Gamma(\theta_j - \theta_i) \quad \forall i, j \quad (4.12)$$

where  $\Gamma$  is the coupling function when it is identical for all pairs  $(i, j)$ . Furthermore, Kuramoto took a simple trigonometric function to represent the coupling function. The resulting phase variation equation was:

$$\dot{\theta}_i = \omega_i + \frac{K}{N} \sum_{j=1}^N \sin(\theta_j - \theta_i) \quad i = 1, \dots, N \quad (4.13)$$

where  $K \in \mathbb{R}$  is the coupling strength. This equation explicitly defines the phase relationship of each oscillator with others.

Up to this point, it has been defined how the oscillator phases vary, but they have not been treated as a collective. A parameter to assess the synchronization status of the full collective may be defined. This parameter is the *order parameter*, in analogy to

## 4.1. Coupled Oscillators

---

the thermodynamic phase transitions (Kuramoto, 1984). It is a macroscopic quantity that can be interpreted as the collective rhythm produced by oscillators (Strogatz, 2000). Oscillator phases may be represented on a unit circle so that the oscillator phases are unit length vectors. These vectors start from the origin and their tilts represent the oscillator phases, as shown in Figure 4.6. The order parameter is defined in terms of the oscillator phases, according to the following equation:

$$r \cdot e^{i\Theta} = \frac{1}{N} \sum_{j=1}^N e^{i\theta_j} \quad (4.14)$$

where  $r$  is the phase coherence,  $\Theta$  is the average phase and  $i$  is the imaginary unit. Returning to the representation in the unit circle, the order parameter is the average of the oscillator vectors, as shown in Figure 4.6 with bold arrows. The synchronization of a collective of oscillators can be assessed by  $r$  which is in the range  $[0, 1]$ . If all oscillators have their phases close,  $r \approx 1$ ; the sum of individual oscillations perform a coherent state and the collective oscillates in unison. Figure 4.6a shows an example of this situation. On the other hand, if the oscillators are scattered around the circle,  $r \approx 0$ ; the sum of individual oscillations perform an incoherent state and no macroscopic effects are appreciable. Figure 4.6b shows an example of this situation.

The Kuramoto model can be rewritten by means of the order parameter, multiplying both sides of Equation 4.14 by  $e^{-i\theta_i}$ :

$$r \cdot e^{i(\Theta - \theta_i)} = \frac{1}{N} \sum_{j=1}^N e^{i(\theta_j - \theta_i)} \quad (4.15)$$

It is an equality of complex numbers. Taking the imaginary parts:

$$r \cdot \sin(\Theta - \theta_i) = \frac{1}{N} \sum_{j=1}^N \sin(\theta_j - \theta_i) \quad (4.16)$$

By combining this equation with Equation 4.13:

$$\dot{\theta}_i = \omega_i + K \cdot r \cdot \sin(\Theta - \theta_i) \quad (4.17)$$

Although this equation represents mathematically the same as Equation 4.13, it has a practical implication which is exploited in this Thesis. Due to the fact that the coupling depends on the order parameter and not on the phase of every oscillator, the synchronization of the full collective may be achieved without explicit communication between each of the oscillators, as explained in detail in Chapter 5.

### 4.1.1 Oscillators as signals

At this point of this Section, the explanation has focused on the coupling between oscillators without specifically defining what an oscillator is. At the beginning of this Section, the oscillators were the pendulums of the clock of Huygens. Later, the oscillators became biological elements representing the coordination of life-processes, as Winfree exposed. And finally, oscillators have been used to represent chemical phenomena through the Kuramoto studies. In general, an oscillator represents a system which can be characterized by a state variable that varies periodically.

In this Thesis, oscillators are approached from a systemic point of view. Their outputs are considered as signals that vary periodically in time.  $x_i^{osc}(t)$  represents the output signal of the oscillator  $i$ . Due to the fact that these signals are periodic, they satisfy that  $x_i^{osc}(t) = x_i^{osc}(t + T_i)$  where  $T_i$  is the period of the oscillator  $i$ . For simplicity, these signals are presented as sinusoidal functions, such that:

$$x_i^{osc}(t) = \sin(\theta_i(t)) \tag{4.18}$$

$$\theta_i = \omega_i t + \phi_i(t)$$

where  $\omega_i = 2\pi/T_i$  is the natural angular frequency of the oscillator  $i$  and  $\phi_i(t)$  is the phase difference compared to a reference phase. In this case, a collective of oscillators is a set of signals which are differentiated by their natural angular frequency and phase differences.

The synchronization between oscillators affects the behavior of the collective which leads to macroscopic effects. An example of these macroscopic effects is a crowd clapping at the end of a performance (Néda et al., 2000). The audiences begin clapping disorderly and, suddenly, they synchronize by increasing the intensity of the applause. This intensity may be observed as a macroscopic effect of the synchronization phenomenon. In the signal representation, the macroscopic effect stands for a *signal superposition* that can be observed through the aggregated (or resulting) signal. Figure 4.7 shows a sketch of the macroscopic effect of this signal superposition. The aggregated signal  $s(t)$  is the sum of the output signals of the oscillators:

$$s(t) = \sum_{i=1}^N x_i^{osc}(t) \tag{4.19}$$

The shape of  $s(t)$  depends on the phase relationship of the output signals of all oscillators. In analogy to wave interference, a coherent state of the collective of

## 4.1. Coupled Oscillators

---

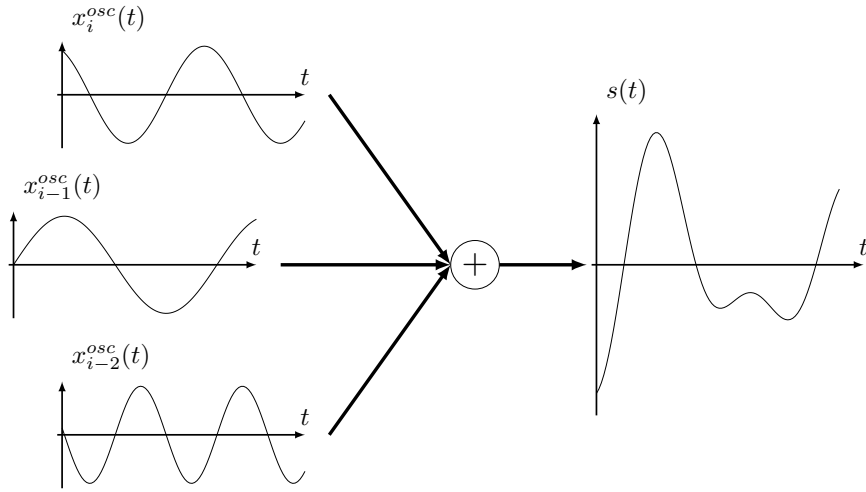


Figure 4.7: Sketch of the wave interference as sum of signals, where  $x_i^{osc}(t)$  are the output signals of the oscillators and  $s(t)$  is the resulting or aggregated signal.

oscillator ( $r(t) \rightarrow 1$ ) corresponds to a *constructive interference*. It means that all signals have the same phase and the amplitude of  $s(t)$  is the sum of all signal amplitudes. On the other hand, an incoherent state ( $r(t) \rightarrow 0$ ) corresponds to a *destructive interference*. It means that the signals are in phase opposition and the amplitude of  $s(t)$  is zero.

The shape of the aggregated signal  $s(t)$  is directly affected by the coupling of the oscillators because it modifies the phase relationships. The following equation defines the coupling for the signal representation, which is based on the Kuramoto model:

$$\begin{aligned}\dot{\theta}_i &= \omega_i + \dot{\phi}_i(t) \\ \dot{\phi}_i(t) &= K \cdot r \cdot \sin(\Theta - \theta_i)\end{aligned}\tag{4.20}$$

$$\phi_i(0) \in [-\pi, \pi]$$

The coupling performs a phase modulation through this representation. In general, the initial phases of every oscillator may take any phase value. The initial phase distribution defines the initial coherence of the collective of oscillators. For example, if the initial phases are the same for every oscillator ( $\phi_i(0) = \phi_0, \forall i$ ) the collective

#### 4. Grid framework background

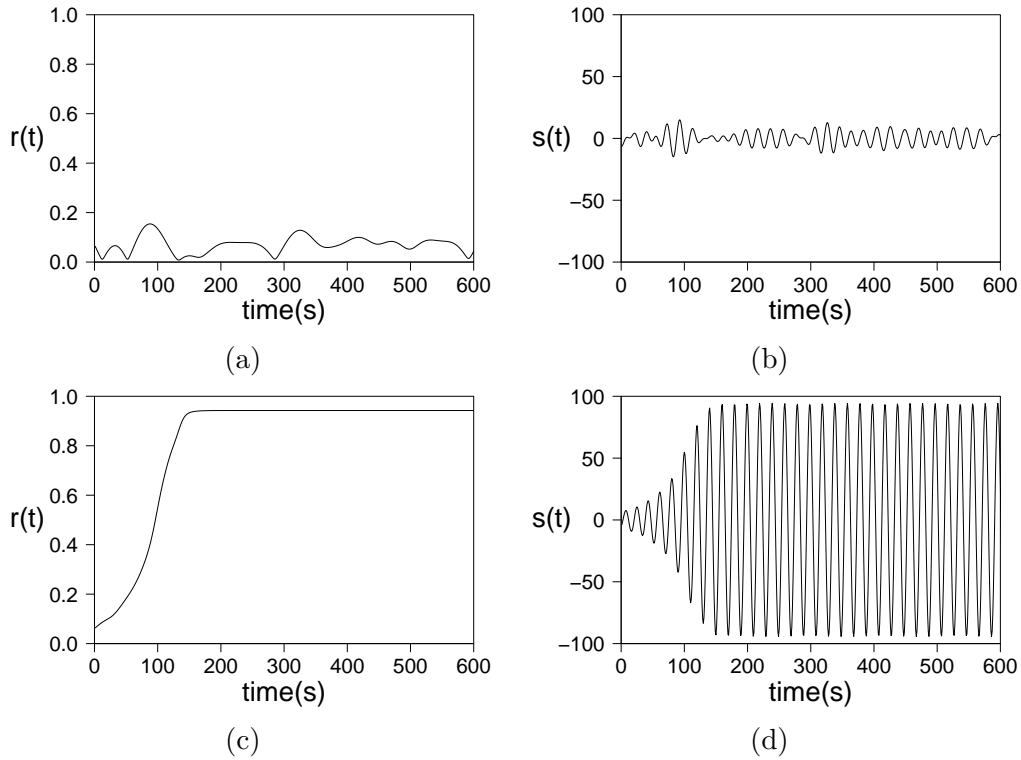


Figure 4.8: Example of oscillator coupling from their output signals for  $N = 100$ ,  $\omega_i$  randomly distributed following a Gaussian density function with a central frequency  $\omega_c = 2\pi \cdot 0.05$  and a variance of  $\sigma^2 = 0.005$  and initial phases uniformly distributed  $\in [-\pi, \pi]$ : a)  $r(t)$  and b)  $s(t)$  development in time for  $K = 0$  (no coupling) and c)  $r(t)$  and d)  $s(t)$  development in time for  $K = 0.1$ .

begins fully synchronized ( $r(0) \rightarrow 1$ ). This situation implies that the amplitude of the aggregated signal will be the amplitude of the sum of all signals.

Figure 4.8 shows an example of oscillator coupling. This example consists of two experiments with a collective of oscillators with and without coupling. These oscillators are executed during a time interval of 600s and their aggregated signal and phase coherence are plotted in the graphs. There are  $N = 100$  oscillators with  $\omega_i$  randomly distributed following a Gaussian density function. The initial phases are uniformly distributed in the phase circle. This phase and frequency distribution provokes a low coherence at the beginning of the experiments. Figure 4.8a

## 4.1. Coupled Oscillators

---

shows the development of  $r(t)$  in time without coupling. It maintains low values during the experiments because the initial phase and frequency distribution and the lack of synchronization. The development of  $s(t)$  without coupling is shown in Figure 4.8b. Corresponding to  $r(t)$ ,  $s(t)$  takes low values during the whole experiment. The coupling turns this situation around. Figure 4.8c shows the development of  $r(t)$  during the experiment with coupling. It takes low values at the beginning of the experiments but it rapidly increases its value reaching full synchronization ( $r \approx 1$ ). This synchronization is also evident in the development of  $s(t)$ , as shown in Figure 4.8d.  $s(t)$  behaves as a “big” single oscillator as in a constructive interference, increasing its amplitude to values close to 100 which corresponds to the number of oscillators.

Kuramoto assumed that the coupling strength  $K$  is positive, synchronizing the oscillator phases. In the previous example, where oscillators were signals, the positive coupling provokes a constructive interference. From the signal point of view, it is obvious to ask whether it is possible to get a destructive interference, or, in other words, an incoherent state of the oscillator phases. This incoherent state may be achieved through a negative coupling. In Tsimring et al. (2005) the authors investigate the dynamics of repulsively coupled phase oscillators. They conclude that the system dynamics converge to a regime that minimizes the mean field (regarding the phase coherence). Therefore, the Kuramoto model may be used to achieve an incoherent state of the phases of the oscillators.

In Hong and Strogatz (2011b) the authors studied a system where there are two groups of qualitatively different oscillators. In the first group, oscillators have positive coupling and they are called “conformists”. In the second group, oscillators have negative coupling and they are called “contrarians”. In this study, the authors modified the proportion of “conformists” and “contrarians” in a collective of oscillators and conclude that the collective always settles into one of three kinds of long-term behavior: i) *incoherent state*, the oscillators are completely desynchronized, ii)  $\pi$  *state*, the “conformists” converge to a partially synchronized state and iii) *traveling wave state*, the phase distributions spontaneously travel at constant speed, maintaining a constant separation. By continuing the idea of two groups of qualitatively different oscillators, the same authors published a few months later a study in which all oscillators are assumed to have the same natural frequency (Hong and Strogatz, 2011a). Curiously, this system of oscillators exhibit more complicated dynamics than a system with heterogeneous natural frequencies.

#### 4. Grid framework background

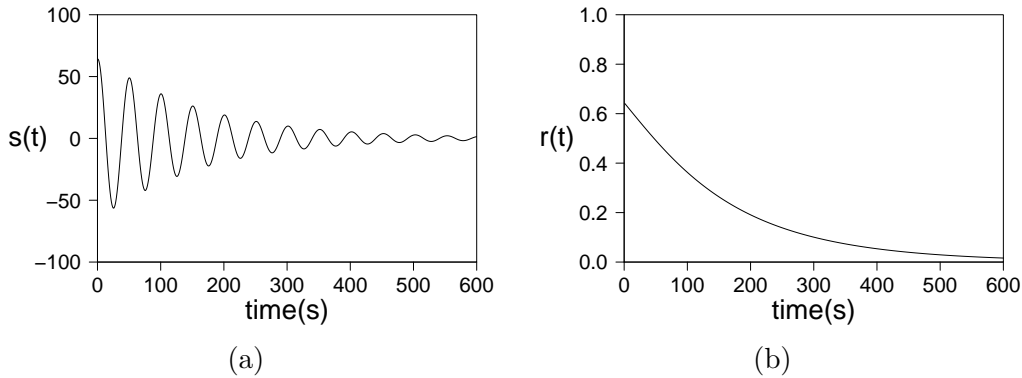


Figure 4.9: Example of oscillator coupling from their output signals with negative coupling  $K = -0.01$  for  $N = 100$ , common natural angular frequency of  $\omega_i = 2\pi \cdot 0.05\forall i$  and initial phases uniformly distributed  $\in [-\pi/2, \pi/2]$ : a)  $r(t)$  and b)  $s(t)$  development in time.

Concretely a new stable state appears: the *blurred  $\pi$  state*, corresponding to non uniformly distributed populations of conformist and contrarians in the unit circle.

The incoherent state is of special interest for the development of this Thesis. Back to the signal example, an incoherent state avoids macroscopic effects in the aggregation of signals provoking a destructive interference. Figure 4.9 shows an example of oscillators with negative coupling. The procedure is the same as in the example of Figure 4.8 with the only difference that there is a common natural angular frequency for all oscillators. The initial phases are uniformly distributed in the range  $[-\pi/2, \pi/2]$  in order to have high initial phase coherence, being easier to see the negative coupling effect. Figure 4.9a shows the development of  $r(t)$  during the experiment. It takes high values at the beginning of the experiments but rapidly decreases its value reaching an incoherent state ( $r \approx 0$ ). This effect is also observed in the development of  $s(t)$ , as is shown in Figure 4.9b. The amplitude of  $s(t)$  is reduced from the beginning of the experiment until it reaches zero. The negative coupling allows to remove the aggregated signal of a set of signals. It can be used as a filter of frequency components in a distributed framework, as will be explained in detail in Chapter 5. This frequency filter approach is used to develop consumption patterns which can be used by the consumers of the grid to smooth the aggregated consumption—see Chapter 6.

## 4.2. Swarm intelligence

---

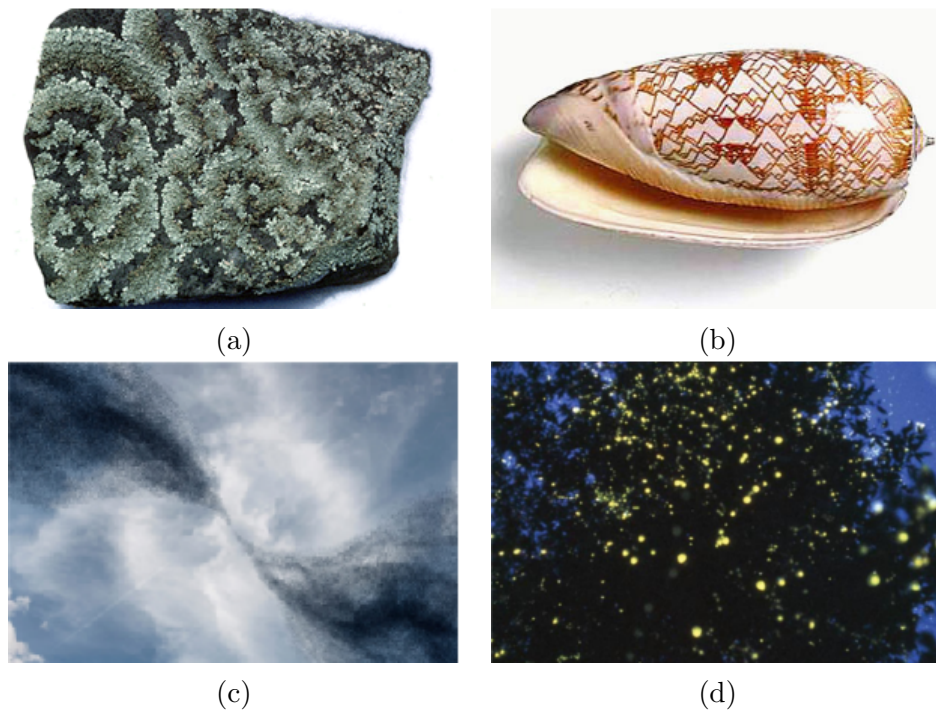


Figure 4.10: Self-organization examples in biological systems: a) lichen growth, b) pigmentation pattern of a porphyry olive shell (*Olivia porphyria*), c) birds flocking and d) fireflies synchronization.

## 4.2 Swarm intelligence

Swarm intelligence was born from biological insights about the abilities of eusocial animal species, mainly social insects, to organize and adapt to the environment. It is based on the study of self-organized behaviors of these species. Self-organization is a set of dynamical mechanisms whereby structures appear at the global level of a system from interactions among its lower-level components, without being guided or managed by a supervising entity (Garnier et al., 2007). Examples of self-organization in biology can be found in lichen growth (Camazine et al., 2003) (Figure 4.10a), pigmentation pattern on shells (Meinhart, 2009) (Figure 4.10b), the flocking of birds (Emlen, 1952) (Figure 4.10c) or the fireflies synchronization (Buck, 1938, 1988) (Figure 4.10d). In Bonabeau et al. (1999) the authors state that self-organization relies on four basic ingredients:

## 4. Grid framework background

---

- *Positive feedback*: it is a process in which the effects of a small disturbance on a system provokes an increase in the magnitude of the perturbation. In the context of swarm intelligence, it is typically composed by simple behavioral rules that promote the creation of structures.
- *Negative feedback*: it occurs when the result of a process influences the operation of the process itself in such a way as to reduce changes. It helps to stabilize the collective pattern: it may take the form of saturation, exhaustion, or competition.
- *Randomness*: a random process is a repeating process where its outcomes do not follow a deterministic pattern. Not only do structures emerge despite randomness, but randomness is often crucial, since it enables the discovery of new solutions, and fluctuations can act as seeds from which structures nucleate and grow.
- *Multiple interactions*: self-organization requires multiple interactions among individuals to apparently produce deterministic outcomes and the appearance of large and enduring structures.

In Garnier et al. (2007) the authors state that self-organization may also be characterized by four key properties:

- *Self-organized systems are dynamic*: the production of structures as well as their persistence requires permanent interactions between the members of the swarm and with their environment.
- *Self-organized systems exhibit emergent properties*: they display more complex properties than the simple contribution of each agent. These properties arise from the nonlinear combination of the interactions between the members of the colony.
- *Self-organized systems may have multiple stable states*: the system can reach different stable states depending on the initial conditions and on the random fluctuations.
- *Self-organized systems have bifurcations*: a bifurcation is the appearance of new stable solutions when some of the system parameters change. This change corresponds to a qualitative modification in the collective behavior.

## 4.2. Swarm intelligence

---

A self-organized system requires interactions between its composing elements. In the case of swarm intelligence, the interactions between individuals are paramount for the performance of a collective behavior. These interactions may be both direct and indirect. Direct interaction occurs when there is an explicit information exchange between individuals: antennation, trophallaxis, mandibular contact, visual contact, chemical contact, etc. Indirect interaction occurs when one individual modifies the environment and other responds to the new environment at a later time: this interaction is called *stigmergy*. It is one of the most important theoretical concepts of swarm intelligence.

### 4.2.1 Stigmergy

In [Theraulaz and Bonabeau \(1999\)](#) the authors divided the stigmergy in two types: quantitative stigmergy and qualitative stigmergy. With quantitative stigmergy, the stimulus-response sequence comprises stimuli that do not differ qualitatively and do only modify the probability of response of the individuals to such stimuli (as pheromone fields and gradients). Qualitative stigmergy differs from quantitative stigmergy in that individuals interact through, and respond to, a discrete set of stimuli which are not quantifiable as the shape of different objects or different smells. Note that stigmergy only refers to interactions between individuals, thus it has to be supplemented with an additional mechanism that makes use of these interactions to coordinate and regulate the collective behavior in a particular way. For this reason, two examples of both stigmergy types are presented below along with two of the best known collective behaviors of social insects: ants foraging and nest building.

An example of quantitative stigmergy can be observed in the *ants foraging*. This collective behavior is defined as the ability to find, select and exploit food resources, which is crucial for the survival of the colony ([Deneubourg et al., 1990](#); [Camazine et al., 2003](#)). Many species of ants are able to trace paths of hundreds of meters from the nest to a food source. This collective behavior is probably one of the best known examples of stigmergy. The ants are able to trace this path through the use of pheromones. These pheromones are chemical substances that attract other ants ([Hölldobler and Wilson, 1990](#)). Once an ant finds food, it moves from the food source to the nest depositing pheromones. When a forager ant smells the pheromone, it follows the pheromone trail to the food source. The forager ant returns to the nest depositing more pheromone, performing a positive feedback which traces a path between the nest and the food source.

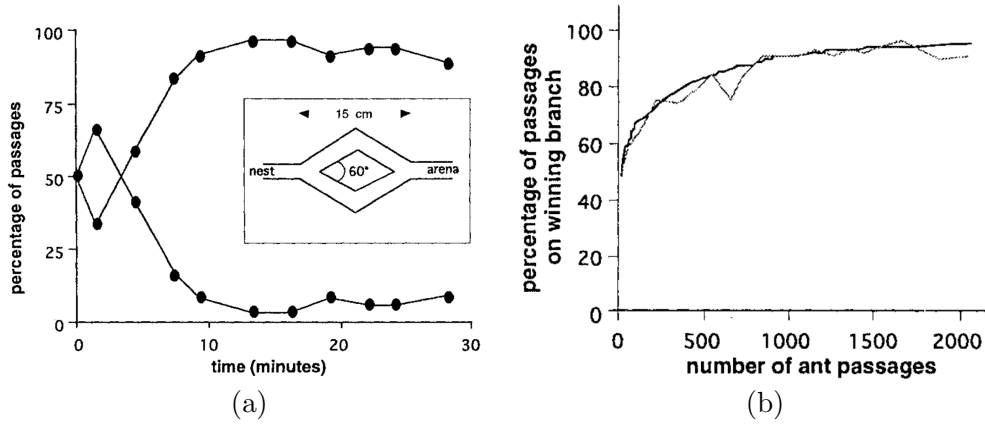


Figure 4.11: Results of the foraging experiment presented in [Deneubourg et al. \(1990\)](#): a) The inset is an schematic representation of the experiment setup with the two bridges and the graph represents the percentage of passages on each bridge along the experiment; b) comparison between the real experiments and Monte Carlo simulations which relates the number of ants and the percentage of passages on the chosen bridge. Source: [Deneubourg et al. \(1990\)](#).

This simple but very successful mechanism was studied in detail in laboratory. This work was presented in [Deneubourg et al. \(1990\)](#). The authors proposed a setup where the food was separated from the nest by two equally long bridges  $A$  and  $B$ —see [Figure 4.11a](#) inset. The bridges are initially chemically unmarked and the ants explore both bridges randomly. However, each ant that crosses a bridge leads a pheromone trail. After initial fluctuations, one of the two bridges becomes to be preferred by the colony. In [Figure 4.11a](#) the percentage of passages for each bridge is shown. This behavior is modeled by a probability function that is dependent on the pheromone intensity; the bridge  $A$  pheromone intensity is denoted by  $A_i$  and  $B_i$  for the bridge  $B$ . The probability that an ant chooses the bridge  $A$  is:

$$P_A = \frac{(k + A)^n}{(k + A)^n + (k + B)^n} = 1 - P_B \quad (4.21)$$

where  $n$  determines the degree of nonlinearity of the choice function and  $k$  quantifies the degree of attraction of an unmarked branch. This model was analyzed by means of Monte Carlo simulations and the results are in perfect agreement with the experiments, as shown in [Figure 4.11b](#).

## 4.2. Swarm intelligence

---

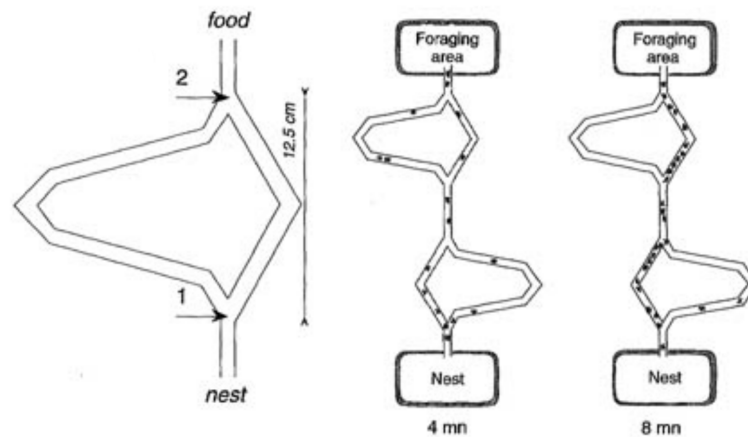


Figure 4.12: Experiment of ant foraging studied in Goss et al. (1989), from left to right: i) schematic representation of the no symmetric bridges, ii) experiment situation after 4 min where the ants have not defined a path and iii) experiment situation after 8 min where the ants have found the shortest path. Source: Goss et al. (1989).

Later, the experiment was extended by increasing the complexity of the bridges. In Goss et al. (1989) the authors presented an experiment where the bridge lengths were not symmetric. Figure 4.12 shows a schematic of the experiment setup where one bridge is considerably longer than the other. By the same mechanism of the previous experiment, the ants trace a pheromone trail from the nest to the food source, but interestingly, the ants choose the shortest path. This choice emerges from the interactions of ants through the quantitative stigmergy from a self-organized way: the ants that choose the shortest path take less time to go from the nest to food and back. This provokes that pheromone intensity in the shortest path increases faster and more ants choose this path. Figure 4.12 shows the experiment situation after 4 min and 8 min, where the swarm chooses the shortest path.

An example of the qualitative stigmergy can be observed in the nest building process. Several species of animals are able to build complex architectures that satisfy multiple functionalities. In Theraulaz and Bonabeau (1995) the authors defined a formal model of distributed building inspired by wasp colonies, concretely in the primitively eusocial wasp *Polistes*. This wasp specie uses long wood fibers and plant hairs that are mixed with salivary secretions, resulting a sort of cardboard which is used to build the nest. A nest consists of a single round shaped comb that can contain

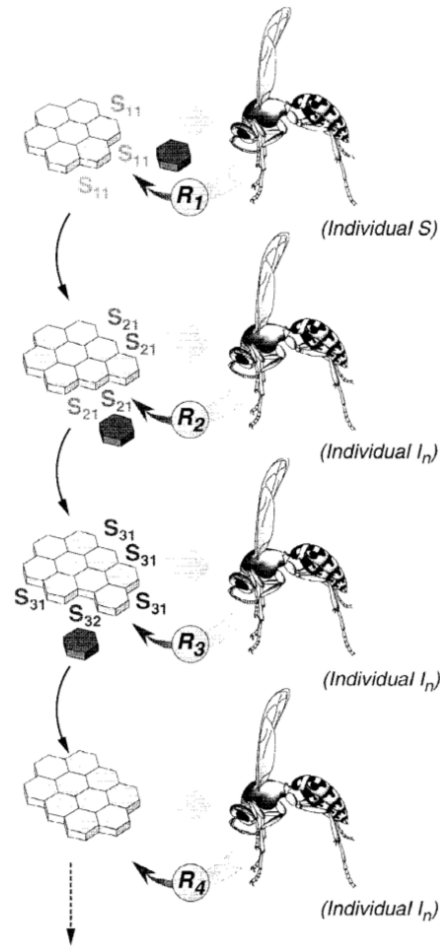


Figure 4.13: Qualitative stigmergy represented by the successive stages leading to the construction of a comb. Each building stage correspond to the addition of a new cell. From top to bottom: i) an individual faces to the pre-existing comb and all possible places for the new cell have the same stimulus ( $S_{11}$ ) and the individual performs the action  $R_1$ , ii) another individual faces to the comb and the new places have the same stimuli  $S_{21}$  provoking the action  $R_2$ , iii) the current structure presents different stimuli because the comb shape  $S_{31}$  and  $S_{32}$ , the individual is stimulated by  $S_{32}$  and performs the action  $R_3$ , iv) the new structure has the same stimuli and the process continues. Source: [Theraulaz and Bonabeau \(1999\)](#).

## 4.2. Swarm intelligence

---

about 150 cells. New cells are added to the comb during nest growth and the number of potential sites where a new cell can be added increases as construction proceeds. In addition, several building actions may take place in parallel. The model proposes that the building process is defined by a set of predefined rules. When an individual approaches to a already built zone, it observes the surrounding area. This individual adds a new cell in its current position if the surrounding area has a specific shape. A graphical example of this process is shown in Figure 4.13. In this model, the stimuli are the actual structure of the nest and the action is to add or not a new cell.

In general, qualitative stigmergy is based on a set of discrete stimuli with a set of discrete actions. For example, when an individual senses a stimulus of type-1, it performs action *A*. Extending this idea to a large number of stimuli and actions, several responses may be defined. Moreover, more complex relationships can be established by considering that actions affect the stimuli of the environment. For example, a stimulus of type-1 provokes that an individual performs action *A* which modifies the environment so that other individual senses a stimulus of type-2 and performs action *B*. Coordination and regulation are more difficult to see in qualitative stigmergy because the feedback loops cannot be analyzed as in quantitative stigmergy.

A wide variety of collective behaviors can emerge from the previously explained self-organization processes and stigmergy. In Garnier et al. (2007) the authors divided the possible collective behaviors in four different sorts which are not mutually exclusive:

- *Coordination*: it is the appropriate organization in space and time of the tasks required to solve a problem. The ant foraging is an example of coordination. The pheromone trails building allows to organize the foraging ants connecting a food source and the nest (Hölldobler and Wilson, 1990). Another coordination example is the birds flocking (Emlen, 1952). In the movements of large groups of birds, they make complex formations in which hundreds or thousands of individuals coordinate.
- *Cooperation*: it occurs when individuals achieve together a task that could not be done by a single one. The individuals must combine their efforts in order to successfully solve a problem that goes beyond their individual abilities. An example of cooperation is the “self-assemblages”, that means the formation of physical structures from the bodies of many individuals (Anderson and Franks, 2001; Anderson et al., 2002).

- *Deliberation*: deliberation refers to mechanisms that occur when a colony faces several opportunities. These mechanisms result in a collective choice for at least one of the opportunities.
- *Collaboration*: it means that different activities are performed simultaneously by groups of specialized individuals. This sort of collective behavior is frame in the division of labor capability of eusocial societies, that is widely explained in the next section.

### 4.2.2 Division of labor and task allocation

Societies of insects can perform different tasks simultaneously, distributing the workload among their individuals. In general, eusocial insect societies show differentiation between individuals, which is reflected in the way collective tasks are organized (Theraulaz et al., 1991). This phenomenon is called division of labor and is one of the most basic and widely studied aspects of colony behavior (Bonabeau et al., 1999; Robinson, 1992). Simultaneous task performance by specialized individuals may be more efficient than the sequential task performance because the task switching is avoided, reducing energy and time costs (Robinson, 2009; Brutschy et al., 2011). A well known example of this phenomenon is the reproductive division of labor: often a single individual, called “queen”, reproduces in a colony and the remaining individuals do not have reproductive capability. Thus, the task allocation in a swarm is characterized by the division of labor and the individuals’ responses to task needs. For instance in Polite wasps, division of labor is based on behavioral castes, and the task allocation process results from a complex set of interactions among insects and the brood state (Theraulaz et al., 1991; Garnier et al., 2007).

In Bonabeau et al. (1999) the authors defined three basic forms of division of labor, which may coexist:

- *Temporal polyethism*: individuals of the same age tend to perform identical sets of tasks. Individuals in the same age class form an *age caste* (Hölldobler and Wilson, 1990). For example, an adult worker of honey bee is performing tasks inside the hive as brood care and nest work during its first 20 days. After this period, it switches to outside tasks as foraging (Wiston, 1987; Beshers et al., 2001).
- *Worker polymorphism*: some species exhibit worker polymorphism where workers have different morphologies. Workers with different morphologies tend

## 4.2. Swarm intelligence

---

to perform different tasks, forming *morphological* or *physical castes* (Hölldobler and Wilson, 1990). An example of a worker caste is the soldier of major caste which is observed in several species of ants (Tschinkel, 1988).

- *Individual variability*: even within an age or morphological caste, differences among individuals in the frequency and sequence of task performance may exist. Individuals that perform the same set of tasks within a given period belong to a *behavioral caste* (Detrain and Pasteels, 1991).

The division of labor often adapts to changes in the environment, becoming the task allocation an elastic behavior. In Wilson (1984), the author experimentally confirmed this behavior. He altered the population ratio of two different morphological castes of some ants species from the *Pheidole* genus: i) the “minors”, which take care of most of the quotidian tasks of the colony and ii) the “major” (often called soldiers), which take care of the swarm defense. Wilson artificially reduces the number of “minors” in the colony and observed a behavioral change of the “major” population. The “major” performed tasks usually performed by the “minors”, replacing the missing population. As Wilson remarked, this individual elasticity determines the resiliency of the colony as a whole, that is, the degree to which the colony responds to environmental alterations through changes in the behavioral repertoires of the constituent castes and individuals.

The study of this collective behavior has originated multiple models in order to understand this resiliency. Division of labor models indicate how individuals are distributed to perform tasks in an appropriate way to the current situation (Gordon, 2002). In Beshers and Fewell (2001) the authors did a complete review of these models. They described six classes of models based on various hypotheses about the causes of division of labor:

- *Response threshold*: response threshold models operate under the assumption that individuals have internal thresholds associated to stimulus intensities. These stimuli are related to specific tasks and may be any environmental information sensed by individuals e.g. pheromone concentration or number of encounters with other individuals (Bonabeau et al., 1999; Theraulaz and Bonabeau, 1999). The probability of acting or the intensity of an action depend on the stimulus intensities and the response thresholds of the individuals (Bonabeau et al., 1998). Thus, differences in these thresholds among individuals in a colony generate division of labor.

#### 4. Grid framework background

---

- *Integrated information transfer:* in [Fewell and Bertram \(1999\)](#) the authors developed an analytical model which they integrated between the questions of how do workers receive information about a task, and how does variation in stimulus perception affect worker task performance. They began with the basic assumption of the threshold model that workers perform a task when the stimulus they encounter matches an intrinsic threshold. Both the threshold distribution for a task and the process by which workers perceived the task stimulus could be varied in the model. However, the integrated information transfer model assumes no explicit genetic effects on task performance.
- *Self-reinforcement:* these models ask whether division of labor can be generated by the effects of experience. Self-reinforcement is a postulated mechanism in which successful performance of a task increases the probability of performing that task again, while unsuccessful performance or lack of opportunity reduces the probability of performance ([Theraulaz et al., 1998](#)). It has been suggested that self-reinforcement can potentially explain the occurrence of specialists and generalists in a wide variety of biological systems ([Spencer et al., 1998](#)).
- *Social inhibition:* social inhibition models explain temporal polyethism as an interaction between an intrinsic process of behavioral development and inhibitory effects of other workers. Thus, these models are concerned with the behavioral state of a worker (the internal physiological state as it relates to task performance) and with the external factor of worker-worker interactions ([Beshers et al., 2001](#); [Huang and Robinson, 1992, 1996](#)).
- *Foraging for work:* this class of models shows how a flexible division of labor with temporal polyethism could emerge from a simple algorithm for individual task performance that is not causally related to worker age or size ([Tofts, 1993](#)). Foraging for work has two main components, a behavioral algorithm for task performance and a spatial arrangement of tasks.
- *Network task allocation:* in [Gordon et al. \(1992\)](#) and [Pacala et al. \(1996\)](#), the authors used models to explore how task allocation and the dynamics of colony behavior can be explained by simple interactions among workers. These models assume no intrinsic differences among workers; instead, changes in task allocation result from simple interactions among workers that effectively communicate information about the number of workers that are active or inactive for a given task.

## 4.2. Swarm intelligence

---

The class of models that has been most extensively studied is the *response threshold* model class. Moreover, other class of models are based on it: the *integrated information transfer* models is based on the distribution of the response thresholds and *self-reinforcement* is often defined as a learning process of a response threshold model as discussed below. In a response threshold model every individual has a response threshold for each possible task that it can perform (Page and Mitchell, 1990). Thus, the likelihood to perform a task depends on an intrinsic parameter of the individual, which is the response threshold, and an extrinsic variable measured from the environment, which is the task-associated stimulus intensity. In general, individuals with a low threshold value have a higher probability to perform a task than individuals with a high threshold value for the same stimulus intensity. From an individual point of view, the higher the task-associated stimulus intensity compared to its threshold, the higher the likelihood to perform such task. In addition, response threshold models establish that the increment of the number of individuals performing a task reduces the stimulus intensity associated to this task (Bonabeau et al., 1996). Therefore, the action of the individuals modifies and is modified by the stimulus intensities, closing a negative feedback loop.

In Bonabeau et al. (1996) the authors defined a response threshold model implementation to emulate the previously explained Wilson experiment. They assumed that only one task is performed by a swarm of  $N$  individuals. There are two castes, characterized by their response threshold to the stimulus intensity, “minors” and “majors”.  $\Theta_1$  is the response threshold for “minors” and  $\Theta_2$  is for “majors”, where  $\Theta_1 < \Theta_2$ . This implies that “minors” have a higher probability to perform the task than the “majors”. The probability to perform the task is:

$$P_i(X_i = 0 \rightarrow X_i = 1) = \frac{s^2}{s^2 + \Theta_i^2} \quad (4.22)$$

where  $s$  is the stimulus intensity and  $X_i$  is a binary state variable which indicates whether the  $i$  individual is working or not.

Figure 4.14a shows an example of the probability of performing the task in relation to the stimulus intensity for “minors” and “majors”. An active individual gives up task performance and becomes inactive with probability  $p$  per unit time. This probability is considered equal for both castes:

$$P(X = 1 \rightarrow X = 0) = p \quad (4.23)$$

#### 4. Grid framework background

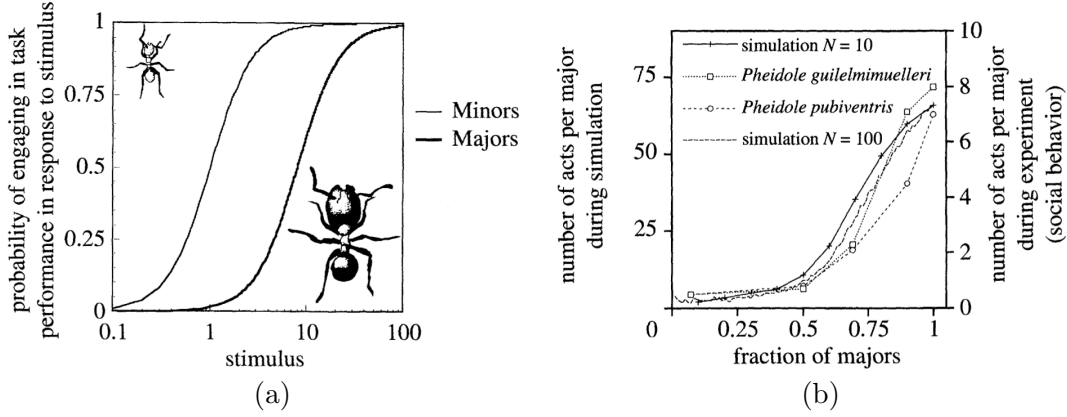


Figure 4.14: The response threshold model presented in Bonabeau et al. (1996): a) the probability of perform the task in relation to the stimulus intensity for “minors” and “majors” and b) comparison between simulations results with  $N = 10$  and  $N = 100$  individuals and the same quantities obtained in experiments reported by Wilson (1984) for *Pheidole guilelmimuelleri* and *Pheidole pubiventris*. Source: Bonabeau et al. (1996).

The stimulus intensity is modified by two factors: i) the number of the individuals performing the task and ii) a natural increase of the task demand  $\delta$ , which is considered constant in this example. The number of individuals performing the task is divided in two groups dependent on the caste;  $N_1$  is the number of “minors” performing the task and  $N_2$  is the number of “majors” performing the task. The stimulus intensity dynamics is defined by the following equation:

$$s(t+1) = s(t) + \delta - \frac{\alpha}{N}(N_1 + N_2) \quad (4.24)$$

where  $\alpha$  is a scale factor measuring the efficiency of task performance. Figure 4.14b shows a comparison between simulations results with  $N = 10$  and  $N = 100$  individuals and the same quantities obtained in experiments reported by Wilson (1984). As the authors of this study mentioned, the qualitative overlap between these curves is striking.

In general, the behavior of a swarm in relation to a certain task is marked by the dynamics of the task-associated stimulus intensity. The swarm may converge to a certain state depending on these dynamics. For instance, Equation 4.24 for a given parameter configuration ( $\Theta_i$ ,  $N$ ,  $\delta$ ,  $\alpha$  and  $p$ ) converges to the solution

## 4.2. Swarm intelligence

---

presented in Figure 4.14b. Another parameter configuration will converge to a different solution and the stimulus intensity will converge to another value. Thus, different dynamical behavior may be represented by a response threshold model as any dynamical system (Guckenheimer and Holmes, 1983). The two most common behaviors are: i) asymptotically stable, the stimulus converges to a certain value that implies that most individuals always take the same decision (perform the task or not) and ii) limit cycle or oscillatory, the stimulus oscillates between a set of values that implies that most individuals are continuously changing their decision.

In previous works, some authors emphasize that stimuli provided by the environment, as well as the history of each individual, are likely to play an important role in the structure of response threshold models (Theraulaz et al., 1998). These studies suggest that the response thresholds should be variable, implementing an adaptive process. This process is typically explained by a reinforcement mechanism. Several experiments support the reinforcement hypothesis (Theraulaz et al., 1998; Sendova-Franks and Franks, 1994). In Withers et al. (1993) the authors observed that important changes in some regions of the brain are associated with ageing in honeybees: the brain of a forager (more than 20 days old) is significantly different from that of a one-day-old bee. While their observations could result from absolute ageing, further experiments, where worker bees were forced to start foraging early, showed that precocious foragers were similar in brain organization to normal, older foragers. This suggests that behavior influences brain organization, which in turn certainly influences under what conditions tasks are performed. In Theraulaz et al. (1998) the authors proposed a simple reinforcement process: a threshold decreases when the corresponding task is performed, and increases when the corresponding task is not performed. This mechanism is also called specialization in the literature because this threshold variation provokes that different groups of individuals always perform the same task (Bonabeau et al., 1999; Sutton and Barto, 1998). The dynamical equation that defines the threshold variation of the  $i$  individual is:

$$\Theta_i(t+1) = \Theta_i(t) - \xi\chi_i(t) + \varphi(1 - \chi_i(t)) \quad (4.25)$$

where  $\xi$  is the threshold decrement,  $\varphi$  is the threshold increment and  $\chi_i(t)$  is a binary variable that takes the value 1 if the individual  $i$  is performing the task and 0 in the other case. In Castillo-Cagigal et al. (2014b), the authors perform a detailed study about the division of labor dynamics and they propose a variable threshold algorithm based on this dynamical study.

### 4.3 Discussion

At the beginning of this Chapter, the signal approach of the DSM was explained. The smoothing of the aggregated consumption  $P(t)$  may be achieved by modifying the controllable part of this consumption  $P^c(t)$ . This smoothing process is summarized in the reduction of the amplitude of the sinusoidal functions of  $P(t)$  through the control of amplitudes  $A_n^c$  and phases  $\phi_n^c$  of the *Fourier* series—see Figure 4.3. In addition, the controllable consumption is not only a single big consumer, but there are several facilities connected to the electric grid. These facilities have a controllable consumption  $p_i^c(t)$  that is managed by the proposed DSM algorithm. In addition, these facilities have not a direct communication system and they can only coordinate by observing the aggregated signal  $P(t)$ . The shape of  $p_i^c(t)$  must be controlled in a distributed way such that  $A_n^c$  and  $\phi_n^c$  are modified to smooth the aggregated consumption. In this Thesis, the distributed control of  $p_i^c(t)$  is performed by the use of local consumption patterns.

A local consumption pattern is a function  $f_i(t)$  that denotes the objective shape of the consumption of the facility  $i$ . This objective shape should be generated in order that the sum of all objective shapes of all facilities achieves a common goal. In this case, the goal is the aggregated consumption smoothing. Therefore, if the controllable consumption of every facility is able to shape its local consumption pattern, the aggregated consumption will be smoothed.

The local consumption patterns can be used to control  $A_n^c$  and  $\phi_n^c$ . They may be sinusoidal functions which are in turn oscillators, so that:

$$f_i(t) = x_i(t) = \sin(\omega_i t + \phi_i) \quad (4.26)$$

where  $\omega_i$  is the *operating frequency* that is the angular frequency at which the pattern  $i$  works and  $\phi_i$  is the phase of the pattern  $i$ . The controllable part of the consumption of a local facility may be approximated by its local consumption pattern (this issue is further discussed in Chapter 6). Notice that  $f_i(t)$  has no magnitude because it represents the consumption shape. The power of the loads in the local facility will define the magnitude of the local consumption. For example, if a facility has a HVAC<sup>3</sup> system of 5 kW and another one of 10 kW, the latter will consume two times the first. Therefore, the controllable local consumption will be proportional to  $f_i(t)$  if the facility loads are scheduled using this pattern and its magnitude depends on local

<sup>3</sup> HVAC (heating, ventilation, and air conditioning) is the technology of indoor and vehicular environmental comfort. Its goal is to provide thermal comfort and acceptable indoor air quality.

### 4.3. Discussion

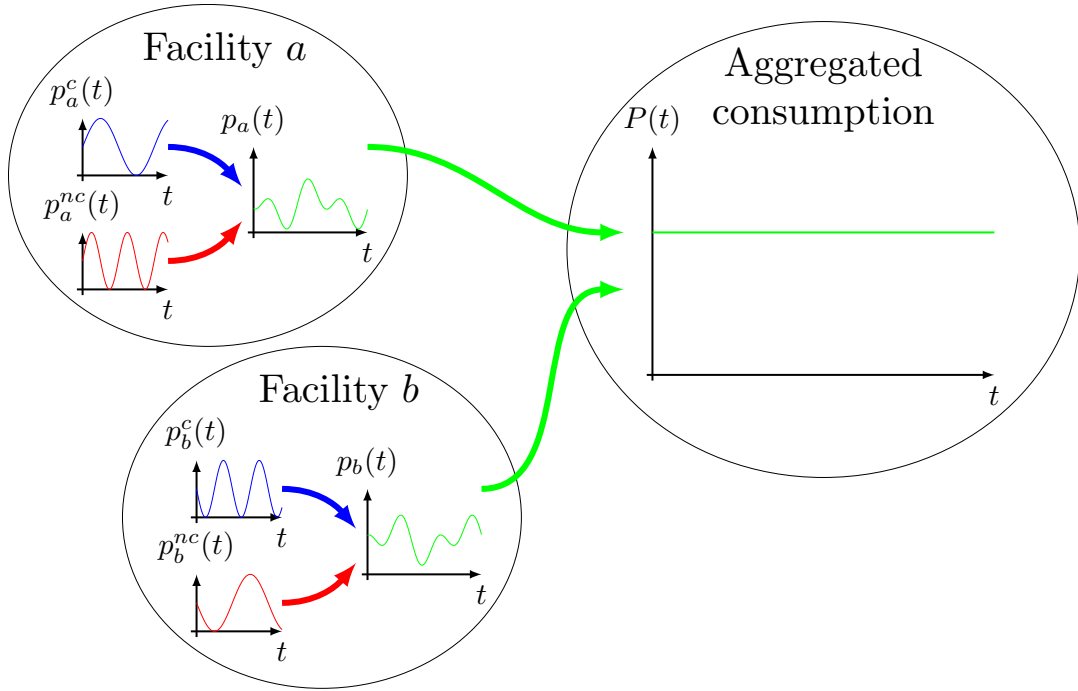


Figure 4.15: Conceptual scheme of an electrical grid divided in local facilities. There are two facilities  $a$  and  $b$  which are added to compose the aggregated consumption. Both facilities are divided in two parts: the non-controllable consumption in red lines and the controllable consumption in blue lines. Both parts are sinusoidal functions with are removing each other, resulting a constant aggregated consumption.

conditions, such that:

$$p_i^c(t) \approx A_i f_i(t) = A_i \sin(\omega_i t + \phi_i(t)) \quad (4.27)$$

where  $A_i$  is the maximum power consumption which depends on the loads of the facility  $i$ . Under this approach,  $P^c(t)$  tends to a sum of sinusoidal functions, so that:

$$P^c(t) = \sum_{i=1}^N p_i^c(t) \approx \sum_{i=1}^M A_i \sin(\omega_i t + \phi_i(t)) \quad (4.28)$$

This equation links the local consumption patterns to the modification of the controllable consumption shape. If these sinusoidal functions are in counterphase with the sinusoidal functions of the non-controllable consumption, the aggregated

consumption is smoothed. Figure 4.15 shows a schematic representation of this process. In both facilities, the non-controllable and controllable consumptions are sinusoidal functions. These functions have a concrete configuration in this example:  $p_a^c(t)$  has the same frequency as  $p_b^{nc}(t)$  but with the opposite phase and with  $p_a^{nc}(t)$  and  $p_b^c(t)$  the same applies. This means that the local consumptions of both facilities are not constant but the controllable consumption of one facility compensates the non-controllable consumption of the other. In summary, the aggregated consumption is constant as desired. This process is performed in a distributed way by the **Multi-Frequency Coupled Oscillators (MuFCO)** algorithm. This algorithm is based on the coupled oscillators and task allocation. The **MuFCO** algorithm is in charge of generating the consumption patterns. Its development and operation are extensively explained in Chapter 5.

Once the patterns are generated, the local controllable consumption must be scheduled. The **MuFCO** algorithm generates patterns considering the whole grid consumption, but there are other local energy factors that influence the load schedule. These factors are related to the local **Photovoltaic (PV)** generation and the consumers requirements. The algorithm that considers these local energy factors and the grid is called **Swarm Grid (SG)** algorithm. It implements the **DSM** mechanism proposed in this Thesis. The **SG** algorithm development and operation are explained in detail in Chapter 6.

## Chapter 5

# Multi-Frequency Coupled Oscillators

In this Chapter, the **Multi-Frequency Coupled Oscillators (MuFCO)** algorithm is described. This algorithm controls a collective of oscillators in environments where there is a non-controllable component. This non-controllable component and the environment itself can be modeled as signals. Thanks to **MuFCO** algorithm, the oscillators are able to adapt to the non-controllable component in order to modify the environment. This adaptation process is designed so that the environment meets certain predefined characteristics or goal. This design procedure is typical in the design of artificial systems where there are several elements, oscillators in this case, that interact with the environment ([Martín H. et al., 2009](#)). The performance of the oscillators is modified by the state of the environment, closing a feedback loop that defines the adaptive process. In this loop, the non-controllable component plays a passive role; it does not adapt, but modifies the environment. Hence, the oscillators should be able to adapt to the non-controllable component and achieve the predefined goal.

As explained in Chapter 4, the grid can be modeled as a sum of signals, such that: the aggregated consumption is the environment where **MuFCO** algorithm operates and the non-controllable consumption is the non-controllable component. The consumption patterns of the local facilities are oscillators, modeled as sinusoidal functions—see Section 4.3. These sinusoidal patterns are not the real consumption, they are a guide to how a facility should consume to perform a collective **Demand-Side Management (DSM)**. However, the real consumption of these facilities is considered as oscillators in this Chapter, so that the consumption behaves as shown in Figure 4.15.

This allows the operation of the algorithm to be checked in the ideal case, where the consumption behaves as the patterns. The coordination and smoothing capabilities can be analyzed through this approach.

This Chapter is organized as follows. In Section 5.1, the environment is defined as signals. The components of the environment are described as *Fourier series* and related between them with the order parameter. The coupling equations of the oscillators with the environment are defined in Section 5.2. Section 5.3 describes the whole operation of the **MuFCO** algorithm. It explains the multi-frequency behavior and how the algorithm is able to smooth signals. An operation example of the **MuFCO** algorithm in the grid is shown in Section 5.4. Finally, Section 5.5 concludes the Chapter.

### 5.1 The environment as signals

The environment signal  $s(t)$  is the sum of a non-controllable signal  $z(t)$  and a collective of oscillators  $x_i^{osc}(t)$ , such that:

$$s(t) = z(t) + \sum_{i=1}^M x_i^{osc}(t) \quad (5.1)$$

where  $M \in \mathbb{N}$  is the population of controllable signals. The oscillators are modeled as sinusoidal functions because of two main reasons: *i*) they are the simplest functions and *ii*) any periodic signal can be implemented as a combination of sinusoidal functions (Oppenheim et al., 1996). Thus, the oscillator  $i$  is defined by the following equation:

$$x_i^{osc}(t) = \sin(\omega_i t + \phi_i) \quad (5.2)$$

where  $\omega_i \in \mathbb{R}$  is the operating frequency and  $\phi_i \in [-\pi, \pi]$  is the phase difference relative to a reference. The instantaneous phase of each oscillator is defined as  $\theta_i = \omega_i t + \phi_i$ . The proposed **MuFCO** algorithm controls these oscillators through the modification of  $\omega_i$  and  $\phi_i$ .

The non-controllable signal  $z(t)$  may be of any nature. Following the same procedure as in Equation 4.3, it is presented as a *Fourier series* and an error term:

$$z(t) = \sum_{n=0}^N A_n^z \cdot \sin(n\omega_0 t + \phi_n^z) + e^z(t) \quad (5.3)$$

where  $N \in \mathbb{N}$  is the number of components of the *Fourier series*,  $\omega_0$  is the fundamental frequency,  $A_n^z$  and  $\phi_n^z$  are the amplitude and phase of the  $n$  component of  $z(t)$

## 5.1. The environment as signals

---

respectively and  $e^z(t)$  is the error term of  $z(t)$ . In the same way, the environment signal can be expressed as *Fourier series* plus an error term. In addition,  $s(t)$  can be decomposed in series with the same number of components  $N$  and the same fundamental frequency  $\omega_0$ , such that:

$$s(t) = \sum_{n=0}^N A_n^s \cdot \sin(n\omega_0 t + \phi_n^s) + e^s(t) \quad (5.4)$$

where  $A_n^s$  and  $\phi_n^s$  are the amplitude and phase of the component  $n$  of  $s(t)$  respectively and  $e^s(t)$  is the error term of  $s(t)$ .

The operating frequency  $\omega_i$  of the oscillators can be chosen by the **MuFCO** algorithm. To bind  $x_i^{osc}(t)$  with  $s(t)$  and  $z(t)$ , it is established that the operating frequencies are contained in the set of frequencies of the *Fourier series* components:  $\omega_i \in \omega_0, 2\omega_0, 3\omega_0, \dots, N\omega_0$ . By combining equations 5.1, 5.2, 5.3 and 5.4 together with this approach, it leads to the following equation:

$$\sum_{n=0}^N A_n^s \cdot \sin(n\omega_0 t + \phi_n^s) + e^s(t) = \sum_{i=1}^M \sin(l_i \omega_0 t + \phi_i) + \sum_{n=0}^N A_n^z \cdot \sin(n\omega_0 t + \phi_n^z) + e^z(t) \quad (5.5)$$

where  $l_i \in [0, \dots, N]$  defines the operating frequency of the oscillator  $i$  in the *Fourier series*. Notice that the error terms, which represent the part of the signals that cannot be represented as a periodic function, are equal through this approach  $e^s(t) = e^z(t)$ . Therefore, the relationship between  $s(t)$ ,  $z(t)$  and  $x_i^{osc}(t)$  is reduced to a relationship between components of the *Fourier series*.

The *Fourier series* representation allows to split the relationship of Equation 5.5 in the relationship between each of the individuals components, such that:

$$A_n^s \cdot \sin(n\omega_0 t + \phi_n^s) = A_n^z \cdot \sin(n\omega_0 t + \phi_n^z) + \sum_{i=1}^{M_n} \sin(l_i \omega_0 t + \phi_i) \quad (5.6)$$

where  $M_n$  is the number of oscillators which satisfy that  $l_i = n$ . It means that the problem can be taken apart in subsets of *Fourier series* where all sinusoidal functions have the same frequency. By using the *Euler's formula*, Equation 5.6 can be represented as:

$$A_n^s e^{i\phi_n^s} = A_n^z e^{i\phi_n^z} + \sum_{i=1}^{M_n} e^{i\phi_i} \quad (5.7)$$

This relationship is applied to every component of series.

## 5. Multi-Frequency Coupled Oscillators

---

The relationship between the non-controllable signal  $z(t)$  and the oscillators  $x_i^{osc}(t)$  can be assessed by an order parameter. This parameter was defined in Equation 4.14 and it was used to evaluate the coherence of a group of oscillators. In this case, there are not only oscillators but also a non-controllable signal. Thanks to the *Fourier series* representation,  $z(t)$  can be introduced in the order parameter. Let  $r_n e^{i\Phi_n}$  be the order parameter of the component  $n$  of *Fourier series*, such that:

$$r_n e^{i\Phi_n} = \frac{1}{M_n + A_n^z} \left( A_n^z e^{i\phi_n^z} + \sum_{i=1}^{M_n} e^{i\phi_i} \right) \quad (5.8)$$

where  $r_n$  is the coherence of the component  $n$  and  $\Phi_n$  is the average phase. The order parameters are related with the amplitudes and phases of the  $s(t)$  components. By combining equations 5.7 and 5.8:

$$r_n = \frac{A_n^s}{M_n + A_n^z} \quad \Phi_n = \phi_n^s \quad (5.9)$$

This relationship means that the order parameter may be calculated through the observation of the environment components. In turn, the coherence between the non-controllable signal and the oscillators may be known, allowing to perform a coupling process. For example, if  $A_n^s \rightarrow 0$  then  $r_n \rightarrow 0$  and  $z(t)$  and  $x_i^{osc}(t)$  are in an incoherent state. On the other hand, if  $A_n^s \rightarrow M_n + A_n^z$  then  $r_n \rightarrow 1$  and  $z(t)$  and  $x_i^{osc}(t)$  are fully synchronized. Section 5.2 shows how Equation 5.9 is used to perform the Kuramoto model only with information about the environment signal.

Thanks to the *Fourier series* representation, the signals that compose the environment can be easily studied in the frequency domain. It means that  $s(t)$  can be analyzed through a *Fourier analysis* and its frequency components can be obtained. **MuFCO** algorithm is designed to work as a digital controller. It means that the signal must be sampled at a certain period called *sample period* ( $T^{smp}$ ). In addition, **MuFCO** algorithm is a real-time algorithm that works with a finite number of samples of  $s(t)$ . For this reasons, the frequency analysis is performed by a **Discrete Fourier Transform (DFT)**. The **DFT** is a finite sequence of frequency components that corresponds to samples, equally spaced in frequency, of the Fourier transform of the signal. The number of samples of  $s(t)$  considered in the frequency analysis is the *processing window* that is denoted by  $W$ . The number of frequency components obtained from the **DFT** is  $W/2$  because  $s(t)$  is a real signal (Oppenheim and Schaffer, 2009) and the spectrum is symmetrical. For example, if  $W = 64$  samples, the **DFT** requires 64 samples of  $s(t)$  and the lower frequency of a frequency component that

## 5.2. Single frequency coupling

---

can be obtained is  $\omega_0 = 2\pi/(64 \cdot T^{sm})$  and the higher frequency is  $\omega_0 = 2\pi/(2 \cdot T^{sm})$ . The use of the **DFT** implies that the information obtained from the frequency components of  $s(t)$  is not the same as if working in continuous time. These calculus error must be taken into account and both  $T^{sm}$  and  $W$  are parameters to be tuned when the algorithm is applied to a concrete use.

## 5.2 Single frequency coupling

In this Section, the coupling of a single frequency component is studied. It means that the non-controllable signal  $z(t)$  is reduced to a single sinusoidal function and all oscillators work on this operating frequency. Hence, the environment signal is also a sinusoidal function whose amplitude and phase depend on the amplitude of  $z(t)$ , the number of oscillators and the phase relationship. The subscript  $n$ , which indicates the component of the *Fourier series*, has been removed from the equations because the procedure followed in this Section is valid for any component. In this case, **MuFCO** algorithm can only modify the phase differences of the oscillators because the operating frequencies are fixed. This phase difference modifications are based on the Kuramoto model, previously introduced in Section 4.1. Two variations of this model are proposed, where the oscillators and  $z(t)$  are coupled through the **DFT**.

### 5.2.1 Coupling equations

The Kuramoto model defines the coupling between a collective of oscillators which usually differ in frequency and phase. In this Section, all oscillators have the same operating frequency, thus they only differ in the phase. The non-controllable signal is also included in the coupling process. It is simplified to a single sinusoidal function and, under this assumption, it can be considered as a non-controllable oscillator. This oscillator is not controllable because its phase is not involved in the coupling process. Although  $z(t)$  is a passive element, it affects the coupling process through the order parameter—see Equation 5.8. Therefore, the phases of the oscillators vary in time  $\phi_i \rightarrow \phi_i(t)$  but the phase of  $z(t)$  keeps constant  $\phi^z = const$ . The Kuramoto model in the order parameter form applied to the oscillator phases leads the following coupling equation:

$$\dot{\phi}_i(t) = K \cdot r(t) \cdot \sin(\Phi(t) - \phi_i(t)) \quad (5.10)$$

where  $K \in \mathbb{R}$  is the Kuramoto coupling strength. Notice that the time has been included in  $r(t)$  and  $\Phi(t)$  because the order parameter is modified during the coupling

## 5. Multi-Frequency Coupled Oscillators

---

process.  $K$  defines the oscillator's coupling from a qualitative and quantitative point of view. The absolute value of  $K$  affects the coupling velocity which in turn affects the stability of the coupling process. The sign of  $K$  defines qualitatively the interaction between the oscillators and  $z(t)$ . Positive  $K$  values correspond to an attractive interaction. It implies that oscillator phases tend to  $z(t)$  phase because  $z(t)$  does not modify its phase. On the other hand, negative  $K$  values produces a repulsive interaction. Oscillator phases and  $z(t)$  phase tend to separate each other.

Figure 5.1 shows an example of coupling between oscillators and  $z(t)$  using Equation 5.10. The frequency of the non-controllable signal  $z(t)$  is  $\omega^z = 2\pi/32 \text{ rad/s}$  and the operating frequencies of the oscillators are the same  $\omega_i = 2\pi/32 \text{ rad/s} \forall i$ . The amplitude of  $z(t)$  is  $A^z = 5$ . The oscillators population is  $M = 10$ . It means that if the oscillators are fully synchronized with  $z(t)$ , the amplitude of the environment signal  $s(t)$  takes the value  $A^s = A^z + M = 15$ . On the other hand, if the oscillators and  $z(t)$  are in an incoherent state, the amplitude of  $s(t)$  takes the value  $A^s = 0$ . The phase of  $z(t)$  is the phase reference, thus,  $\phi^z = 0$  and the phase difference of the oscillators  $\phi_i(t)$  are referenced to this phase. The initial oscillator's phase differences are uniformly distributed in  $[-\pi, \pi]$ . This example shows the coupling effect in two cases: with positive coupling  $K = 0.01$  and negative coupling  $K = -0.01$ . Figure 5.1a shows the development in time of  $s(t)$  for positive coupling, where  $s(t)$  begins with an amplitude  $A^s \approx 10$  to converge to a coherent state with  $A^s = 15$ . The coupling effect can also be observed in the phase differences—see Figure 5.1b. All phase differences  $\phi_i(t)$  and  $\Phi(t)$  converge to zero. Figure 5.1c shows the development in time of  $r(t)$  which converges to 1. On the other hand, the negative coupling has the opposite effect. Figure 5.1d shows how  $s(t)$  develops in time for the negative coupling.  $s(t)$  begins with an amplitude  $A^s \approx 10$  but converges to an incoherent state with  $A^s = 0$ . In this case, the phase differences converge to an incoherent state—see Figure 5.1e. It implies that they are spread in the range  $[-\pi, \pi]$  such that the phase coherence is reduced to zero. Figure 5.1f shows the development in time of  $r(t)$ .

This example has been analyzed by the DFT. It has been applied to  $s(t)$  by using a sample period of  $T^{smp} = 1 \text{ s}$ . The *processing window* is set to  $W = 64$  samples. The DFT gives the amplitude  $A^s(t)$  and phase difference  $\phi^s(t)$  of the frequency component analyzed in this example  $\omega_0 = 2\pi/32 \text{ rad/s}$ . Figures 5.1b and 5.1e show the development of  $\phi^s(t)$  calculated by the DFT over the example. According to Equation 5.9,  $\phi^s(t)$  and  $\Phi(t)$  should be equal, but the information obtained from the Fourier analysis is not exact because the use of a DFT. In general, the *processing window* affects to this result causing a certain delay between the instantaneous phase  $\Phi(t)$  and the phase

## 5.2. Single frequency coupling

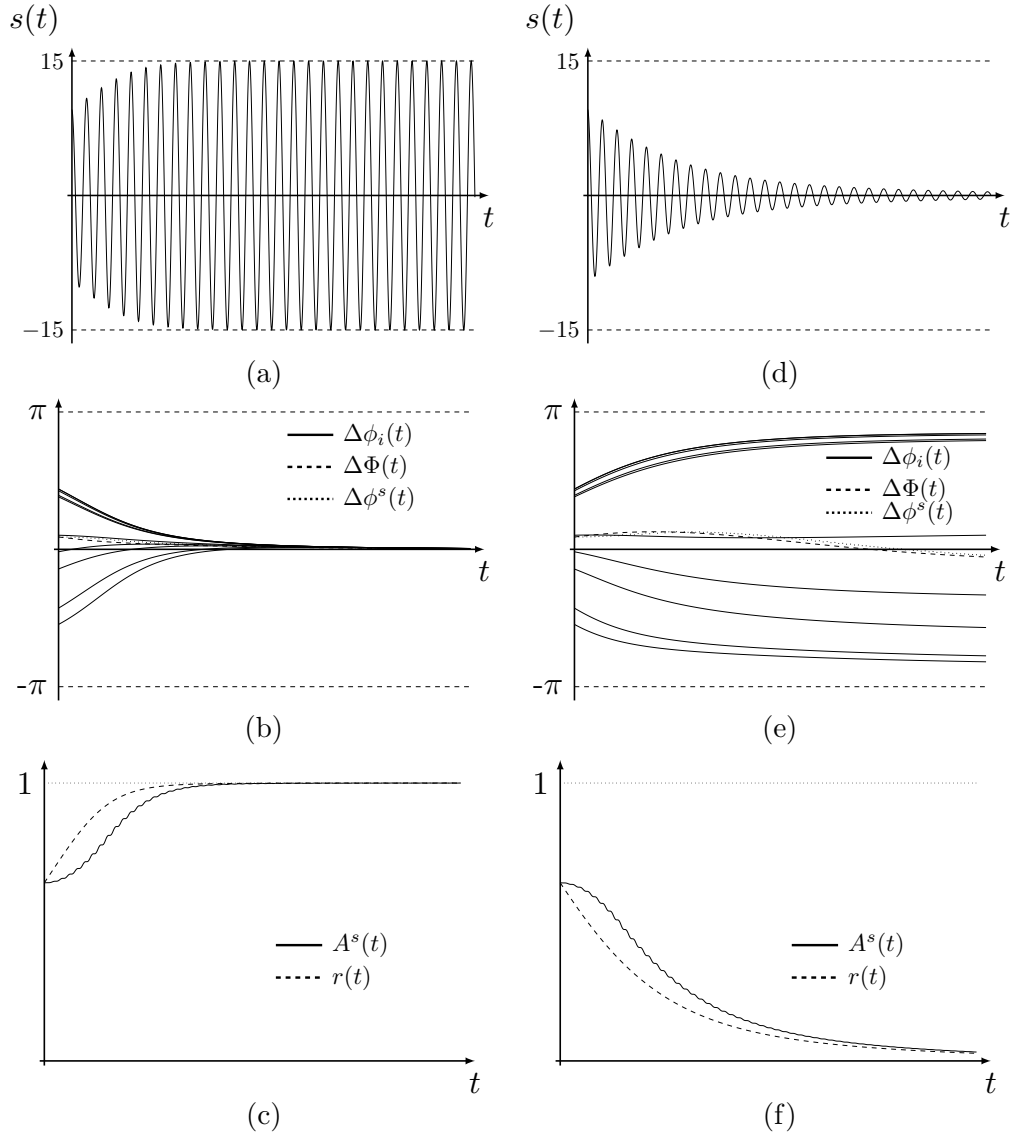


Figure 5.1: Example of coupling between oscillators and  $z(t)$  using Equation 5.10 with  $M = 10$ ,  $\omega^z = \omega_i = 2\pi/32 \text{ rad/s } \forall i$ ,  $A^z = 5$ ,  $W = 64$  samples and  $T^{smp} = 1$  s: a)  $s(t)$  for  $K = 0.01$ , b)  $\phi_i(t)$ ,  $\Phi(t)$  and  $\phi^s(t)$  for  $K = 0.01$ , c)  $r(t)$  and normalized  $A^s(t)$  for  $K = 0.01$ , d)  $s(t)$  for  $K = -0.01$ , e)  $\phi_i(t)$ ,  $\Phi(t)$  and  $\phi^s(t)$  for  $K = -0.01$  and f)  $r(t)$  and normalized  $A^s(t)$  for  $K = -0.01$ .

## 5. Multi-Frequency Coupled Oscillators

---

calculated through the **DFT**  $\phi^s(t)$ . Figures 5.1c and 5.1d show the development of the normalized  $A^s(t)$  calculated by the **DFT** over the example.  $A^s(t)$  has been normalized by  $A^z + M$  to restrict it in the range  $[0, 1]$  and to be compared with the phase coherence. According to the Equation 5.9, normalized  $A^s(t)$  should be equal to  $r(t)$ , but a certain delay can be observed as in the case of the phase differences.

The use of the order parameter to perform the coupling equation 5.10 implies that every oscillator knows the phases of all oscillators. This requirement means that the coupling process is not a local phenomenon and depending on the situation may hinder its application on distributed systems. For example, situations where oscillators are spread over a large zone and the information exchange implies a complex communication system. The order parameter may be approximated by the **DFT** of  $s(t)$ . Through this approach, every oscillator may obtain the required coupling information only by observing the environment signal  $s(t)$ . Combining equations 5.9 and 5.10 leads the following coupling equation:

$$\dot{\phi}_i(t) = K \cdot \frac{A^s(t)}{A^z + M} \cdot \sin(\phi^s(t) - \phi_i(t)) \quad (5.11)$$

Figure 5.2 shows an example of coupling between oscillators and  $z(t)$  using Equation 5.11. This example has the same setup as the previous example presented in Figure 5.1. The development of the oscillators and  $s(t)$  over the example for positive coupling are shown in figures 5.2a, 5.2b and 5.2c. The use of the  $A^s(t)$  and  $\phi^s(t)$  obtained from the **DFT** does not alter the coupling process. The oscillators achieve a coherent state with  $z(t)$  as in the example with the order parameter. Figures 5.2d, 5.2e and 5.2f show the effect of the negative coupling. The development of the oscillators and  $s(t)$  over the example is similar to the example with the order parameter. Therefore, the use of the **DFT** to calculate  $A^s(t)$  and  $\phi^s(t)$  and to replace  $r(t)$  and  $\Phi(t)$  allows to perform a coupling process without every oscillator knowing the phases of all others.

Although the **DFT** allows the coupling process without the knowledge of oscillator phases, Equation 5.11 requires  $M$  and  $A^z$  to be implemented. This information is not always easy to obtain in a distributed system. The developed algorithm in this Thesis aims to adapt to unknown environments and populations. Hence, the normalization of  $A^s$  by  $M + A^z$  should be modified by another normalization factor which does not require the knowledge of  $M$  and  $z(t)$ . For this reason, it is proposed to replace  $M + A^z$  by the historical maximum of the component of the environment signal  $\max(A^s)$ . The reason of this proposal is that the maximum value attainable by a  $s(t)$  component is

## 5.2. Single frequency coupling

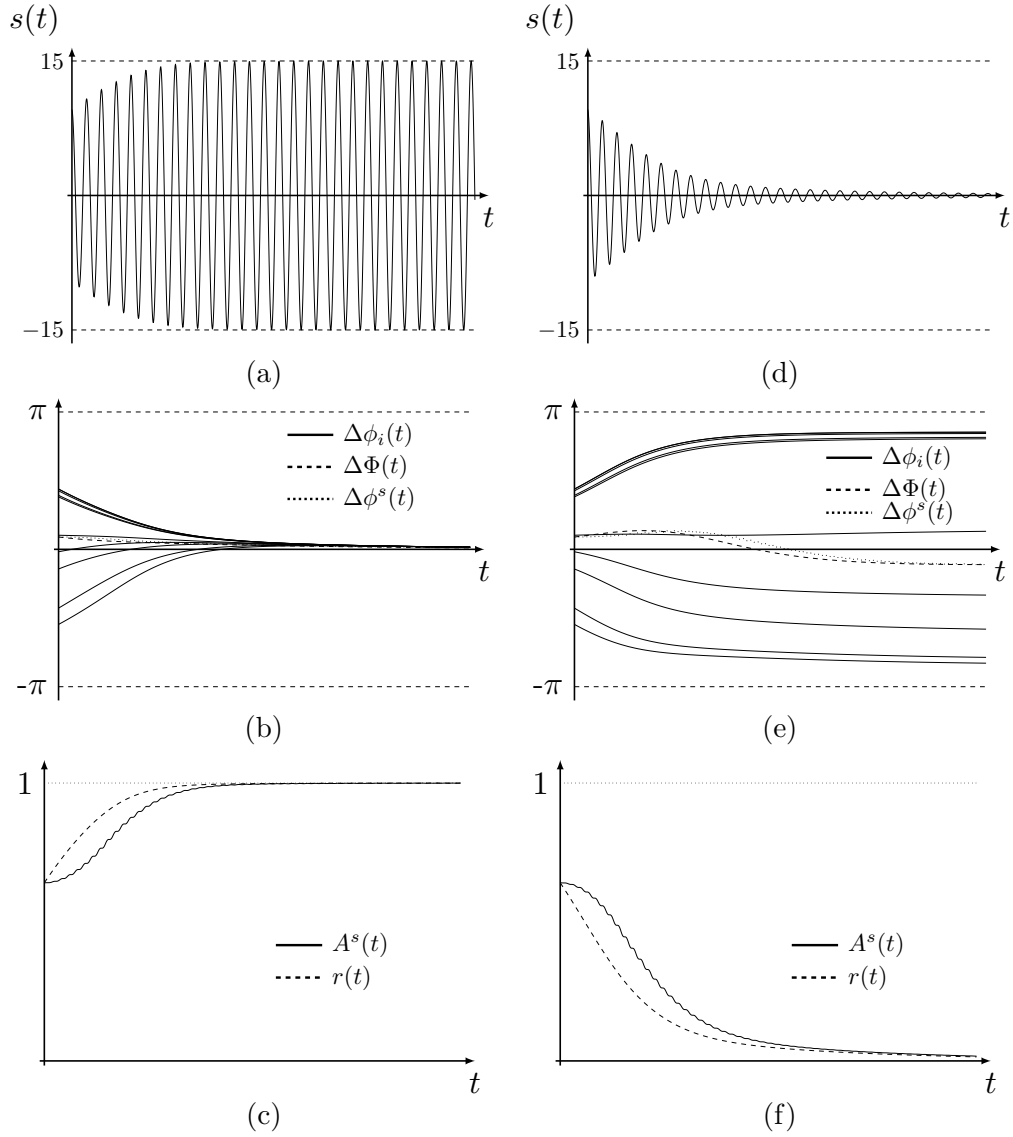


Figure 5.2: Example of coupling between oscillators and  $z(t)$  using Equation 5.11 with  $M = 10$ ,  $\omega^z = \omega_i = 2\pi/32 \text{ rad/s } \forall i$ ,  $A^z = 5$ ,  $W = 64$  samples and  $T^{smpl} = 1$  s: a)  $s(t)$  for  $K = 0.01$ , b)  $\phi_i(t)$ ,  $\Phi(t)$  and  $\phi^s(t)$  for  $K = 0.01$ , c)  $r(t)$  and normalized  $A^s(t)$  for  $K = 0.01$ , d)  $s(t)$  for  $K = -0.01$ , e)  $\phi_i(t)$ ,  $\Phi(t)$  and  $\phi^s(t)$  for  $K = -0.01$  and f)  $r(t)$  and normalized  $A^s(t)$  for  $K = -0.01$ .

## 5. Multi-Frequency Coupled Oscillators

---

$M + A^z$ . The proposed coupling equation is:

$$\dot{\phi}_i(t) = K \cdot \frac{A^s(t)}{\max(A^s)} \cdot \sin(\phi^s(t) - \phi_i(t)) \quad (5.12)$$

Notice that  $\max(A^s) \leq M + A^z$ . It implies that the coupling strength is higher than a common coupling.

Figure 5.3 shows an example of coupling between oscillators and  $z(t)$  using Equation 5.12. This example has the same setup as the examples presented in figures 5.1 and 5.2. Both positive and negative coupling are shown in this example too. The effect of the positive coupling in the development of the oscillators and  $s(t)$  is shown in figures 5.3a, 5.3b and 5.3c. The oscillators achieve a coherent state despite using the  $\max(A^s)$  approximation. As aforementioned, the use of this approximation speeds up the coupling process because it is always lower than the ideal value. The negative coupling presents the same effect, as shown in figures 5.3d, 5.3e and 5.3f.

### 5.2.2 Coupling strength K analysis

In this Section, the effect of the coupling strength  $K$  on the coupling process is analyzed. The coupling process varies depending on the different coupling equations 5.10, 5.11 and 5.12. Hence, a scanning of the coupling strength  $K$  has been performed for each coupling equation. This scanning consists in the execution of a set of coupling process experiments for different  $K$  values. These values are consecutive and equally spaced discrete values of  $K$  in the range  $[-0.1, 0.1]$ . The space between  $K$  values is 0.001, thus, 200 values of  $K$  are studied. The execution of an experiment lasts for 1000 s. After this execution, the phase coherence is calculated ( $r(1000)$ ). The frequency of the non-controllable signal  $z(t)$  is  $\omega^z = 2\pi/32 \text{ rad/s}$  and the operating frequencies of the oscillators are the same  $\omega_i = 2\pi/32 \text{ rad/s} \forall i$ . The amplitude of  $z(t)$  is  $A^z = 50$  and the population of oscillators is  $M = 100$ . The initial oscillator phases are randomly distributed in the range  $[-\pi, \pi]$ . The experiments are grouped in sets because the randomness of the initial oscillator phases. For a set of experiments,  $K$  takes the same value but each experiment is executed with different initial values. Through this repetition of the experiments, the coupling process can be analyzed without the spurious effects of the random initial phases. In this analysis, each set of experiments has 30 repetitions. The operation window of the DFT is  $W = 64$  samples and the sampling period  $T^{smpl} = 1 \text{ s}$ .

Figure 5.4 shows the results of the  $K$  analysis performed for the three coupling equations. The three quartiles Q1, Q2 and Q3 and the maximum and minimum value

## 5.2. Single frequency coupling

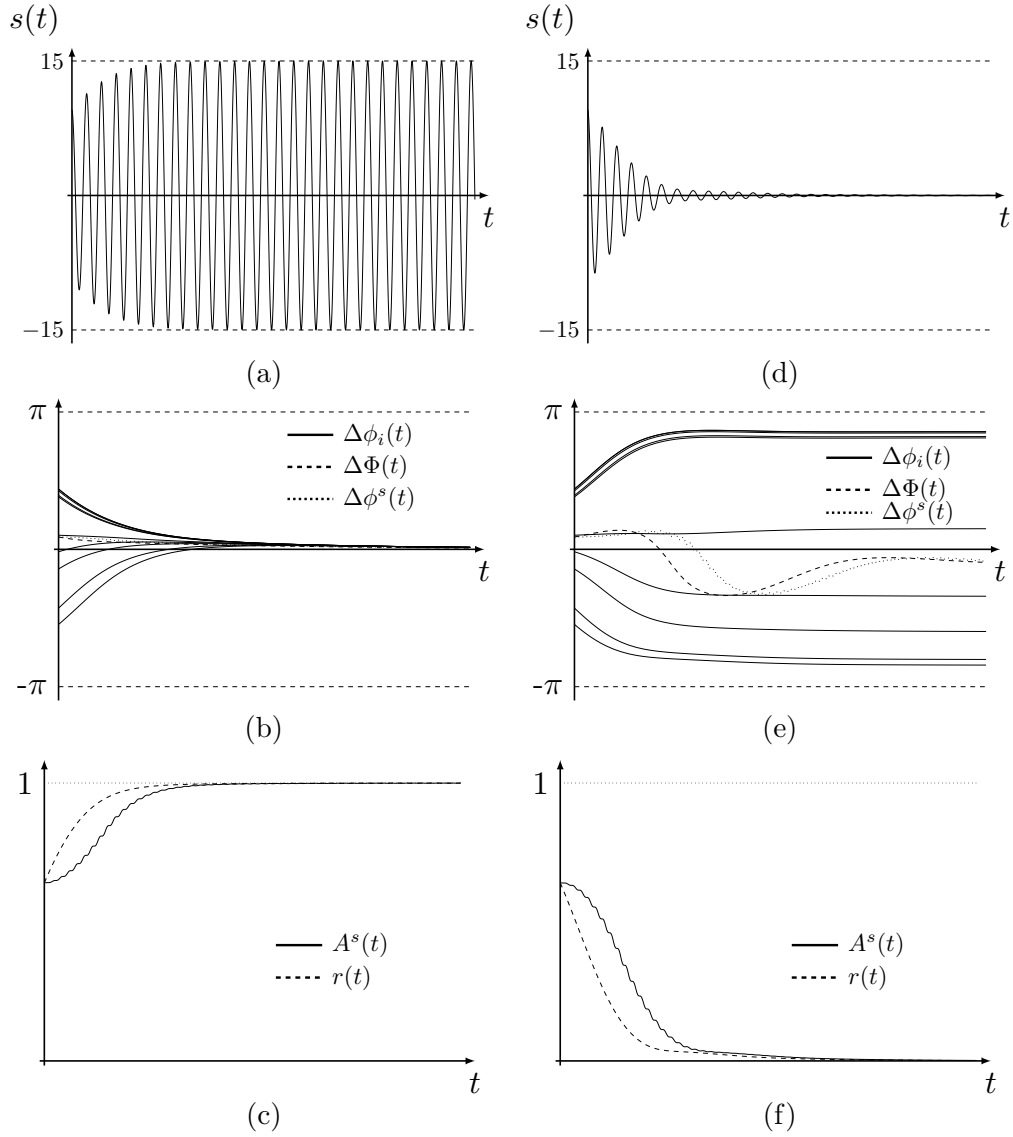


Figure 5.3: Example of coupling between oscillators and  $z(t)$  using Equation 5.12 with  $M = 10$ ,  $\omega^z = \omega_i = 2\pi/32 \text{ rad/s } \forall i$ ,  $A^z = 5$ ,  $W = 64$  samples and  $T^{smp} = 1$  s: a)  $s(t)$  for  $K = 0.01$ , b)  $\phi_i(t)$ ,  $\Phi(t)$  and  $\phi^s(t)$  for  $K = 0.01$ , c)  $r(t)$  and normalized  $A^s(t)$  for  $K = 0.01$ , d)  $s(t)$  for  $K = -0.01$ , e)  $\phi_i(t)$ ,  $\Phi(t)$  and  $\phi^s(t)$  for  $K = -0.01$  and f)  $r(t)$  and normalized  $A^s(t)$  for  $K = -0.01$ .

## 5. Multi-Frequency Coupled Oscillators

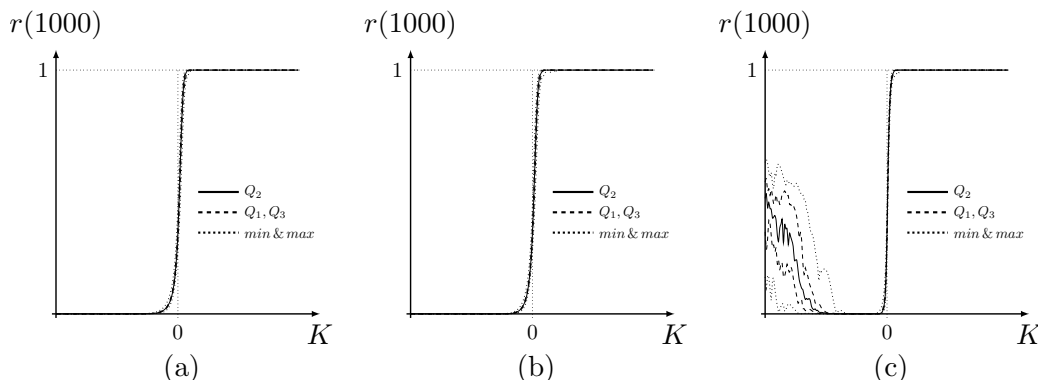


Figure 5.4: Result of the  $K$  analysis, where  $Q_1$ ,  $Q_2$ ,  $Q_3$ , maximum and minimum values are represented with the coupling equations: a) Equations 5.10, b) Equations 5.11 and c) Equations 5.12.

obtained for each set of experiments are represented in the graphs. Figure 5.4a shows the response in  $r(1000)$  of the oscillators and  $z(t)$  for Equations 5.10. For the positive and negative  $K$  values, the phase coherence converges to 1 or 0 respectively. For  $K$  values close to zero, there is a transition from 0 to 1 where the phase coherence takes an intermediate value. Figure 5.4b shows the response in  $r(1000)$  for Equations 5.11. The phase coherence has a similar development than the previous case. Although, the coupling equation is using the phase taken from the DFT, the convergence is similar. Figure 5.4c shows the response in  $r(1000)$  for Equations 5.12. In this case, the normalization of  $A^s$  is approximated by the historical maximum of  $A^s$ . The response in  $r(1000)$  is modified for negative  $K$  values. It differs from the ideal behavior of the negative coupling where  $r(1000)$  should converge to 0. The mean of the experiments  $Q_2$  increases its  $r(1000)$  value. This implies that the oscillators and  $z(t)$  cannot achieve an incoherent state. However, there is a region of negative  $K$  values close to zero which can achieve the incoherent state. Therefore, the  $K$  value should be chosen in this range if a negative coupling behavior is desired.

The coupling equation 5.12 is used by MuFCO algorithm during the remainder of the Thesis because it does not require information about the number of oscillators or the amplitude of the non-controllable component. Thereby, oscillators can be coupled only by observing the environment signal. As consideration, this equation depends on the processing window size  $W$ . The coupling process with equation 5.12 has been also analyzed with three different sizes of  $W$ : 32, 64 and 128 samples. The experiments

### 5.3. Multi-frequency coupling

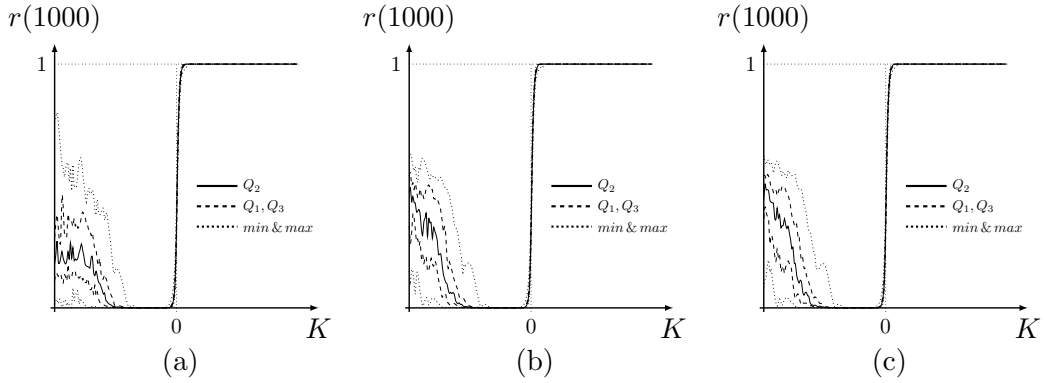


Figure 5.5: Result of the effects of the different  $W$  values in  $K$  analysis with the coupling equation 5.12, where  $Q_1$ ,  $Q_2$ ,  $Q_3$ , maximum and minimum values are represented for: a)  $W = 32$  samples, b)  $W = 64$  samples and c)  $W = 128$  samples.

setup is the same than the previous analysis, including the  $K$  number of values and the number of experiments for each set of experiments. Figure 5.5 shows the result of the effects of the different  $W$  values in  $K$  analysis. The three quartiles  $Q_1$ ,  $Q_2$  and  $Q_3$  and the maximum and minimum values obtained for each set of experiments are also represented in the graphs. The different  $W$  values affect to the negative coupling behavior. It can be appreciated that the smaller  $W$  is, the lower the means of  $r(1000)$  values are. The coupling is more stable when  $W$  is closer to the operation frequency because the window is smaller and the calculus delay is shorter. Notice that if  $W$  must be long enough to contain a whole period of the studied frequency component. In this case with  $\omega^z = 2\pi/32$  rad/s, the shortest windows is  $W = 32$  samples.

### 5.3 Multi-frequency coupling

The previous coupling equations consider that all oscillators and  $z(t)$  operate at the same frequency. However, the non-controllable signal and consequently the environment rarely are a sinusoidal function. It is commonly formed by several frequency components or even stochastic signals. The modification of the operating frequency of the oscillators is required to adapt them to complex environments. The operating frequency modification mechanism, also called frequency switching, is described in this Section. This mechanism allows that the collective of oscillators works on different operating frequencies, where each oscillator has a certain operating

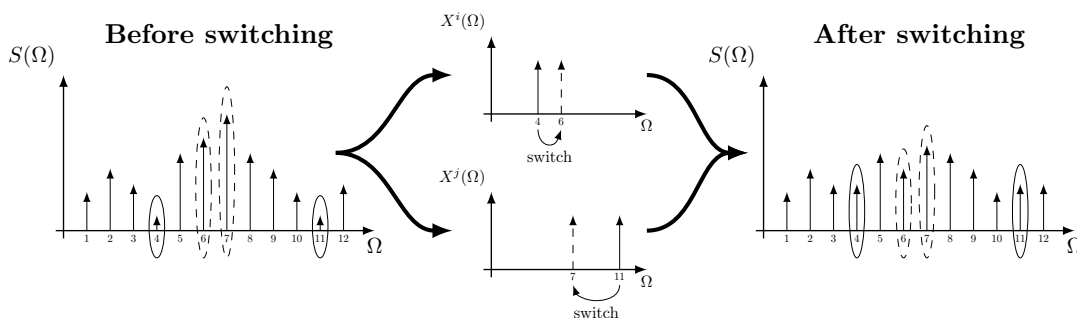


Figure 5.6: Conceptual scheme of the **MuFCO** algorithm operation.

frequency and is coupled to its frequency component through Equation 5.12. This multi-frequency coupled behavior names **MuFCO** algorithm.

Let  $S(\Omega)$  be the **DFT** of  $s(t)$ . The goal of **MuFCO** algorithm is to achieve a *target shape* of  $S(\Omega)$ . Figure 5.6 shows a conceptual scheme of the **MuFCO** algorithm operation. Firstly,  $S(\Omega)$  has a certain shape because  $z(t)$  and the initial  $\omega_i(0)$  of every oscillator. Notice that the number of frequency components of the Fourier transform is  $W/2$ .  $\omega_i$  are contained in these components. In the example of Figure 5.6,  $W$  is 24 samples, thus, there are 12 frequency components in the **DFT**.  $\omega_i(0)$  is in the 4<sup>th</sup> component of the **DFT** and  $\omega_j(0)$  is in the 11<sup>th</sup> component. If the objective is to smooth  $s(t)$ , the target shape of  $S(\Omega)$  is zero for every frequency component. It means that  $s(t)$  becomes constant and the oscillators operate like a bank of filters, removing every frequency component. The coupling strength is paramount to achieve the goal of the algorithm. In this case, negative coupling is required. Therefore, the oscillators should switch to frequency components with higher amplitude values and the negative coupling will reduce the amplitude of these components. Figure 5.6 shows an example of this frequency switching: the oscillator  $i$  switches from the 4<sup>th</sup> component to the 6<sup>th</sup> and the oscillator  $j$  switches from the 11<sup>th</sup> component to the 7<sup>th</sup>. The amplitudes of the higher frequency components is reduced through the frequency switching, smoothing the  $S(\Omega)$  shape. The switching and coupling processes are repeated every  $T^{smp}$  with a recalculated  $S(\Omega)$ .

**MuFCO** algorithm is a distributed algorithm which implies that each oscillator selects its operating frequency. The operation of the algorithm performed by every oscillator individually is described in the pseudo-code of Algorithm 3. Firstly, the oscillator decides whether switch or not—see from line 1 to 10 of Algorithm 3.

### 5.3. Multi-frequency coupling

---

**Algorithm 3** High-level description of the **MuFCO** algorithm.

---

```
1: /* Frequency switching */
2: /* Stop condition */
3:  $S(\Omega) \leftarrow$  DFT of  $s(t)$ 
4:  $E(S(\Omega)) \leftarrow$  Calculate  $E(S(\Omega))$  with Equation 5.13
5:  $rnd \leftarrow$  Generate random number  $\in [0,1]$ 
6: if  $rnd \leq E(S(\Omega))$  then
7:   /* Target frequency */
8:    $\omega_{target} \leftarrow$  Get frequency with distribution  $P(S(\Omega))$ , Equation 5.14
9:    $\omega^i = \omega_{target}$ 
10: end if
11: /* Coupling Equation */
12:  $\Delta\phi^i \leftarrow$  Calculate phase difference modification with coupling Equation 5.12
13:  $\phi^i = \phi^i + \Delta\phi^i$ 
```

---

Secondly, this oscillator modifies its phase by using Equation 5.12—see from line 11 to 13 of Algorithm 3. In this Section, the frequency switching process is explained in detail.

#### 5.3.1 Frequency switching

The frequency switching of the oscillators is based on concepts of task allocation. A frequency component is considered as a task to be performed. An oscillator chooses a concrete component of the **DFT** with a certain probability. For example, if  $W = 4$  samples, there are two possible frequency components to be chosen:  $\omega_A$  and  $\omega_B$ . Each oscillator should choose one of these two components. This selection is done by means of task allocation, so in this example there are two tasks to be allocated:  $task_A$  and  $task_B$ . The probability of performing a task depends on the task associated stimulus, as in Equation 4.22. In this case, the stimuli are just the amplitude of the frequency components.

The frequency switching is divided in two steps: *i*) the switching decision, where the algorithm decides to stay in the current frequency component or switch, and *ii*) the new frequency component selection, which is based on the task associated stimuli. The switching decision is done through the calculation of the *shape error function*  $E(S(\Omega))$ . It evaluates the difference between the target shape and the current shape of  $S(\Omega)$ . The output range of  $E(S(\Omega))$  is  $[0, 1]$ , where 0 denotes that both signals are

## 5. Multi-Frequency Coupled Oscillators

---

equal and 1 that they are completely different.  $E(S(\Omega))$  is used as the stop condition so that the lower its value is, the lower the probability that an oscillator moves to another frequency component. This behavior is observed in the conditional of the line 6 of Algorithm 3. The following equation defines the proposed shape error function:

$$E(S(\Omega)) = P_{switch} \cdot \sum_{j=1}^{w/2} \left( \frac{A_j^y[k]}{\max(S(\Omega))} \right)^4 \quad (5.13)$$

where  $P_{switch}$  is the *switching factor* that denotes the probability that an oscillator moves to another frequency component and  $\max(S(\Omega))$  is the historical maximum amplitude of any frequency component measured during the algorithm execution.  $\max(S(\Omega))$  normalizes the frequency components amplitudes and ensures that  $E(S(\Omega)) \in [0, 1]$ . Notice that the zero frequency component is not included in the equation because this component represents the constant value.

If the oscillator decides to move to another frequency component, it uses the *transition rule*. It is based on a typical random proportional rule used in swarm intelligence. The transition rule generates a probability density function of the spectrum and a frequency component is selected following this density function. This procedure is similar to that indicated by Equation 4.22 in which the probability to perform the  $task_i$  is a function of the associated stimulus. The probability of each frequency component  $p_n$  is calculated such that:

$$p_n = \frac{(A_n^s)^2}{\sum_{j=1}^{w/2} (A_j^s)^2} \quad (5.14)$$

In this case, the associated stimulus to a certain frequency component is  $A_n^s$ , thus, the higher the value of  $A_n^s$ , the higher the probability to switch to the frequency component  $n$ . Notice that an oscillator can select the same frequency as the operation one, thus no movement occurs. After a frequency has been selected, the oscillator modifies its operation frequency and restarts its phase randomly, with a uniform distribution between  $[-\pi, \pi]$ .

Figure 5.7 shows an example of MuFCO algorithm operation.  $z(t)$  is composed by three frequency components:  $\omega_2^z = 2\pi/32$  rad/s,  $\omega_4^z = 2\pi/16$  rad/s and  $\omega_8^z = 2\pi/8$  rad/s. The amplitudes of the frequency components are  $A_2^z = 50$ ,  $A_4^z = 30$  and  $A_8^z = 20$ . The DFT of  $s(t)$  is calculated with  $T^{sm} = 1$  s and  $W = 64$  samples. Figure 5.7a shows the spectrum of  $z(t)$ . There are 100 oscillators with  $K = -0.01$  and  $P_{switch} = 0.01$ . The initial operating frequencies of oscillators are uniformly distributed over

### 5.3. Multi-frequency coupling

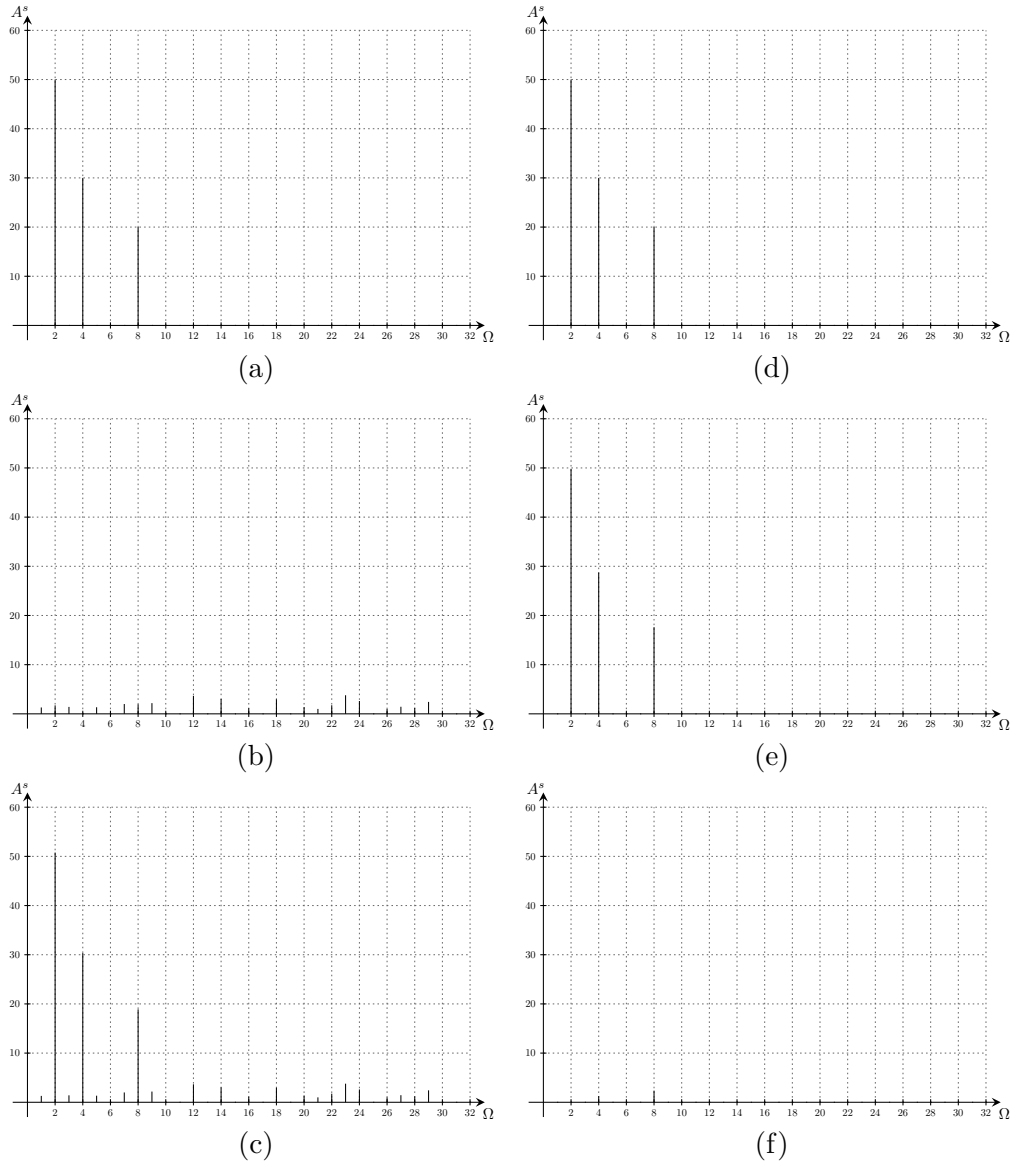


Figure 5.7: MuFCO algorithm operation example, where: a) initial DFT of  $z(t)$ , b) initial DFT of  $x_i^{osc}(t)$ , c) initial DFT of  $s(t)$ , d) final DFT of  $z(t)$ , e) final DFT of  $x_i^{osc}(t)$  and f) final DFT of  $s(t)$ .

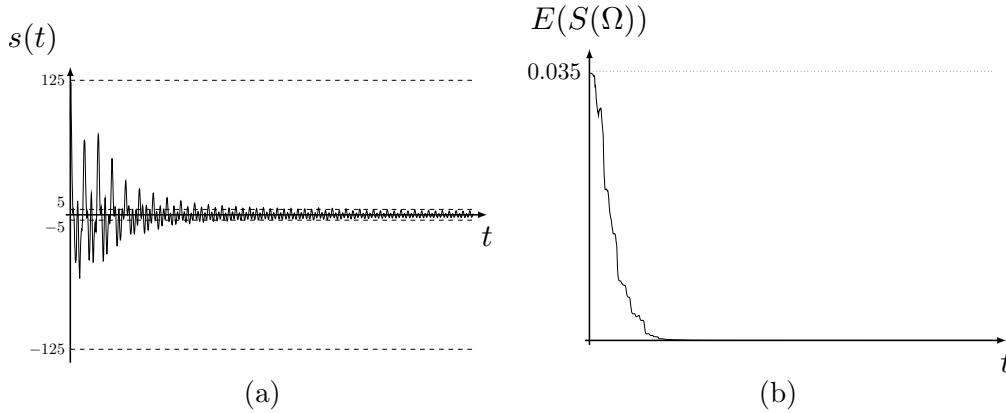


Figure 5.8: **MuFCO** algorithm operation example, where: a)  $s(t)$  development and b)  $E(S(\Omega))$  development in time.

the spectrum. In addition, the initial phase differences are uniformly distributed in  $[-\pi, \pi]$ . Figure 5.7b shows the initial oscillators **DFT**. Notice that the sum of  $A_2^z + A_4^z + A_8^z = 100$ . It means that in the ideal case oscillators will be able to cancel all frequency components. Figure 5.7c shows the initial  $S(\Omega)$  which is the sum of the spectrums of  $z(t)$  and oscillators.

In this example, the **MuFCO** algorithm is executed during 1000s. Thus, Algorithm 3 is executed 1000 times for each oscillator. The spectrum of  $z(t)$  keeps constant because this signal has been defined as a fixed number of sinusoidal functions—compare figures 5.7a and 5.7d. On the other hand, the oscillators switch their operating frequencies and they couple to their respective frequency components. They switch to the frequency components with the higher amplitudes of  $S(\Omega)$ . For this reason, their operating frequencies end up being the same that the initial main components of  $S(\Omega)$ —see Figure 5.7e. Thanks to the negative coupling, these components are removed. Figure 5.7f shows  $S(\Omega)$  at the end of the example, where  $A_2^s$ ,  $A_4^s$  and  $A_8^s$  are almost zero.

Figure 5.8a shows the development of  $s(t)$  over the duration of the example.  $s(t)$  begins as a periodic signal. The frequency components of the signal are canceled during the example, converging to a continuous value. The oscillators behave as a filter. Figure 5.8b shows the development of the shape error function  $E(S(\Omega))$ . As the frequency components of  $S(\Omega)$  are reduced,  $E(S(\Omega))$  converges to zero. This

## 5.4. Operation example

---

results in oscillators keeping the same frequency component, stopping the frequency switching.

### 5.4 Operation example

The **MuFCO** algorithm is designed for signal smoothing in a self-organized way. It may be applied in several applications where the environment and the action of the individuals can be modeled as signals. In this Section, an example of tuning and operation of the **MuFCO** algorithm in a real environment is proposed. The environment chosen for this example is the aggregated consumption of the electricity grid. The electrical grid is divided in two parts: *i*) the base consumption which is the non-controllable signal  $z(t)$  and *ii*) the local facilities which are the oscillators  $x_i^{osc}(t)$ . Therefore, the aggregated consumption may be modified through the phase coupling and operating frequency switching of the oscillators. This example has been implemented in *GridSim* simulation framework—see Appendix A.

The electrical grid chosen for this example is the peninsular Spanish grid during the year 2013. This consumption was measured by the Spanish grid operator R.E.E. with a sampling period of 1 hour. These real measurements have been interpolated in order to use an aggregated consumption with a sampling period of 1 min because the simulation time step of *GridSim* has been set to 1 min. Hence,  $z(t)$  is the aggregate consumption of Spain. Figure 5.9a shows the aggregated consumption during 2013. This consumption varies along the year with a yearly average consumption of 28.1 GW, a maximum consumption around 39.5 GW and minimum consumption around 17.2 GW. The daily difference between peak and valley has also been calculated so that the maximum difference throughout the year is 15.5 GW, the minimum is 7.6 GW and the average is 11.7 GW. Figure 5.9b zooms on a signal segment showing the aggregated consumption during two weeks. The intra-day variation can be appreciated in this figure. This variation is the strongest in the aggregated consumption signal and it is the one that more affects the electricity grid operation. The spectrum of the aggregated consumption is shown in Figure 5.9c, where the main frequency components are in the low frequencies. The strongest frequency component has a period of 24 hour verifying the importance of intra-day variation. The next strongest component is in the 12 hour period. It corresponds to the half-day variations which also affects considerably to the electricity grid operation. For periods longer than 24 hour, the main frequency component corresponds to the weekly variations with a 168 hour period.

## 5. Multi-Frequency Coupled Oscillators

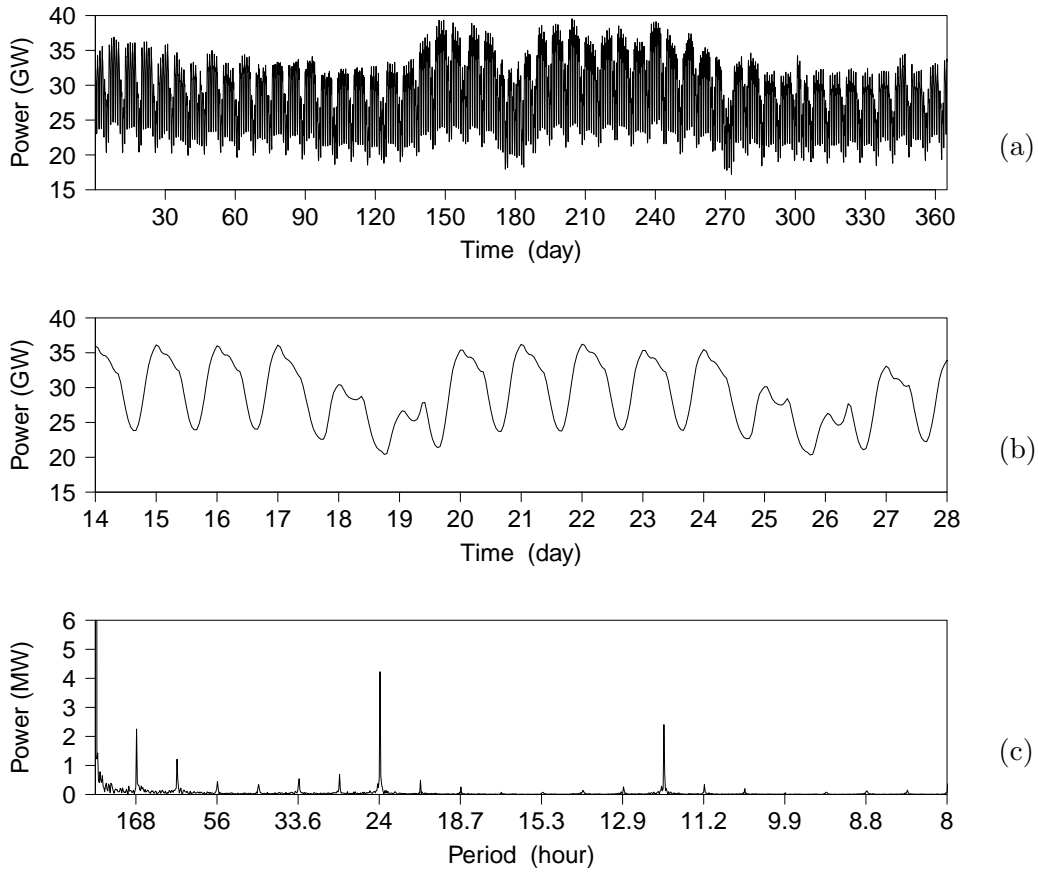


Figure 5.9: Aggregated consumption signal of Spain during 2013: a) aggregated consumption in time  $P(t)$ , b) zoom on two weeks of  $P(t)$ , c) **DFT** of the signal.

The variations of the aggregated consumption are assessed through the *crest factor*—see Equation 3.8. This factor can be applied to different time intervals, where the maximum peak is divided by the root mean square of the aggregated consumption during the studied interval. Four types of crest factors are used:  $C_{year}$ ,  $C_{month}$ ,  $C_{week}$  and  $C_{day}$ . These crest factors are averaged during the assessment period as in Equation 3.9, where  $\bar{C}_{day}$  represents the average of the crest factors of the 365 days of simulated year,  $\bar{C}_{week}$  is the average of the 52 weeks and  $\bar{C}_{month}$  is the average of the 12 months. Table 5.1, “without **MuFCO**” column, shows the crest factor averages for the aggregated consumption exposed in Figure 5.9.

## 5.4. Operation example

<b>crest factors</b>	<b>Without MuFCO</b>	$\mathcal{C}_{\text{day}}$	$\mathcal{C}_{\text{week}}$	$\mathcal{C}_{\text{mix}}$
$C_{\text{year}}$	1.3893	1.2843	1.3375	1.3042
$\bar{C}_{\text{month}}$	1.2856	1.1772	1.1705	1.1795
$\bar{C}_{\text{week}}$	1.2411	1.1340	1.1306	1.1365
$\bar{C}_{\text{day}}$	1.1657	1.0751	1.0779	1.0801

Table 5.1: Crest factors of the aggregated consumption example.

Variations in the aggregated consumption cause different problems in electricity grids, as explained in Chapter 1. These variations may be reduced by using **DSM** techniques. From a frequency domain point of view, **DSM** can be understood as the reduction of the frequency components of the aggregated consumption signal. Therefore considering the oscillators as consumers with a sinusoidal profile, the **MuFCO** algorithm can be applied to **DSM**. Clearly there are no consumers in the electricity grid whose profile is just a sinusoidal function, but their use for real consumptions is explained in detail in Chapter 6. This example is focused on the tuning and validation of the **MuFCO** algorithm with the aggregated consumption.

The **MuFCO** algorithm has four configurable parameters:  $K$ ,  $P^{\text{switch}}$ ,  $T^{\text{smp}}$  and  $W$ . They depend on the environment nature and optimization conditions. The optimization condition refers to a concrete smoothing objective. In this example, the algorithm is tuned to three smoothing objectives: *i*) to reduce the intra-day variations, *ii*) to reduce the weekly variations and *iii*) to achieve an equilibrium between intra-day and weekly variation reduction. The tuning process has been performed by using the *irace*<sup>1</sup> package, which implements the *iterated racing* procedure (López-Ibáñez et al., 2011). Its main purpose is to automatically configure optimization algorithms by finding the most appropriate settings given a set of instances of an optimization problem. The smoothing of aggregated consumption by the **MuFCO** algorithm must be translated to an optimization problem by formalizing a cost function and a set of instances of the problem. *irace* executes different instances of the problem with different configurable parameter combinations of the **MuFCO** algorithm. Its goal is to find the best combination of configurable parameters that minimizes the cost function for the different instances.

<sup>1</sup> <http://iridia.ulb.ac.be/irace/>

## 5. Multi-Frequency Coupled Oscillators

<b>MuFCO</b> parameter	$\mathcal{C}_{\text{day}}$	$\mathcal{C}_{\text{week}}$	$\mathcal{C}_{\text{mix}}$
$W$	16	32	16
$T_{\text{smp}}$	90	315	90
$K$	-0.03	-0.03	-0.02
$P_{\text{switch}}$	0.02	0.29	0.04

Table 5.2: *irace* optimization results.

An instance of the problem represents a specific execution framework where the **MuFCO** algorithm is assessed by the cost function. The instance definition is paramount to tune the algorithm to the problem. In this example, each instance consist of the execution of the **MuFCO** algorithm during 1,051,200 min which correspond to 2 years. The first year is used to adapt the algorithm and the second one to assess the **MuFCO** algorithm performance. All instances are performed with 200 oscillators of 100 MW of peak power. The instances have been divided in two groups:

- *The group of instances without  $z(t)$* : represents the instances in which there are only oscillators and  $z(t)$  is zero. These instances ensure that the optimum parameters obtained from the tuning process are able to meet the optimization criterion in situations where the oscillator power is higher than  $z(t)$  power. This provides scalability to the algorithm because it is able to self-synchronize in absence of  $z(t)$ .
- *The group of instances with  $z(t)$* : allows to find the optimum configuration parameters for this concrete example. In these instances,  $z(t)$  is the aggregated consumption. Additionally, both instance groups are composed of 6 different instances each, where each instance only differs in the random number generator seed. This ensures that the optimum parameters are not affected by the initial conditions.

After the execution of an instance, the **MuFCO** algorithm performance must be assessed through the *cost function*  $\mathcal{C}$ . The cost function definition is paramount to find the optimum parameters that reach the proposed goal. In order to assess the intra-day variations, the cost function is the average daily crest factor for the second

## 5.4. Operation example

---

year of simulation:

$$\mathcal{C}_{\text{day}} = \bar{\mathcal{C}}_{\text{day}} \quad (5.15)$$

where  $\mathcal{C}_{\text{day}}$  denotes the cost function to assess the intra-day variation. After each instance is simulated, the cost function of Equation 5.15 is calculated. *irace* optimization has been performed using this cost function in the different instances previously explained. Table 5.2,  $\mathcal{C}_{\text{day}}$  column, shows the result of the optimization process. It is noteworthy that the sample period is 90 min because the execution of the **MuFCO** algorithm only takes place in this interval. This means that low computing power is required.

Figure 5.10 shows an example of the **MuFCO** algorithm operation optimized to reduce intra-day variations. This example corresponds to the execution of one instance used for the *irace* procedure. It means that the example configuration is the same as in the *irace*'s instances. Figure 5.10a shows the aggregated consumption during the second year of simulation. The intra-day variations of the aggregated consumption have been considerably reduced in comparison with the situation of Figure 5.9a. The yearly average consumption is 28.1 GW, a maximum consumption is 35.8 GW and minimum consumption is 17.9 GW. The maximum daily difference between peak and valley throughout the year is 11.2 GW, the minimum is 1.3 GW and the average is 4.7 GW. This effect can be better appreciated by observing Figure 5.10b. The Fourier Transform of the aggregated consumption also shows the intra-day variation reduction. Figure 5.10c shows that the frequency components of 24 hour and 12 hour period has almost been removed in comparison with Figure 5.9c. The crest factor averages for this example are shown in Table 5.1,  $\mathcal{C}_{\text{day}}$  column. All crest factors have been reduced with special emphasis on the daily factor.

Despite the reduction of the intra-day variations, there are still very marked intra-week variations. These variations may be reduced if the **MuFCO** algorithm is optimized with a cost function that only considers the intra-week variations. In this case, the cost function is the average weekly crest factor:

$$\mathcal{C}_{\text{week}} = \bar{\mathcal{C}}_{\text{week}} \quad (5.16)$$

where  $\mathcal{C}_{\text{week}}$  denotes the cost function to assess the intra-week variation. Table 5.2 shows the result of the optimization process using  $\mathcal{C}_{\text{week}}$ . The weekly component is not dismissed from the **DFT** analysis of the **MuFCO** algorithm. Thus, the oscillators can oscillate at this operating frequency.

Figure 5.11 shows an example of the **MuFCO** algorithm operation optimized to reduce intra-week variations. As in the previous example, the configuration of

## 5. Multi-Frequency Coupled Oscillators

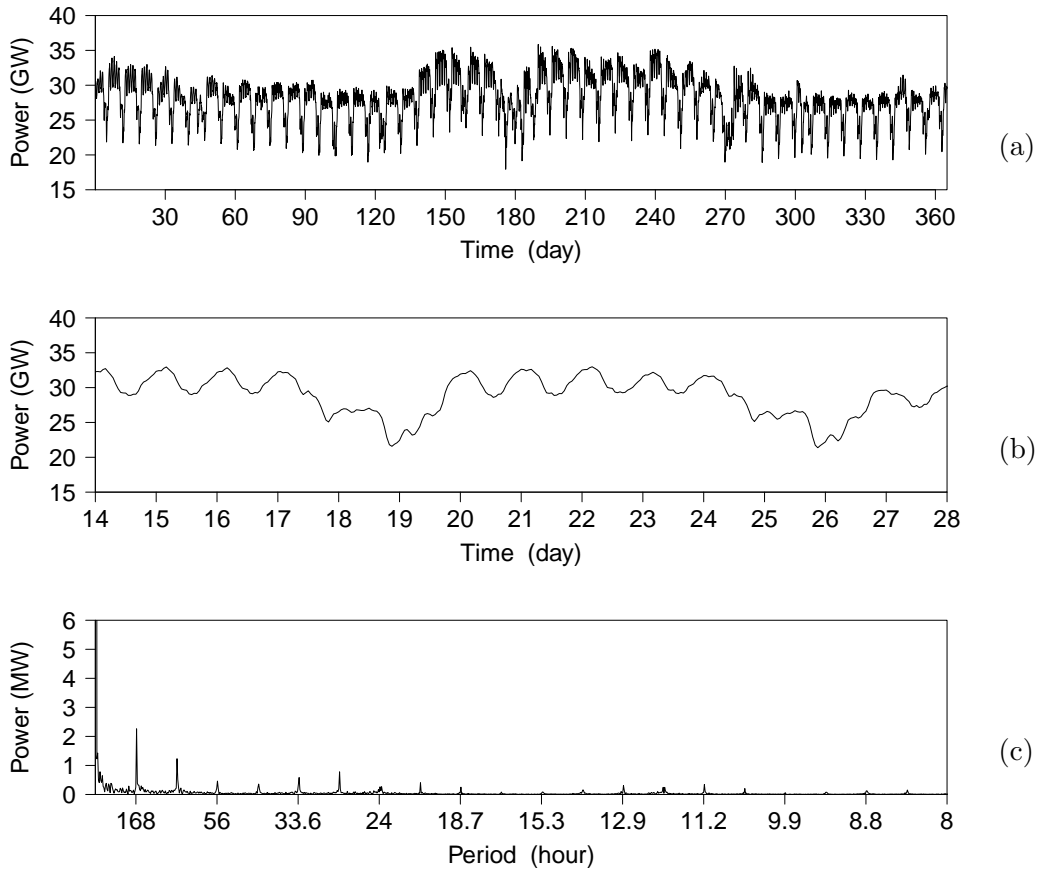


Figure 5.10: Aggregated consumption signal of Spain during 2013 using **MuFCO** algorithm with daily optimization: a) aggregated consumption in time  $P(t)$ , b) zoom on two weeks of  $P(t)$ , c) **DFT** of the signal.

the experiment is the same than an *irace*'s instance configuration. Figure 5.11a shows the aggregated consumption during the second year of simulation. The aggregated consumption variations have been also considerably reduced. The yearly average consumption is 28.1 GW, a maximum consumption is 37.4 GW and minimum consumption is 15.5 GW. The maximum daily difference between peak and valley throughout the year is 11.2 GW, the minimum is 1.6 GW and the average is 4.4 GW. In this case, the difference between the weekdays and the weekend is not so pronounced. This reduction in the intra-week variations causes that the intra-day

## 5.4. Operation example

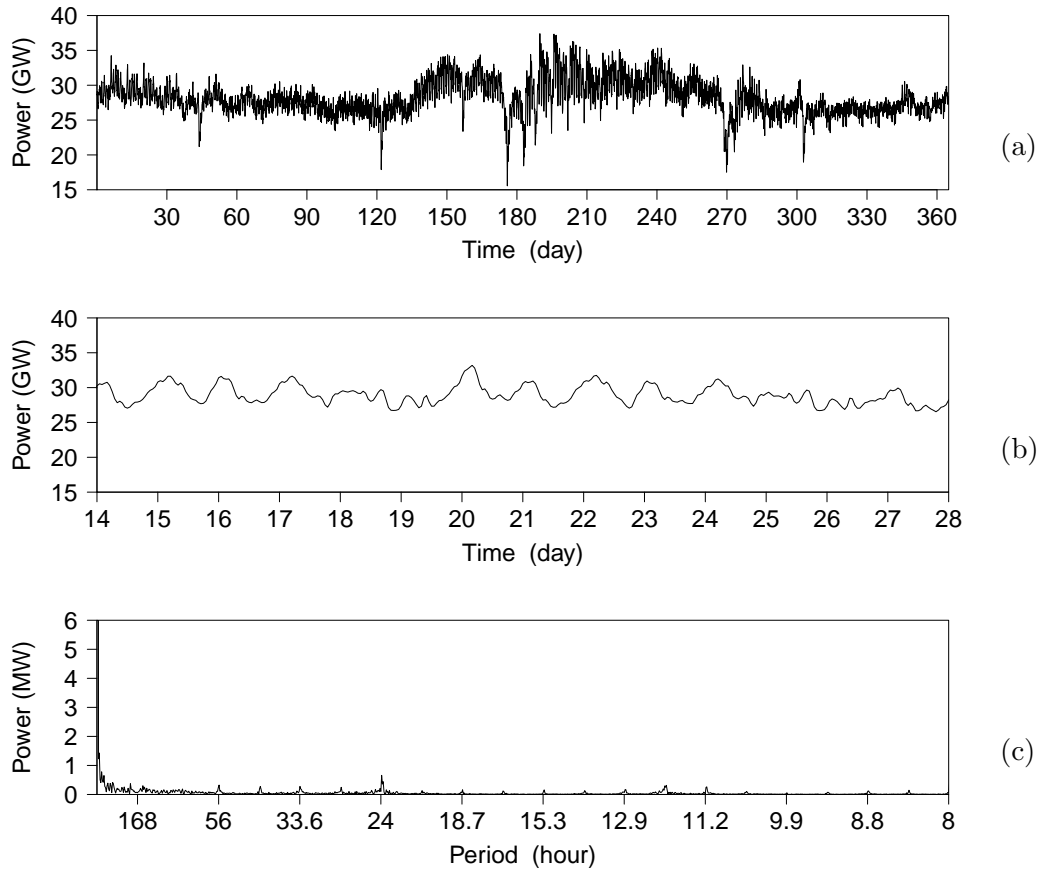


Figure 5.11: Aggregated consumption signal of Spain during 2013 using **MuFCO** algorithm with weekly optimization: a) aggregated consumption in time  $P(t)$ , b) zoom on two weeks of  $P(t)$ , c) **DFT** of the signal.

variation increases—see Figure 5.11b. Figure 5.11c shows the Fourier Transform of the aggregated consumption. The weekly component (168 hour period) is reduced compared with the figures 5.9c and 5.10c. Despite this reduction, the frequency components of 24 hour and 12 hour period have increased slightly compared to intra-day optimization. Table 5.1 shows the crest factor averages for this example.  $\bar{C}_{week}$  is the lowest of all examples.

## 5. Multi-Frequency Coupled Oscillators

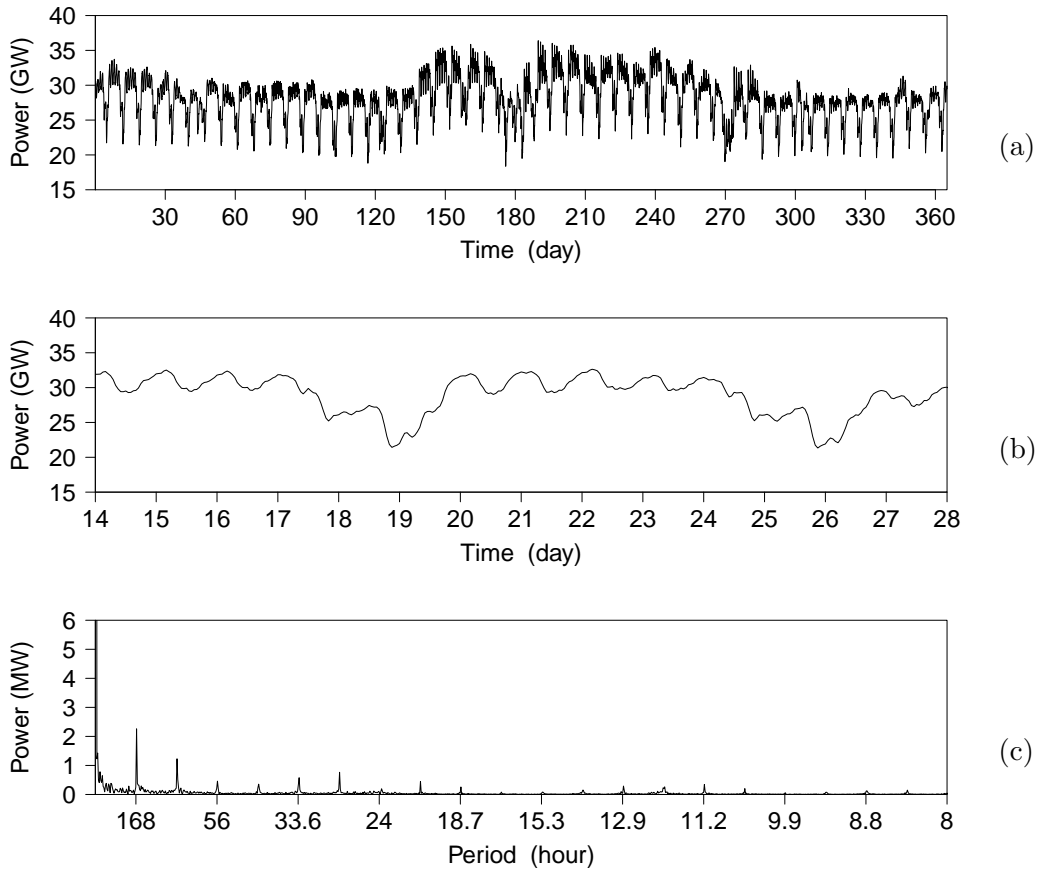


Figure 5.12: Aggregated consumption signal of Spain during 2013 using **MuFCO** algorithm with mixed optimization: a) aggregated consumption in time  $P(t)$ , b) zoom on two weeks of  $P(t)$ , c) **DFT** of the signal.

An equilibrium may be found between the daily and weekly optimization. The following equation defines a cost function that considered both optimization criteria:

$$\mathcal{C}_{\text{mix}} = \frac{\bar{C}_{\text{week}} + \bar{C}_{\text{day}}}{2} \quad (5.17)$$

where  $\mathcal{C}_{\text{mix}}$  is the cost function for the mix of both criteria. Through this function the intra-day and intra-week variations may be reduced at the same time. Table 5.2 shows the result of the optimization process using  $\mathcal{C}_{\text{mix}}$ .

## 5.4. Operation example

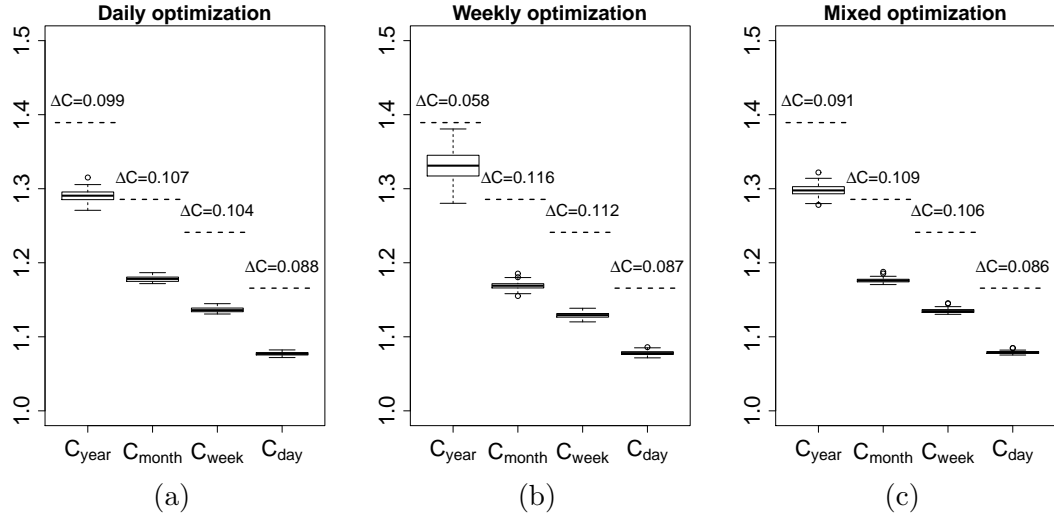


Figure 5.13: Boxplot representation of the statistical analysis of the **MuFCO** optimization.

Figure 5.12 shows an example of the **MuFCO** algorithm operation optimized using Equation 5.17. This example uses the same configuration than an *irace*'s instance, as all previous examples. Figure 5.12a shows the aggregated consumption during the second year of simulation for this example. Both intra-day and intra-week variations have been considerably reduced. The yearly average consumption is 28.1 GW, a maximum consumption is 36.4 GW and minimum consumption is 18.4 GW. The maximum daily difference between peak and valley throughout the year is 12 GW, the minimum is 1 GW and the average is 4.7 GW. Figure 5.12b shows that the difference between weekdays and weekend is not so low than Figure 5.11b but lower than Figure 5.10b. The difference between peaks and valleys during a daily period has been also reduced. The frequency components of 168 hour, 24 hour and 12 hour period have been reduced—see Figure 5.12c. Table 5.1 shows the crest factor averages for this example.

In the previous examples, it has been shown the reduction of the crest factors using the optimized parameters with different optimization criteria. These examples are not representative until they are not statistically analyzed because of the random component. To carry out this analysis, 100 experiments have been performed by using the optimized parameters of each optimization criterion. These experiments have the same configuration as the previous examples. They only differ in the seed of

the random number generator. Figure 5.13 shows the result of the statistical analysis through a boxplot representation. Each graph shows the boxplot for the four types of crest factors for each optimization criterion. The crest factors of the aggregated consumption without oscillators are also represented with discontinuous lines. They correspond to the example of Figure 5.9, where there are no random components. These crest factors are used as reference of the improvement brought by the MuFCO algorithm. For this reason, the *crest factor improvement*  $\Delta C$  is also shown in the graphs.  $\Delta C$  is the difference between the crest factors without oscillators and the mean of the crest factors obtained for each optimization criterion.

The results of the statistical analysis for the daily optimization criteria is shown in Figure 5.13a. All crest factors are reduced by using MuFCO algorithm with this criteria. The most prominent  $\Delta C$  is caused in the  $\bar{C}_{day}$ . Figure 5.13b shows the results of the analysis for the weekly optimization criteria. In this case, the most prominent  $\Delta C$  is caused in the  $\bar{C}_{week}$ . Figure 5.13b shows the result for the mixed optimization criteria.

### 5.5 Discussion

The coupling process by using DFT information is a novel approach which allows the synchronization to be applied to more practical applications. The calculus of the DFT through the Fast Fourier Transform (FFT) is a widely use technique in signal processing. On the other hand, the introduction of a non-controllable signal or oscillator in the coupling equation presents a new synchronization approach. It may be used as an adaptive process where the oscillators adapt to the phase of the non-controllable signal and between them. All this can be performed from a distributed point of view, where no accurate information is required of all system elements. The elements only require information about the environment as an interaction through stigmergy.

The switching between frequency components is based on concepts of task allocation. This is a broadly used technique in decision making processes in swarm intelligence. The oscillators choose the frequencies component by considering their amplitudes as stimuli. Thereby, these components are like tasks in a task allocation process. The use of this technique allows to choose the operating frequency of each oscillator in a distributed way. The only information required is the FFT of the aggregated consumption.

## 5.5. Discussion

---

In the operation example of **MuFCO** algorithm in the electrical grid, it was considered that the consumers are oscillators and their consumptions have sinusoidal function shape. This consideration is far from the actual power consumption in the electrical grids, where there are millions of different devices. However, this sinusoidal functions can be considered as consumption patterns as discussed in Section 4.3. This means that the consumers can schedule their consumption following these sinusoidal functions. When the number of consumers is very large, their consumption may take the shape of the consumption pattern. Hence, the consumption will have the same features as the sinusoidal functions of the **MuFCO** algorithm. This issue is extensively explained in Chapter 6.

## 5. Multi-Frequency Coupled Oscillators

---

## Chapter 6

# Swarm Grid

The **Swarm Grid (SG)** algorithm is described in this Chapter. This algorithm uses the sinusoidal consumption patterns generated by the **Multi-Frequency Coupled Oscillators (MuFCO)** algorithm. Through these patterns, the **SG** algorithm schedules the deferrable consumption in order to smooth the aggregated consumption of the electrical grid. In addition, **SG** algorithm takes into account the local generation. It follows a similar procedure than the **Active Demand-Side Management (ADSM)** algorithm presented in Chapter 3. Combining the sinusoidal patterns and the local generation forecast, the **SG** algorithm is able to achieve an equilibrium between self-consumption enhancement and aggregated consumption smoothing.

### 6.1 The Swarm Grid algorithm

The proposed **SG** algorithm is designed to schedule deferrable loads in local facilities. Its objective is to smooth the aggregated consumption of the electrical grid and to increase the self-consumption of these facilities. The scheduling consists of the assignment of an *activation time*  $t_{i,j}^{act}$ <sup>1</sup> for each deferrable load controlled by the **SG** algorithm, where the subscript  $i$  denotes that the deferrable load belongs to the facility  $i$  and the subscript  $j$  is an identifier of the deferrable load. The number of these deferrable loads are defined by the user of the local facility: when the user requires to perform a deferrable load, the user indicates to the **SG** algorithm which load must be performed together with its *running range*  $[t_{i,j}^{beg}, t_{i,j}^{end}]$ <sup>2</sup>. The algorithm is responsible

---

<sup>1</sup> The activation time is the time instant when the deferrable load begins to work, as defined in Section 2.1.3.

<sup>2</sup> The running range represents a time constraint required by the user, as defined in Section 3.1.1.

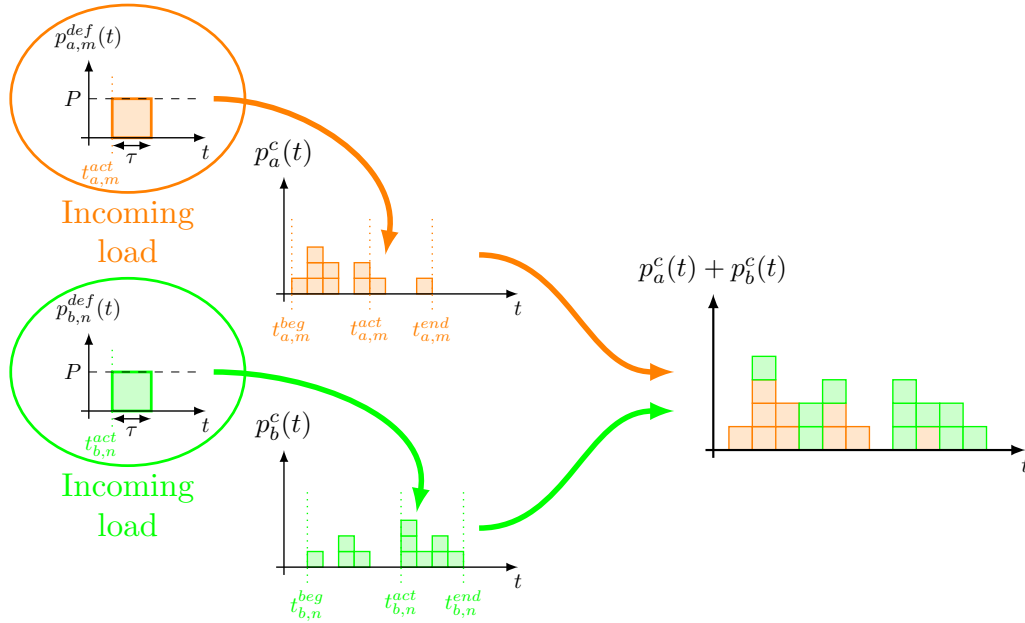


Figure 6.1: Conceptual example of the **SG** algorithm's load scheduling. There are two facilities  $a$  and  $b$ , both facilities schedule one deferrable load each one, which are denoted by  $m$  and  $n$  respectively. The resulting scheduling shapes the local controllable consumptions  $p_a^c(t)$  and  $p_b^c(t)$ . The local consumptions are aggregated composing the aggregated consumption.

to schedule the task deciding the  $t_{i,j}^{act}$ , satisfying that this time instant is within the running range. Figure 6.1 shows a conceptual example of the **SG** algorithm's load scheduling. In this example, the deferrable loads have been simplified as *energy packages* that consume a constant power  $P$  during a time period  $\tau$ . The consumption of these deferrable loads is expressed by the following equation:

$$p_{i,j}^{def}(t) = \begin{cases} P & t \in [t_{i,j}^{act}, t_{i,j}^{act} + \tau] \\ 0 & t \notin [t_{i,j}^{act}, t_{i,j}^{act} + \tau] \end{cases} \quad (6.1)$$

There is a running range for each deferrable load. In the example of Figure 6.1, the incoming orange load  $m$  of the facility  $a$  is scheduled in a different time interval than the green load  $n$  of the facility  $b$ . The **SG** algorithm can schedule an unlimited number of loads. The local scheduling shapes the controllable consumption of the local facility

## 6.1. The Swarm Grid algorithm

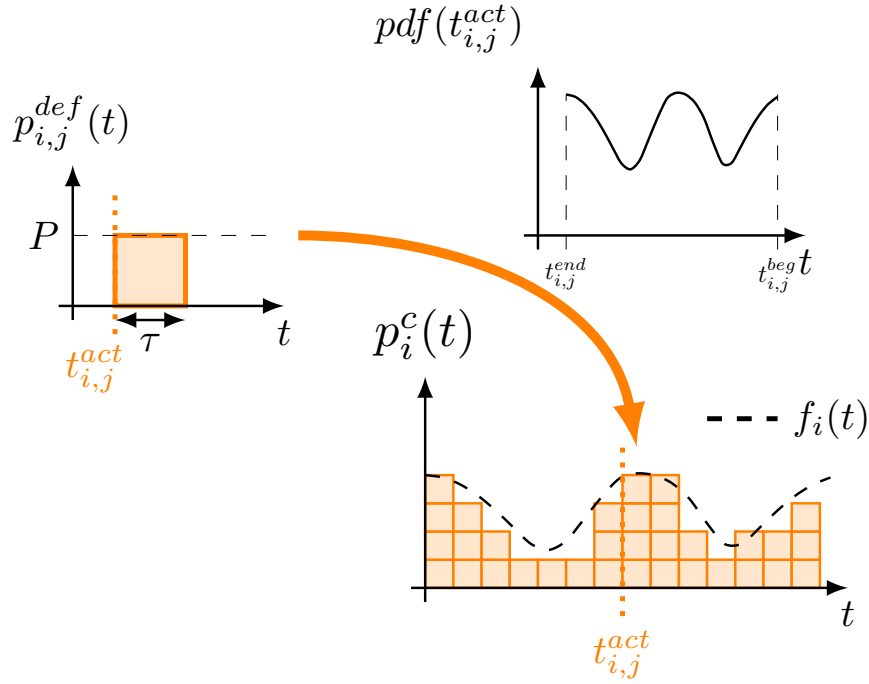


Figure 6.2: Conceptual example of the  $t_{i,j}^{act}$  calculation by SG algorithm.

which is denoted by  $p_i^c(t)$ . In the example of Figure 6.1, the resulting schedules are different as can be observed comparing  $p_a^c(t)$  with  $p_b^c(t)$ . The consumptions of all facilities connected to an electrical grid are aggregated. This procedure was defined in Section 4.3. For example,  $p_a^c(t)$  is aggregated with  $p_b^c(t)$ . Hence, the local schedules shape, at the same time, the aggregated consumption of the whole grid.

As aforementioned, the scheduling consist on the assignment of  $t_{i,j}^{act}$  for each incoming deferrable load. This assignment is performed by using a local consumption pattern  $f_i(t)$ —see Section 4.3. These patterns define the objective shape of the local consumption. It means that the deferrable load should be scheduled such that the local consumption has the same shape than  $f_i(t)$ . In order to achieve this objective, the local consumption patterns have been used as *probability density functions*  $pdf(t_{i,j}^{act})$ . The activation time is considered as a random variable which takes on a value with a certain probability described by  $pdf(t_{i,j}^{act})$ . Notice that  $t_{i,j}^{act}$  should take a value in the running range. The following equation connects the  $f_i(t)$

with  $pdf(t_{i,j}^{act})$ :

$$pdf(t_{i,j}^{act}) = \frac{1}{C} f_i(t_{i,j}^{act}) \quad \text{for } t_{i,j}^{act} \in [t_{i,j}^{beg}, t_{i,j}^{end}]$$

$$C = \int_{t_{i,j}^{beg}}^{t_{i,j}^{end}} f_i(t) dt \quad (6.2)$$

where  $C$  is a normalizing factor which is required for  $pdf(t_{i,j}^{act})$  is a probability density function.

Figure 6.2 shows a conceptual example of this procedure. The incoming deferrable load is activated at  $t_{i,j}^{act}$  which has been assigned by using the probability density function. The time range of  $pdf(t_{i,j}^{act})$  is defined by the user through  $t_{i,j}^{beg}$  and  $t_{i,j}^{end}$ . Thereby,  $t_{i,j}^{act}$  takes always a value in this time interval, satisfying the requirements of the user. In addition,  $pdf(t_{i,j}^{act})$  is calculated using  $f_i(t)$  in the running interval. The local consumption  $p_i^c(t)$  is shaped by the scheduling of the deferrable loads that is in turn shaped by the local consumption pattern.

The local consumption patterns have two objectives on the **SG** algorithm: to smooth the aggregated consumption and to increase the self-consumption. In order to achieve this objectives,  $f_i(t)$  has been divided in two parts. The first part is the sinusoidal function from the **MuFCO** algorithm  $f_i^{MuFCO}(t)$ . This function is able to smooth the aggregated consumption. The second part is the **Photovoltaic (PV)** generation forecast function  $f_i^{PV}(t)$ . This function is able to increase the self-consumption of the local facility. Both parts are combined in the following equation:

$$f_i(t) = \beta \cdot f_i^{PV}(t) + (1 - \beta) \cdot f_i^{MuFCO}(t) \quad (6.3)$$

where  $\beta \in [0, 1]$  is a parameter which regulates the importance of the previous two functions in  $f_i(t)$ . It means that if  $\beta \rightarrow 0$  the local consumption pattern tends to  $f_i^{MuFCO}(t)$  and the scheduling tends to smooth the aggregated consumption. On the other hand, if  $\beta \rightarrow 1$  the local consumption pattern tends to  $f_i^{PV}(t)$  and the scheduling tends to increase the self-consumption.

### 6.1.1 Scheduling with MuFCO

**MuFCO** algorithm generates sinusoidal functions from a distributed way to smooth the aggregated consumption. The deferrable consumption rarely behaves as a sinusoidal function, but this function may be used as a pattern of how the consumption should behave. In this Section, the **SG** algorithm is configured with  $\beta = 1$ , thus, it only uses  $f_i^{MuFCO}(t)$  to generate the local consumption pattern.  $f_i^{MuFCO}(t)$  is the

## 6.1. The Swarm Grid algorithm

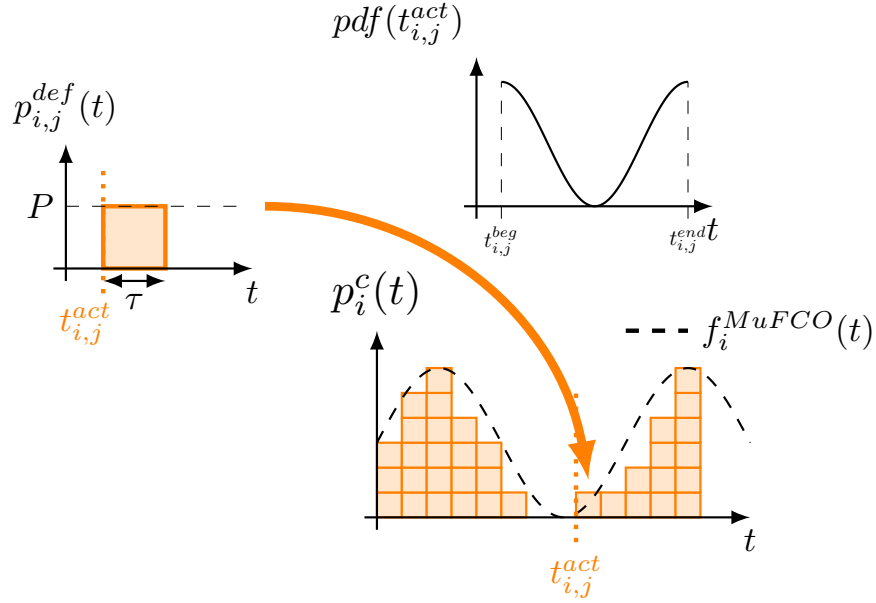


Figure 6.3: Conceptual example of the  $t_{i,j}^{act}$  calculation by **SG** algorithm taking into account the **MuFCO** sinusoidal patterns.

sinusoidal function obtained from the **MuFCO** algorithm for a single oscillator in the range  $[0, 1]$ . The sinusoidal function has been shifted to this range to have a positive function. Thus, a facility is considered as an oscillator which is shifted in magnitude, such that:

$$f_i^{MuFCO}(t) = \frac{1 + x_i(t)}{2} = \frac{1 + \sin(\omega_i t + \phi_i)}{2} \quad (6.4)$$

The definition of an oscillator was explained in Chapter 5 together with Equation 5.2. Therefore, the sum of all facilities has the same properties than the collective of oscillators generated by the **MuFCO** algorithm. The facilities observe the aggregated consumption signal and generate sinusoidal functions such that they adapt to the non-controllable consumption and smooth the aggregated consumption. For this reason, the use of the sinusoidal functions as local consumption patterns allows to achieve this objective.

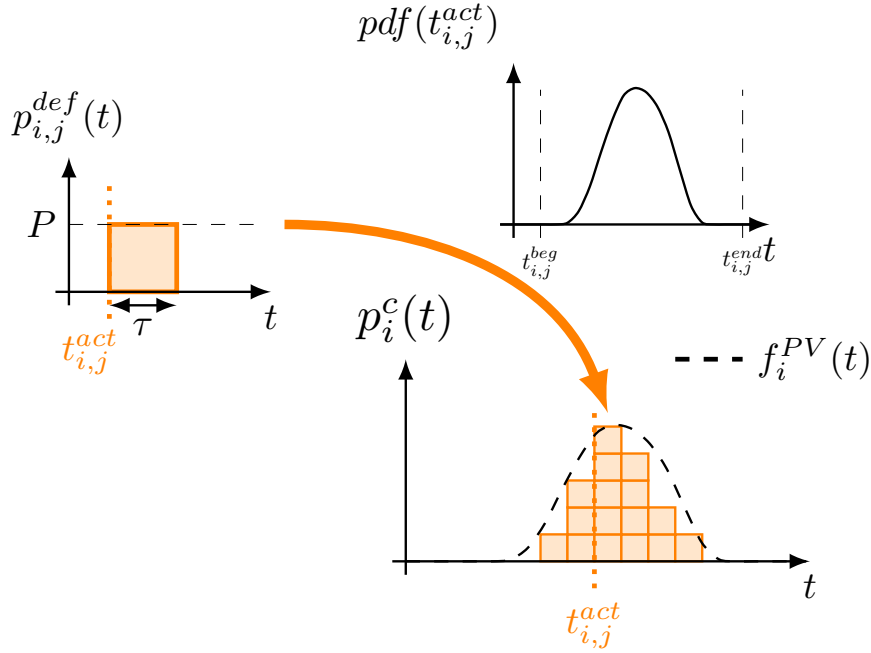


Figure 6.4: Conceptual example of the  $t_{i,j}^{act}$  calculation by **SG** algorithm taking into account the **PV** forecast.

The sinusoidal function for a local facility  $i$  is directly used as a probability density function when  $\beta = 1$ , such that:

$$pdf(t_{i,j}^{act}) = \frac{1}{C} f_i^{MuFCO}(t_{i,j}^{act}) \quad \text{for } t_{i,j}^{act} \in [t_{i,j}^{beg}, t_{i,j}^{end}] \quad (6.5)$$

$$C = \int_{t_{i,j}^{beg}}^{t_{i,j}^{end}} f_i^{MuFCO}(t) dt$$

Figure 6.3 shows an example of the load scheduling with a sinusoidal function. If several loads are scheduled using this distribution, the resulting aggregated consumption will shape as a sinusoidal function. This means that the load scheduling has the same smoothing property as the **MuFCO** algorithm.

### 6.1.2 Scheduling with PV forecast

In order for **SG** algorithm to improve the self-consumption of the locally generated electricity, the local energy generation forecast should be included in the scheduling

## 6.1. The Swarm Grid algorithm

---

**Algorithm 4** High-level description of the Swarm Grid algorithm in the facility  $i$ .

---

- 1: /\* Deferrable load information from the user \*/
  - 2:  $\tau \leftarrow$  Get duration of the deferrable load
  - 3:  $t_{i,j}^{beg} \leftarrow$  Get beginning time of the time interval
  - 4:  $t_{i,j}^{end} \leftarrow$  Get end time of the time interval
  - 5: /\* Calculate  $f_i(t)$  \*/
  - 6:  $f_i^{MuFCO}(t) \leftarrow$  Get sinusoidal from MuFCO algorithm
  - 7:  $f_i^{PV}(t) \leftarrow$  Get normalized local generation forecast
  - 8:  $f_i(t) = \beta \cdot f_i^{MuFCO}(t) + (1 - \beta) \cdot f_i^{PV}(t)$
  - 9: /\* Calculate  $t_{i,j}^{act}$  \*/
  - 10:  $pdf(t_{i,j}^{act}) \leftarrow$  Calculate the p.d.f. by using Equation 6.2
  - 11:  $t_{i,j}^{act} \leftarrow$  Get value of random variable with  $pdf(t_{i,j}^{act})$
- 

process. In this Section, the **SG** algorithm is configured with  $\beta = 0$ , thus, it only uses  $f_i^{PV}(t)$  to generate the local consumption pattern.  $f_i^{PV}(t)$  is the normalized **PV** generation forecast for the facility  $i$ . This function is normalized by the maximum generation of the **PV** generator. It means that  $f_i^{PV}(t)$  is in the range  $[0, 1]$ . The normalized **PV** generation forecast for a local facility  $i$  is directly used as a probability density function when  $\beta = 0$ , such that:

$$pdf(t_{i,j}^{act}) = \frac{1}{C} f_i^{PV}(t_{i,j}^{act}) \quad \text{for } t_{i,j}^{act} \in [t_{i,j}^{beg}, t_{i,j}^{end}] \quad (6.6)$$

$$C = \int_{t_{i,j}^{beg}}^{t_{i,j}^{end}} f_i^{PV}(t) dt$$

Figure 6.4 shows an example of the load scheduling using the **PV** generation forecast. The deferrable loads are scheduled so that the local consumption takes the shape of the **PV** generation forecast. This implies that the consumption is bigger as higher the local generation is. This procedure increases the local self-consumption.

### 6.1.3 Real-time execution

The **SG** algorithm has been designed to run in real-time. It is executed when a new deferrable load is required by the user and this event can occur at any time. Thus, the **SG** algorithm is an asynchronous algorithm. The execution of the **SG** algorithm is summarized by the Algorithm 4: When a new deferrable load is required, this algorithm is executed. The algorithm begins by obtaining the information of

the deferrable load to be scheduled—see from line 2 to 4. This information comes directly from the user. Once the user has indicated the required information, the **SG** algorithm calculates  $f_i^{MuFCO}(t)$  from the **MuFCO** algorithm. This means that **SG** algorithm asks for  $\omega_i$  and  $\phi_i$  to the **MuFCO** algorithm and calculates the sinusoidal function—see Equation 6.5.  $f_i^{PV}(t)$  is also calculated through the Equation 6.6. The local consumption pattern  $f_i(t)$  is calculated by using the Equation 6.3. Once  $f_i(t)$  is obtained,  $pdf(t_{i,j}^{act})$  can be calculated in the range  $[t_{i,j}^{beg}, t_{i,j}^{end}]$  by using the Equation 6.2. Finally,  $t_{i,j}^{act}$  is calculated for this deferrable load. The value of  $t_{i,j}^{act}$  is taken on from  $pdf(t_{i,j}^{act})$  as the execution of a random variable.

## 6.2 Operating examples

In this Section, the **SG** algorithm’s operation is analyzed. This analysis is focused on validating the **SG** algorithm and studying the improvement that it brings to the electrical grid. This Section is divided in three parts in order to analyze three different scenarios:

- *The grid without DERs:* in this scenario, there are not **Distributed Energy Resources (DERs)** and the **SG** algorithm just manages the consumption of the electrical grid to smooth the aggregated consumption. This situation is similar to the example of Section 5.4, where the **MuFCO** algorithm was tuned to smooth the aggregated consumption following different optimization criterion. **SG** algorithm schedules the deferrable loads only by using the sinusoidal patterns generated by **MuFCO**, thus,  $\beta = 0$  for this scenario.
- *The grid with DG:* in this scenario, local **PV** generators are included in the local facilities as **Distributed Generation (DG)** without electrical storage. The presence of this generation may increase the variability of the electrical grid, as shown in Section 3.3.2. **SG** algorithm should schedule the deferrable loads in order to achieve an equilibrium between self-consumption and aggregated consumption smoothing.
- *The grid with DER:* in this scenario, the local facilities are equipped with **DERs**. These resources are composed by **PV** generators and storage systems. As in the previous scenario, the **SG** algorithm should schedule the loads and achieve an equilibrium between self-consumption and aggregated consumption smoothing.

This analysis has been done throughout simulations of an electrical grid by using *GridSim* simulator—see Appendix A. The simulated electrical grid is divided in 600

## 6.2. Operating examples

---

nodes. Each node is a facility which is equipped with a **PV** generator, storage system and local consumption. Depending on the scenario, these elements of the local facility are used or not. The time step of simulation is 1 min. In this analysis, a virtual user is used in order to generate the consumption profile. This user belongs to a concrete facility, it means that if there are 600 nodes, there are 600 virtual users.

### 6.2.1 Virtual users

The consumption of the local facilities (nodes) is created by virtual users in *GridSim* simulator. In this analysis, the virtual users only create deferrable loads, as in the analysis of Section 3.3. Thus, the user of each facility requires a number of deferrable loads during the execution of any simulation. This requirement is an asynchronous event which represents a new deferrable load creation in the local facility. It could happen at any time step of the simulation. Every new deferrable load is created at a concrete time instant denoted by  $t_{i,j}^{NDL}$ . If any controller does not schedule the load, it is activated when it is created such that  $t_{i,j}^{act} = t_{i,j}^{NDL}$ . Figure 6.5 shows an example of this procedure for two facilities where one facility is equipped with the **SG** algorithm and the other has not any controller.

Virtual users create new deferrable loads randomly. There is a probability density function which defines the probability that a new deferrable load is created at a given time instant. This function is denoted by  $P^{NDL}(t)$ . Thus, the creation of a new deferrable load is a binary random variable  $NDL$ . Every time step of the simulation, it is checked if there is a new deferrable load  $P^{NDL}(t) \rightarrow NDL = 1$ . For the analysis presented in this Section,  $P^{NDL}(t)$  is the real aggregated consumption of peninsular Spain during 2013. This implies that the consumption of the virtual users has a similar shape than this aggregated consumption. **SG** controllers modify the activation time of the deferrable loads, thus, it is satisfied that  $t_{i,j}^{act} \neq t_{i,j}^{NDL}$ .

*GridSim* accepts different models of deferrable loads. In this Section, the deferrable loads model has been simplified. They are modeled as *energy packets*. These packets consume a constant nominal power  $P$  during a certain time interval  $\tau$ —see Figure 6.5. To perform the following analysis, the nominal power is  $P = 50$  MW and duration is  $\tau = 60$  min. In addition, it is considered that the deferrable loads have a running range of one day (1440 min):  $t_{i,j}^{beg} = t_{i,j}^{NDL}$  and  $t_{i,j}^{end} = t_{i,j}^{NDL} + 1440$ . Each user creates around 12200 deferrable loads per year. Thus, a local facility consumes around 410 GWh per year. The sum of all local facilities has a yearly energy consumption around 246 TWh, as the Spanish yearly consumption. In a real electrical grid, the facilities do not consume as much electrical energy as the simulated facilities. These

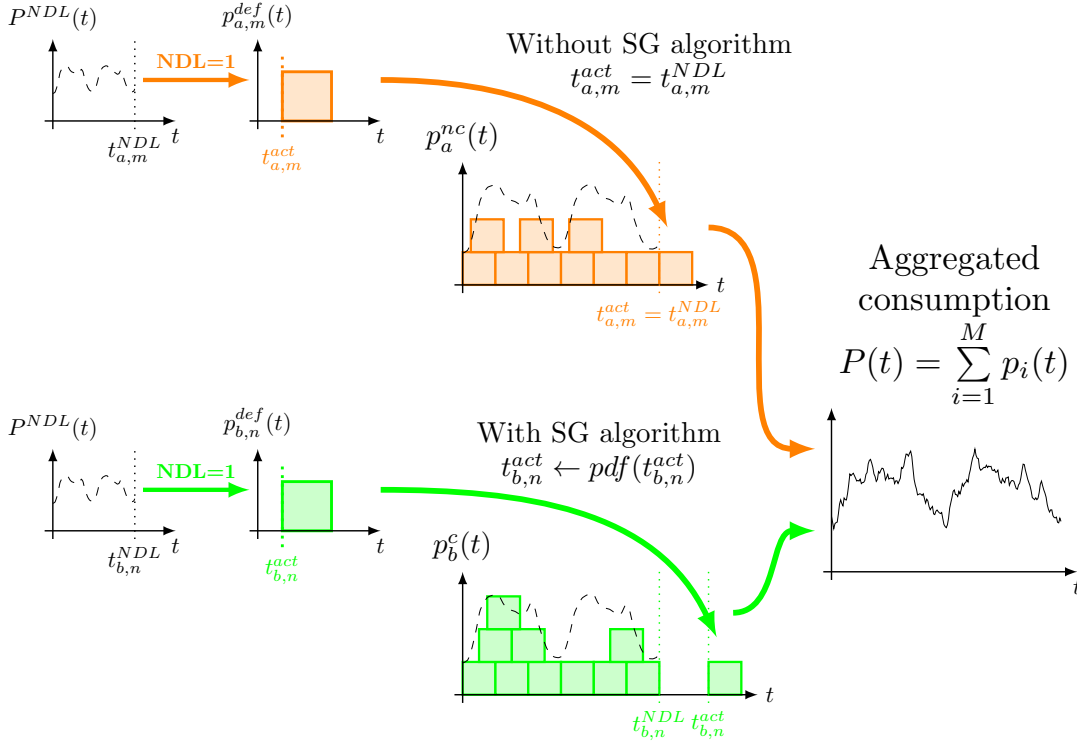


Figure 6.5: Conceptual example of the deferrable consumption created by the virtual users.

energy amounts have been chosen because the grid has been divided in 600 facilities to reduce the computing load. To simulate an electrical grid with thousands or millions of facilities causes a very high computation time. On the other hand, 600 facilities are enough to observe the coordination and smoothing capacity of the SG algorithm.

### 6.2.2 The grid without DER

In this scenario, the facilities are purely consumers without local generation. It is the common scenario if the SG algorithm is deployed in buildings without DER where the classical Demand-Side Management (DSM) mechanisms are performed. Part of this consumption is controlled by the SG algorithm and the other part is directly set by the user. The percentage of consumption controlled by the algorithm is denoted by  $\rho^{ctr}$ . For example, if  $\rho^{ctr} = 50\%$  and the yearly consumption is 246 TWh, it means

## 6.2. Operating examples

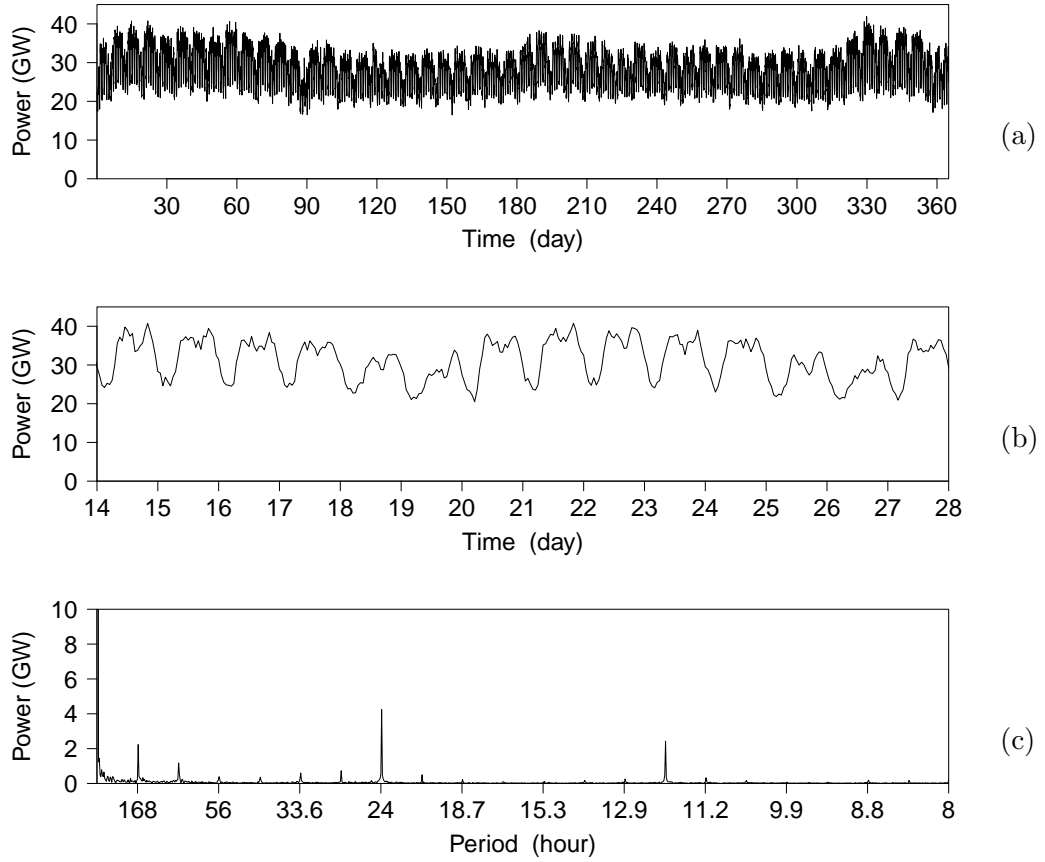


Figure 6.6: Example of the aggregated consumption of the simulated electrical grid without DER, where the SG algorithm does not control any load  $\rho^{ctr} = 0\%$ : a) one year of simulation, b) one week of this simulation and c) DFT. The crest factors for these example:  $C_{year} = 1.52$ ,  $\bar{C}_{month} = 1.37$ ,  $\bar{C}_{week} = 1.32$  and  $\bar{C}_{day} = 1.22$ .

that the SG algorithm controls 123 TWh of deferrable loads along the year. Notice that  $\beta = 0$  for all experiments performed in this scenario because there is not local generation.

Figure 6.6 shows the aggregated consumption for an example of this scenario where the SG algorithm does not control any load  $\rho^{ctr} = 0\%$ . In this example, the deferrable loads are activated at the same time that they are generated by the virtual user, such that  $t_{i,j}^{act} = t_{i,j}^{NDL}$ . Thus, the aggregated consumption shown in Figure 6.6 represents

the common behavior of the Spanish electrical grid. This example is equivalent to that shown in Figure 3.16 in Section 3.3. The Fourier Transform of this consumption has some prominent frequency components at 168 h, 24 h and 12 h periods, as the typical aggregated consumption—see Figure 6.6c. The simulated grid reaches a maximum yearly peak of 41.9 GW, a minimum valley of 16.4 GW and a average consumption of 28.1 GW. The daily difference between peak and valley has also been calculated so that the maximum difference throughout the year is 20.5 GW, the minimum is 6.8 GW and the average is 12.2 GW.

A campaign of experiments has been performed to study how the percentage of consumption controlled by the SG algorithm affects the crest factors of the aggregated consumption. For each  $\rho^{ctr}$  value, 100 experiments have been performed with different seeds of the random number generator. An experiment consists on the simulation of the previously explained electrical grid during one year and a half (788400 min) with a concrete  $\rho^{ctr}$  value and a concrete seed. The first half year is used to adapt the SG algorithm to the grid, after that, the crest factors are calculated for the remainder year. This algorithm operates with the tuned parameters to reduce the daily variability obtained in Section 5.4:  $W = 16$ ,  $T_{smp} = 90$  min,  $K = -0.03$  and  $P_{switch} = 0.02$ .

Figure 6.7 shows the development of the crest factors for different percentages of consumption controlled by the SG algorithm. For each  $\rho^{ctr}$  value, the mean and the maximum and minimum values have been calculated from the 100 different seeds. Figure 6.7 is divided in four graphs where each graph plots the statistical analysis for each type of crest factor. The common trend is that the greater the amount of consumption controlled by the algorithm is, the lower the crest factors are. In addition, the dispersion of the experiments is higher as greater is the range of time covered by the crest factor. For instance, the difference between *max* and *min* is much lower for the daily crest factor average than for the yearly crest factor average. In all graphs, the crest factors achieve a plateau value when the SG algorithm controls over the 50% of the whole consumption. The following conclusions come from these results:

- *Regardless  $\rho^{ctr}$ , the algorithm reduces the electrical grid variability:* In general, the higher the  $\rho^{ctr}$ , the lower the crest factors. This implies that the smoothing objective is met by the SG algorithm. This relationship is satisfied until the crest factors achieve the plateau value. When this value is achieved, the algorithm self-organizes and the crest factors may not be reduced.

## 6.2. Operating examples

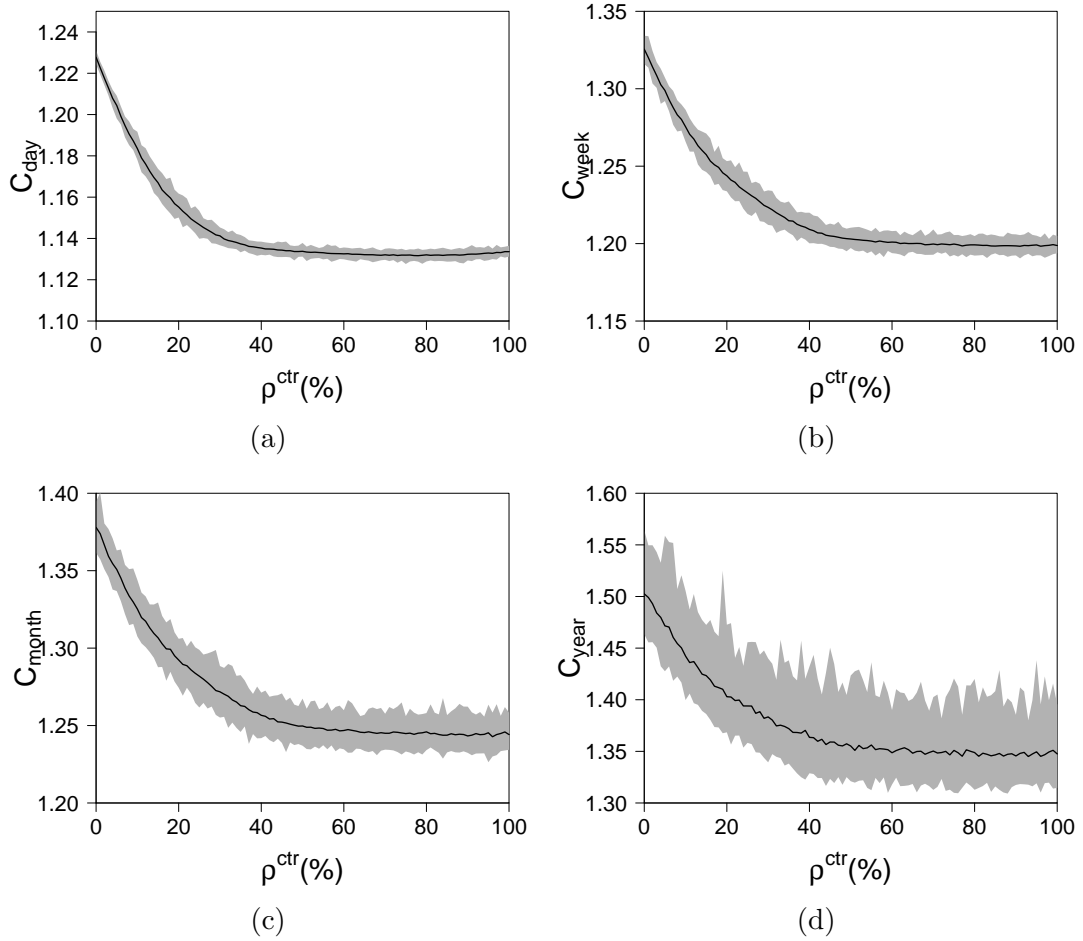


Figure 6.7: Development of the crest factors for different percentages of consumption controlled by the SG algorithm. The solid line represents the mean of the crest factors from the 100 simulated seed. The shaded area is between the maximum and the minimum value obtained from the 100 simulated seed: a)  $\bar{C}_{day}$ , b)  $\bar{C}_{week}$ , c)  $\bar{C}_{month}$  and d)  $C_{year}$ .

- *The algorithm self-organizes:* For  $\rho^{ctr} < 50\%$  values, the controllable part of grid's consumption is lower than the non-controllable one. SG algorithm adapts to the non-controllable consumption, reducing the variability of the grid. On the other hand, when  $\rho^{ctr} > 50\%$ , SG algorithm should also self-organize. It

means that the controllable consumption must coordinate with itself to achieve a neutral effect. For example, if  $\rho^{ctr} = 60\%$  there are 240 facilities without the **SG** algorithm, thus, 240 facilities with the **SG** algorithm are required at least to fully smooth their consumption. The other 120 facilities with the **SG** algorithm should coordinate between to provoke a constant aggregated consumption. This feature is verified because the crest factors do not increase for  $\rho^{ctr} > 50\%$ . It implies that the controlled consumption is able to coordinate to reduce the crest factors for  $\rho^{ctr} < 50\%$  values and to maintain them for  $\rho^{ctr} > 50\%$ .

Figure 6.8 shows the aggregated consumption for an instance of this scenario where the **SG** algorithm controls the whole consumption  $\rho^{ctr} = 100\%$ . In this example, the deferrable loads are scheduled by the **SG** algorithm and  $t_{i,j}^{act} \neq t_{i,j}^{NDL}$ . The reduction of the aggregated consumption variability can be easily observed by comparing Figure 6.6 with Figure 6.8. The intra-day variations of the aggregated consumption have been considerably reduced. Figure 6.8b shows how this variability has been almost entirely eliminated. By comparing the Fourier transform of both experiments, with and without **SG** algorithm, it can be observed how the frequency components at 24 h and 12 h periods have been reduced to almost zero. The difference between the crest factors of both examples is also considerable, reaching reductions of 12% in the yearly crest factor or 7.5% in the daily crest factor average. In this example, the maximum yearly peak reaches 36.1 GW, reducing by 5.8 GW in relation to the example without the **SG** algorithm. The minimum yearly valley is 19.8 GW and the average is 28.1 GW. Regarding the daily difference between peak and valley, the maximum difference is 9.4 GW, the minimum is 2.4 GW and the average is 4.7 GW.

### 6.2.3 The grid with DG

The presence of **DG** in the electrical grid may increase the variations in the aggregated consumption. This issue was analyzed in Section 3.3.2. In this scenario, the effects of the **PV** generation together with the **SG** algorithm are analyzed. The simulated generation follows the same procedure as in Section 3.3.2. The generation profiles from six different cities of Spain have been used. There are 100 virtual facilities (nodes) for each city. The combination of these cities allows different climate regions to be considered. The maximum nominal **PV** power generation is 240 MWp in each facility, such that the sum of the generation of all facilities is 144 GWp. This generation power corresponds to a yearly energy generation around 246 TWh which is the same energy amount than the yearly energy consumption of Spain. In this Section, the effects

## 6.2. Operating examples

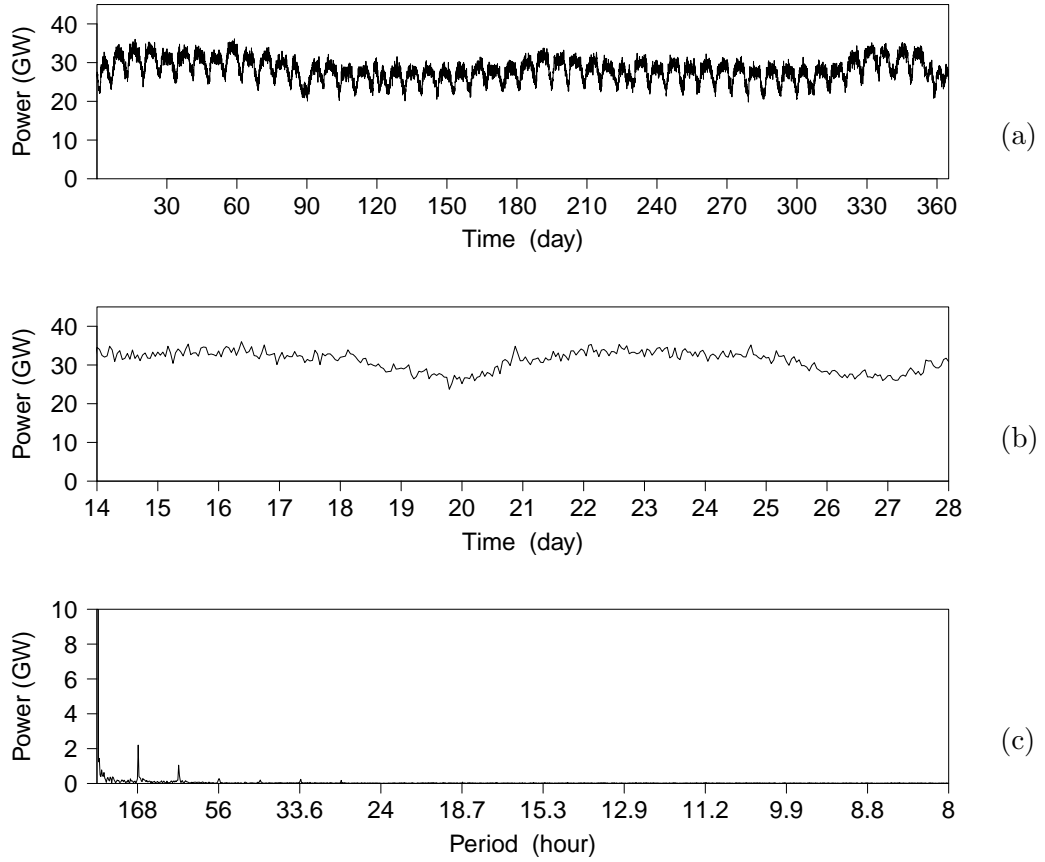


Figure 6.8: Example of the aggregated consumption of the simulated electrical grid without **DER**, where the SG algorithm controls all loads  $\rho^{ctr} = 100\%$ : a) one year of simulation, b) one week of this simulation and c) **DFT**. The crest factors for these example:  $C_{year} = 1.34$ ,  $\bar{C}_{month} = 1.24$ ,  $\bar{C}_{week} = 1.20$  and  $\bar{C}_{day} = 1.13$ .

of the **PV** penetration in the electrical grid have also been studied by using the **PV penetration factor**  $\rho^{PV}$ .

Figure 6.9 shows an example of the aggregated consumption of the simulated electrical grid with  $\rho^{PV} = 50\%$  and  $\rho^{ctr} = 0\%$ . This penetration of **PV** generation in the electrical grid increases its variability. The maximum yearly peak reaches 41.9GW as the example without **PV** generation. There are times during the year where the aggregated consumption is reduced to zero. The average of the aggregated

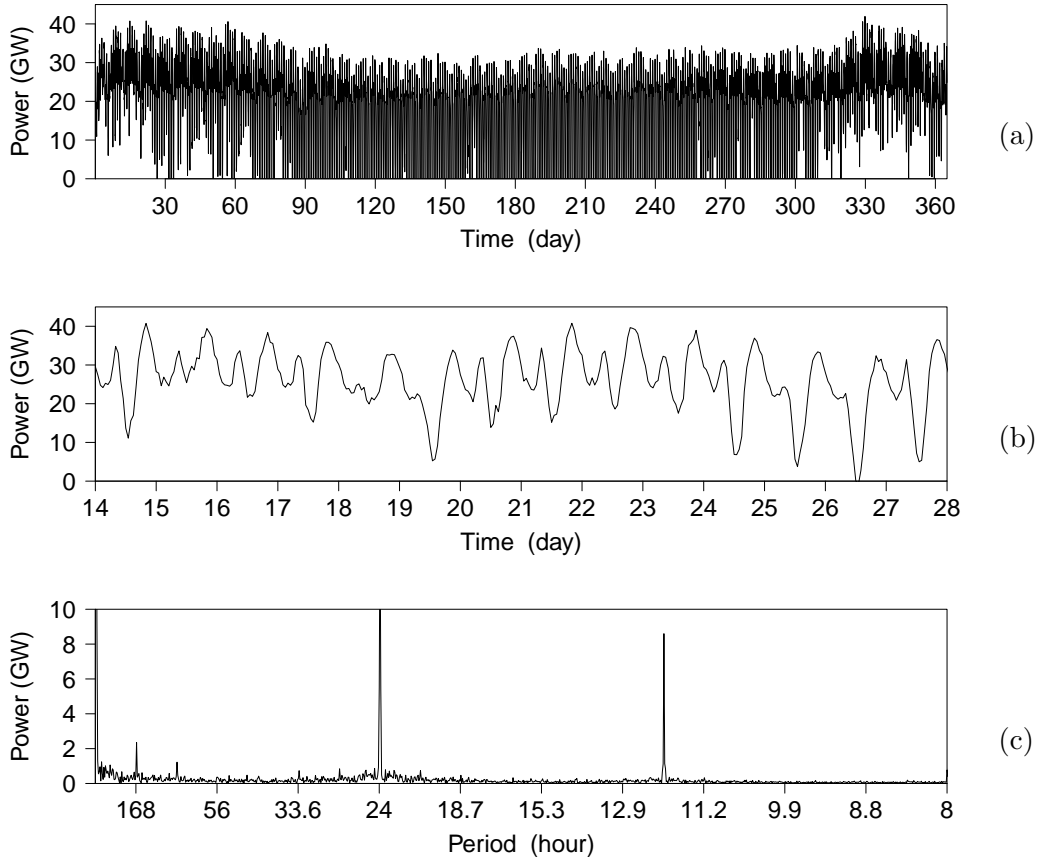


Figure 6.9: Example of the aggregated consumption of the simulated electrical grid with  $\rho^{PV} = 50\%$  and  $\rho^{ctr} = 0\%$ : a) one year of simulation, b) one week of this simulation and c) **DFT**. The crest factors for these example:  $C_{year} = 1.94$ ,  $\bar{C}_{month} = 1.79$ ,  $\bar{C}_{week} = 1.72$  and  $\bar{C}_{day} = 1.6$ . The self-consumption for this example:  $\xi = 0.24$ .

consumption is 18.3 GW. Regarding the daily difference between peak and valley, the maximum difference is 39.8 GW, the minimum is 10.4 GW and the average is 28.3 GW. In this example, the **SG** algorithm is not controlling any load, thus, this values are considered as reference for the next examples.

**SG** algorithm modifies the aggregated consumption shape and the self-consumption of the local facilities depending on the  $\beta$  parameter when there is **PV** generation. A campaign of experiments has been performed to study how  $\rho^{PV}$  and  $\beta$  affects

## 6.2. Operating examples

---

the crest factors of the aggregated consumption and the self-consumption. In this campaign,  $\rho^{ctr} = 100\%$  for all experiments so that the effect of  $\beta$  parameter could be better observed. Different combinations of  $\rho^{PV}$  and  $\beta$  have been studied. For each combination of these parameters, 3 experiments have been performed with different seeds of the random number generator. An experiment consists on the simulation of the previously explained electrical grid during one year and a half (788400 min) with a concrete combination of  $\rho^{PV}$  and  $\beta$  and a concrete seed. The first half year is used to adapt the **SG** algorithm to the grid, after that, the crest factors are calculated for the remainder year. The crest factors and the self-consumption of the local facilities are calculated for each experiment. **SG** algorithm operates with the tuned parameters to reduce the daily variability obtained in Section 5.4:  $W = 16$ ,  $T_{smp} = 90$  min,  $K = -0.03$  and  $P_{switch} = 0.02$ .

Figure 6.10 shows the development of the crest factors for different combinations of  $\rho^{PV}$  and  $\beta$  with  $\rho^{ctr} = 100\%$ . In general, the lower the  $\beta$  parameter is, the lower the electrical grid variability. When  $\beta$  takes values close to one, the variability of the grid increases exponentially. This behavior is similar to that observed with the **ADSM** algorithm in Section 3.3.3. The greater the  $\beta$  parameter is, the greater the importance that is given to the **PV** generation forecast. In these situations, all facilities schedule the deferrable loads following a similar pattern (the **PV** forecast) without synchronization. It implies that days with low **PV** generation or forecast errors causes a great mismatch between consumption and generation. These results suggest that **SG** algorithm works better for  $\beta = 0$  from the grid point of view.

Figure 6.11 shows the development of the self-consumption for different combinations of  $\rho^{PV}$  and  $\beta$  with  $\rho^{ctr} = 100\%$ . In general, the higher the  $\rho^{PV}$  and  $\beta$ , the higher the self-consumption. The increase of the self-consumption because of  $\beta$  takes place for  $\beta$  values close to one. This effect coincides with the exponential increases of the grid variability. Therefore, the decision of which  $\beta$  value should be used depends on the designer priority: whether the self-consumption is more important than the grid variability or not. On the other hand, the increase of the self-consumption because of  $\rho^{PV}$  is trivial: the greater the presence of **PV** power is, the greater the amount of **PV** energy used in the local facilities. During the remainder of this chapter,  $\beta$  is zero to focus on the smoothing of the aggregated consumption.

Figure 6.12 shows an example of the aggregated consumption of the simulated electrical grid with  $\rho^{PV} = 50\%$ ,  $\rho^{ctr} = 100\%$  and  $\beta = 0$ . The maximum yearly peak reaches 50.9 GW as the example without **PV** generation. There are times during the year where the aggregated consumption is reduced to zero. The average of the

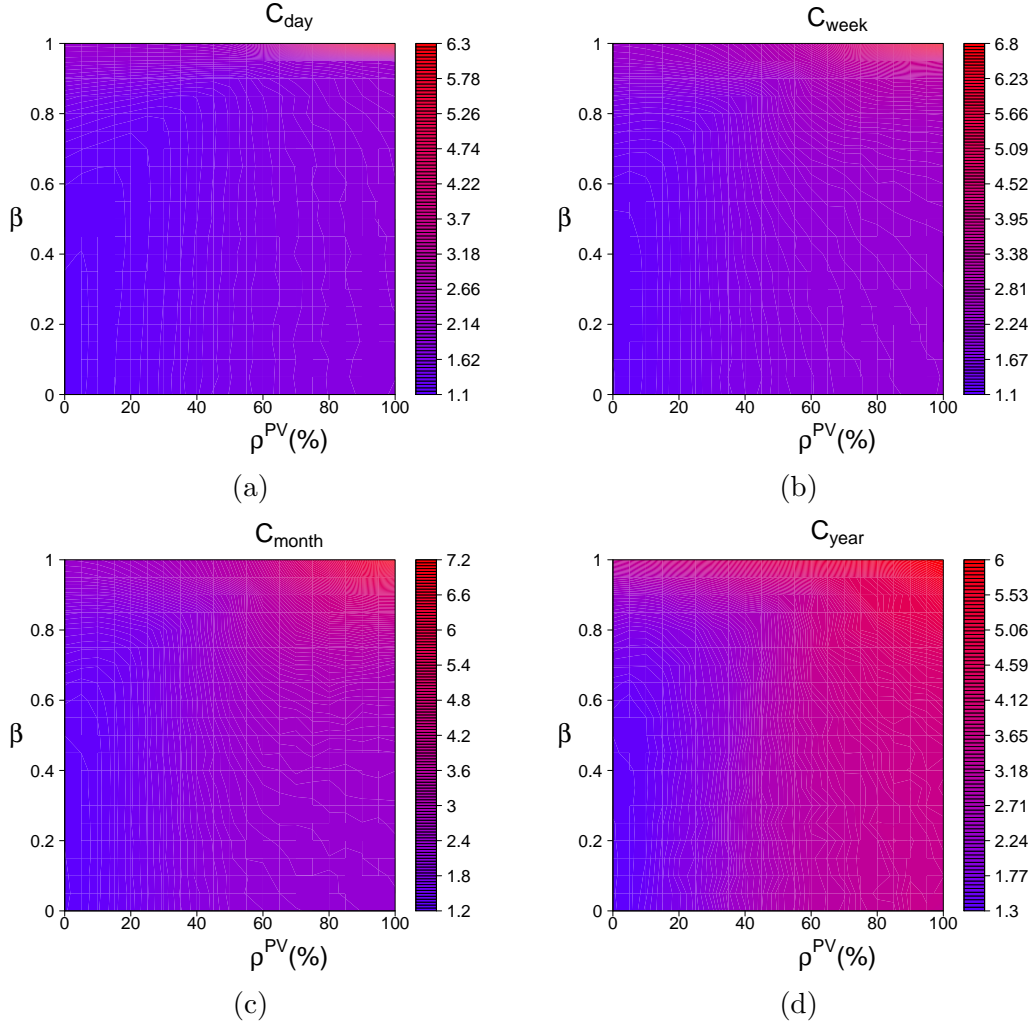


Figure 6.10: Heat map representing the development of the crest factors for different combinations of  $\rho^{PV}$  and  $\beta$  with  $\rho^{ctr} = 100\%$ : a)  $\bar{C}_{day}$ , b)  $\bar{C}_{week}$ , c)  $\bar{C}_{month}$  and d)  $C_{year}$ .

aggregated consumption is 16.2 GW. Regarding the daily difference between peak and valley, the maximum difference is 35.7 GW, the minimum is 4.9 GW and the average is 17.6 GW. The use of SG algorithm has increased the maximum yearly peak in relation to the example of Figure 6.9 where it reached 41.9 GW. This is because of the high variability introduced by the PV generation which makes difficult

## 6.2. Operating examples

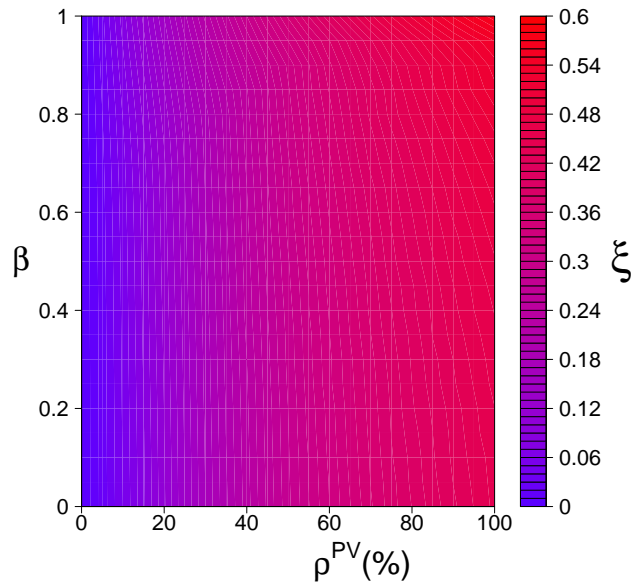


Figure 6.11: Heat map representing the development of the self-consumption for different combinations of  $\rho^{PV}$  and  $\beta$  with  $\rho^{ctr} = 100\%$ .

the synchronization process. This can be observed in Figure 6.12a: after the high generation period during summer, the aggregated consumption signal varies abruptly and the SG algorithm should synchronize to this change. On the other hand, the daily difference between peaks and valleys has been reduced regarding the case without SG algorithm. It means that the algorithm is able to perform the objective for which it has been optimized even with high  $\rho^{PV}$  values.

The effect of the percentage of consumption controlled by SG algorithm on the aggregated consumption depends on the PV penetration. A campaign of experiments has been performed to study how  $\rho^{PV}$  and  $\rho^{ctr}$  affects the crest factors of the aggregated consumption and the self-consumption. In this campaign,  $\beta$  is zero because of the results of the previous analysis. Different combinations of  $\rho^{PV}$  and  $\rho^{ctr}$  have been studied. For each combination of these parameters, 3 experiments have been performed with different seeds of the random number generator. An experiment consists on the simulation of the previously explained electrical grid during one year and a half (788400 min) with a concrete combination of  $\rho^{PV}$  and  $\rho^{ctr}$  and a concrete seed. The first half year is used to adapt the SG algorithm to the grid, after that, the crest factors are calculated for the remainder year. The crest factors

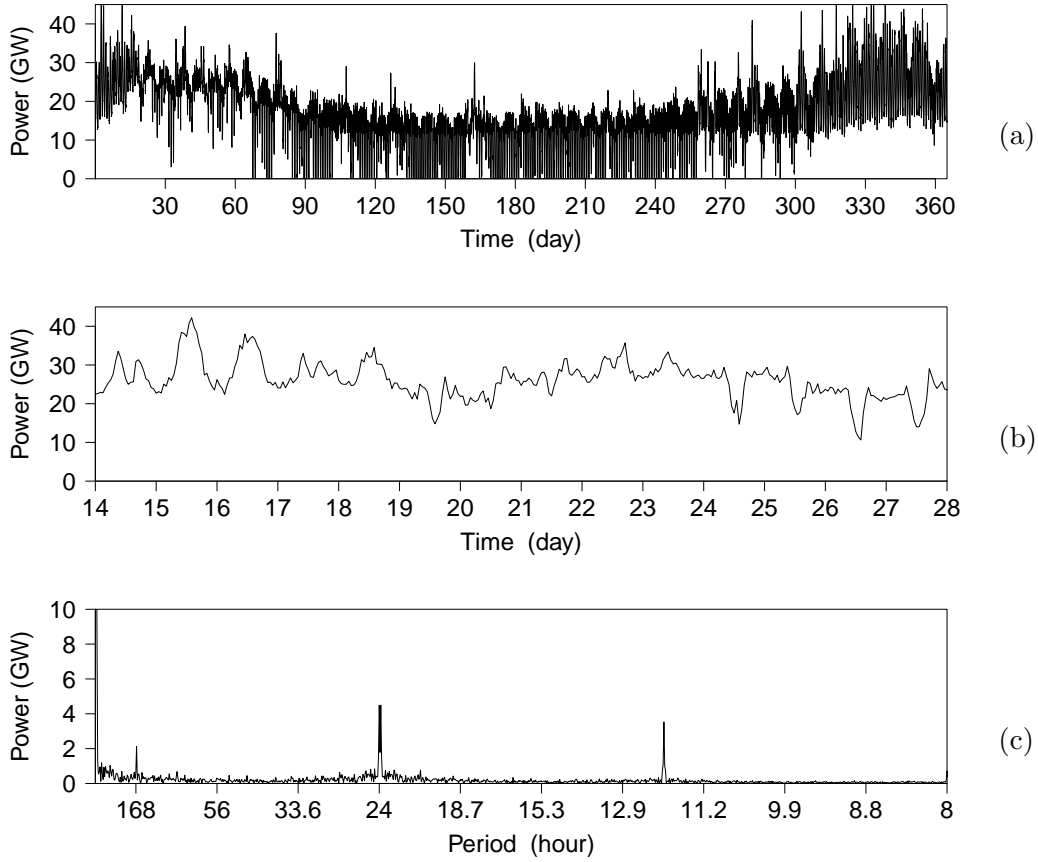


Figure 6.12: Example of the aggregated consumption of the simulated electrical grid with  $\rho^{PV} = 50\%$ ,  $\rho^{ctr} = 100\%$  and  $\beta = 0$ : a) one year of simulation, b) one week of this simulation and c) **DFT**. The crest factors for these example:  $C_{year} = 2.78$ ,  $\bar{C}_{month} = 2.17$ ,  $\bar{C}_{week} = 1.81$  and  $\bar{C}_{day} = 1.55$ . The self-consumption for this example:  $\xi = 0.28$ .

and the self-consumption of the local facilities are calculated for each experiment. **SG** algorithm operates with the tuned parameters to reduce the daily variability obtained in Section 5.4:  $W = 16$ ,  $T_{smp} = 90$  min,  $K = -0.03$  and  $P_{switch} = 0.02$ .

Figure 6.13 shows the development of the crest factors for different combinations of  $\rho^{PV}$  and  $\rho^{ctr}$  with  $\beta = 0$ . The effect of the **SG** algorithm on these factors changes depending on the **PV** penetration. For low values of  $\rho^{PV}$ , the higher  $\rho^{ctr}$ , the smoother

## 6.2. Operating examples

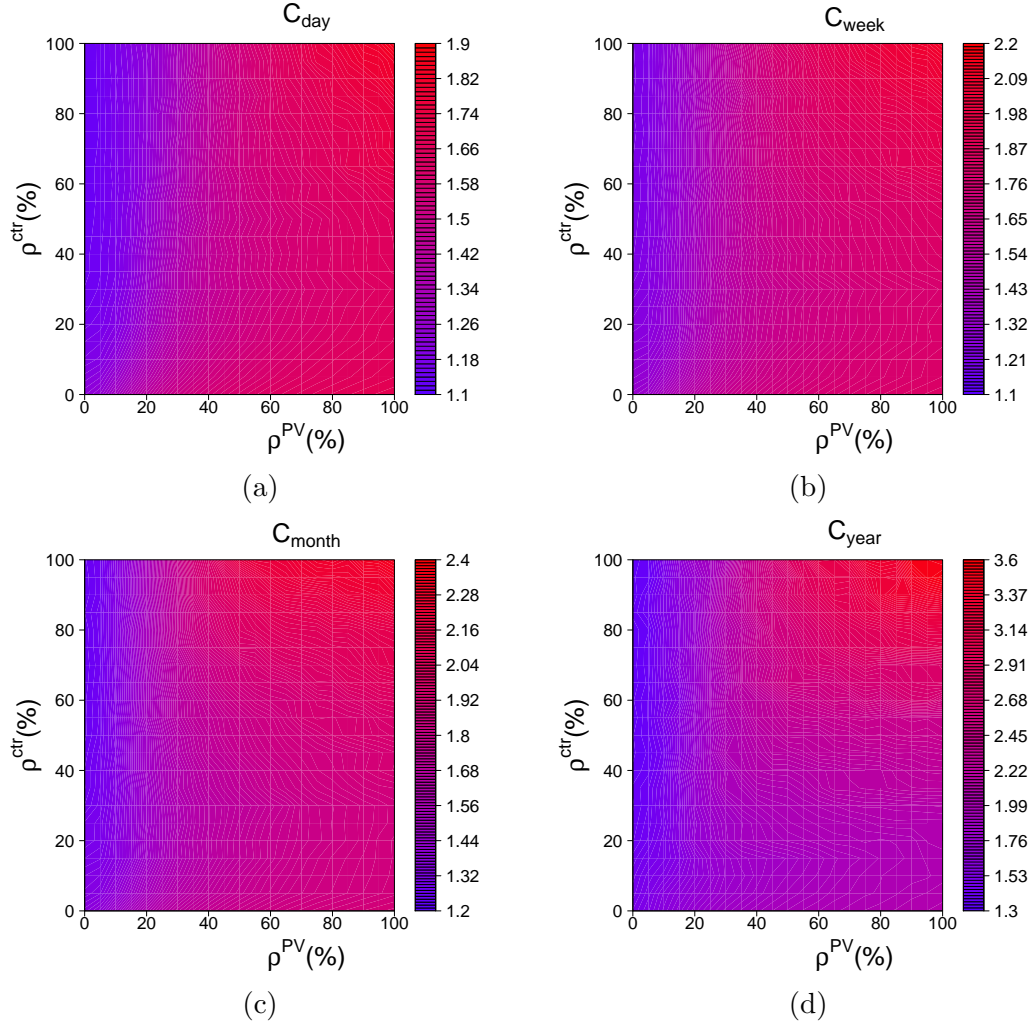


Figure 6.13: Heat map representing the development of the crest factors for different combinations of  $\rho^{PV}$  and  $\rho^{ctr}$  with  $\beta = 0$ : a)  $\bar{C}_{day}$ , b)  $\bar{C}_{week}$ , c)  $\bar{C}_{month}$  and d)  $C_{year}$ .

the aggregated consumption. **SG** algorithm is able to synchronize with the electrical grid and to reduce the crest factors. On the other hand, for high values of  $\rho^{PV}$ , the increase of  $\rho^{ctr}$  intensifies the variability introduced by the **PV** generation. This effect has been observe in the example of Figure 6.12: the **SG** algorithm is not able to synchronize with the climate dependency of the **PV** resource.

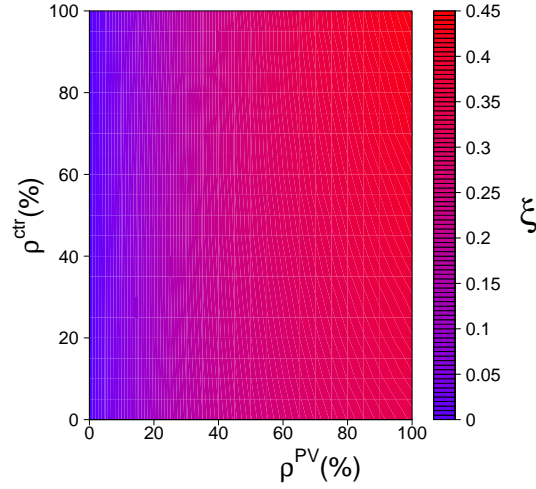


Figure 6.14: Heat map representing the development of the self-consumption for different combinations of  $\rho^{PV}$  and  $\rho^{ctr}$  with  $\beta = 0$ .

Figure 6.13 shows the development of the self-consumption for different combinations of  $\rho^{PV}$  and  $\rho^{ctr}$  with  $\beta = 0$ . As in previous analysis, the self-consumption increases with  $\rho^{PV}$  because the PV resource availability. Moreover,  $\rho^{ctr}$  enhances the self-consumption too. This implies that the SG algorithm synchronizes with the PV generation because it is included in the aggregated consumption signal.

Figure 6.15 shows an example of the aggregated consumption of the simulated electrical grid with  $\rho^{PV} = 50\%$ ,  $\rho^{ctr} = 50\%$  and  $\beta = 0$ . The maximum yearly peak reaches 41.8 GW as the example without PV generation. There are times during the year where the aggregated consumption is reduced to zero. The average of the aggregated consumption is 17 GW. Regarding the daily difference between peak and valley, the maximum difference is 29.8 GW, the minimum is 6.9 GW and the average is 19.8 GW. Comparing this example with the example with  $\rho^{ctr} = 100\%$  of Figure 6.12, the seasonal effect of the PV generation on the synchronization can be observed. The consumption peak that is close to the day 150 in Figure 6.12a does not occur in Figure 6.15a.

#### 6.2.4 The grid with DER

The presence of *Distributed Energy Resources* in the electrical grid is increasing over time. In turn, these resources are increasing in complexity and functionality. In

## 6.2. Operating examples

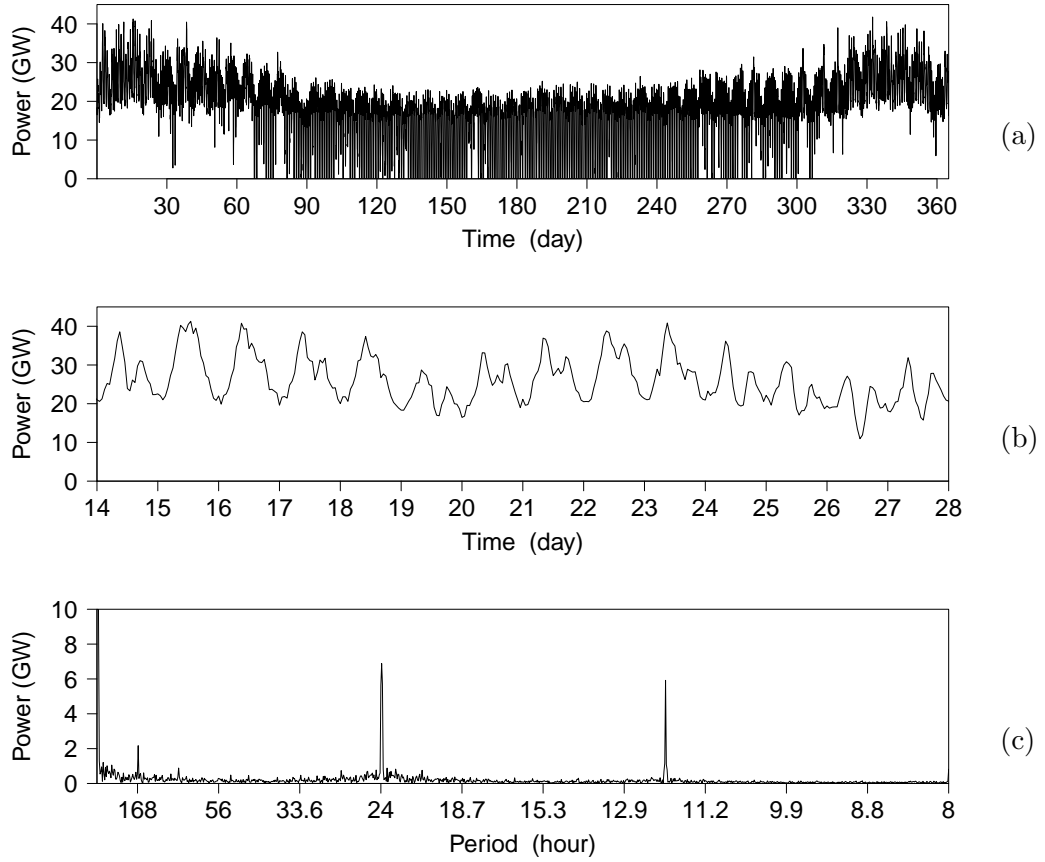


Figure 6.15: Example of the aggregated consumption of the simulated electrical grid with  $\rho^{PV} = 50\%$ ,  $\rho^{ctr} = 50\%$  and  $\beta = 0$ : a) one year of simulation, b) one week of this simulation and c) **DFT**. The crest factors for these example:  $C_{year} = 2.25$ ,  $\bar{C}_{month} = 1.8$ ,  $\bar{C}_{week} = 1.68$  and  $\bar{C}_{day} = 1.5$ . The self-consumption for this example:  $\xi = 0.26$ .

this scenario, the effects of the **PV** generation together with storage systems and the SG algorithm are analyzed. The storage systems are included in this analysis from a similar way than in the analysis of Section 3.3. These systems are part of a facility and are managed by the battery controller explained in Section 3.1.2. The capacity is a key parameter whose value completely modifies the effects of the storage system on the power balances. When this systems are installed in a local facility

which has a certain consumption, the capacity is defined in *days of autonomy*. A day of autonomy is the average consumed energy of this facility. In this scenario, each facility consumes 410 GWh per year, thus, the average daily consumption is around 1.12 GWh. In addition, the battery controller is designed to optimize the self-consumption with  $SoC^{min} = 40\%$  and  $SoC^{max} = 60\%$ .

A campaign of experiments has been performed to study how  $\rho^{PV}$  and  $Cap^*$  affects the crest factors of the aggregated consumption and the self-consumption. In this campaign, the **SG** algorithm controls the whole consumption  $\rho^{ctr} = 100\%$  because it is the most critical situation when there is high **PV** penetration.  $\beta$  is zero because of the results of the previous analysis. Different combinations of  $\rho^{PV}$  and  $Cap^*$  have been studied. For each combination of these parameters, 3 experiments have been performed with different seeds of the random number generator. An experiment consists on the simulation of the previously explained electrical grid during one year and a half (788400 min) with a concrete combination of  $\rho^{PV}$  and  $Cap^*$  and a concrete seed. The first half year is used to adapt the **SG** algorithm to the grid, after that, the crest factors are calculated for the remainder year. The crest factors and the self-consumption of the local facilities are calculated for each experiment. **SG** algorithm operates with the tuned parameters to reduce the daily variability obtained in Section 5.4:  $W = 16$ ,  $T_{smp} = 90$  min,  $K = -0.03$  and  $P_{switch} = 0.02$ .

Figure 6.16 shows the development of the crest factors for different combinations of  $\rho^{PV}$  and  $Cap^*$  with  $\rho^{ctr} = 100\%$  and  $\beta = 0$ . As in the previous analysis, the crest factors increase with  $\rho^{PV}$ . On the other hand, the effects of  $Cap^*$  on the crest factors depend on the analyzed period. For the shorter periods,  $\bar{C}_{day}$  and  $\bar{C}_{week}$  the crest factors increase with  $Cap^*$  for high **PV** penetration values. This is because the storage systems are able to isolate the facilities while they have enough energy to supply or capacity to store energy. Otherwise, the facilities export or consume energy to/from the electrical grid causing an abrupt change in the aggregated consumption shape. For the shorter periods,  $\bar{C}_{month}$  and  $\bar{C}_{year}$  the crest factors decrease with  $Cap^*$  for high **PV** penetration values. Despite the problem mentioned above, the main monthly and yearly peaks are reduced through the use of storage systems. These systems can store **PV** energy and supply it during the evening hours, at the same time as the largest consumption peaks.

Figure 6.16 shows the development of the self-consumption for different combinations of  $\rho^{PV}$  and  $Cap^*$  with  $\rho^{ctr} = 100\%$  and  $\beta = 0$ . The controller of the storage system is designed to maximize the self-consumption of the local facilities. Therefore, the higher the  $Cap^*$ , the higher the  $\xi$ .

## 6.2. Operating examples

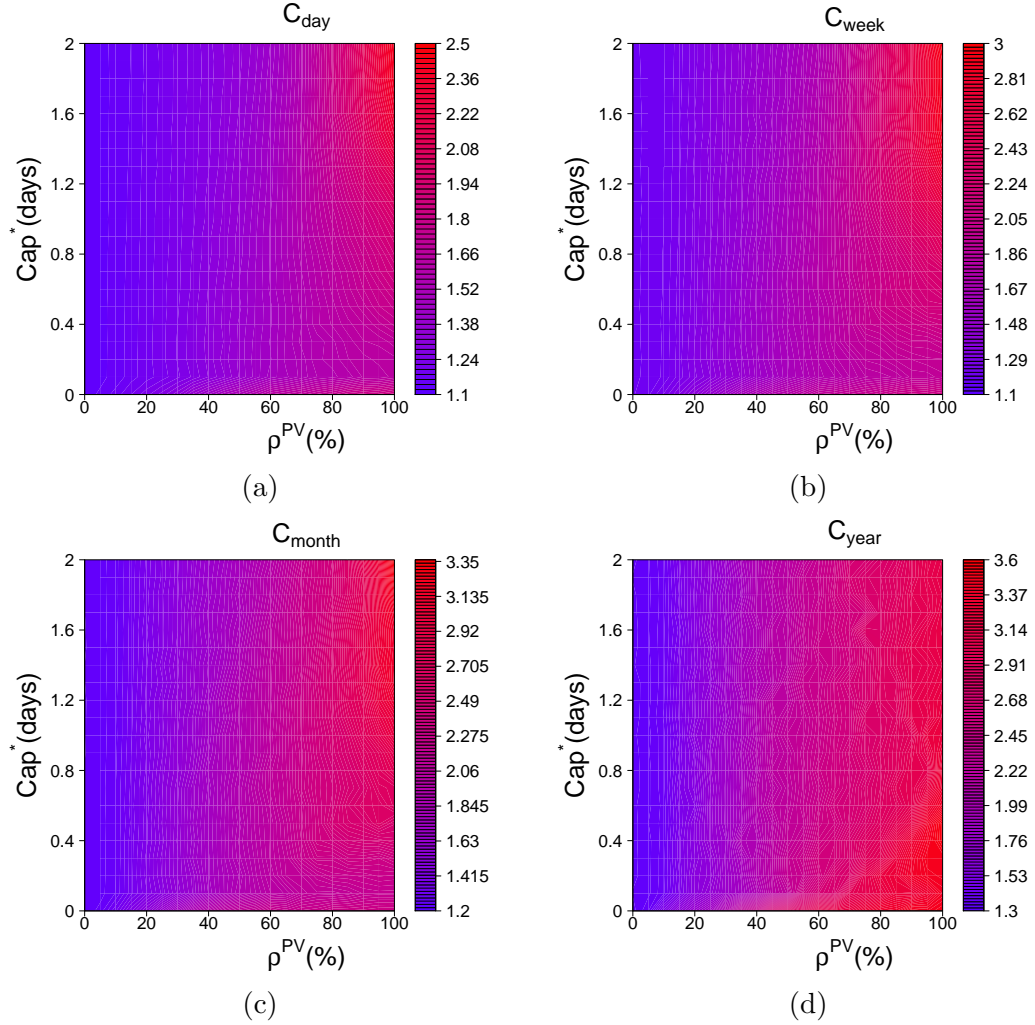


Figure 6.16: Heat map representing the development of the crest factors for different combinations of  $\rho^{PV}$  and  $Cap^*$  with  $\rho^{ctr} = 100\%$  and  $\beta = 0$ : a)  $\bar{C}_{day}$ , b)  $\bar{C}_{week}$ , c)  $\bar{C}_{month}$  and d)  $C_{year}$ .

Figure 6.18 shows an example of the aggregated consumption of the simulated electrical grid with  $\rho^{PV} = 50\%$ ,  $\rho^{ctr} = 50\%$ ,  $\beta = 0$  and storage systems of 1 day of autonomy. The maximum yearly peak reaches 40.5 GW as the example without PV generation. There are times during the year where the aggregated consumption is reduced to zero. The average of the aggregated consumption is 17.8 GW. Regarding

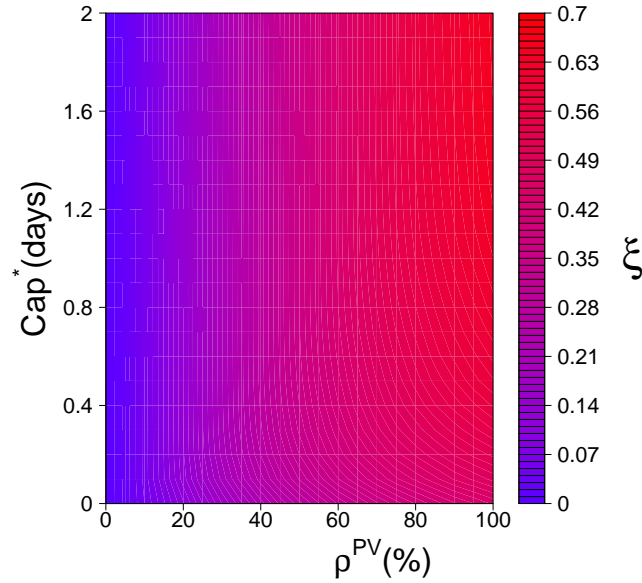


Figure 6.17: Heat map representing the development of the self-consumption for different combinations of  $\rho^{PV}$  and  $Cap^*$  with  $\rho^{ctr} = 100\%$  and  $\beta = 0$ .

the daily difference between peak and valley, the maximum difference is 19.6 GW, the minimum is 3.6 GW and the average is 11.8 GW.

### 6.3 Discussion

In this Chapter, the operation of the **SG** algorithm has been explained together with some operating examples on an electrical grid. The algorithm has a number of valuable features for **DSM** that it borrows from swarm intelligence and coupled oscillators:

- *Self-organization*: an electrical grid with facilities equipped with the **SG** algorithm is able to self-organize. All facilities schedule the deferrable loads following a common goal. Without an explicit information exchange and without the presence of a central agent, the consumption of these facilities organizes over time. This feature could be observed in Section 6.2.2 when the amount of controllable consumption exceeds the amount of non-controllable

### 6.3. Discussion

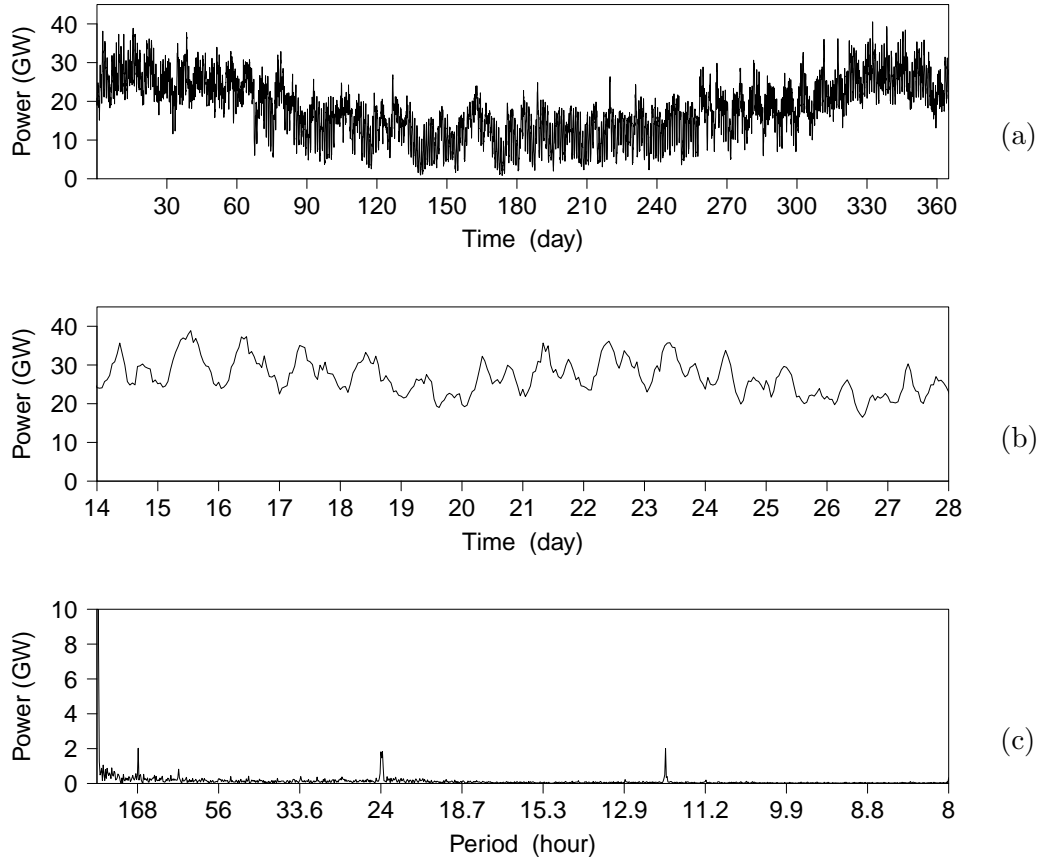


Figure 6.18: Example of the aggregated consumption of the simulated electrical grid with  $\rho^{PV} = 50\%$ ,  $\rho^{ctr} = 50\%$ ,  $\beta = 0$  and storage systems of 1 day of autonomy: a) one year of simulation, b) one week of this simulation and c) **DFT**. The crest factors for these example:  $C_{year} = 2.18$ ,  $\bar{C}_{month} = 1.83$ ,  $\bar{C}_{week} = 1.63$  and  $\bar{C}_{day} = 1.41$ . The self-consumption for this example:  $\xi = 0.36$ .

consumption. In this situation, the controllable consumption should self-organize to consume at a constant power.

- *Adaptability*: facilities are able to adapt to the aggregated consumption of the grid. A non-controllable consumption was introduced in the simulated

electrical grid. **SG** algorithm schedules the deferrable loads adapting to the non-controllable consumption and smoothing the aggregated consumption.

- *Low information exchange:* **SG** algorithm requires a very low information exchange. The facilities only require the aggregated consumption signal which should be provided by the electrical grid operator. In addition, the sample period of this signal implies a low computing load compared to the current electronic:  $T^{smp} = 90$  min in the examples shown.
- *Local conditions:* **SG** algorithm takes into account local conditions. It schedules the deferrable loads by considering the grid and the local **PV** generation forecast. In addition, this algorithm could be designed to satisfy other local conditions because its distributed nature. This issue is further discussed in the conclusions of this Thesis—see Chapter 7.

The smoothing of the aggregated consumption by the **SG** algorithm could be observed in different scenarios in Section 6.2. In general, **SG** algorithm reduces the crest factors of the electrical grid proportionally to the amount of controlled energy. This issue is easily observed in the analysis of the **SG** operation without **DER** technologies. In this case, the **SG** algorithm schedules a certain percentage of energy of the electrical grid. The results conclude that for an amount of energy controlled by the **SG** algorithm lower than 50%, the higher the percentage of controlled energy, the lower the crest factors. For percentages higher than 50%, the crest factors achieve a plateau value. This is because the **SG** algorithm adapts to the non-controllable consumption and schedules the remainder controllable consumption so that the variability of the aggregated consumption does not increase. This is indicative of the self-organization capacity of the algorithm. Two examples have been proposed to show how the **SG** algorithm affects to the shape of the aggregated consumption and its difference between peaks and valleys. Thanks to the use of the algorithm, the maximum yearly peak has been reduced from 41.9 GW to 36.1 GW maintaining the same average consumption. This implies that the size of the electrical grid has been improved because the average consumption is closer to the maximum peak: less electrical infrastructure is required and this is used more time in average. In addition, the average daily difference between peaks and valleys has been reduced from 12.2 GW to 4.7 GW. This implies that the daily use of the electrical grid has also been improved: the difference between peaks and valleys is much lower and, thus, the grid does not have to respond to such abrupt power variations increasing its stability. Thus, the **SG** algorithm meets the main objective sought in this Thesis.

### 6.3. Discussion

---

The presence of large amounts of **PV** generation makes difficult the smoothing process of the aggregated consumption. In Section 3.3.2, the effect of the **PV** penetration on the aggregated consumption was already observed. The use of the **PV** forecast may cause wrong load scheduling. A similar phenomenon was observed in the operation of **ADSM** algorithm in Chapter 3.3.3. In both cases, the cause of this malfunction is the same: all facilities schedule the deferrable loads to run during the same time period without considering other facilities. This causes a consumption peak at this period which may be increased because of a lack of generation or a bad forecast. On the other hand, the local self-consumption is enhanced when  $\beta \rightarrow 1$ . Thus, a compromise between aggregated consumption smoothing and self-consumption should be found. This compromise depends on the specific requirements where the **SG** algorithm is implemented.

The other analyses have been done considering that  $\beta \rightarrow 0$ : the **SG** algorithm does not use **PV** forecast, only the sinusoidal functions from the **MuFCO** algorithm. In these cases, the **SG** algorithm reduces the crest factors for low **PV** penetration levels. On the other hand, when **PV** penetration levels increase above the 50%, The use of the **SG** algorithm may increase the crest factors. The reason is that high **PV** penetration levels increase the difficulty of synchronization because more no periodic components are introduced in the aggregated consumption signal. The use of **DER** may improve the power behavior of the local facilities. In general, they can smooth the energy exchange between these facilities and the electrical grid. This behavior may become detrimental to high **PV** penetration levels because when the facilities exchange energy with the electrical grid, they do it more abruptly than without **DER**. This phenomenon could also be observed in Section 3.3.4.



## **Part III**

# **Conclusions and Future Works**



## Chapter 7

# Conclusions and Future Works

This Chapter summarizes and concludes this Thesis. The main contributions and improvements are remarked, both in the energy management and the algorithmic fields. This Chapter is divided in four sections. The first two sections refer to each part of this Thesis: local framework and grid framework. Section 7.3 shows some proposals of future research lines for this Thesis. Finally, Section 7.4 summarizes the main contributions of the author over the course of his doctorate.

### 7.1 Local Framework

In this part of the Thesis, Photovoltaic (PV) generation, Demand-Side Management (DSM) and storage systems have been tackled from a local point view. This means that the local energy management only responds to local conditions without considering the electrical grid status. The local facilities are equipped with: PV generation, battery storage systems, grid connection and controllable consumption. Three types of consumption have been defined in this Thesis: *i*) fixed, which is uncontrollable, *ii*) deferrable, which can be displaced in time and *iii*) elastic, whose instantaneous power can be directly controlled. In order to evaluate the power flows in the local facilities, an assessment methodology has been developed which includes the definition of six energy variables and the self-consumption factor.

A new concept called Active Demand-Side Management (ADSM) has been defined for the combination of DSM with an automatic control of the local consumption. It has been implemented together with local generation and storage technologies adding local conditions to the management problem. Two controllers have been designed: the *ADSM algorithm* and the *battery controller*. The ADSM algorithm is responsible

## 7. Conclusions and Future Works

---

for scheduling and running the deferrable loads. The battery controller monitors the power flows and some storage system variables, and actuates over the battery power flows. Both controllers have been designed to maximize the self-consumption of the local facilities.

The operation of the previous controllers has been analyzed through simulated and real experiments. The local facility chosen to perform this study is “Magic Box”—see Section 2.3. This solar house has been modeled to simulate its energy behavior in different situations. For the real experiments, both controllers have been implemented in a real-time system in “Magic Box”. The experiments have shown the house electrical energy balances in daily and yearly studies, activating and deactivating the ADSM system and modifying the battery capacity. It has been demonstrated that the use of both techniques increases the self-consumption considerably. In addition, these techniques allow the implementation of different electric behaviors in order to achieve different energy objectives.

The relationship between electrical energy flows and the storage capacity is not linear. There is a different variation of these flows for low capacity levels, achieving a plateau for capacities higher than two days of autonomy. The change of this trend takes place with storage capacities close to one day of autonomy. As expected, the relationship between the self-consumption factor and the capacity follows a similar evolution than the electrical energy flows. This relationship is an important design criterion, which involves that oversized storage does not produce relevant energy benefits with regard to the local energy optimization. Designers must also take into account the battery float charge consumption: they are not normally considered, but are very important for small battery capacities, which will be expected to arrive at the residential sector.

ADSM presents important improvements in the local electricity flows, integrating the generation and the user demand patterns. The effects of ADSM are not constant with the storage capacity, increasing considerably the self-consumption factor for low storage and disappearing for high capacity levels: for  $Cap^*$  higher than one day of autonomy in the experiments of Section 3.2. In any case, this technique reduces the use of the storage systems and therefore reduces the losses with regard to the storage system efficiency. In conclusion, the ADSM performs many advantages, which the main ones are:

- *To decrease energy losses:* the use of ADSM increases the direct use of the local sources to the detriment of the storage use, reducing the losses with regard to the efficiency. Moreover, the ADSM systems have no physical contact with

## 7.1. Local Framework

---

the energy system and therefore their use does not affect the global system efficiency.

- *To reduce the storage size:* the same effects produced by a system without **ADSM** can be obtained with **ADSM** by reducing at the same time the battery capacity. It involves that the storage system capacity can be reduced and therefore it decreases the related costs. Moreover, less waste will be generated when recycling batteries at the end of their useful life and therefore it reduces the environmental impact associated to the storage systems.
- *To increase the electricity management possibilities:* by actuating on the demand, the number of variables involved in the energy management of local electric power systems increases. In this Chapter, this management has been focused in the self-consumption maximization. By modifying this target, different energy strategies can be carried out depending on the user needs, e.g. the load displacement to low-cost electricity hours or to avoid power consumption over a defined threshold.
- *Easy scalability:* because **ADSM** can be implemented by simple electronics and software controllers, the system size is not an important constraint to this technique. On the other hand, the principal limit of **ADSM** is the percentage of deferrable loads, which in most cases is difficult to increase.
- *User collaboration:* **ADSM** usually involves the user in the house energy management, by informing the user about the energy situation of the local facility. It makes the user aware of the energy demand which usually involves the consumption reduction.

In this Thesis, the main challenges of the **ADSM** have been addressed—see Chapter 1. An **Information and Communications Technology (ICT)** infrastructure has been developed by using the irradiance forecasts from the Spanish State Meteorological Agency and the house communication network supported by the electrical appliances. The local control system takes the local conditions information and decides when loads should be placed in order to optimize the self-consumption. The complexity of the system increases, but this may be acceptable if one takes into account the improvements arising from a technical and economical point of view.

Despite the local benefits produced by the **ADSM** and the battery controller, they may cause a great variability on the electric grid. In Section 3.3, the effects of the **PV** generation, **ADSM** algorithm and storage systems on the grid have been shown.

The use of these techniques without taking into account the electrical grid status may be detrimental to this grid for high **PV** penetration levels. For example, the **ADSM** algorithm runs every load in every facility at the same time because it only takes into account the **PV** resource, which is similar for all facilities. This analysis leads to the conclusion that coordination between facilities and the grid is required. The search of this coordination has been the aim of the second part of this Thesis.

### 7.2 Grid Framework

In this part of the Thesis, **DSM** has been tackled from the electrical grid point of view. It means that the local consumption is managed to smooth the aggregated consumption of the grid in addition to respond to local conditions. A **DSM** algorithm has been developed to address this issue. As mentioned in the previous Section, coordination between facilities and the grid should be performed. The proposed algorithm is posed from a distributed point of view, thus, the **DSM** is not performed by a central agent but each consumer is actively involved in its implementation. Direct communication between facilities has also been avoided. Thus, the coordination is performed with the sole information of the aggregated consumption of the grid. To smooth the aggregated consumption considering these constraints, two collective coordination techniques have been used: *coupled oscillators* and *swarm intelligence*.

The aggregated consumption is a complex signal which depends on the behavior of multitude of users connected to the electrical grid. However, this signal has a periodic behavior. This periodicity has been used in this Thesis to implement a **DSM** algorithm which is able to smooth the aggregated consumption. The aggregated consumption signal is divided in Fourier series and an error term. This implies that this signal is composed by a sum of sinusoidal functions. Every facility schedules its deferrable loads by using a local pattern. This local pattern has also a sinusoidal function shape. The sinusoidal functions are tuned in counterphase of the aggregated consumption Fourier series. Therefore, the deferrable loads are scheduled shaping sinusoidal functions in counterphase with the aggregated consumption. This procedure causes that the oscillatory behavior of the aggregated consumption is removed and thus it is smoothed.

The proposed **Multi-Frequency Coupled Oscillators (MuFCO)** algorithm is responsible for generating the sinusoidal functions and ensuring that the aggregated consumption is smoothed—see Chapter 5. It is able to generate a sinusoidal function in each facility in a distributed manner, using the aggregated consumption as the

## 7.2. Grid Framework

---

sole information. The aggregated consumption has been called environment during the definition of the **MuFCO** algorithm to generalize the explanation. The **MuFCO** algorithm considers each facility as an oscillator which operates in a certain frequency. The oscillators are coupled by using a coupling equation similar to the Kuramoto's coupled oscillators. The most relevant modification to the common coupling equation is the use of the **Discrete Fourier Transform (DFT)**. The phase information of all oscillators is contained in the frequency components calculated by the **DFT**. Thus, the oscillators are coupled between them and the environment. Besides the energy management application, this procedure has multiple applications in the coupled oscillator field. It allows coupling a group of oscillators to unknown signals in order to modify its shape.

In addition, the oscillators can modify their operating frequencies performing a multifrequency behavior. To perform this modification, a probability decision function has been defined, inspired by the task allocation algorithms of swarm intelligence. Through this function, every oscillator chooses its operating frequency, such that the collective achieves a common objective. Thus, the whole collective (or swarm) of oscillators can shape complex signals with multiple frequency components, adapting to the environment. The **MuFCO** algorithm can be tuned to adapt to different signals with different objectives. For example, in this Thesis, the objective is to remove every frequency component by making the collective of oscillators to work in counterphase with the environment. But this objective can be modified, for example, by doing the opposite and increasing every frequency component, performing a synchronized behavior with the environment. This algorithm opens up a new approach to the application of such techniques and to adaptation of collectives of individuals to complex environments.

The proposed **Swarm Grid (SG)** algorithm uses the sinusoidal consumption patterns generated by the **MuFCO** algorithm and takes into account the local generation. It generates a pattern by combining sinusoidal patterns and **PV** generation forecasts to schedule the deferrable loads. Section 6.2 shows the **SG** algorithm behavior in different scenarios. In general, the **SG** algorithm is able to smooth the aggregated consumption in every scenario. The improvement caused by the **SG** algorithm is more relevant for low percentages of controllable power. It achieves a plateau value after the controllable energy of the whole electrical grid reaches the 50%. It means that the deferrable power controlled by the **SG** algorithm is able to adapt to the non-controllable power. Thanks to the use of this algorithm,

## 7. Conclusions and Future Works

---

the maximum yearly peak and the daily difference between peaks and valleys are reduced. Thus, the **SG** algorithm meets the main objective sought in this Thesis.

The **SG** algorithm represents an important contribution to the **DSM** and the Smart Grids. It has several advantages that are required for the widespread implementation of this kind of electrical grids:

- *Robustness*: the local consumption is managed from a fully decentralized way. Each facility is able to schedule its own loads. In addition, the connection loss by a facility implies that this facility operates as a non-controllable consumption. Thus, the other facilities can adapt to this “disconnected” facility and the **DSM** mechanism continues working. In the worst case, where all facilities are disconnected, the aggregated consumption has the same shape than an electrical grid without the **SG** algorithm.
- *Data privacy*: there is not communication between facilities, it means that a user cannot know what are other users doing. In addition, the facilities do not send information to a central agent. This implies that there is not a central agent which knows what all users are doing.
- *Scalability*: every facility adapts to the aggregated consumption without knowing how many facilities are cooperating. Thus, there is not a minimum number of facilities equipped with the **SG** algorithm for proper operation. On the other hand, the facilities coordinate between them, even in absence of non-controllable consumption. Thus, there is not a maximum number of facilities equipped with the **SG** algorithm for proper operation. This implies that the **SG** algorithm is completely scalable and it smooths the aggregated consumption regardless the number of facilities.
- *Low cost*: the **SG** algorithm adapts to the current grids without any topological requirements. Thus, structural modifications are not required. In addition, the computing power required by the **SG** algorithm is very low. From the results of the tune process, it could be observed that the **MuFCO** algorithm must be updated every 90 minutes (the sample period). To schedule a deferrable load, the calculation of a pattern which is the sum of a sinusoidal function and the **PV** generation forecast is only required. This implies that the computing power and therefore the cost of the electronics is very low.
- *Quick deployment*: the high scalability and the low cost allow a quick deployment of the **SG** algorithm in the electrical grids. In addition, the high

### 7.3. Future Work

---

resilience of this algorithm to the environment makes it easy to install. The main drawback is the reception of the aggregated consumption signal in every facility. Nowadays, it is not a reality, despite the efforts to deploy SmartMeters in every house. However, this signal may be received from other ways as internet.

## 7.3 Future Work

This Thesis has explored and combined two very different fields: the energy management and the collective systems. For both fields, this Thesis has presented a novel approach that may be further developed. In this Section, these further developments are discussed.

### 7.3.1 Energy Management Framework

There are several areas for future studies in the energy framework related to this Thesis. The **SG** algorithm is a novel proposal for the **DSM** in Smart Grids. This algorithm is still in a early state of its development. The algorithm may be improved from the local to the grid points of view. In general, every improvement is related to a practical implementation of the algorithm to be used in final user applications.

The **SG** algorithm has been designed to schedule deferrable loads, but it is not the only type of load. In Section 2.1.3 three types of load were defined: *fixed*, *deferrable* and *elastic*. The scheduling generated by the **SG** algorithm is based on the calculus of consumption patterns. Despite this fact, the deferrable loads are a discrete consumption, in the sense that they are considered as energy packages, but the consumption patterns are continuous. This implies that these patterns may also be applied to elastic loads whose consumption can be controlled directly. For example, the power of an electric pump can be modified to shape a sinusoidal pattern. Although ideally the power of elastic loads can be controlled, this fact is not always true in the real world. Several loads are a mix between deferrable and elastic consumption. For example, the power of HVAC systems may be modified but only in a number of discrete values in a certain range and it usually has time constraints as minimum operation time. In general, many devices have a complex operation way. This operation form must be taken into account in the **SG** algorithm. It implies that every device where the **SG** algorithm is installed must contain a specific module which translates the consumption patterns generated by **SG** algorithm to the operation form of this device. This module must ensure that the consumption shape of this device tends to the consumption pattern. Therefore, the adaptation of different operation

## 7. Conclusions and Future Works

---

forms to the **SG** algorithm brings a big number of studies about the controllability of many types of consumption.

On the other hand, the fixed consumption is uncontrollable. It means that this consumption cannot be shaped as the consumption patterns generated by the **SG** algorithm. Another possible approach is to take the fixed consumption into account in the generation of consumption patterns. The fixed consumption is produced by the local user in its facility. It usually follows a certain periodicity or behavioral pattern. This consumption may be acquired by a learning algorithm. A learning mechanism of the local fixed consumption may be added to the **SG** algorithm. Therefore, the local scheduling may take into account the fixed consumption. The development of this learning algorithm can constitute a new research.

Another research line related to the local energy management is the study of new local constraints. For example, the power limits is a well known constraint in the local facilities as the power limit by electricity contract in dwellings. In addition, facilities with **Distributed Energy Resource (DER)** may have different power limits depending of the local electricity availability. For example, a facility which has an electrical grid connection of 3kW may be equipped with a storage system of 7kW. It means that if there is enough energy in the storage system, the facility can consume 7kW, but if the storage system runs out of energy, the facility can only consume 3kW. These limits may be also related to certain time range or to the local distributed generation. The **SG** algorithm schedules the loads without considering whether these loads can be run or whether their operation may cause any electrical problem. The inclusion of this new type of constraints in the **SG** algorithm increases the number of variables to be taken into account for the scheduling. On the other hand, the inclusion of these constraints will allow the **SG** algorithm to be useful to different scenarios.

This Thesis has been focused on the **PV** technology as **Distributed Generation (DG)**. There are other **DG** technologies among which are multiple renewable energy technologies. They can also be included in the operation of the **SG** algorithm. Probably one of the most interesting **DG** technology for the algorithm's use is the *wind power*. This technology has a similar problem as the **PV** generation: the resource availability is not controllable. A similar procedure as the **PV** forecast use can be followed. The **SG** algorithm may be used to increase the self-consumption or to smooth the aggregated consumption with the presence of high wind power penetration levels.

By combining these previous research lines, the control of one of the major future electricity consumption challenge can be addressed from the local perspective: the

### 7.3. Future Work

---

**Electric Vehicle (EV).** The widespread inclusion of EVs in the car park is expected in the coming years. To convert the transport consumption from fossil fuels to electricity will cause an unprecedented growth of the electricity consumption. Thus, problems associated with the resource availability and the aggregated consumption variability will be accentuated. The EV consumption has an uncontrollable part because the use of the vehicle cannot be controlled by an automated system. This can be considered as fixed consumption and its behavior should be learned by a DSM mechanisms for a proper energy management. On the other hand, once the EV is connected to the grid to be charged, there are several variables to be taken into account. Depending on the user requirements, the EV should be charged to a certain speed. It means that if a user is going to do a tour of 100 km in one hour, the EV must be charged with the required energy in one hour. Thus, the power is restricted by this kind of requirements and cannot be directly controlled as an elastic load. A future version of the SG algorithm should take into account this kind of restrictions to schedule the charge of the EV without forgetting the initial objectives of the algorithm: to smooth the aggregated consumption and to increase the self-consumption.

From the electrical grid point of view, another research lines may follow. SG algorithm tackles the aggregated consumption by smoothing it from a technical point of view. This issue can also be addressed from other perspectives, for example from the economical point of view. The electricity market can also be considered as a signal. It varies continuously during the day. The electricity market is not only affected by the demand, but by the resources availability and the financial market too. The SG algorithm can be used to adapt to this market by considering other variables that affect the electricity price. The required variables to achieve this new objective should be studied and how they could be included in the algorithm.

Another research line is related to the structure of the grid. As mentioned in the introduction, the electrical grids have a hierarchical structure—see Chapter 1. This structure has not been considered in the SG algorithm because every consumption is added to form an aggregated consumption and the structure of the grid does not affect to the operation of the algorithm. This fact is not completely true if the SG algorithm is widely expanded. The grid is connected by using transmission lines which have a certain capacity. This capacity is not able to drive the whole power of the electrical grid everywhere. Actually, the grid has different zones with different generation and consumption capacities such that the produced energy has not to travel long distances. This could be linked with another new concept about the electrical grid design: the

*microgrids*<sup>1</sup>. The **SG** algorithm may be applied to manage the consumption in these different structures. In this case, the **SG** algorithm should take into account the aggregated consumption of the microgrid where it is deployed. In addition, it could consider other signals from other surrounding microgrids. Hence, the **SG** algorithm could be use to coordinate the consumption of different microgrids.

### 7.3.2 Collective System Framework

The **MuFCO** algorithm may be the grounds of new researches about collective systems. This algorithm is a novel proposal in the collective system field whose development is still in an initial state. Moreover, the **MuFCO** algorithm may be applied to different fields instead of the energy management. Some examples of these further applications are discussed below.

The **MuFCO** algorithm is not able to respond to non-periodic events. The adaptive process and the actuation of the **MuFCO** algorithm is designed to work from a periodic point view. It adapts to periodic components of the environment and acts through sinusoidal functions. Although this procedure has shown a very stable and robust behavior, some events cannot be tackled by the **MuFCO** algorithm. An abrupt and sporadic change in the value of the environment signal does not modify the behavior of the **MuFCO** algorithm. Depending on the application, this effect can be detrimental. To act against this kind of events, the **MuFCO** algorithm should be provided with a reactive behavior. It should be able to modify the value of the swarm of oscillators instantaneously by reacting to abrupt changes of the value of the environment signal which cannot be observed through the **DFT**. This procedure could be performed through a subsumption architecture where the current **MuFCO** algorithm may be a bottom layer and another reactive algorithm an upper layer. In this case, the **MuFCO** algorithm will operate as the “long term” behavior. A reactive layer could suppress the **MuFCO** algorithm when a reactive behavior is required.

The current version of the **MuFCO** algorithm operates with a fixed **DFT** window. This window may be optimized for a certain application. The main drawback of this procedure is that this window cannot adapt to the environment signal in real time. It means that if the algorithm is not well optimized or the periodic behavior of the environment signal changes to another frequency range, the **MuFCO** algorithm will not operate properly. A mechanism to modify the **DFT** window should be designed to increase the real-time adaptation of the **MuFCO** algorithm.

---

<sup>1</sup>A microgrid is a localized grouping of electricity generation, energy storage, and loads that normally operates connected to a traditional centralized grid (macrogrid).

## 7.4. Review of Contributions

---

The proposed developments about collective synchronization and swarm intelligence can be applied to any purposes other than the energy management. For example, the author has begun to explore the use of the collective synchronization in swarm robotics, where the movement of a swarm of robots is synchronized with the environment. The swarm has to reallocate its workforce periodically, performing a temporal task allocation that must be synchronized with the environment to be effective (Castillo-Cagigal et al., 2014a). The environment proposed in this work operates at a single frequency. In other environments that present more complex behaviors, the multifrequency concept developed in the **MuFCO** algorithm may be applied to adapt the workforce of the swarm to the appearance of tasks.

The real-time resource allocation is a common problem in engineering, not only in the energy management field. This problem is usually associated to the coordination of several elements, as in the **MuFCO** algorithm framework. For example, the coordination and scheduling of the computing load in a cluster. This load is spread over several nodes that consume energy and are heated during the process. The energy consumption and the heat distribution in a cluster may be interesting criteria for the computing load scheduling. The nodes of a cluster could be considered as oscillators that synchronize their computing power to stabilize their consumption and heating. This concept can be also applied to *distributed computing*<sup>2</sup>. In this case, the **MuFCO** algorithm could coordinate not only the computing power between nodes of a cluster, but the computing load between clusters or computers spread over a common network too.

## 7.4 Review of Contributions

This dissertation describes original research carried out by the author. Some studies have been done to study different aspects of the energy management or collective systems. In this Section, all papers published or accepted for publication by the author (10 journals and 9 conferences), together with a number of co-workers, are explained and linked with this Thesis. The corresponding publications are detailed in the following.

---

<sup>2</sup> Distributed computing is a field of computer science that studies distributed systems. A distributed system is a software system in which components located on networked computers communicate and coordinate their actions by passing messages. The components interact with each other in order to achieve a common goal.

## 7. Conclusions and Future Works

---

The early works published by the author were in 2009 in two conferences: *i)* the *I Congreso de Gestión Distribuida* in Madrid and *ii)* the *24th European Photovoltaic Solar Energy Conference* in Hamburg. In the first conference, two papers were published. One paper about the effect of the DSM on the use of a PV system (Caamaño-Martín et al., 2009b) and another paper about the distributed control techniques for the DSM on the residential sector (Castillo-Cagigal et al., 2009). In the second conference, a paper was published about how much the use of PV energy in the residential sector can be increased by using DSM techniques (Caamaño-Martín et al., 2009a). These studies were pioneers in their time and opened the research line of the first part of this Thesis: the local framework.

The research on the DSM with PV generation was continued by including the use of local storage systems. The works on this field were performed under the GeDELOS-FV project<sup>3</sup> framework. Thanks to this project and the prototype of solar house called “MagicBox”, these studies could be done in simulation and real frameworks. Some conference publications followed these studies in 2010: a paper about the self-consumption of PV electricity together with ADSM were published in the *25th European Photovoltaic Solar Energy Conference* in Valencia (Castillo-Cagigal et al., 2010), another paper about the implementation of the DSM in the GeDELOS-FV project was published in the *IV Conferencia Latinoamericana de Energía Solar* in Cuzco (Caamaño-Martín et al., 2010) and finally a paper about the design of battery controller to optimize the self-consumption were published in the *5th International Renewable Energy Storage Conference*.

In addition, the development of the GeDELOS-FV project allowed the publication of different results of this project in journals. These results are the grounds of the first part of this Thesis. The first journal paper was published in *Energy Conversion and Management* in July 2011. It is entitled *A Semi-Distributed Electric Demand-Side Management System with PV Generation for Self-Consumption Enhancement* (Castillo-Cagigal et al., 2011b) and it addresses the ADSM system developed in the project by the author and presented in this Thesis in Section 3.1.1. Latter, in September 2011, another journal paper entitled *PV self-consumption optimization with storage and Active DSM for the residential sector* was published in *Solar Energy* (Castillo-Cagigal et al., 2011a). This paper addresses the improvements caused by the combination of ADSM and storages systems. Another paper was

---

<sup>3</sup> GeDELOS-FV: *Gestión de la demanda eléctrica doméstica con tecnología solar fotovoltaica*, supported by the Plan Nacional de Investigación Científica, Desarrollo e Innovación Tecnológica, 2007-2010, (ENE-2007-66135/ALT).

## 7.4. Review of Contributions

---

published in *Sensors* in December 2011. This paper is entitled *Heterogeneous Collaborative Sensor Network for Electrical Management of an Automated House with PV Energy* (Castillo-Cagigal et al., 2011c) and it addresses the monitoring and analysis system developed for the GeDELOS-FV project.

Further works have been performed following the research line marked by GeDELOS-FV project. In September 2011, a conference paper was published in the *26th European Photovoltaic Solar Energy Conference* in Hamburg. This paper addresses an economical analysis of the self-consumption in small grids (Matallanas et al., 2011). It was based on the energy variables obtained from the experiments performed in “MagicBox”. A journal paper entitled *Neural Network Controller for Active Demand Side Management with PV Energy in the Residential Sector* was published in *Applied Energy* in March 2012 (Matallanas et al., 2012). This paper addresses the **ADSM** from a neural network approach. Finally, the last publication on this research line was the journal paper entitled *Improving photovoltaics grid integration through short time forecasting and self-consumption* (Masa-Bote et al., 2014). It was published in *Applied Energy* in July 2014.

The **ADSM** and battery controllers are not exclusive from **PV** common panels. They may be used with other renewable energy sources. With this aim, the SIGMAPLANTAS<sup>4</sup> project was created. In this project, the author participate in the implementation of **ADSM** and local storage in office buildings with CPV<sup>5</sup> as local generation source. In this framework, two papers were published. The first one was published in the *8th International Conference on Concentrating Photovoltaic Systems* in April 2012 in Toledo (Trujillo et al., 2012). The second paper was published in *Progress in Photovoltaics* in September 2013. This publication is entitled *ISFOC: concentration photovoltaics hybrid system first year of operation and improvements* (Trujillo et al., 2013).

Up to this point of this Section, the publications about local facilities have been presented. The author has also contributed in projects with an electrical grid perspective. The main relevant project of this topic is the *Solar Decathlon Europe*<sup>6</sup>

---

<sup>4</sup> SIGMAPLANTAS: La innovación en las plantas y modelos de sistemas de Concentración Fotovoltaica en España. Ministerio de Ciencia e Innovación, programa INNPACTO (CIN/699/2011) IPT-2011-1468-920000.

<sup>5</sup> Concentrated **PV** (CPV) technology uses optics such as lenses or curved mirrors to concentrate a large amount of sunlight onto a small area of solar **PV** cells to generate electricity.

<sup>6</sup> Solar Decathlon Europe 2012 is an international competition created through an agreement signed between the Ministry of Housing of the Government of Spain and the United States Government, co-organized by Universidad Politécnica de Madrid in which universities from all over the world meet to design, build and operate an energetically self-sufficient house, grid-connected,

## 7. Conclusions and Future Works

---

which took place in September 2012 in Madrid. The development of this project allowed to submit three papers all published in *Energy and Buildings*. The first paper is entitled *Experiences and methodology in a multidisciplinary energy and architecture competition: Solar Decathlon Europe 2012* (Navarro et al., 2014) and it makes an overview of the assessment and analysis of the electrical grid deployed in this project. The second paper is entitled *Electrical energy balance contest in Solar Decathlon Europe 2012* (Matallanas et al., 2014) and it analyzes the energy balances in the grid of the project. Finally, the third paper is entitled *Passive design strategies and performance of Net Energy Plus Houses* (Rodriguez-Ubiñas et al., 2014) and it addresses the use of passive techniques, broadly architectonics techniques, to reduce the energy consumption in the electrical grid.

Besides the energy studies of the electrical grid, some works about the control theory and swarm intelligence have been performed. These works have been carried out together with the development of the **MuFCO** and **SG** algorithms. A journal paper has been submitted containing these works. This paper is entitled *Variable Threshold Algorithm for Division of Labor Analyzed as a Dynamical System* (Castillo-Cagigal et al., 2014b). It has been published online in *Transactions on Cybernetics* and it is waiting for final publication. In this paper, a division of labor model as a discrete-time dynamical system is defined, in order to study the equilibrium points and their properties related to convergence and stability. In addition, an algorithm that varies the response thresholds in order to modify the dynamic behavior of the system has been designed and tested. It is able to achieve an asymptotically stable behavior of the system in different environments and independently of the number of individuals. These works are not directly related to the topic of this Thesis but they have helped to understand some unstable behaviors that appear in distributed algorithms, mainly when the number of individuals or elements are not known.

In this Thesis, a simulator of electrical grids has been developed which is called *GridSim*<sup>7</sup>—see Appendix A. This simulator is able to simulate electrical grids by dividing them in different nodes with different energy properties. The main advantage of *GridSim* is the ease in which the controllers are added to the elements of the grid. Local controllers can be added to the simulated nodes. They can control the

---

using solar energy as the only energy source and equipped with all of the technologies that permit maximum energy efficiency. The author took over the task of designing, implementing and installing the monitoring system in charge of logging these variables, process them and show them in the monitoring web of the competition.

<sup>7</sup> *GridSim* is released under GPLv3.0. It can be downloaded from: <https://github.com/Robolabo/gridSim.git>

#### 7.4. Review of Contributions

---

generation, the storage and the consumption of the grid from a distributed or a centralized way. For this reason, *GridSim* is a useful tool for the design of Smart Grids algorithms. In addition, it has the possibility of parallel computing which allows the execution of simulations in computer clusters. *GridSim* is an open source simulator that has been released under a license GPLv3.0.

During the swarm intelligence algorithms development, the author has also worked on swarm robotics<sup>8</sup>. The concepts of collective synchronization developed on the second part of this Thesis have been applied to this research field. The robots have been considered as oscillators that have to perform task allocation in an environment with periodic properties. In this environment, tasks appear in different areas following periodic temporal patterns. The swarm of robots has to reallocate its workforce periodically, performing a *temporal task allocation* that must be synchronized with the environment to be effective. This work has been published in a paper entitled *Temporal Task Allocation In Periodic Environments: An Approach Based on Synchronization* (Castillo-Cagigal et al., 2014a). This paper has been published in the *9th International Conference on Swarm Intelligence* in September 2014.

---

<sup>8</sup> Swarm robotics is a new approach to the coordination of multirobot systems which consist of large numbers of mostly simple physical robots. It is supposed that a desired collective behavior emerges from the interactions between the robots and interactions of robots with the environment. This approach emerged on the field of artificial swarm intelligence, as well as the biological studies of insects, ants and other fields in nature, where swarm behavior occurs.

## 7. Conclusions and Future Works

---

## Appendix A

# GridSim simulation framework

*GridSim*<sup>1</sup> is an open source simulator developed to analyze the power balances on a virtual electrical grid. Figure A.1 shows a scheme of its modular architecture. The grid is composed by lines. A line represents a set of nodes with the same features. The nodes are complex elements connected to the lines which can be equipped with different types of consumption, *Distributed Energy Resources* (DER) technologies and control systems. These nodes can represent from a single device which only consumes as a single device to a complex microgrid. In addition, a base consumption function can be added to the grid. It represents an uncontrollable consumption which is added to the aggregated consumption of the simulated grid.

The structure of a grid is defined by an XML file. In this file, the number of lines and the number of nodes per line can be defined. Each line has a concrete type of node; it means that all the nodes of each line have the same features. *GridSim* can run multiple executions in parallel. This feature of the simulator has been implemented by making use of the MPI<sup>2</sup> protocol.

*GridSim* calculates the power balances of every node and they are aggregated in their common line. The aggregated consumption of the virtual electrical grid is calculated as the sum of the power balances of every line plus the base consumption function. The nodes can be equipped with different controllers to control the possible

---

<sup>1</sup> *GridSim* is released under GPLv3.0. It can be downloaded from: <https://github.com/Robolabo/gridSim.git>

<sup>2</sup> Message Passing Interface (MPI) is a standardized and portable message-passing system designed by a group of researchers from academia and industry to function on a wide variety of parallel computers. The standard defines the syntax and semantics of a core of library routines useful to a wide range of users writing portable message-passing programs in different computer programming languages.

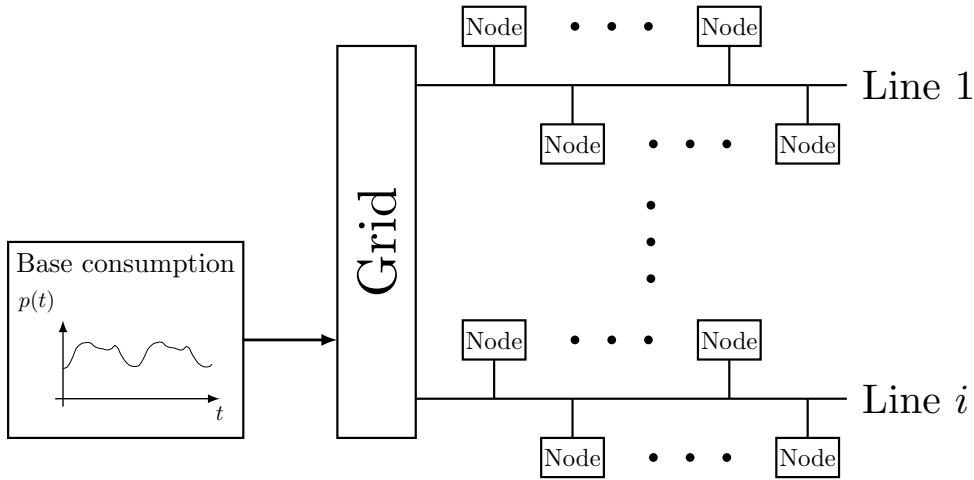


Figure A.1: Scheme of the modular architecture of *GridSim* simulator.

elements which a node is composed of. For example, the charge power of the storage system can be controlled by a battery controller. The controllers can obtain information from every element of the *GridSim* simulator.

Algorithm 5 describes the operation of *GridSim*. In the first place, the simulator is initialized—see from line 1 to 3. The virtual electrical grid is created by using a configuration file which indicates structure of the grid. In addition, the counter of *time steps* is set to zero. A time step is one execution of the main loop of the simulator. It is the virtual clock of a simulation which marks the events that happen. A time step is related to an amount of time in the real world. For example, if a time step represents one minute, in each execution of the main loop, the power balances are calculated for one minute in the real world. The lower the amount of time in the real world is, the higher the accuracy of the simulator is, but also the greater the computing power. After *GridSim* is initialized, the main loop begins. The main loop simulates the virtual electrical grid, the virtual users and controllers in each time step. The counter of time steps is increased at the end of this loop. When the main loop finishes, the simulation finishes. This condition is satisfied when the counter of time steps reaches a certain value indicated in the configuration file—see the condition of line 5.

---

**Algorithm 5** High-level description of the main loop of *GridSim* simulator.

---

```
1: /* Initialization */
2: createGrid(< configurationFile >)
3: TimeStep ← 0
4: /* Main Loop */
5: while TimeStep < TimeStepLimit do
6:   /* Execute main control function */
7:   mainControlFunction()
8:   /* Execute virtual user functions on all nodes */
9:   for i < numNodes do
10:    node[i] → userFunction()
11:   end for
12:   /* Execute control functions on all nodes */
13:   for i < numNodes do
14:    node[i] → controlFunction()
15:   end for
16:   /* Execute grid energy balance - physics engine */
17:   gridExecutionFunction()
18:   TimeStep ++
19: end while
```

---



# Bibliography

- Abdelaziz, E. A., Saidur, R., and Mekhilef, S. (2011). A review on energy saving strategies in industrial sector. *Renewable and Sustainable Energy Reviews*, 15(1):150–168.
- Anderson, C. and Franks, N. R. (2001). Teams in animal societies. *Behavioral Ecology*, 12(5):534–540.
- Anderson, C., Theraulaz, G., and Deneubourg, J. L. (2002). Self-assemblages in insect societies. *Insectes Sociaux*, 49(2):99–110.
- Barker, P. P. and Mello, R. W. D. (2000). Determining the impact of distributed generation on power systems: radial distribution systems. In *Proceedings of the Power Engineering Society Summer Meeting, 2000. IEEE*, volume 3, pages 1645–1656, Piscataway, NJ.
- Baughman, M. L. and Siddiqi, S. N. (1991). Real-time pricing of reactive power: theory and case study results. *IEEE Transactions on Power Systems*, 6(1):23–29.
- Bennett, M., Schatz, M. F., Rockwood, H., and Wiesenfeld, K. (2002). Huygens’s clocks. *Proc. R. Soc. Lond.*, 458(2019):pp. 563–579.
- Beshers, S. N. and Fewell, J. H. (2001). Models of division of labor in social insects. *Annual Review of Entomology*, 46(1):413–440.
- Beshers, S. N., Huang, Z. Y., Oono, Y., and Robinson, G. E. (2001). Social inhibition and the regulation of temporal polyethism in honey bees. *Journal of Theoretical Biology*, 213(3):461–479.
- Beyea, J. (2010). The smart electricity grid and scientific research. *Science*, 328(5981):979–980.

## BIBLIOGRAPHY

---

- Bonabeau, E., Dorigo, M., and Theraulaz, G. (1999). *Swarm Intelligence: From Natural to Artificial Systems*. Oxford University Press, New York, NY.
- Bonabeau, E., Theraulaz, G., and Deneubourg, J. L. (1996). Quantitative study of the fixed threshold model for the regulation of division of labor in insect societies. *Proc. R. Soc. Lond.*, 263(1376):1565–1569.
- Bonabeau, E., Theraulaz, G., and Deneubourg, J. L. (1998). Fixed response thresholds and the regulation of division of labor in insect societies. *Bulletin of Mathematical Biology*, 60(4):753–807.
- Bopp, G., Gabler, H., Preiser, K., Sauer, D. U., and Schmidt, H. (1998). Energy storage in photovoltaic stand-alone energy supply systems. *Progress in Photovoltaics: Research and Applications*, 6(4):271–291.
- Brandon, G. and Lewis, A. (1999). Reducing household energy consumption: a qualitative and quantitative field study. *Journal of Environmental Psychology*, 19(1):75–85.
- Brutschy, A., Tran, N.-L., Baiboun, N., Frison, M., Pini, G., Roli, A., Dorigo, M., and Birattari, M. (2011). Costs and benefits of behavioral specialization. In Gro, R., Alboul, L., Melhuish, C., Witkowski, M., Prescott, T. J., and Penders, J., editors, *Towards Autonomous Robotic Systems*, pages 90–101. Springer Berlin Heidelberg.
- Buck, J. (1988). Synchronous rhythmic flashing of fireflies ii. *The Quarterly Review of Biology*, 63(3):265–289.
- Buck, J. B. (1938). Synchronous rhythmic flashing of fireflies. *The Quarterly Review of Biology*, 13(3):301–314.
- Caamaño-Martín, E., Castillo-Cagigal, M., Masa-Bote, D., Gutiérrez, A., Matallanas, E., Monasterio-Huelin, F., and Jiménez-Leube, F. J. (2010). Autoconsumo de energía solar fotovoltaica con gestión activa de la demanda: El sistema GeDELOS-FV. In *Actas del IV Conferencia Latinoamericana de Energía Solar (IV ISES CLA) y XVII Simposio Peruano de Energía Solar (XVII- SPES)*, Cuzco, Perú. Asociación Peruana de Energía Solar y del Ambiente.
- Caamaño-Martín, E., Egido, M. A., Neila, J., Bedoya, C., Santos, A. G., Jiménez, F. J., and Magdalena, L. (2005). Spanish participation in the “Solar Decathlon 2005” competition: new proposal for zero-energy houses. In *Proceedings of the*

## BIBLIOGRAPHY

---

- 20th European Photovoltaic Solar Energy Conference*, pages 2587–2590, Munich, Germany. WIP-Renewable Energies.
- Caamaño-Martín, E., Laukamp, H., Jantsch, M., Erge, T., Thornycroft, J., Moor, H. D., Cobben, S., Suna, D., and Gaiddon, B. (2008). Interaction between photovoltaic distributed generation and electricity networks. *Progress in Photovoltaics: Research and Applications*, 16(7):629–643.
- Caamaño-Martín, E., Masa, D., Gutiérrez, A., Monasterio-Huelin, F., Castillo-Cagigal, M., Jiménez, J., and Porro, J. (2009a). Optimizing pv use through active demand side management. In *Proceedings of the 24th European Photovoltaic Solar Energy Conference*, pages 3149–3155, Munich, Germany. WIP-Renewable Energies.
- Caamaño-Martín, E., Masa, D., Gutiérrez, A., Monasterio-Huelin, F., Jiménez-Leube, F. J., Porro, J., and Castillo-Cagigal, M. (2009b). Optimización del uso de un sistema fotovoltaico mediante gestión activa de la demanda. In *Proceedings of the I Congreso de Generación Distribuida*, pages 121–126, Madrid, Spain. Fundación de la Energía de la Comunidad de Madrid.
- Caamaño-Martín, E., Novo, S., Egidio, M. A., and Masa, D. (2007). Demand side management in PV-powered homes: A supervision and decision making tool. In *Proceedings of the 22th European Photovoltaic Solar Energy Conference and Exhibition*, pages 2478–2483, Munich, Germany. WIP-Renewable Energies.
- Calvo-Fernández, M., Vega, J. E., Egidio, M. A., and Caamaño-Martín, E. (2005). Spanish participation in the “Solar Decathlon 2005” competition: design and simulation of the photovoltaic system. In *Proceedings of the 20th European Photovoltaic Solar Energy Conference*, pages 1958–1963, Munich, Germany. WIP-Renewable Energies.
- Camazine, S., Deneubourg, J.-L., Franks, N. R., Sneyd, J., Theraulaz, G., and Bonabeau, E. (2003). *Self-Organization in Biological Systems*. Princeton Studies in Complexity. Princeton University Press, Princeton, NJ.
- Castillo-Cagigal, M., Brutschy, A., Gutiérrez, A., and Birattari, M. (2014a). Temporal task allocation in periodic environments: An approach based on synchronization. In *Proceedings of the 9th International Conference on Swarm Intelligence*, pages 182–193, Brussels, Belgium. Springer International Publishing.

## BIBLIOGRAPHY

---

- Castillo-Cagigal, M., Caamaño-Martín, E., Gutiérrez, A., Masa-Bote, D., Monasterio, F., Porro, J., Matallanas, E., and Jiménez-Leube, F. J. (2010). Self-consumption of pv electricity with active demand side management: the gedelos-pv system. In *Proceedings of the 25th European Photovoltaic Solar Energy Conference*, pages 4866–4870, Munich, Germany. WIP-Renewable Energies.
- Castillo-Cagigal, M., Caamaño-Martín, E., Matallanas, E., Masa-Bote, D., Gutiérrez, A., Monasterio-Huelin, F., and Jiménez-Leube, J. (2011a). PV self-consumption optimization with storage and active DSM for the residential sector. *Solar Energy*, 85(9):2338–2348.
- Castillo-Cagigal, M., Gutiérrez, A., Monasterio-Huelin, F., Caamaño-Martín, E., Masa, D., and Jiménez-Leube, J. (2011b). A semi-distributed electric demand-side management system with PV generation for self-consumption enhancement. *Energy Conversion and Management*, 52(7):2659–2666.
- Castillo-Cagigal, M., Gutiérrez, A., Monasterio-Huelin, F., Masa, D., Caamaño-Martín, E., Jiménez-Leube, F. J., and Porro, J. (2009). Sistema de control distribuido para la gestión de la demanda en el sector residencial. In *Proceedings of the I Congreso de Generación Distribuida*, pages 275–280, Madrid, Spain. Fundación de la Energía de la Comunidad de Madrid.
- Castillo-Cagigal, M., Matallanas, E., Gutiérrez, A., Monasterio-Huelin, F., Caamaño-Martín, E., Masa-Bote, D., and Jiménez-Leube, J. (2011c). Heterogeneous collaborative sensor network for electrical management of an automated house with PV energy. *Sensors*, 11(12):11544–11559.
- Castillo-Cagigal, M., Matallanas, E., Navarro, I., Caamaño-Martín, E., Monasterio-Huelin, F., and Gutiérrez, A. (2014b). Variable threshold algorithm for division of labor analyzed as a dynamical system. *IEEE Transactions on Cybernetics*, PP(99):1–11.
- Deneubourg, J. L., Aron, S., Goss, S., and Pasteels, J. M. (1990). The self-organizing exploratory pattern of the Argentine ant. *Journal of Insect Behavior*, 3(1):159–168.
- Denholm, P. and Margolis, R. M. (2007). Evaluating the limits of solar photovoltaics (PV) in electric power systems utilizing energy storage and other enabling technologies. *Energy Policy*, 35(9):4424–4433.

## BIBLIOGRAPHY

---

- Depuru, S. S. S. R., Wang, L., and Devabhaktuni, V. (2011). Smart meters for power grid: Challenges, issues, advantages and status. *Renewable and Sustainable Energy Reviews*, 15(6):2736–2742.
- Detrain, C. and Pasteels, J. M. (1991). Caste differences in behavioral thresholds as a basis for polyethism during food recruitment in the ant *Pheidole Pallidula* (Nyl.) (Hymenoptera: Myrmicinae). *Journal of Insect Behavior*, 4(2):157–176.
- Dondi, P., Bayoumi, D., Haederli, C., Julian, D., and Suter, M. (2002). Network integration of distributed power generation. *Journal of Power Sources*, 106(12):1–9.
- Driesen, J. and Katiraei, F. (2008). Design for distributed energy resources. *Power and Energy Magazine, IEEE*, 6(3):30–40.
- Edenhofer, O., Pichs-Madruga, R., Sokona, Y., Seyboth, K., Matschoss, P., Kadner, S., Zwickel, T., Eickemeier, P., Hansen, G., Schlömer, S., and von Stechow, C. (2011). Special report on renewable energy sources and climate change mitigation. Technical Report 1472, IPCC.
- El-Khattam, W. and Salama, M. M. A. (2004). Distributed generation technologies, definitions and benefits. *Electric Power Systems Research*, 71(2):119–128.
- Emlen, J. T. J. (1952). Flocking behavior in birds. *The Auk*, 69(1):160–170.
- Eto, J., Koomey, J., Lehman, B., Martin, N., Mills, E., Webber, C., and Worrel, E. (2001). Scoping study on trends in the economic value of electricity reliability to the U.S. economy. Technical Report LBLN-47911, Lawrence Berkeley National Laboratory, Berkeley.
- Farhangi, H. (2010). The path of the smart grid. *Power and Energy Magazine, IEEE*, 8(1):18–28.
- Fewell, J. H. and Bertram, S. M. (1999). Division of labor in a dynamic environment: response by honeybees (*Apis Mellifera*) to graded changes in colony pollen stores. *Behavioral Ecology and Sociobiology*, 46(3):171–179.
- Foidart, F., Oliver-Solá, J., Gasol, C. M., Gabarrel, X., and Rieradevall, J. (2010). How important are current energy mix choices on future sustainability? Case study: Belgium and Spain – projections towards 2020-2030. *Energy Policy*, 38(9):5028–5037.

## BIBLIOGRAPHY

---

- Garnier, S., Gautrais, J., and Theraulaz, G. (2007). The biological principles of swarm intelligence. *Swarm Intelligence*, 1(1):3–31.
- Glova, A. F. (2003). Phase locking of optically coupled lasers. *Quantum Electronics*, 33(4):283–306.
- Gordon, D. M. (2002). The organization of work in social insect colonies. *Complexity*, 8(1):43–46.
- Gordon, D. M., Goodwin, B. C., and Trainor, L. E. H. (1992). A parallel distributed model of the behaviour of ant colonies. *Journal of Theoretical Biology*, 156(3):293–307.
- Goss, S., Aron, S., Deneubourg, J. L., and Pasteels, J. M. (1989). Self-organized shortcuts in the Argentine ant. *Naturwissenschaften*, 76(12):579–581.
- Groppi, F. (2002). Grid connected photovoltaic power systems: power value and capacity value of PV systems. Technical Report IEA-PVPS T5-11, International Energy Agency.
- Guckenheimer, J. and Holmes, P. (1983). *Nonlinear Oscillations, Dynamical Systems and Bifurcations of Vector Fields*. Springer, New York, NY.
- Hadjipaschalis, I., Poullikkas, A., and Efthimiou, V. (2009). Overview of current and future energy storage technologies for electric power applications. *Renewable and Sustainable Energy Reviews*, 13(6-7):1513–1522.
- Herter, K. (2007). Residential implementation of critical-peak pricing of electricity. *Energy Policy*, 35(4):2121–2130.
- Hölldobler, B. and Wilson, E. O. (1990). *The Ants*. Belknap Press, Cambridge, MA.
- Hong, H. and Strogatz, S. H. (2011a). Conformists and contrarians in a kuramoto model with identical natural frequencies. *Phys. Rev. E.*, 84(4):046202.
- Hong, H. and Strogatz, S. H. (2011b). Kuramoto model of coupled oscillators with positive and negative coupling parameters: An example of conformist and contrarian oscillators. *Phys. Rev. Lett.*, 106(5):054102.
- Huang, Z. Y. and Robinson, G. E. (1992). Honeybee colony integration: worker-worker interactions mediate hormonally regulated plasticity in division of labor. volume 89, pages 11726–11729, Bethesda, MD. National Academy of Science of USA.

## BIBLIOGRAPHY

---

- Huang, Z. Y. and Robinson, G. E. (1996). Regulation of honey bee division of labor by colony age demography. *Behavioral Ecology and Sociobiology*, 39(3):147–158.
- INDEL, P. (1998). Atlas de la demanda eléctrica española. Technical Report Project Final Report, R.E.E.
- Järventausta, P., Repo, S., Rautiainen, A., and Partanen, J. (2010). Smart grid power system control in distributed generation environment. *Annual Reviews in Control*, 34(2):277–286.
- Jenkins, D. P., Patidar, S., and Simpson, S. A. (2014). Synthesising electrical demand profiles for UK dwellings. *Energy and Buildings*, 76(0):605–614.
- Jiang, Z. and McCall, M. (1993). Numerical simulation of a large number of coupled lasers. *Journal of the Optical Society of America B*, 10(1):155–163.
- Kiessling, R. (1987). Lead/acid batteries for load-levelling applications. *Journal of Power Sources*, 19(23):227–230.
- Kim, J. H. and Shcherbakova, A. (2011). Common failures of demand response. *Energy*, 36(2):873–880.
- Kirtley, J. L. (2010). *Electric Power Principles: Sources, Conversion, Distribution and Use*. John Wiley & Sons, Chichester, UK.
- Kjaer, S. B., Pedersen, J. K., and Blaabjerg, F. (2005). A review of single-phase grid-connected inverters for photovoltaic modules. *IEEE Transactions on Industry Applications*, 41(5):1292–1306.
- Koeppel, G. and Korpas, M. (2008). Improving the network infeed accuracy of non-dispatchable generators with energy storage devices. *Electric Power Systems Research*, 78(12):2024–2036.
- Kuramoto, Y. (1975). Self-entrainment of a population of coupled non-linear oscillators. In Araki, H., editor, *International Symposium on Mathematical Problems in Theoretical Physics*, volume 39 of *Lecture Notes in Physics*, pages 420–422. Springer Berlin Heidelberg.
- Kuramoto, Y. (1984). *Chemical Oscillations, Waves, and Turbulence*. Springer, Berlin, Germany.

## BIBLIOGRAPHY

---

- Leygue, C., Ferguson, E., Skatova, A., and Spencer, A. (2014). Energy sharing and energy feedback: affective and behavioral reactions to communal energy displays. *Frontiers in Energy Research*, 2(29):1–12.
- Li, F., Qiao, W., Sun, H., Wan, H., Wang, J., Xia, Y., Xu, Z., and Zhang, P. (2010). Smart transmission grid: Vision and framework. *IEEE Transactions on Smart Grid*, 1(2):168–177.
- Lior, N. (2008). Energy resources and use: The present situation and possible paths to the future. *Energy*, 33(6):842–857.
- Liu, C., Weaver, D. R., Strogatz, S. H., and Reppert, S. M. (1997). Cellular construction of a circadian clock: Period determination in the suprachiasmatic nuclei. *Cell*, 91(6):855–860.
- Lopes, J. A. P., Hatziargyriou, N., Mutale, J., Djapic, P., and Jenkins, N. (2007). Integrating distributed generation into electric power systems: A review of drivers, challenges and opportunities. *Electric Power Systems Research*, 77(9):1189–1203.
- Lopes-Ferreira, H., Garde, R., Fulli, G., Kling, W., and Pecas-Lopes, J. (2013). Characterisation of electrical energy storage technologies. *Energy*, 53(0):288–298.
- López-Ibáñez, M., Dubois-Lacoste, J., Stützle, T., and Birattari, M. (2011). The irace package, Iterated Race for Automatic Algorithm Configuration. Technical Report TR/IRIDIA/2011-004, IRIDIA, Université Libre de Bruxelles, Belgium.
- Loulas, N. M., Karteris, M. M., Pilavachi, P. A., and Papadopoulos, A. M. (2012). Photovoltaics in urban environment: A case study for typical apartment buildings in Greece. *Renewable Energy*, 48(0):453–463.
- Luque, A. and Hegedus, S. (2011). *Handbook of Photovoltaics Science and Engineering*. John Wiley & Sons, Chichester, UK.
- Martín H., J. A., De Lope, J., and Maravall, D. (2009). Adaptation, anticipation and rationality in natural and artificial systems: computational paradigms mimicking nature. *Natural Computing*, 8(4):757–775.
- Marvin, S., Chappells, H., and Guy, S. (1999). Pathways of smart metering development: shaping environmental innovation. *Computers, Environment and Urban Systems*, 23(2):109–126.

## BIBLIOGRAPHY

---

- Masa, D. (2014). *Contribución a la integración de sistemas fotovoltaicos conectados a la red eléctrica: recurso solar y predicción de generación*. PhD thesis, Universidad Politécnica de Madrid.
- Masa-Bote, D. and Caamaño-Martín, E. (2010). Forecast of energy production for pv systems 24 hours ahead. In *Proceedings of the 25th European Photovoltaic Solar Energy Conference*, pages 4813–4819, Munich, Germany. WIP-Renewable Energies.
- Masa-Bote, D., Castillo-Cagigal, M., Matallanas, E., Caamaño-Martín, E., Gutiérrez, A., Monasterio-Huelin, F., and Jiménez-Leube, J. (2014). Improving photovoltaics grid integration through short time forecasting and self-consumption. *Applied Energy*, 125(0):103–113.
- Matallanas, E., Castillo-Cagigal, M., Caamaño-Martín, E., Masa-Bote, D., Gutiérrez, A., and Monasterio-Huelin, F. (2011). Analysis of the self-consumption possibilities in small grid-connected photovoltaic systems in Spain. In *Proceedings of the 26th European Photovoltaic Solar Energy Conference*, pages 4619–4624, Munich, Germany. WIP-Renewable Energies.
- Matallanas, E., Castillo-Cagigal, M., Gutiérrez, A., Monasterio-Huelin, F., Caamaño-Martín, E., Masa, D., and Jiménez-Leube, J. (2012). Neural network controller for Active Demand-Side Management with PV energy in the residential sector. *Applied Energy*, 91(1):90–97.
- Matallanas, E., Solórzano, J., Castillo-Cagigal, M., Navarro, I., Caamaño-Martín, E., Egido, M. A., and Gutiérrez, A. (2014). Electrical energy balance contest in Solar Decathlon Europe 2012. *Energy and Buildings*, 83(0):36–43.
- McKinstry, G., Galloway, S., and Kockar, I. (2010). An initial assessment of the potential impact of smart metering on a decentralised energy network. In *Proceedings of the Universities Power Engineering Conference (UPEC), 2010 45th International*, pages 1–4, Cardiff, UK.
- Mecrow, B. C. and Jack, A. G. (2008). Efficiency trends in electric machines and drives. *Energy Policy*, 36(12):4336–4341.
- Meinhart, H. (2009). *The Algorithmic Beauty of Sea Shells*. Springer-Verlag, Berlin, Germany.

## BIBLIOGRAPHY

---

- Michaels, D. C., Matyas, E. P., and Jalife, J. (1987). Mechanisms of sinoatrial pacemaker synchronization: a new hypothesis. *Circulation Research*, 61(5):704–714.
- Mohsenian-Rad, A. H. and Leon-Garcia, A. (2010). Optimal residential load control with price prediction in real-time electricity pricing environments. *IEEE Transactions on Smart Grid*, 1(2):120–133.
- Moslehi, K. and Kumar, R. (2010). A reliability perspective of the smart grid. *IEEE Transactions on Smart Grid*, 1(1):57–64.
- Nair, N.-K. C. and Garimella, N. (2010). Battery energy storage systems: Assessment for small-scale renewable energy integration. *Energy and Buildings*, 42(11):2124–2130.
- Navarro, I., Gutiérrez, A., Montero, C., Rodríguez-Ubiñas, E., Matallanas, E., Castillo-Cagigal, M., Porteros, M., Solórzano, J., Caamaño-Martín, E., Egado, M. A., Páez, J. M., and Vega, S. (2014). Experiences and methodology in a multidisciplinary energy and architecture competition: Solar Decathlon Europe 2012. *Energy and Buildings*, 83(0):3–9.
- Néda, Z., Ravasz, E., Brechet, Y., Vicsek, T., and Barabási, A. L. (2000). Self-organizing processes: The sound of many hands clapping. *Nature*, 403(6772):849–850.
- Newsham, G. R. and Bowker, B. G. (2010). The effect of utility time-varying pricing and load control strategies on residential summer peak electricity use: A review. *Energy Policy*, 38(7):3289–3296.
- Onovwiona, H. I. and Ugursal, V. I. (2006). Residential cogeneration systems: review of the current technology. *Renewable and Sustainable Energy Reviews*, 10(5):389–431.
- Oppenheim, A. V. and Schaffer, R. W. (2009). *Discrete-Time Signal Processing*. Prentice-Hall, New Jersey, USA.
- Oppenheim, A. V., Willsky, A. S., and Nawab, S. H. (1996). *Signals & Systems (2Nd Ed.)*. Prentice-Hall, Inc., Upper Saddle River, NJ.

## BIBLIOGRAPHY

---

- Pacala, S. W., Gordon, D. M., and Godfray, H. C. J. (1996). Effects of social group size on information transfer and task allocation. *Evolutionary Ecology*, 10(2):127–165.
- Page, R. E. J. and Mitchell, S. D. (1990). Self organization and adaptation in insect societies. pages 289–298, Chicago, IL. The University of Chicago Press.
- Pagliarini, G. and Rainieri, S. (2012). Restoration of the building hourly space heating and cooling loads from the monthly energy consumption. *Energy and Buildings*, 49(0):348–355.
- Papagiannis, G., Dagoumas, A., Lettas, N., and Dokopoulos, P. (2008). Economic and environmental impacts from the implementation of an intelligent demand side management system at the european level. *Energy Policy*, 36(1):163–180.
- Pepermans, G., Driesen, J., Haeseldonckx, D., Belmans, R., and D’haeseleer, W. (2005). Distributed generation: definition, benefits and issues. *Energy Policy*, 33(6):787–798.
- Peterson, S. B., Whitacre, J. F., and Apt, J. (2010). The economics of using plug-in hybrid electric vehicle battery packs for grid storage. *Journal of Power Sources*, 195(8):2377–2384.
- R.A. of Engineering (2013). Gb electricity capacity margin. Technical Report 293074, Royal Academy of Engineering.
- Rahimi, F. and Ipakchi, A. (2010). Demand response as a market resource under the smart grid paradigm. *IEEE Transactions on Smart Grid*, 1(1):82–88.
- Richards, G., Noble, B., and Belcher, K. (2012). Barriers to renewable energy development: A case study of large-scale wind energy in Saskatchewan, Canada. *Energy Policy*, 42(0):691–698.
- Robinson, G. E. (1992). Regulation of division of labor in insect societies. *Annual Review of Entomology*, 37:637–665.
- Robinson, G. E. (2009). Chapter 77 - division of labor in insect societies. In Resh, V. H. and Cardé, R. T., editors, *Encyclopedia of Insects (Second Edition)*, pages 297–299. Academic Press, San Diego.

## BIBLIOGRAPHY

---

- Rodriguez-Ubiñas, E., Montero, C., Porteros, M., Vega, S., Navarro, I., Castillo-Cagigal, M., Matallanas, E., and Gutiérrez, A. (2014). Passive design strategies and performance of net energy plus houses. *Energy and Buildings*, 83(0):10–22.
- Santiago, I., Lopez-Rodríguez, M. A., Trillo-Montero, D., Torriti, J., and Moreno-Muñoz, A. (2014). Activities related with electricity consumption in the Spanish residential sector: Variations between days of the week, autonomous communities and size of towns. *Energy and Buildings*, 79(0):84–97.
- Sendin, A., Berganza, I., Arzuaga, A., Pulkkinen, A., and Kim, I. H. (2012). Performance results from 100,000+ PRIME smart meters deployment in Spain. In *Smart Grid Communications (SmartGridComm), 2012 IEEE Third International Conference on*, pages 145–150, Piscataway, NJ.
- Sendova-Franks, A. B. and Franks, N. R. (1994). Social resilience in individual worker ants and its role in division of labour. *Proc. R. Soc. Lond.*, 256(1347):305–309.
- Sioshansi, R. and Short, W. (2009). Evaluating the impacts of real-time pricing on the usage of wind generation. *IEEE Transactions on Power Systems*, 24(2):516–524.
- Solórzano, J. (2014). *Distributed control strategies for photovoltaics systems in urban environments*. PhD thesis, Universidad Politécnica de Madrid.
- Spencer, A. J., Couzin, I. D., and Franks, N. R. (1998). The dynamics of specialization and generalization within biological populations. *Journal of complex systems*, 1(1):1–14.
- Strbac, G. (2008). Demand side management: Benefits and challenges. *Energy Policy*, 36(12):4419–4426.
- Strogatz, S. H. (2000). From Kuramoto to Crawford: exploring the onset of synchronization in populations of coupled oscillators. *Physica D: Nonlinear Phenomena*, 143(1-4):1–20.
- Strogatz, S. H. (2003). *Sync: The Emerging Science of Spontaneous Order*. Hyperion Press, New York, NY.
- Sutton, R. S. and Barto, A. G. (1998). *Reinforcement Learning: An introduction*. MIT Press, Cambridge, MA.

## BIBLIOGRAPHY

---

- Theraulaz, G. and Bonabeau, E. (1995). Modeling the collective building of complex architectures in social insects with lattice swarms. *Journal of Theoretical Biology*, 177(4):381–400.
- Theraulaz, G. and Bonabeau, E. (1999). A brief history of stigmergy. *Artificial Life*, 5(2):97–116.
- Theraulaz, G., Bonabeau, E., and Deneubourg, J. L. (1998). Response threshold reinforcement and division of labor in insect societies. *Proc. R. Soc. Lond.*, 265(1393):327–332.
- Theraulaz, G., Gervet, J., and Tian-Chanski, S. S. (1991). Social regulation of foraging activities in polistes dominulus christ: a systemic approach to behavioural organization. *Behavior*, 116(3/4):292–320.
- Tofts, C. (1993). Algorithms for task allocation in ants. (a study of temporal polyethism: Theory). *Bulletin of Mathematical Biology*, 55(5):891–918.
- Torriti, J., Hassan, M. G., and Leach, M. (2010). Demand response experience in europe: Policies, programmes and implementation. *Energy*, 35(4):1575–1583.
- Trujillo, P., Alamillo, C., Gil, E., Óscar de la Rubia, Martínez, M., Rubio, F., Cadavid, A., Navarro, J., Hillenbrand, S., Ballesteros-Sánchez, I., Castillo-Cagigal, M., Masa-Bote, D., Matallanas, E., Caamaño-Martín, E., and Álvaro Gutiérrez (2012). Cpv hybrid system in isfoc building, first results. In *Proceedings of the 8th International Conference on Concentrating Photovoltaic Systems*, pages 360–363, Melville, NY. American Institute of Physics.
- Trujillo, P., Alamillo, C., Martínez, M., Óscar de la Rubia, Rubio, F., Masa-Bote, D., Castillo-Cagigal, M., Matallanas, E., Caamaño-Martín, E., and Gutiérrez, A. (2013). Instituto de sistemas fotovoltaicos de concentración concentration photovoltaics hybrid system first year of operation and improvements. *Progress in Photovoltaics: Research and Applications*, 21(6):1260–1275.
- Tschinkel, W. R. (1988). Colony growth and the ontogeny of worker polymorphism in the fire ant, solenopsis invicta. *Behavioral Ecology and Sociobiology*, 22(2):103–115.
- Tsimring, L. S., Rulkov, N. F., Larsen, M. L., and Gabbay, M. (2005). Repulsive synchronization in an array of phase oscillators. *Phys. Rev. Lett.*, 95(1):014101.

## BIBLIOGRAPHY

---

- Vojdani, A. (2008). Smart integration. *Power and Energy Magazine, IEEE*, 6(6):71–79.
- Vu, K., Begouic, M. M., and Novosel, D. (1997). Grids get smart protection and control. *Computer Applications in Power, IEEE*, 10(4):40–44.
- Wagner, R. (1997). Large lead/acid batteries for frequency regulation, load levelling and solar power application. *Journal of Power Sources*, 67(1-2):163–172.
- Walker, T. J. (1969). Acoustic synchrony: Two mechanisms in the snowy tree cricket. *Science*, 166(3907):891–894.
- Wiener, N. (1958). *Nonlinear problems in Random Theory*. MIT Press, Cambridge, MA.
- Wiesenfeld, K., Colet, P., and Strogatz, S. H. (1996). Synchronization transitions in a disordered josephson series array. *Phys. Rev. Lett.*, 76(3):404–407.
- Wilson, E. O. (1984). The relation between caste ratios and division of labor in the ant genus *pheidole* (Hymenoptera: Formicidae). *Behavioral Ecology and Sociobiology*, 16(1):89–98.
- Winfree, A. T. (1967). Biological rhythms and the behavior of populations of coupled oscillators. *Journal of Theoretical Biology*, 16(1):15–42.
- Wiston, M. L. (1987). *The biology of the honey bee*. Harvard University Press, Cambridge, MA.
- Withers, G. S., Fahrbach, S. E., and Robinson, G. E. (1993). Selective neuroanatomical plasticity and division of labour in the honeybee. *Nature*, 364(6434):238–240.
- Wood, G. and Newborough, M. (2003). Dynamic energy-consumption indicators for domestic appliances: environment, behaviour and design. *Energy and Buildings*, 35(8):821–841.
- York, R. A. and Compton, R. C. (1991). Quasi-optical power combining using mutually synchronized oscillator arrays. *IEEE Transactions on Microwave Theory and Techniques*, 39(6):1000–1009.